Phase separation and mechanical properties of epoxy / thermoplastic blends

Emmerson, Gordon T.

Phase Separation And Mechanical Properties Of Epoxy / Thermoplastic Blends

By

Gordon T. Emmerson

Of

Durham University

A dissertation submitted to the University of Durham for the degree of Doctor of Philosophy

December 2003

Table of Contents

To Carol.....

Acknowledgements

Many people have helped and supported me along the way to completing this PhD thesis and several need to be singled out for special acknowledgement.

Dr Terry McGrail of CytecFiberite Research Support Group. This thesis would not have been undertaken without the considerable support, encouragement and advice that Terry has continuously offered. Terry's own outstanding contribution to the area of polymer blends inspired me to learn more about the topic. I am forever indebted to his contribution towards this thesis and my career.

Dr Nigel Clarke of Durham University. I could not have wished for a better academic supervisor for this project than Nigel. His teaching, advice and direction have largely dictated the successful outcome of this project. Nigel and I discussed this work on many occasions over great food and fine wine in many wonderful locations around the world, he has taught me that this is a great forum for scientific debate and learning.

Dr Roy Moore of Imperial College London. The mechanical testing and fracture mechanics studies in this thesis were professionally undertaken under his advice and direction, he offered many useful discussions during this thesis. Roy taught me two lessons of great importance; firstly the essential attention to detail that is required in any scientific research and secondly to never miss a golfing opportunity when one comes along.

My thanks go to the following people who have assisted and contributed to the completion of this thesis: Dr Andrew Burgess, Dr Gordon Seeley, Mrs Lizzie Egginton, Miss Jayne Baker, Miss Ivana Fodale, Mrs Jessica Chappel and Mrs Margaret Derbyshire of ICI Strategic Technology Group at Wilton. Mr Julian Barwick, Dr Phil Wilcocks, Mr Andrew Broadhurst and Mrs Alyson Dunn of ICI Measurement Science Group at Wilton.

Abstract

Thermosetting epoxy resins blended with aromatic thermoplastics are of significant commercial interest in several areas including aerospace, transportation and electronics. These materials offer an excellent combination of mechanical properties ease of processing and overall component cost. A more complete and fundamental understanding of these materials could potentially lead to a new generation of thermoplastic-thermoset blends with enhanced properties that would extend their use into new applications. This thesis studies the reaction induced phase separation behaviour of a thermosetting epoxy resin blended with an aromatic polyethersulphone thermoplastic and explores the link between morphology and physical properties.

The phase separation behaviour of the thermoplastic-thermoset blend is studied using a combination of Small Angle Light Scattering (SALS), Differential Scanning Calorimetry (DSC) and Polarised Light Microscopy. A large part of this thesis involved the design and build of specialised SALS equipment that enabled the phase separation of the thermoplastic-thermoset blends to be studied dynamically. The studies show that in this thermoplastic-thermoset blend the mechanism of phase separation appears to be, without exception, spinodal decomposition. There was no evidence of phase separation occurring by nucleation and growth in these blends. The particulate morphologies seen in the thermoplastic-thermoset blends appear to form by the break up of a percolating network that initially forms by spinodal decomposition. This behaviour is termed Percolation to Cluster Transformation (PCT).

Cahn-Hilliard theory was used to analyse the SALS data from the reacting thermoplastic-thermoset blends to give kinetic information about the phase separation process. These studies show that this particular blend exhibits Lower Critical Solution Temperature (LCST) behaviour. The work also shows that Cahn-Hilliard theory does not fully describe the spinodal decomposition processes occurring in these thermoplastic-thermoset blends.

The effect of blend composition, cure temperature and epoxy functionality on phase separation behaviour are studied. This shows that in certain formulations especially around the critical formulation of the blend both primary and secondary spinodal decompositions occur during cure. This can lead to thermoplastic-thermoset blend formulations that have very unique, and previously unreported, morphologies for these systems. These novel morphologies resemble sub-included or salami morphologies similar to that observed in rubber modified polystyrene (HIPS) but have in fact formed by multiple PCT occurring during cure.

This study shows that moisture can significantly influence the properties of epoxy resin based systems. It also appears that a phase inverted morphology consisting of a continuous thermoplastic rich phase with a dispersed thermosetting rich phase appears to offer great advantage in terms of fracture and mechanical properties after both dry and moisture conditioning. The phase-inverted morphology also appears to significantly reduce the moisture ingress of the epoxy blend.

Chapter 1

Introduction

Thermosetting polymeric materials such as epoxy resins are used commercially in a wide range of different applications. These include adhesives, coatings, encapsulants, electronic packaging and composite matrices. The reason why thermosetting polymers are used in such a diverse range of application is because they offer an excellent combination of properties, which include low cost, ease of processing, good chemical resistance, and mechanical properties. However thermosetting materials such as epoxy resins are rarely used in an unmodified form, they are usually formulated or blended with other components to enhance their properties to fit the application in question.

One major problem that inhibits the more extensive use of crosslinked thermosetting polymers is their inherent brittleness and poor fatigue performance. This is due to the highly crosslinked structure that is produced after curing, resulting in a glassy brittle polymer. This produces a polymer that has inherently low fracture toughness. It is for this reason that many thermosetting-based systems that are used successfully in commercial application are generally blends formulated to improve the fracture toughness of the system without significantly impacting the inherent advantages of thermosetting systems. This is the reason why it is important to understand in detail the behaviour of thermosetting polymer blends and how their morphology influences mechanical properties such as toughness, Tg and modulus. This thesis studies the behaviour of a thermoplastic-thermoset blend that is typical of those used in aerospace applications as a matrix system for a continuous carbon fibre reinforced composite.

This system is a blend of an epoxy resin and a high Tg thermoplastic; such systems were developed to give a good combination of toughness, modulus and high Tg. The thesis initially studies the reaction induced phase separation behaviour of the thermoplastic-thermoset blend and how temperature, composition and degree of crosslinking influence the morphology of the system. Then the thesis discusses how the morphology influences the final properties of the system.

1.1 Applications Of Thermosetting Polymers

1.1.1 Adhesives

Adhesive bonding is rapidly replacing conventional joining techniques such as welding and soldering in many manufacturing processes. Adhesive bonding can offer significant advantages but the primary advantage is lower cost rapid assembly of components. However it has also been discovered that from a performance point of view adhesives offer several significant performance advantages over conventional joining processes. In particular adhesive bonding can produce structures that are more reliable, durable and less prone to fatigue and impact failure. This is because a compliant polymeric adhesive joining two solid structures together can offer a reduction in residual stresses compared to conventional welding or joining methods. One excellent example of how adhesives can replace conventional joining and give performance advantages is the world land speed record holding vehicle Thrust 2. This set a world land speed record of 633mph in 1984. The constriction of the Thrust 2 vehicle was a tubular steel frame with aluminium alloy panels. The initial test vehicle attached the aluminium panels to the steel alloy frame using traditional bolts. Holes were drilled through the aluminium panels and threaded holes were drilled into the steel substructure. The bolts were tightened and the threads locked with an anaerobic acrylic adhesive. During the initial vehicle trials the levels of vibration caused the bolts to fail due to fatigue and panels became detached from the structure. Fatigue cracks were also observed on both the aluminium panels and steel tube frame initiating from the holes drilled into the structure. Bonding the aluminium panels to the steel substructure using a rubber toughened thermally cured epoxy adhesive

solved all of these problems. This bonding method is now used extensively in aerospace and automotive applications removing the need for slow expensive welding and riveting processes and imparting improved durability. An example of this is the Lotus Elise sports car adhesive bonding is extensively used in the construction.

Figure 1.1.1.1 Thrust 2 SSC. This vehicle set the current land speed record of 633.48mph in 1984. Its panel structure was bonded together using a toughened epoxy adhesive (Picture Courtesy of Jeremy Davey of Permabond)

Figure 1.1.1.2 Lotus Elise Sports Car. The construction of this car relies heavily upon toughened epoxy adhesives (picture courtesy of rsportscars.com)

Thermosetting adhesives are also extensively used in the construction of silicon chip integrated circuits. At present this is one of the most rapidly growing markets for thermosetting resins adhesives. These are very specialised adhesives that are used to package silicon chips for subsequent use in electronic components. A typical example here is for a die attach adhesive that bonds a silicon die to a metal leadframe. Traditionally this was done using solder. The application needs the adhesive to bond the die to the leadframe and be electrically and thermally conductive.

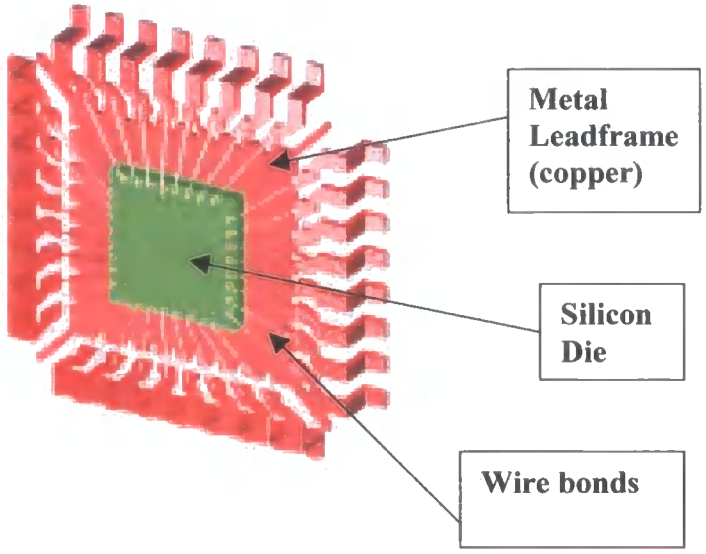

Figure 1.1.1.3 Figure showing the internal structure of a typical silicon chip integrated circuit. Here a conductive adhesive is used to bond the die to the leadframe.

Typical adhesives used as die attach materials are silver filled thermosetting resins which can be epoxy based but the latest generation adhesives use BMI resins due to their improved thermal stability. The use of thermosetting adhesives in this application has many advantages over conventional solder. Firstly it can reduce the stress in the bonded joint and make it a more reliable tougher joint. Also the use of adhesives enables more rapid lower processing temperature manufacturing. As electronic components become smaller adhesives are the only viable option. The major drawback with polymers in this application is their moisture sensitivity. On storage of the integrated circuit, the package picks up moisture. Subsequent soldering into a component board where the processing is around 260°C causes rapid moisture out-gassing and package cracking. This is referred to as popcorning.

Newer generation integrated circuits permit more complex operations to be carried out on a single silicone chip. An example of this technology is the latest generation computer central processing units (CPU). This uses flipchip technology where the silicon chip contacts are no longer small wires from the periphery of the top of the silicon chip but tiny balls of solder on the underside of the chip. With flipchips the die is attached to the substrate by the solder ball connectors. However to improve reliability of the chip on thermal cycling a toughened thermoset resin is used to fill the gaps between the board and the chip, this material is a nonconductive underfil resin.

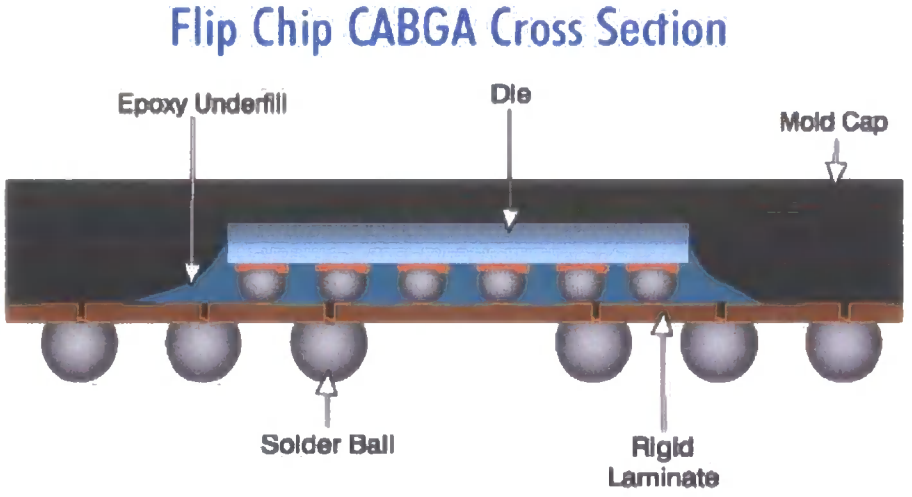

Figure 1.1.1.4 Cross section of a flipchip IC showing the epoxy underfill material.

The underfill material needs to be low viscosity for processing and highly toughened to prevent thermal fatigue failure in use.

Due to the legislation that restricts the use of lead base solders that comes into force in Europe in 2006 a new generation of highly conducting filled thermosetting systems are currently being developed as alternatives to solder. These are likely to offer rapid processing and improved reliability.

Epoxy resins that are liquids in their uncured form are commonly used in a wide range of adhesive applications. Typical liquid epoxy resins are based on diglycidylether of bisphenol acetone commonly referred to as (DGEBA). There is however a range of liquid epoxy resins which are commercially available and can be used in adhesive applications. These liquid epoxy resins are formulated with a curing agent that is selected to meet the application requirements. For example for room

temperature curing adhesives an aliphatic diamine may be used as a curing agent. Where a higher Tg or improved chemical resistance is required aromatic diamines may be used as curing agents, which require thermal curing. Chapter 4 of this thesis discusses the different cure reactions of epoxy resins and how this influences the properties of the system

The advantage of epoxy resins in adhesive applications is that they have excellent adhesion to a wide range of substrates due to their highly polar nature. Also they wet polar surfaces very effectively and can be cured to form a strong and chemically resistant crosslinked solid. These characteristics make epoxy resins ideally suited to adhesive applications. However epoxy resins do have some limitations such as slow cure speed , sensitivity to moisture, low toughness and poor thermal stability above 200°C. This has lead to the development of new and alternative chemistries to be used in adhesive applications; these include acrylic, cyanate esters and bismaleimide. These alternatives to epoxy resins offer many of the advantages of epoxy resins but have improved thermal stability and reduced sensitivity to moisture however they still show low fracture toughness that is inherent in crosslinked thermosetting systems. These systems still require formulating with toughening agents to allow them to be successfully used in commercial adhesive applications.

1.1.2 Coatings

Toughened thermosetting materials find use in many coating applications. The advantage of polymer thermoset coatings is often to provide corrosion protection or barrier properties. One of the world's major uses of epoxy resins is roller coatings for paper converting. Here the epoxy coating is used on metal rollers in the paper drying process. Metal finished rollers cannot be used in these applications due to the severe combination of temperature, moisture and acidity to which the roller surface coating is subjected. Also textures and patterns can be easily applied to the thermoset coating surface which enables the production of textured papers.

Can coatings is another application for epoxy resins. The inside of tin cans for food applications is coated with a cured epoxy resin to prevent the corrosion of the tin can and the subsequent spoiling of the can contents.

Epoxy resins are also used as highly specialised paints that provides both decoration and corrosion protection for a range of different substrates. Also filled epoxy resins are used as coatings on concrete to protect from moisture ingress and concrete corrosion.

1.1.3 Composites

Fibre reinforced composite materials are used extensively in aerospace applications where low weight and high modulus structures are essential. Continuous carbon fibre reinforced composites offer an excellent combination of low weight, high stiffness(modulus), good thermal properties and durability which makes then find application in high performance aerospace type applications.

Figure 1.1.3.1 The USA Navy latest generation of fighter aircraft, the Joint Strike Fighter, extensively uses carbon fibre reinforced toughened epoxy resins composites in both primary and secondary structure to reduce weight and improve performance. (Picture courtesy of Boeing Aerospace, Seattle)

Military aircraft such as the new Joint Strike fighter (figure 1.1.3.1) uses fibre reinforced thermosetting composites extensively in both load bearing primary structure and secondary non-load bearing structure. This produces an aircraft that has exceptionally high power to weight ratio and is reported to be highly manoeuvrable due to its low weight and high rigidity

Fibre reinforced thermosetting composites are also finding ever increasing application in commercial aircraft. Their use produces lighter stiffer structures than conventional aluminium alloys and this results in a significant weight advantage in the final aircraft. This can produce commercial aircraft with higher payloads, greater economy and longer range.

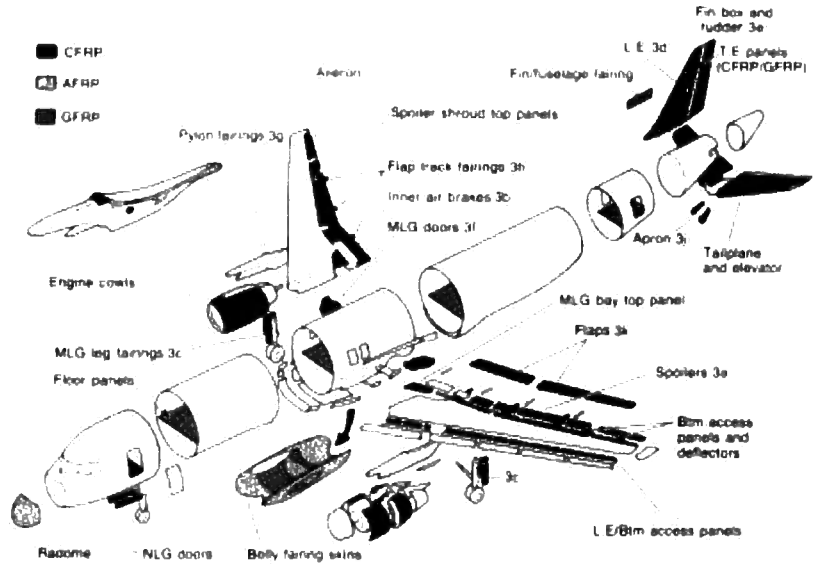

Figure 1.1.3.2 This picture shows the secondary structures of commercial aircraft that are produced from fibre reinforced thermosetting materials (picture courtesy of Boeing Aerospace)

Other areas where carbon fibre reinforced composite materials find applications in areas where performance and low weight are of vital importance such as formula one racing cars. Here carbon fibre reinforced epoxy resins are used extensively due to both their specific modulus and their ability to absorb energy on impact and deformation. Due to these properties these materials are used to build the drivers 'tub' of formula one racing cars because they are both lightweight and improve safety.

Figure 1.1.3.3 This figure shows a cockpit or so called 'tub' of a formula one car. This is made exclusively from woven carbon fibre reinforced toughened thermosetting epoxy resin

Thermosetting resins can be compounded with fibres to produce fibre reinforced composite materials. Typical fibres include carbon, glass and alumina. Such composites result in materials that have excellent specific modulus that makes them ideal for use in aircraft and other aerospace applications where low weight high stiffness structures are necessary.

Fibre reinforced composites can contain either continuous fibres or discontinuous fibres. In the case of discontinuous fibres chopped fibres are compounded with thermosetting resins to produce what is termed a moulding compound. Typically the fibre lengths are 2-5mm in length and these moulding compounds can be readily processed into complex shapes by simple processing techniques such as injection moulding. The resulting components are thermosetting polymers with random fibre reinforcement. However to fully realise the full properties of high modulus carbon fibres they need to be used in a continuous form. Continuous fibre reinforced thermosetting composites can be prepared from what is termed a prepreg. This is a continuous fibre arrangement that is impregnated with a formulated thermosetting resin. The typical volume fraction of fibres in prepreg is around 70%. The fibres in a prepreg may be either unidirectional or woven in nature. The thermosetting resin has to be formulated to give a unique blend of properties. Firstly the uncured resin need appropriate rheological properties in order for the system to be impregnated into the fibres to fully wet the fibres. A solvent may be used to assist this impregnation

process but this needs to be removed through a thermal treatment prior to use otherwise voiding may occur in the final component. The prepreg needs to have the correct handling characteristics, which requires the correct drape and tack so that it can be easily formed into more complex shapes.

The cure characteristics of the thermosetting system also need to be closely controlled. It is important to formulate a resin that has a latent curing tendency so that the system has a long work life. This is because large structures, which are typically made from continuous fibre composites can take many days even weeks to lay up and prepare, so long work life is essential. Also thick sections may have to be prepared, for this reason the cure reaction needs to have a low, controlled level of exothermic energy release otherwise a runaway exothermic reaction may occur on curing.

To make components out of prepreg systems requires individual layers of the prepreg to be laid up in sequence to produce the component shape. Usually this operation is performed inside a metal mould. This process is called the lay up and can be performed manually or by automated tape laying machines.

Continuous fibre reinforced composite systems are generally moulded at temperatures above 150°C using autoclave moulding which is the most effective method of eliminating void and applying consolidation pressure to the composite system during cure.

The final cured properties of the thermoset matrix system are of vital importance to the overall properties of the system. The thermoset resin system needs to have both good interfacial adhesion to the fibre and also high fracture toughness. The region of lowest toughness where most failures occur in continuous fibre reinforced composites is the matrix resin rich interlaminar region between the individual plies of the moulded system. The toughness of the interlaminar region is dominated by the toughness of the thermosetting matrix. Hence the morphology and the final toughness of the thermoset matrix are of great importance in these materials.

Resin systems formulated for this application generally have good toughness coupled with high modulus and high Tg. This is the reason thermosetting polymers blended with high Tg thermoplastics are extremely successful in this application.

1.2 Toughening Technologies For Thermosetting Resins

The major drawback of thermosetting polymer resins is their inherently low fracture toughness. In their unmodified form cured highly crosslinked thermosetting polymers are glassy solids that are very brittle and have poor impact resistance. For most applications thermosetting resins such as epoxy resins need to be toughened in some way for them to be used successfully in a particular application.

There are several different methods that have been used to toughen thermosetting polymers such as epoxy resins. These are liquid rubbers, thermoplastics, core-shell particles, reactive diluents and inorganic particles. This section briefly summarises the different approaches and their inherent benefits and drawbacks.

1.2.1 Liquid rubber toughening

Blending liquid rubbers with epoxy resins to improve the fracture toughness is used extensively. This approach was first developed by McGarry [1] who incorporated polybutadiene rubbers into epoxy resin. This showed only a marginal improvement in fracture properties and the thermal stability of the epoxy blend was reduced. No mention was made of the phase morphology in these systems, however it was found to be difficult to obtain a homogeneous solution due to the non-polar nature of the polybutadiene rubber.

Much research has since been carried out to develop butadiene-acrylonitrile rubbers with functional end groups[2 ,3, 4] The end groups can be carboxylic acid (CTBN), amine or vinyl. These CTBN liquid rubbers due to their highly polar nature are more miscible with epoxy resins and with the reactive end groups can undergo reaction with the epoxy network. Several workers have reported on the two-phase morphology that results in these systems after cure. Typically these systems produce particles of a rubber rich phase dispersed in an epoxy rich matrix. This can give high levels of toughening and Bucknall et al studied the toughening mechanisms in such systems and showed that a combination of shear yielding and cavitation occur in these systems on deformation which greatly improved the fracture toughness. It was also highlighted that the end group chemistry or the rubber is essential to provide

improved toughness. Non-reactive end group liquid rubbers showed only a minimal improvement in toughness.

The major drawback of these systems is twofold, firstly the Tg, modulus and yield strength of the system are significantly reduced when compared with the unmodified epoxy resin. Secondly the thermal stability of the system is greatly reduced and this is largely due to the poor stability of the unsaturation in the backbone of the liquid rubber [5,6,7,8].

Functionalised liquid acrylic oligomers have also been used to toughen epoxy resins. These provide greater thermal stability due to the lack of unsaturated groups. The fracture toughness of the system is improved, however the Tg and yield strength of the system are significantly reduced. This is largely due to the incomplete phase separation in the system. A small amount of acrylic rubber remains in the continuous epoxy resin phase, which reduced the Tg compared with the unmodified epoxy resin [9].

1.2.2 Toughening by Core-shell particles and cross-linked rubber particles

In order to overcome the drawbacks of adding reactive liquid rubbers to thermosetting systems core shell particles and functionalised cross-linked rubber particles have been developed. The advantage of these systems is that the low Tg rubber phase is crosslinked and is not soluble in the thermoset resin. The rubber particles are preformed and dispersed by shear mixing into the uncured thermosetting resin. The rubber particles are not soluble so no reaction induced phase separation will occur. Therefore after cure the Tg of the continuous thermoset phase remains close to that of the unmodified cured resin.

Core shell particles are of a two-phase nature consisting of a rubber core and an outer shell which has controlled properties to give good compatibility with the matrix resin to which it will be added. This gives good interfacial adhesion between the thermoset and toughening rubber phase. This is essential for toughening to occur. The size of the particles is also carefully controlled to give maximum toughness by inducing shear yielding in the matrix [10]. Typically the diameter of the core shell particles is around 500-700nm. The major draw back of core shell particles is that when the

particles are blended into the thermoset resin the viscosity of the system is significantly increased which has a detrimental effect on handing and processing.

Recent developments in this area include nano-scale crosslinked CTBN rubber particles [11]and functionalised hyper-branched polyethers [12]. These both claim to offer excellent toughness with little impact on Tg and yield strength and minor impact on rheological properties. These systems are currently undergoing evaluation in industrial applications.

1.2.3 Thermoplastic Toughening of Thermosetting Systems.

Liquid rubber-toughened thermoset resins and core-shell particle additives can increase toughness of thermosets however this can only be achieved by sacrificing other important properties such as Tg, modulus, thermal stability or rheological properties. Several industries, such as the aerospace industry, have a significant need for thermoset polymer materials that have high thermal stability, high Tg, high modulus and as well as toughness [13]. To meet this growing need thermoplastic modified thermosets have been developed [14,15]. Typically the thermoplastics used to modify thermosetting resins are high Tg thermoplastics that are thermally and chemically stable and intrinsically have good ductility and toughness. This technology toughens thermoset resins without negatively affecting their Tg or high-temperature performance. This method has significant performance advantages however the major drawback with this approach is that the rheology of the uncured resin may be altered which can be detrimental to processing.

Many commercial high Tg thermoplastics have been evaluated as toughening agents for thermosetting epoxy resins, however not all attempts were successful. Bucknall and Partridge [16] studied blending commercial grades of PES into epoxy resins but this did not significantly improve the fracture toughness, and in some cases, the fracture toughness decreased compared with the untoughened epoxy. This was attributed to poor adhesion and compatibility between the two phase-separated components. Work by McGrail & co workers showed that it is important to increase the compatibility and interfacial adhesion between the two separated phases in order to increase the fracture toughness[17].

Typical thermoplastics that can be used for thermoset toughening are non-crystalline aromatic thermoplastics such as polyimides and polyethersulphones. For these to be successful in this application the thermoplastic needs to be soluble in the uncured thermoset resin and also it is advantageous for the thermoplastic to have some functionality that can react with the thermoset network. On curing of the thermoplastic-thermoset blend the system may undergo reaction induced phase separation to give multi-phase morphology that can give improved toughness and good thermal stability coupled with improved higher temperature properties. This thesis deals exclusively with the area of thermoplastic-thermoset blends and the reaction induced phase separation that occurs in these systems and how the resulting morphology influences the physical properties of the blend.

1.2.4 Inorganic filler particles

Inorganic particulate fillers have also been used as toughening agents for epoxy materials. These act as stress concentrators in the resin matrix and on deformation cause localised yielding and deformation around the individual particles. This dissipates stored energy in the material and therefore improves fracture toughness and impact properties. Inorganic particles that have been used for this purpose are, glass beads[18] silica [19], alumina trihydrate [20] and various metal oxide powders such as copper oxide[21]. It has been demonstrated that the fracture energy of filled epoxies reaches a maximum at a certain volume fraction and also the interfacial adhesion between the filler and the matrix plays a vital role in the toughening mechanism[22,23].

1.2.5 Other Toughening Methods For Thermosetting Systems

Other methods have been used to improve the toughness of thermosetting resins however most of these methods have limited application because they improve the toughness at the expense of other key properties. Yorkgitis et al [24] has reported toughening epoxy resins by incorporating functionalised polyorganic siloxanes, such as hydroxyl-terminated polydimethlysiloxane. Although toughness is improved and

moisture uptake of the system is reduced this method significantly reduces the Tg and modulus of the system as well as reducing adhesion to substrates.

Reactive diluents have been added to thermosetting resins to improve toughness. This method works by reducing the crosslinked density of the system that also reduces modulus and Tg of the system.

Also epoxy resins and amine curing agents have been developed that have flexible spacer groups. For example low Tg flexible aliphatic diols have been functionalised with epoxy groups[25]. These can be blended with other epoxy resins and curing agents to produce cured blends with improved fracture properties. This has the disadvantage of reducing the Tg and modulus of the blend but may be advantageous in adhesive formulations where lower modulus materials are required to relieve stresses in the cured joint.

1.3 Summary

This chapter has described how thermosetting materials are of great commercial significance and their use in advanced technological applications is growing. It has also been outlined that thermosetting systems have some limitations but the most significant drawback is their low fracture toughness, which limits their more widespread use. Much work has been carried out into how to improve the overall fracture toughness of thermosetting materials and these methods have been outlined. One of the most interesting areas from both a commercial and technological viewpoint is in the area of thermoplastic toughened thermosets. These systems have the potential to offer improved toughness without significantly altering other key properties inherent in thermosetting polymers. Therefore a thorough and detailed understanding of the fundamental factors that influence the properties of thermoplastic-thermoset blends is of strategic importance. This thesis presents studies of the phase separation behaviour of a thermoplastic-thermoset blend and also looks at how morphology can influence the properties of such blends.

1.4 References

1 McGarry, F.J., Proc. Roy. Soc. London, A319, 59 (1970)

2 Kunz-Douglass, S., Beaumont, P.W.R., and Ashby, M.F., J. Mater. Sci., 15, 1109 (1980)

3 Kinloch, A.J., Shaw, S.J., Tod, D.A., Hunston, D.L., Polymer, 24 (4), 1355 (1983).

4 Pearson, R.A., and Yee, A.F., J. Mater. Sci., 26, 3828 (1991).

5 Verchere, D., Sautereau, H., and Pascault, J.P., J. Appl. Polym. Sci., 41, 467 (1990).

6 Verchere, D., Pascault, J.P., Sautereau, H., Moschiar, S.M., Riccardi, C.C., and Williams, R.J.J., J. Appl.Polym. Sci., 43, 293 (1991)

7 Hwang, J.F., Manson, J.A., Hertzberg, R.W., Miller, G.A., and Sperling, J.H., Polym. Eng. Sci., 29, 1466 (1989).

8 Kirshenbaum, S.L., Gazit, S., and Bell, J.P., in .Rubber Modified Thermoset Resins., edited by Riew, C.K., and Gillham, J.K., Advances in Chemistry Series, 208, Amer. Chem. Soc., Washington DC, 1984

9 Ochi, M., and Bell, J.P., J. Appl. Polym. Sci., 29, 1381 (1984).

10 C-S toughening ref Bucknall et all

11 http://www.zeonchemicals.com/productgrid.asp?id=419

12 http://www.perstorppolyols.com/product.cfm

13 Hedrick, J.C., Patel, N.M., and McGrath, J.E., in .Toughened Plastics I., edited by Riew, C.K., and Iijima, T., Tomoi, M., Suzuki, A., Eur. Polym. J., 27, 851 (1991).

14 Kim, S.C., and Brown, H.R., J. Mater. Sci., 22, 2589 (1987).

15 Kim, J., and Robertson, R., Polym. Mater. Sci. Eng., 63, 301 (1990).

16 Bucknall, C. B., and Partridge, I.K., Polymer, 24, 639 (1983).

17 A.J. Mackinnon, S.D. Jenkins, P.T. Mcgrail And R.A. Pethrick, Macromolecules 25(1992) 3492.

18 Spanoudakis, J., and Young, R.J., J. Mater. Sci., 19, 473 (1984)

19 Nakamura, Y., Yamaguchi, M., Kitayama, A., Okubo, M., and Matsumoto, T., Polymer, 32, 2976 (1991).

20 Moloney, A.C., Kausch, H.H., and Stieger, H.R., J. Mater. Sci., 18, 208 (1983).

21 Nakamura, Y., Yamaguchi, M., Okubo, M., and Matsumoto, T., J. Appl. Polym. Sci., 45, 1281 (1992).

22 Young, R.J., and Beaumont, P.W.R., J. Mater. Sci., 12, 684 (1977)

23 Srivastava, V.K., Shembekar, P.S., J. Mater. Sci., **25**, 3513 (1990).

24 Yorkgitis, E.M., Tran, C., Eiss, N.S., Hu, T.Y., Yilgor, I., Wilkes, G.L., and McGrath, J.E., in .Rubber- Modified Thermoset Resins., edited by Riew, C.K., and Gillham, J.K., Advances in Chemistry Series, 208, American Chemical Society, Washington, D.C., 1984.

25 Scherzer, N., J. Appl. Polym. Sci., 51, 491 (1994).

Chapter 2

Theory of Phase Separation in Polymer Blends: Thermodynamics and Kinetics

2.1 Introduction

This chapter will discuss the theoretical aspects of phase separation in polymer blends. Firstly the basic concepts of the thermodynamic aspects of polymer blends will be described in terms of the Flory–Huggins (F-H) theory. It will be shown how F-H theory can be used to predict phase diagrams for polymer blends. The relevance of F-H theory to reactive thermoset-thermoplastic blends will be discussed.

The characteristics of the two different kinds of phase separation mechanism, spinodal decomposition and nucleation and growth, will be described and the concepts of secondary phase separation processes and percolation to cluster transformations will also be introduced.

The kinetic aspects of phase separation of polymer blends will be discussed in terms of Cahn-Hilliard (C-H) theory. Linearised C-H theory is only applicable to early stage spinodal decomposition in polymer blends. Other theories covering the kinetics of non-linear and later stage phase separation processes will be described.

2.2 Thermodynamics: Flory-Huggins Theory of Polymer Blends.

The aim of mixing two or more polymers together to produce a blend is to optimise the overall properties of the system. In a polymer blend it is possible to get either complete mixing on a molecular level to give a homogeneous system or alternatively phase separation can occur to produce a multi-phase heterogeneous system. The properties of the blend will be strongly influenced by the resulting phase morphology and this topic will be discussed in chapter 7. Phase diagrams can be a useful tool to map out expected morphologies under different conditions such as composition and temperature. F-H theory [1, 2, 3] can be used to describe the thermodynamic considerations of binary polymer blends and therefore be used to predict phase diagrams.

2.2.1 The Entropy of Mixing for a thermoplastic-thermoset blend.

Consider a blend of a monodisperse thermoset, E, with a monodisperse thermoplastic P. The system has N_E moles of thermoset E and N_P moles of thermoplastic P.
The total number of moles in the system is given by:

$$N_T = N_E + N_P \qquad (1)$$

If the volume fractions of E and P are ϕ_E and ϕ_P respectively the Flory-Huggins expression for the entropy of mixing is given by[4]:

$$\Delta S_{mix} = -R(N_E \ln \phi_E + N_P \ln \phi_P) \qquad (2)$$

The assumption made in this entropy expression is that within the mixture the occupation of any site is independent of it neighbours. This expression does not account for any molecular order that may occur. The expression assumes that the probability of occupation of any particular site by either component E or P is only related to the relative concentration of the component in the mixture.

If V_E and V_P are the molar volumes of E and P respectively and the total volume of the system is V_T then the entropy of mixing per unit volume can be given as:

$$\Delta S^{\circ} = \frac{\Delta S_{mix}}{V_T} = -R\left(\frac{\phi_E}{V_E}\ln\phi_E + \frac{\phi_P}{V_P}\ln\phi_P\right) \qquad (3)$$

The expression (3) indicates that there is always a positive entropy gain on mixing. The system will always have a tendency to maximise its entropy therefore from purely entropic considerations alone a thermoplastic-thermoset blend should always give a homogeneous mixture.

Applying equation 3 to a thermoplastic-thermoset blend, if we assume the case that V_P remains constant during the thermoset curing process, ie the modifying thermoplastic has no functionality, then the ΔS° change during curing is due to variation in V_E only. V_E is a function of the degree of conversion of the thermosetting phase. V_P is typically much larger than V_E so the thermoset phase is generally the major contributor to the entropy of mixing in an uncured blend.

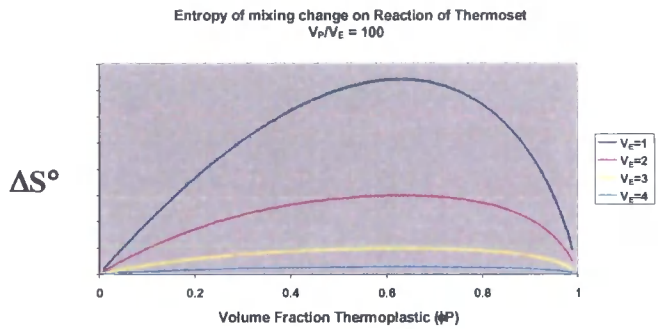

Graph 2.2.1.1 This graph shows how for a thermoplastic-thermoset blend the entropy of mixing ΔS° varies across the composition range and during cure of the thermoset. This assumes that V_P remains constant and V_P/V_E before any cure has taken place is 100.

Graph 2.2.1.1 shows how the entropy of mixing changes as the cure progresses for a thermoplastic-thermoset blend. This is assuming that V_P is constant during cure. It shows that the entropy of mixing ΔS° reduces as the thermoset increases its molar volume during cure. Although ΔS° reduces it always remains positive and hence favours homogeneous mixing.

In some thermoplastic-thermoset blends the thermoplastic or modifying polymer can be reactive. For example reactive end groups can be present that allow the thermoplastic to increase its molar volume during curing. This too will have the effect of reducing the $\Delta S°$ of the blend.

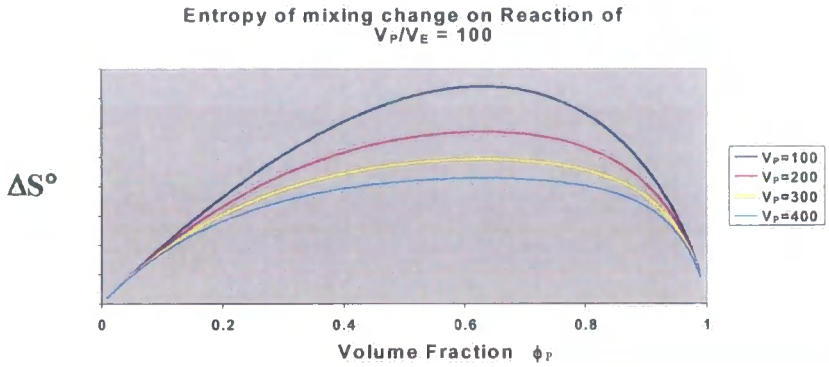

Graph 2.2.1.2 *This graph shows how for a thermoplastic-thermoset blend the entropy of mixing $\Delta S°$ varies across the composition range. This also shows the effect of increasing thermoplastic molar volume during cure with the thermoset molar volume remaining constant. Before any cure V_P/V_E is equal to 100*

Graph 2.2.1.2 shows the influence of increasing the molar volume of the thermoplastic keeping the molar volume of the thermoset constant. The overall influence of increasing the molar volume of the thermoplastic is smaller in comparison to the effect of changing molar volume of the thermoset phase during cure.

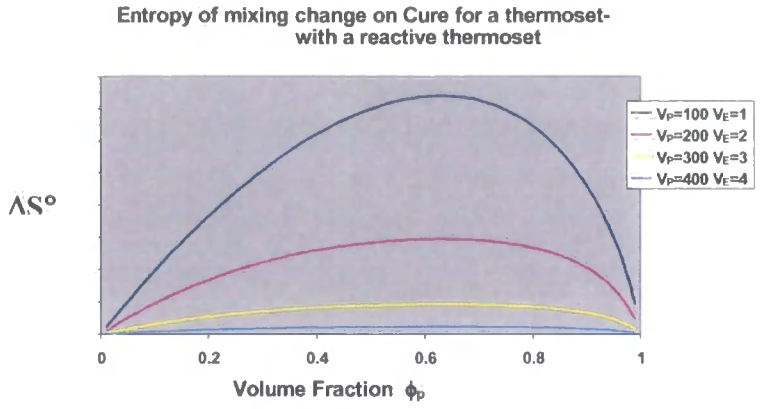

Graph 2.2.1.3 *This graph shows how for a thermoplastic-thermoset blend the entropy of mixing $\Delta S°$ varies across the composition range. In this situation there is a reactive thermoplastic so both V_E and V_P can increase during curing.*

In a thermoplastic-thermoset blend system with a reactive thermoplastic the increase in molar volume of both thermoset and thermoplastic components will cause an overall reduction in the $\Delta S°$ of the system and this effect is shown in Graph 2.2.1.3. This reduction of $\Delta S°$ will cause the initially homogeneous solution to become less thermodynamically stable.

Equation 3 only considers the case for monodisperse components. The polydispersity of both the thermoset and thermoplastic will influence the $\Delta S°$ of the system. This is because both V_E and V_P will not be discrete values and in real systems they will have a distribution spectrum.

However entropy alone does not dictate if a thermoplastic-thermoset blend will phase separate, in fact on entropic considerations alone all blends would mix homogenously. The overall driving force for phase separation is the change in free energy of mixing, $\Delta G°$, which considers the effect of both entropic and enthalpic terms. The Flory-Huggins expression for $\Delta G°$ will be discussed in the next section.

2.2.2 The Enthalpy Of Mixing For A Thermoplastic-Thermoset Blend

In order to express the enthalpy of mixing in a monodisperse thermoplastic-thermoset blend a reference unit cell with a molar volume V_R needs to be defined. This can be selected as the initial molar volume of the thermoset material or as the molar volume of the repeat unit in thermoplastic polymer. In this case the V_R will be equal to V_E prior to any cure reaction occurring. Each reference volume will have a set co-ordination number of nearest neighbours defined as Z_C.

The number of moles of unit cells with reference volume V_R in the total volume of the blend, V_T, is given by:

$$M_{VR} = \frac{V_T}{V_R} \tag{4}$$

Within the blend the probability, Ψ, of having contact between a unit volume containing a molecule of thermoset E and a unit volume containing a monomeric unit of the thermoplastic P can be given by the following expression:

$$\Psi = Z_C \phi_E \phi_P M_{VR} \tag{5}$$

In order to define the enthalpy of mixing it is necessary to define the exchange energy, ε, between the unit cells. In practical terms this is related to the nature of the inter molecular bonding level between the different cells. For example highly polar systems will have higher exchange energy than a non-polar system that only has Van der Waals forces of interaction between the reference cells.

The exchange energy, ε, can be defined by the following equation [4. 5]:

$$\varepsilon = \frac{1}{2}\varepsilon_{EE} + \frac{1}{2}\varepsilon_{PP} - \varepsilon_{EP} \tag{6}$$

where ε_{ij} is the contact energy between components i and j. Multiplying equations 5 and 6 gives lead to an expression for the enthalpy of mixing for a system, ΔH_M,

$$\Delta H_M = Z_C \varepsilon M_{VR} \phi_E \phi_P \tag{7}$$

Expressing the ΔH_M per unit volume to give $\Delta H°$ yields:

$$\Delta H^{o} = \frac{Z_C \varepsilon}{V_R} \phi_E \phi_P \qquad (8)$$

The Flory-Huggins interaction parameter, χ, is defined by:

$$\chi = \frac{Z_C \varepsilon}{RT} \qquad (9)$$

The assumption in this expression for χ, is that the number of neighbours of each type of molecule at any given site is simply given by the overall concentration and there are no fluctuations in concentration in the sample. This is called the mean field theory.

Equation 8 can now be redefined as follows:

$$\Delta H^{o} = \frac{\chi RT}{V_R} \phi_E \phi_P \qquad (10)$$

In the case of a thermoplastic-thermoset blend the value of χ may be either positive or negative depending on the nature of the intermolecular forces of attraction between the thermoset molecules and the thermoplastic molecules. In cases where strong forces of attraction exist between thermoset and thermoplastic molecules, ie polar bonds or hydrogen bonding, χ may be negative.

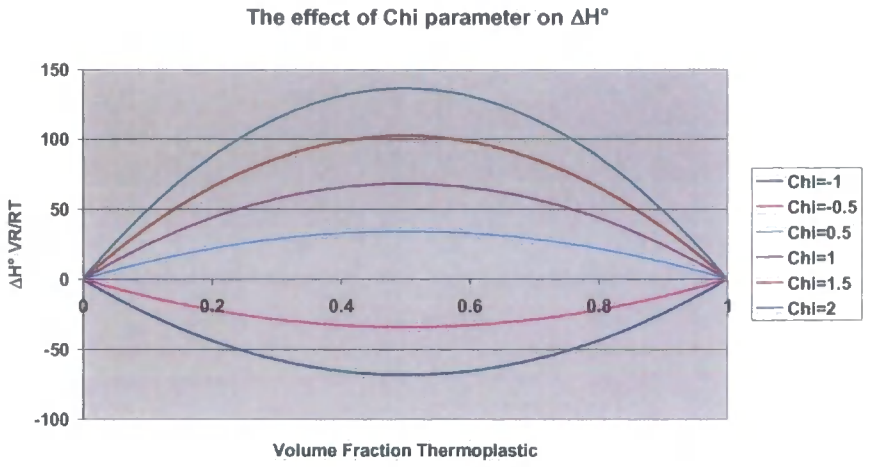

Graph 2.2.2.1 *This graph shows how the enthalpy of mixing $\Delta H°$ varies with composition for different χ values. This shows that the enthalpy of mixing can vary dramatically depending on the nature of the intermolecular forces between the molecules in the blend.*

Graph 2.2.2.1 shows that the enthalpy of mixing contribution may be negative depending on the nature of the intermolecular forces of attraction between the molecules in the blend. In a thermoplastic-thermoset blend during cure it is likely that χ will change as the degree of conversion of the thermoset phase advances. For example in an epoxy thermoset blend as the epoxy molecules react hydroxyl groups are produced. These hydroxyl groups are polar in nature compared with the un-reacted epoxy group, and as the level of conversion increases the exchange energy will change altering the value of χ [6, 7]. This is also the case for cyanate ester blends where initially there is an abundance of highly polar cyanate ester groups. As the resin begins to cure the polar cyanate ester groups are converted to non-polar triazine rings. This again alters the interaction energy changing the value of χ [8].

2.2.3 Flory-Huggins Equation For Free Energy Change Of Mixing In Thermoplastic-Thermoset Blends

In the previous two sections (2.2.1 and 2.2.3) the entropy and enthalpy of thermoplastic-thermoset blends was discussed. The actual thermodynamic driving force for phase separation in polymer blends is the reduction in Gibbs free energy of mixing ΔGm. The free energy of mixing is given by:

$$\Delta G_m^o = \Delta H^o - T\Delta S^o \qquad (11)$$

Equations 3 and 10 can now be combined to produce the Flory-Huggins equation for free energy of mixing in a thermoplastic-thermoset blend:

$$\Delta G_m^o = \left\{\frac{\chi RT}{V_R}\right\}\phi_E\phi_P + RT\left\{\frac{\phi_E}{V_E}\ln\phi_E + \frac{\phi_P}{V_P}\ln\phi_P\right\} \qquad (12)$$

Let Z_i be the ratio of molar volume to the reference volume so:

$$Z_E = \frac{V_E}{V_R} \qquad (13)$$

$$Z_P = \frac{V_P}{V_R} \qquad (14)$$

Equation 12 can now be expressed as follows:

$$\Delta G_m^o = \left(\frac{RT}{V_R}\right)\left\{\frac{\phi_E}{Z_E}\ln\phi_E + \frac{\phi_P}{Z_P}\ln\phi_P + \chi\phi_E\phi_P\right\} \qquad (15)$$

Equation 15 is the Flory-Huggins expression for the free energy change on mixing of a binary polymer blend [1,5]. For a thermoplastic-thermoset blend Z_E is a function of conversion of the thermoset phase and if a non-reactive thermoplastic is used Z_p remains constant during the cure reaction. As Z_E increases during polymerisation of the thermoset phase the entropy of the system is lowered which may drive phase separation in the system. Also as the cure reaction progresses the Flory-Huggins interaction parameter, χ, may also change as the nature of the chemical functionality

changes. If χ increases during the cure reaction this would favor phase separation if it remains constant or becomes lower mixing would be favored. In the case for an epoxy resin the value of χ is likely to increase as polar hydroxyl groups are produced during cure. For an epoxy cured with a primary amine the polar nature of the amine group is lost as the protons on the amine groups are consumed. This too will influence the value χ as the reaction proceeds [7].

Equation 9 above shows that the value of χ is inversely proportional to temperature therefore the cure temperature of a thermoplastic thermoset blend will also have an influence on the phase separation behavior of the blend. Overall there are many factors that may influence the value of χ in a reactive thermoplastic-thermoset blend. The resultant value of χ will be influential in determining the nature of the phase separation process.

Equation 15 represents the case for a blend of monodisperse components. In real systems both thermoset and thermoplastic components will be polydisperse in nature. The following expression describes the case for polydisperse blends[5, 9,10]:

$$\Delta G = RT\left\{\sum \frac{1}{V_{ESy}}\phi_y \ln\phi_y + \sum \frac{1}{V_{PSx}}\phi_x \ln\phi_y + \left(\frac{\chi}{V_R}\right)\phi_P\phi_M\right\} \quad (16)$$

where V_{ESy} is the molar volume of the y-fraction of the thermoset phase, V_{PSx} is the molar volume of the x-fraction of the thermoplastic phase. The summations are over the entire range of distribution fractions for the thermoset and thermoplastic phases, ie

$\phi_E = \sum \phi_y$ and $\phi_p = \sum \phi_x$

In order to solve equation 16 the molar mass distribution as a function of conversion is required for the thermoset phase. In the case of reactive thermoplastics the molar mass distribution as the cure progresses is also required.

The Flory-Huggins expression as outlined in equation 15 is a useful tool to give a general indication of how the free energy of mixing changes as various parameters of the system change. However actual polymer blends can be complex in nature and factors such as polydispersity, polymer chain mobility, Tg, and complex χ relationships make accurate modelling of the free energy difficult. The Flory-Huggins free energy expression does not, for example, account for the effect of

pressure or changes in the overall volume of the system, which may lead to inaccuracies. However the Flory-Huggins is a useful first approximation of the state of free energy of mixing which may be used to estimate equilibrium phase diagrams for polymer blends.

2.2.4 Polymer Blend Phase Diagrams

In section 2.2.3 above the Flory-Huggins expression for $\Delta G°$ was defined for a thermoplastic-thermoset blend. Plotting $\Delta G°$ as a function of composition for a polymer blend can map out the limits of solubility for the system and hence phase diagrams can be predicted [11, 12, 13].

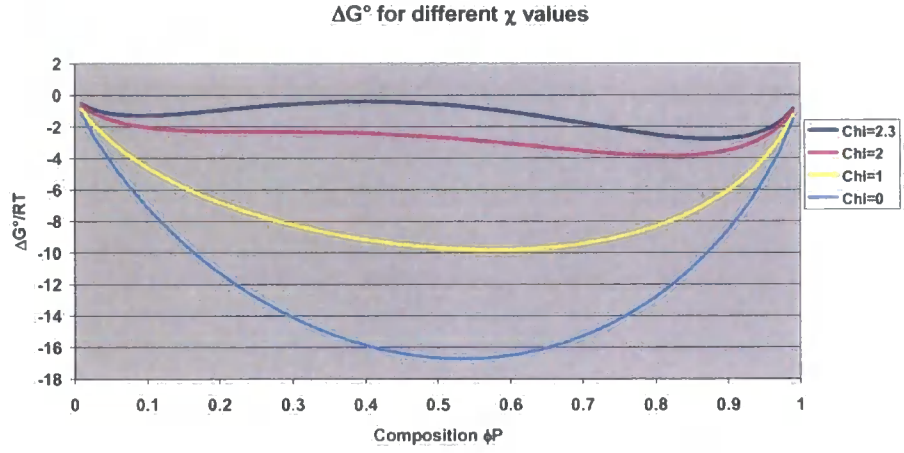

Graph 2.2.4.1 *This graph shows how the value of the Flory-Huggins interaction parameter alters the profile of the $\Delta G°$ versus composition curve. For values of $\chi \geq 2$ two minima occur and the system can lower its overall free energy by phase separating. At $\chi < 2$ the system is homogeneous and will not phase separate. This applies when $V_E = V_P$.*

Graph 2.2.3.1 above shows how the ΔG versus composition profile changes as the value of χ changes for a polymer blend. In the example above when χ =0 and 1 the curves are parabolic with a single minima. The curvature of these lines is positive at all points and the following expression holds:

$$\frac{\partial^2 \Delta G^o}{\partial \phi_P^2} > 0 \qquad (17)$$

Here across the entire ϕ_p range any localised fluctuations in composition will have a higher free energy state than the homogeneous mixture. Therefore phase separation is thermodynamically unfavourable and the system will remain a homogeneous solution. Figure 2.2.4.2 shows that for the case when the curvature of the ΔG° versus composition is positive, i.e. equation 17 is true; phase separation for any composition would lead to an increase in ΔG° and is therefore thermodynamically unfavourable. Hence any localised fluctuations in composition are unstable and the system will remain homogeneous.

However as the value of χ increases there becomes a point where the curve of ΔG° versus composition develops two distinct minima. In the example in figure 2.2.4.2 this point occurs at a χ value of around 2. These minima define the thermodynamic limits of the phase separation and these minima in composition are usually referred to as α and β. These compositions α and β define the compositions between which phase separation is thermodynamically favourable. In this case the equilibrium phases that would form are α and β. The limits of phase separation are defined by $\partial \Delta G^o / \partial \phi_P = 0$.

This applies to a binary blend when degrees of polymerisation are equal. When this is not the case it is necessary to determine the point at which the chemical potentials of each component is equivalent. This may also be done empirically by graphically determining the common tangent of the ΔG° versus composition plot.

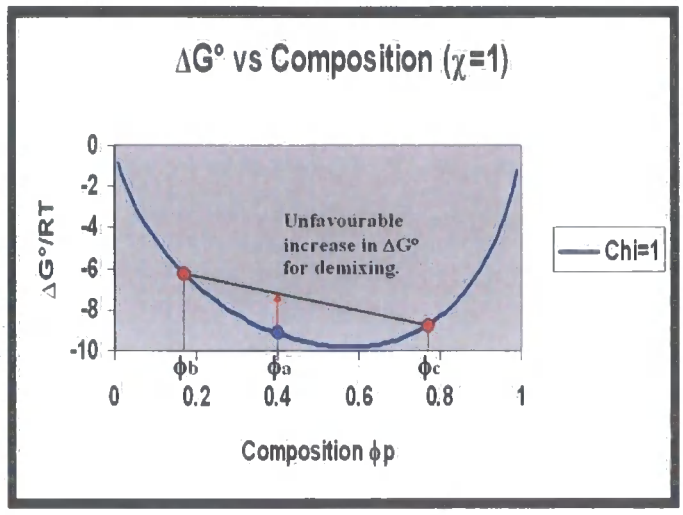

Figure 2.2.4.2 *This graph shows a ΔG° vs ϕ_P curve for the case when the curvature of the line is positive at all points in the curve ie $\partial^2 \Delta G^\circ / \partial \phi^2 > 0$. Here for a composition ϕ_a to phase separate into ϕ_b and ϕ_c would lead to an overall increase in ΔG° and therefore phase separation is thermodynamically unstable. Hence any localised perturbations in fluctuation are unstable and the system remains homogeneous. This applies across the entire composition range.*

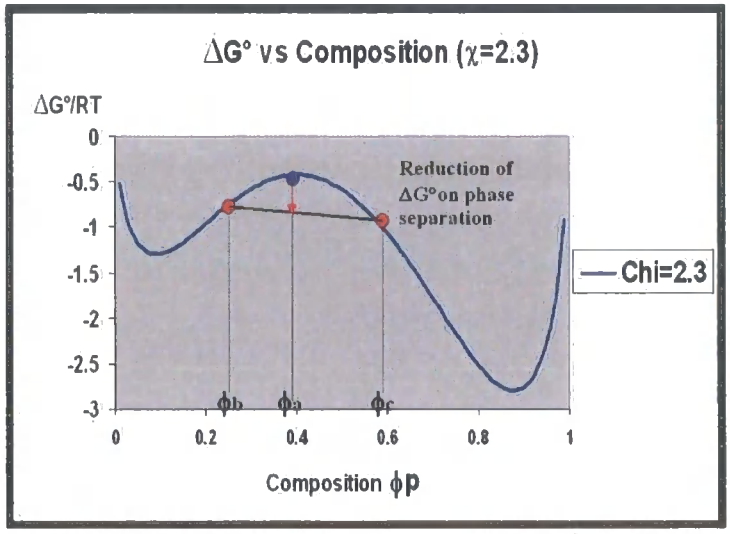

Figure 2.2.4.3 *This figure shows how the ΔG° of composition ϕ_a can be reduced when separation occurs into ϕ_b and ϕ_c. Therefore at composition ϕ_a the system is unstable with respect to small fluctuations in composition. This behaviour is spinodal decomposition.*

In the case where the ΔG° versus ϕ_P curve has two minima there is a composition range where phase separation is thermodynamically favourable. Figure 1.2.4.3

shows a reduction in ΔG° can occur if a composition ϕ_a phase separates into composition ϕ_b and ϕ_c.

The composition ϕ_a in figure 2.2.4.3 can lower its ΔG° by separation into compositions ϕ_b and ϕ_c. Here composition ϕ_a is classed as unstable because localised concentration fluctuation are stable and hence phase separation can occur. This case where fluctuations in concentration are thermodynamically favourable and begin to grow is called spinodal decomposition. This is defined where the curvature of the ΔG° versus ϕ_P curve is negative. Hence the region of instability where spinodal decomposition will occur can be defined by:

$$\frac{\partial^2 \Delta G^o}{\partial \phi_P^2} < 0 \qquad (18)$$

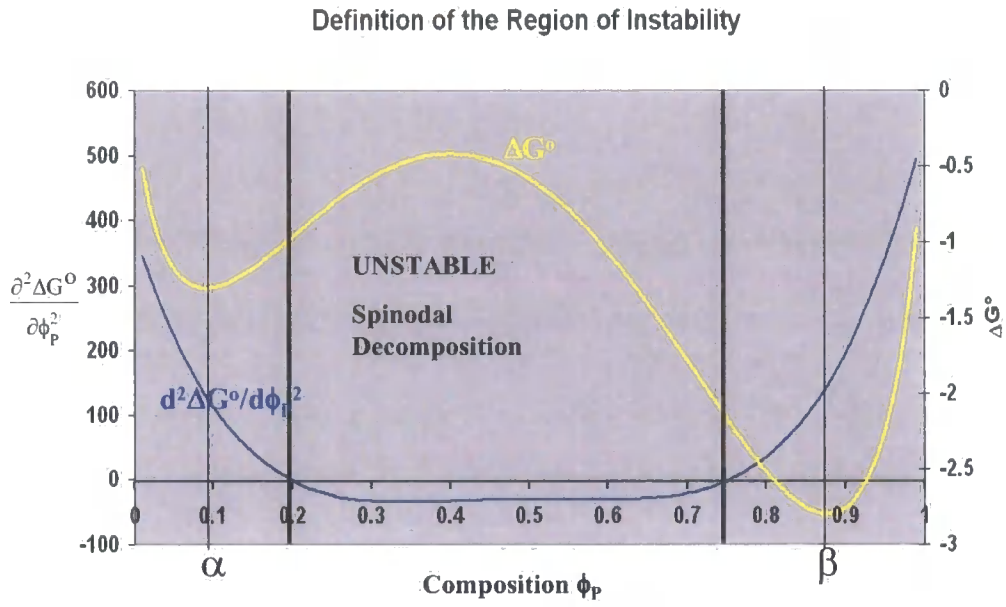

Figure 2.2.4.4 This figure shows how the region of instability can be defined for a thermoplastic-thermoset blend. Within this region phase separation will occur by spinodal decomposition.

Figure 2.2.4.4. shows both the ΔG° versus composition and the corresponding second differential as a function of composition. The positions where $\partial^2 \Delta G^o / \partial \phi_P^2 = 0$ define the limits of the unstable region.

There are regions in the ΔG° versus ϕ_P curve in figure 2.2.4.4 between the α and β

limits of phase separation where the curvature of the line is positive i.e. $\partial^2 \Delta G^\circ / \partial \phi_P^2 > 0$. Here the system can globally lower its overall ΔG° by phase separating into phase's α and β however localised perturbations in concentration around the initial starting composition are energetically unfavourable. In such circumstances the system is described as metastable and in order for the system to phase separate and activation energy needs to be overcome before the system can phase separate into phases α and β. Phase separation under such circumstances requires a nucleation process in order to overcome the activation energy. Hence such phase separation is termed nucleation and growth, which is in contrast to phase separation by spinodal decomposition where there is no initial energy barrier to the separation process. Figure 2.2.4.5 visually demonstrates the concept of metastability.

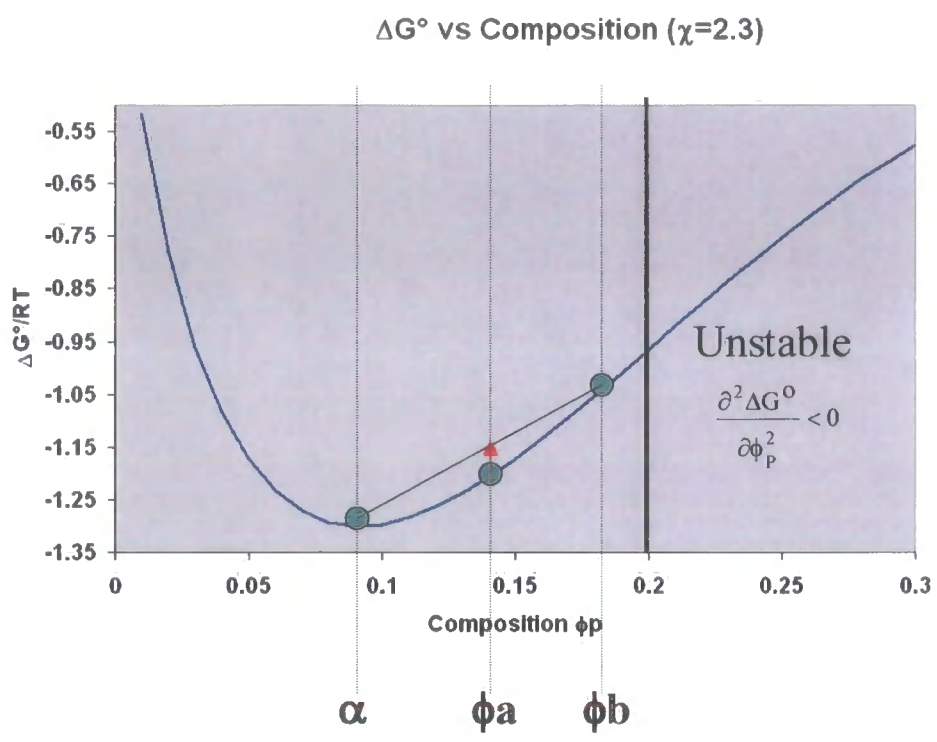

Figure 2.2.4.5 *This graph shows regions in the ΔG° vs ϕ_p curve between the limits of phase separation α and β where $\partial^2 \Delta G^o / \partial \phi_P^2 > 0$. Compositions in this region can globally reduce their ΔG° by phase separating into phases of α and β however an activation energy needs to be overcome. Such formulations are described as metastable.*

Having defined the limits of phase separation, the metastable and unstable regions form the free energy versus composition curve. Figure 2.2.4.6 below summarises how from knowing the ΔG° versus composition relationship at a particular temperature or level of conversion the regions of homogeneous mixing, metastability and instability can be identified.

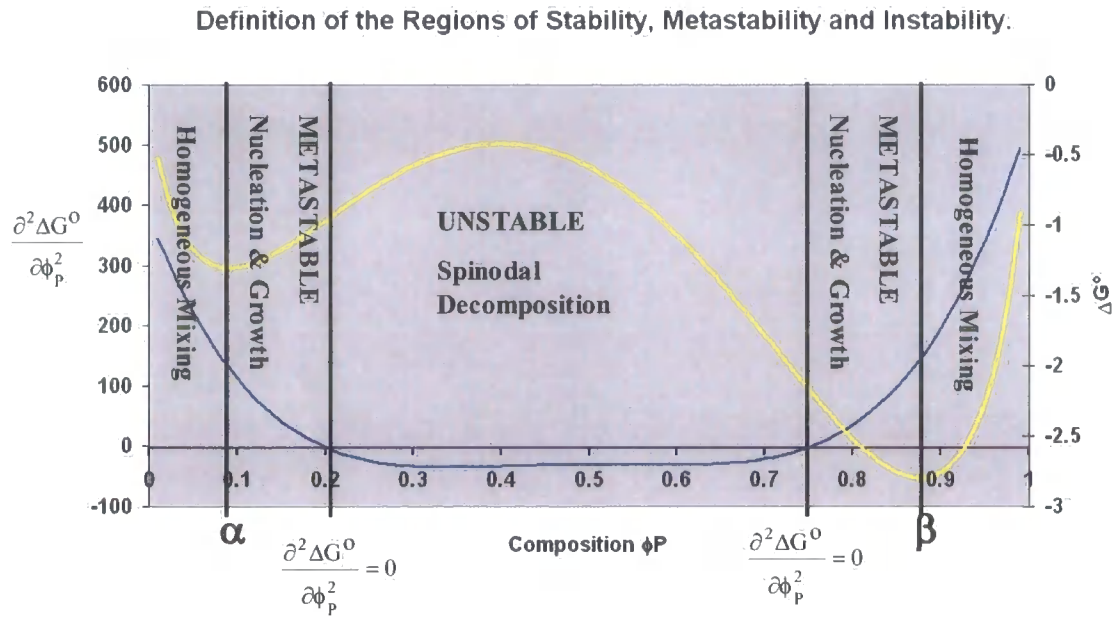

Figure 2.2.4.6 *This figure shows how knowing the ΔG° vs composition behaviour as defined by the Flory-Huggins equation the regions of mixing, metastability and unstable can be identified. The yellow line represents the free energy ΔG^{o} versus Composition relationship and the blue line represents the $\partial^2 \Delta G^{o} / \partial \phi_P^2$ relationship with composition.*

For a thermoplastic-thermoset blend knowing the form of the free energy curves as a function of temperature or thermoset conversion enables the mapping of the limit of solubility $\partial \Delta G^{0} / \partial \phi_P$, which defines the binodal, or cloud point curve can be achieved. Mapping of the spinodal region can also be accomplished where $\partial^2 \Delta G^{o} / \partial \phi_P^2 > 0$. Plotting the bimodal and spinodal curves as a function of composition defines the shape and nature of the phase diagram for the particular blend.

A critical composition may also be defined, this is a formulation that crosses the phase boundary directly into the unstable region, for a critical composition there is no region of metastability. At the critical composition for a symmetrical blend both $\partial^2 \Delta G^{o} / \partial \phi_P^2$ and $\partial \Delta G^{0} / \partial \phi_P = 0$. The expression $\partial^2 \Delta G^{o} / \partial \phi_P^2 = 0$ defines the limits of solubility α and β.

For a blend in which both components are monodisperse the critical point is located at the maximum of the spinodal curve when $\partial^3 \Delta G^o / \partial \phi^3 = 0$

$$\phi_{Mcrit} = \frac{1}{1 + [Z_M / Z_P(pcrit)]^{1/2}}$$

This defines the position of the critical composition in the phase diagram.

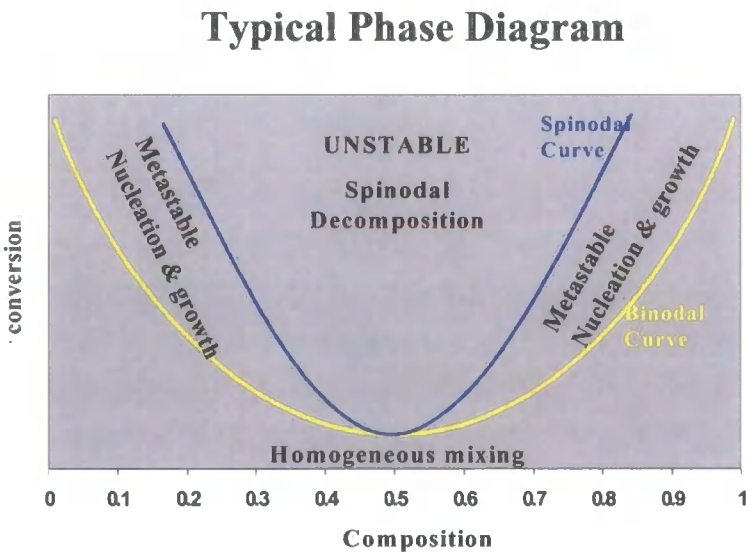

Figure 2.2.4.7 Phase diagram for a thermoplastic-thermoset blend.

Figure 2.2.4.7 shows an example of phase diagram for a thermoplastic-thermoset blend. This particular phase diagram shows phase separation occurring as the conversion increases.

In this section it has been shown how from the relationship between $\Delta G°$ and composition ϕ_P as defined by the Flory-Huggins equation (15) regions of mixing and phase separation may be identified. The $\Delta G°$ for a thermoplastic-thermoset blend varies as conversion increases due to both entropic and enthalpic considerations. Identifying how $\Delta G°$ varies with temperature and conversion allows phase diagrams to be predicted. This however only considers thermodynamics of mixing and in no way accounts for the kinetics of the phase separation process. The kinetics of phase separation in thermoplastic-thermoset blends will be considered later in this chapter.

In the case for reactive thermoplastic-thermoset blends, however, the phase diagram is dynamic and not static. As the reaction progresses due to changes in both entropy (changes in Z_E , Z_P and temperature) and enthalpy (changes in ε and temperature which affect χ) the shape of the phase diagram can alter significantly. This can cause the interesting phenomenon of secondary phase separations.

2.2.5 Secondary phase separations in thermoplastic-thermoset blends

As previously discussed in section 2.2.4 above for the case of reactive thermoplastic-thermoset blends as the cure process progresses significant changes occur in the $\Delta G°$ of the blend. This produces a dynamic phase diagram that in turn can lead to the phenomenon of secondary phase separations; this has been both predicted and observed by several workers [14, 15]. This is the effect where an initially homogeneous thermoplastic-thermoset blend going through a cure process crosses a phase boundary into the unstable region. This formulation can then minimise its free energy by separating into the two equilibrium compositions α and β as defined by the minima in the free energy composition relationship. However due to the dynamic nature of the phase diagram in a thermoset-thermoplastic blend the two equilibrium compositions α and β can now find themselves in a region of either metastability or instability and therefore can undergo a secondary phase separation. Such secondary phase separations in thermoplastic-thermoset blends have been both predicted from theory and also observed in practice [14,15].

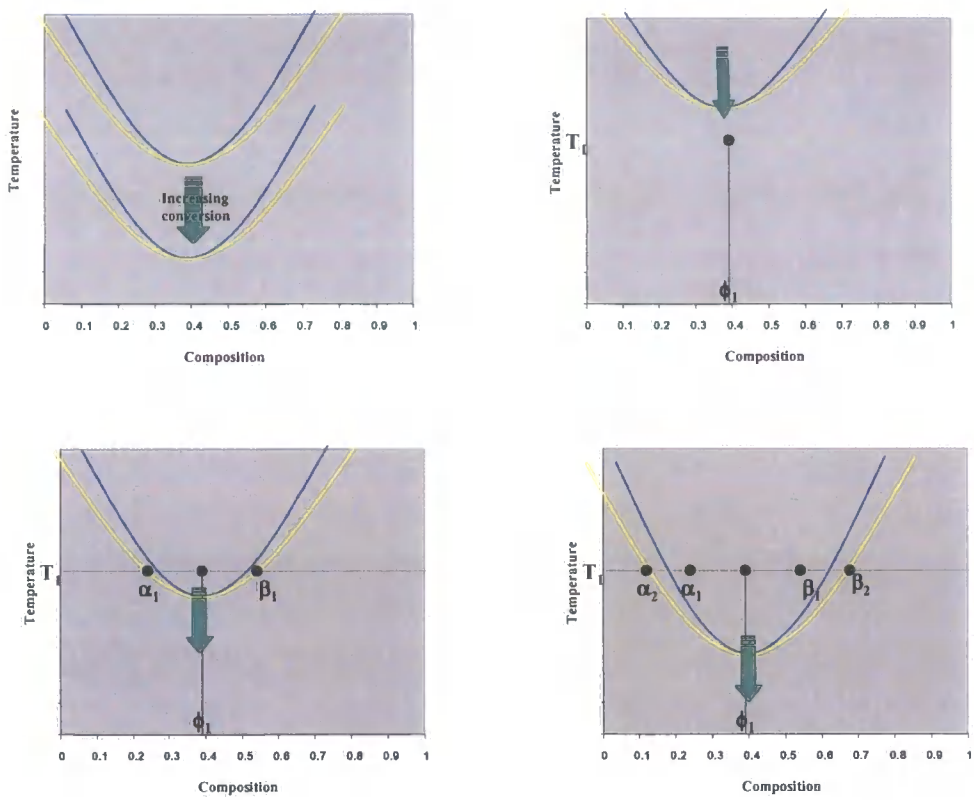

Figure 2.2.5.1 This figure shows how the phase diagram for a LCST thermoplastic-thermoset blend may change during the cure process, and how secondary phase separations can occur in these systems

Figure 2.2.5.1 above shows how the phase diagram can change as cure occurs for a thermoplastic-thermoset blend. The changes are as a result of increasing Z_E and changing χ but this change can lead to secondary phase separation.

The figure 2.2.5.1 show a thermoplastic-thermoset blend undergoing primary and secondary phase separation processes. In this instance both the primary and secondary phase separation processes occur in unstable region and therefore both separations occur by spinodal decomposition. It is also possible for other combinations of primary and secondary phase separation process to occur, for example primary phase separation can occur by spinodal decomposition whereas secondary could occur by nucleation and growth. The nature of both the primary and secondary phase separation process will influence the overall morphology of the

system. How the phase separation process will influence the morphology of the microstructure will be discussed later in this chapter.

2.3 Nucleation and Growth and Spinodal Decomposition.

It has been shown the previous sections that in a polymer blend phase separation can take place by one of two different mechanisms, namely nucleation and growth and spinodal decomposition. In this section we will discuss the characteristics of these processes.

2.3.1 Nucleation and Growth.

In order for phase separation to occur by nucleation and growth initially nuclei of critical size must develop [16, 17]. Sub-critical nuclei are unstable and will re-dissolve back into the solution. Hence for nucleation and growth to occur the activation energy must be overcome to form the initial critical sized nucleus. The process of nucleation is sporadic in nature and produces no characteristic length scale to the forming morphology. Once the nuclei of critical size have formed they can then grow with a rate that is determined by diffusion. When a nuclei of phase α forms it leaves a localised region around the nuclei that is depleted in A. This produces a concentration gradient around the nuclei, which can drive diffusion of A molecules towards the growing nuclei. Hence particles of α begin to develop and grow in size and the concentration of A reduces in the solution. This is represented in figure 2.3.1.1. Nucleation and growth will occur in the metastable region of the thermoplastic-thermoset blend phase diagram.

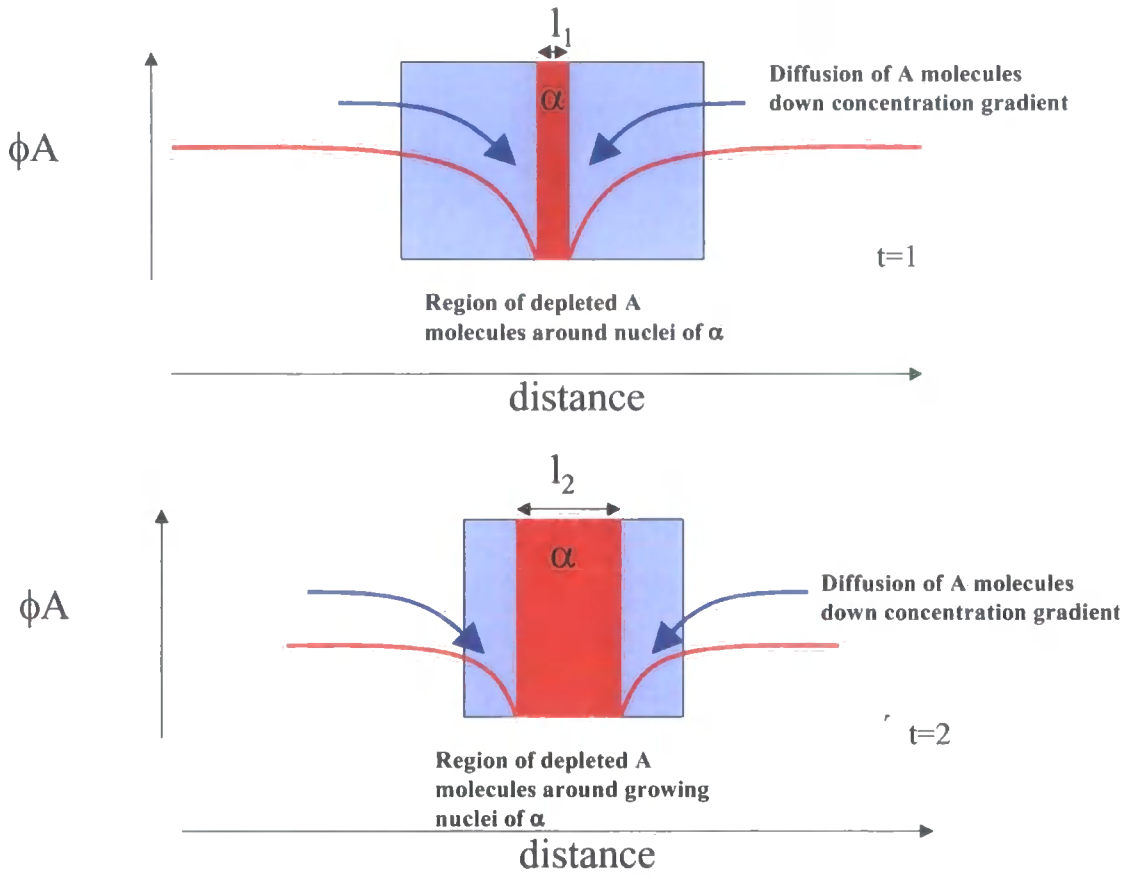

Figure 2.3.1.1 This diagram illustrates phase separation by nucleation and growth. The growth process is driven by diffusion along a concentration gradient which results from a depleted zone around the growing nucleus.

2.3.2 Spinodal Decomposition

In the unstable region of the phase diagram phase separation will occur by spinodal decomposition [16,17]. In this region any localised fluctuation in composition will lower the ΔG° of the blend, therefore concentration fluctuations are stable and are amplified resulting in phase separation. In spinodal decomposition material has to migrate against the local concentration gradient i.e. material migrates from low concentration to high concentration regions. This migration is referred to as uphill diffusion. This occurs because the material is migrating from a region of high chemical potential to an area of low chemical potential with the result of lowering the overall ΔG° of the system. The chemical potential is related to the first derivative of the ΔG° with respect to the composition hence if $\partial^2 \Delta G^\circ / \partial \phi^2 > 0$ then regions of

high concentration also have high chemical potential this means that in the metastable region diffusion will be in the normal direction i.e. down the concentration gradient. However in the spinodal region where $\partial^2 \Delta G^o / \partial \phi^2 < 0$ the chemical potential gradient has the opposite sign to that of the concentration gradient and therefore diffusion occurs against the concentration gradient i.e. uphill diffusion.

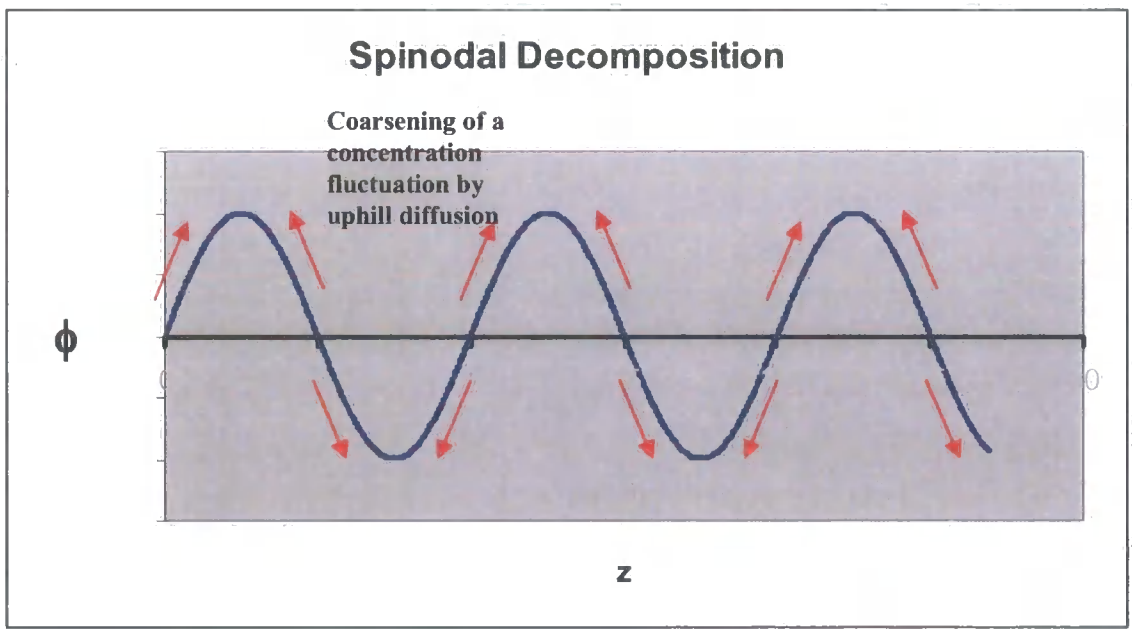

Figure 2.3.2.1 This figure shows how in spinodal decomposition a concentration fluctuation will grow and coarsen by uphill diffusion.

Any fluctuation in composition will have an associated length scale or wavelength as shown in figure 2.3.2.1. In an initially homogeneous mixture that separates by spinodal decomposition wavelengths over a critical size of fluctuation concentration will be thermodynamically stable and will grow. However a particular intermediate wavelength will dominate and its rate of growth will be rapid compared with other wavelengths. This is because large wavelength fluctuations require the diffusion of material over long distances and is therefore slower to grow. Short wavelength concentration fluctuations are suppressed because there is a high free energy associated with such sharp concentration gradients. This is why a certain intermediate wavelength range of concentration fluctuation dominated and grows and ultimately dictates the length scale of the final morphology of the blend.

The process of spinodal decomposition has three well-defined stages. Firstly early stage spinodal decomposition where a length scale composition fluctuation begins to develop and a broad diffuse interphase region forms. In scattering experiments this produces a peak in the S(q) versus q scattering profile [18]. The value of q where the peak occurs corresponds to dominant length scale of the developing morphology.
Secondly the intermediate stage here the compositions defining the limits of phase separation α and β are reached and the interphase width decreases and the morphology becomes well defined.
Finally in the late stages of spinodal decomposition the domain size begins to grow and develop and the interphase width is minimised. This process is expressed graphically in figure 2.3.2.2 below.

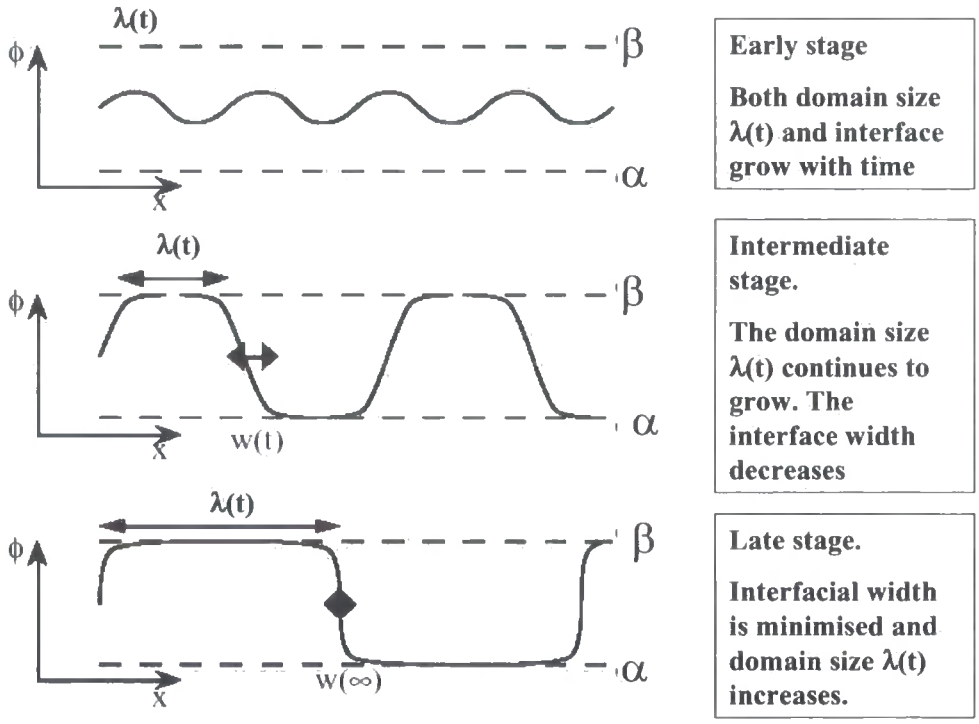

Figure 2.3.2.2 This figure defines the three stages of spinodal decomposition in a binary blend. Here the limits of phase separation are defined by α and β. (Figure courtesy of Prof. Richard Jones of Sheffield University[13])

2.3.3 The Kinetics Of Early Stage Spinodal Decomposition-Cahn-Hilliard Theory

In the previous section the thermodynamics of polymer blends was discussed and the concepts of nucleation and growth and spinodal decomposition were described. The thermodynamics of a thermoplastic-thermoset blend give an insight into the overall tendency of the system to phase separate. The kinetics on the other hand determines the rate at which phase separation proceeds.

The Cahn –Hilliard originally developed their theory [19] for phase separation in metallic alloys undergoing spinodal decomposition. This theory has been applied to describe spinodal decomposition in polymer blends.

Cahn Hilliard theory considers an initially homogeneous system-undergoing phase separating by spinodal decomposition where small concentration fluctuations are thermodynamically stable. The free energy of the separating system is defined by the following equation:

$$G = \int_V [g(\phi) + K(\nabla\phi)^2]dV \qquad (19)$$

Where $g(\phi)$ is the free energy density of the homogeneous system of composition ϕ. The term $K(\nabla\phi)^2$ represents the free energy change associated with concentration gradients in the material. K is associated with the interfacial surface energy between the two forming phases. In a thermoplastic-thermoset blend K will be dependent on the nature of intermolecular forces between the separating phases.

The diffusional flux J during the initial stages of spinodal decomposition of a simple binary composition of A and B, is given by the following equation [20]:

$$J = J_A = -J_B = M\nabla(\mu_A - \mu_B) \qquad (20)$$

where M is given by:

$$M = \frac{1}{2}[(1-\phi)(M_{BB} - M_{AB}) + \phi(M_{AA} - M_{BB})] \qquad (21)$$

M_{xy} are the mobility's and μ_x are chemical potentials of the individual molecules. In order to satisfy thermodynamic considerations mobility, M, must be positive if spontaneous uphill diffusion caused by a chemical potential gradient is to give an overall decrease in free energy. Cahn [21]showed that the difference in chemical potential, μ_A-μ_B, is derived from equation (19) above to give:

$$\mu_A - \mu_B = \frac{\delta G}{\delta \phi} = \frac{\partial g}{\partial \phi} - 2K\nabla^2\phi + \text{higher.order.terms} \qquad (22)$$

By substituting equation (22) ignoring the higher order terms into equation (20) and taking the divergence keeping only the first degree terms the following equation is obtained:

$$\frac{\partial \phi}{\partial t} = M\left(\frac{\partial^2 g}{\partial \phi^2}\right)_0 \nabla^2\phi - 2MK\nabla^4\phi \qquad (23)$$

in which M, K and $(\partial^2 g/\partial\phi^2)_0$ are assumed to be independent of the localised composition, the subscript 0 refers to the fact that the derivative has to be taken for the initial overall average composition ϕ_0. These assumptions are necessary so that equation (22) can be linerised and analytically solved. The diffusion equation above is linerised so it can only hold for small variations in composition fluctuation, i.e. in the early stages of the spinodal decomposition. In reactive thermoplastic-thermoset blend because reaction is proceeding as the phase separation occurs this is likely to be when the length scale of the final morphology of the blend is determined.

The term M $(\partial^2 g/\partial\phi^2)_0$ is associated with the uphill diffusion coefficient for the spinodal decomposition phase separation process and is referred to as the apparent diffusion coefficient D_{app}:

$$D_{app} = -M\left(\frac{\partial^2 g}{\partial \phi^2}\right)_0 \qquad (24)$$

The so called structure function S(q,t) is defined as the square of the Fourier transform of the spatial composition function $\phi(r,t)$,

$$S(q,t) = \left|\int \phi(r,t) e^{iqr} dr\right|^2 \qquad (25)$$

Where $q=2\pi/\Lambda$ is the wave number of a Fourier component and Λ is the wavelength of the concentration fluctuation. Taking the Fourier transform of equation (23) and substituting in (25) the following expression can then be derived:

$$\frac{\partial S(q,t)}{\partial t} = -2M\left[\left(\frac{\partial^2 g}{\partial \phi^2}\right) + 2Kq^2\right] q^2 S(q,t) \qquad (26)$$

Equation (26) is an ordinary differential equation that has the following solution:

$$S(q,t) = S(q,0) e^{2R(q)t} \qquad (27)$$

Here R(q) is the growth rate factor or amplification factor given by the following equation:

$$R(q) = -Mq^2\left[\left(\frac{\partial^2 g}{\partial \phi^2}\right)_0 + 2Kq^2\right] \qquad (28)$$

R(q) is the growth rate for given concentration fluctuation with a wave number q. Whether or not a particular concentration fluctuation grows or decays depends on the value of R(q), if it is positive the fluctuation will be stable and grow, if R(q) is negative the fluctuations will decay. R(q) for a range of wave number q can be calculated from scattering data. Whether R(q) is positive or negative depends on the free energy and composition relationship $(\partial^2 g/\partial \phi^2)_0$. For compositions in the metastable region,

$(\partial^2 g/\partial\phi^2)_0$ is always less than zero causing R(q) to be also negative. Therefore any perturbations in concentration will be unstable and decay.

In the unstable spinodal decomposition region of the phase diagram the expression $(\partial^2 g/\partial\phi^2)_0$ is positive and all concentration fluctuations with $q>q_{crit}$ will decay whereas fluctuations with $q<q_{crit}$ will grow, where,

$$q_{crit} = \left[-\frac{1}{2K}\left(\frac{\partial^2 g}{\partial\phi^2}\right)_0 \right]^{\frac{1}{2}} \qquad (29)$$

In practical terms q_{crit} may be obtained from a plot of R(q) vs q and is the intercept on the x axis.

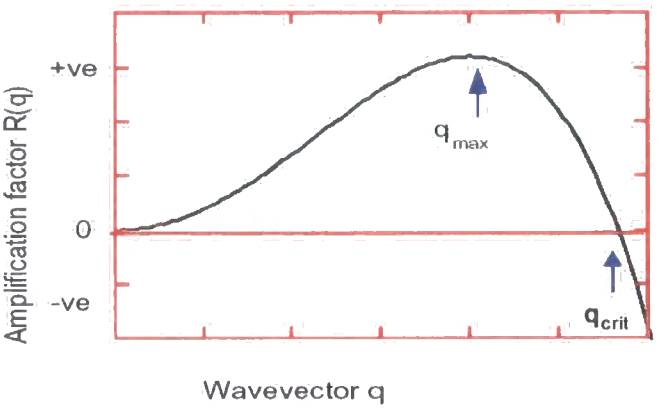

Figure 2.3.3.1 Graph showing R(q) versus q for a polymer blend phase in the early stages of spinodal decomposition. q_{max} defines the dominant length scale of the forming morphology. q_{crit} defines the minimum length scale allowed to develop as phase separation progresses.

Equation (28) also has a maximum, q_{max} given by the following expression:

$$q_{max} = \frac{1}{2}\sqrt{\frac{1}{K}\left[-\left(\frac{\partial^2 g}{\partial\phi^2}\right)_0 \right]} \Rightarrow \frac{q_{crit}}{\sqrt{2}} \qquad (29)$$

Substituting back into equation (28) yields:

$$R(q)_{max} = \frac{M}{8K}\left(\frac{\partial^2 g}{\partial \phi^2}\right)_0^2 = 2KM(q_{max})^4 \qquad (30)$$

With a corresponding wavelength (or spinodal distance) of

$$\Lambda_{max} = \frac{2\pi}{q_{max}} = 4\pi\left[-\frac{1}{K}\left(\frac{\partial^2 g}{\partial \phi^2}\right)_0\right]^{-\frac{1}{2}} \qquad (31)$$

From equations (29) and (30) it can be observed that the rate of formation $R(q)_{max}$ is defined by both the mobility, M and the thermodynamic term $\left(\frac{\partial^2 g}{\partial \phi^2}\right)_0$ whereas q_{max} is controlled only by the thermodynamic term $\left(\frac{\partial^2 g}{\partial \phi^2}\right)_0$.

Equation (28) indicates that a plot of $R(q)/q^2$ vs q^2 should yield a straight line with an intercept on the y axis of D_{app} and a gradient of 2MK.

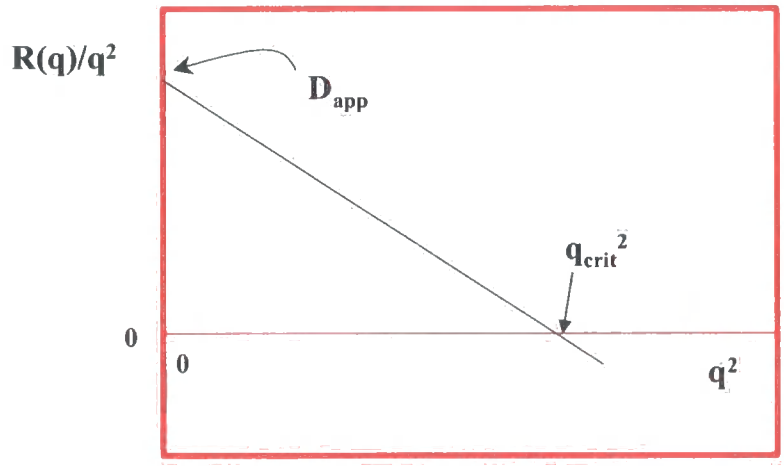

Figure 2.3.3.2 Cahn plot showing apparent diffusion coefficient D_{app} and the critical wave vector q_{crit}.

According to Hill [22] an alternative method of calculating D_{app} is to evaluate both $R(q)_{max}$ and q_{max} and to use:

$$D_{app} = \frac{2R(q)_{max}}{q_{max}^2} \qquad (32)$$

2.3.4 The Kinetics of Late Stage Spinodal Decomposition

In the later stages of spinodal decomposition the growth of the domains is driven by the reduction in interfacial energy of the system [23]. Reducing the area of interfacial contact between the two separating phases will reduce interfacial energy. This reduction in interfacial energy of the system is the driving force for coarsening of morphology. The rate at which the morphology coarsens during the later stages of the phase separation process is therefore dictated by the diffusion of material through the bulk. The Lifshitz-Slyozov law [24] gives the rate of coarsening of the morphology.

$$L(t) \sim (D\gamma t)^{1/3} \qquad (33)$$

Here L(t) is the size of the growing domain, D is the diffusion coefficient for the transport of material and γ is the interfacial energy. Equation (33) shows that the rate of growth of the domains in the later stages is proportional to $t^{1/3}$.

The reduction in interfacial energy of the system is also the driving force for the phenomenon of percolation to cluster transformations observed in polymer blends by Tekano et al [25, 26]. In the early stages of spinodal decomposition the two phase morphology initially comprises of two continuous phases of α and β. Reducing the interfacial energy can lower the overall energy of the system. This can be achieved by one of the continuous phases forming droplets or particles. This process requires material to migrate by uphill diffusion. The final morphology of the system will be two-phase particulate in nature.

Another important factor in thermoplastic-thermoset blends is that the degree of conversion of the thermoset will be increasing as the phase separation progresses. This leads to an increase in the Tg of the separating phases and in some cases the Tg

of one or both of the separation phases can reach the cure temperature. When this occurs the phases become vitrified and rates of diffusion and mobility will fall dramatically effectively fixing the morphology. The vitrification of one of the separating phases may prevent the formation of predicted equilibrium morphological structures.

2.3.5 The Kinetics Of Nucleation And Growth

It has been shown that for a system to phase separate by nucleation and growth there is an activation energy barrier that needs to be overcome for the process to occur and hence the system is described as metastable [12,13,16]. This usually occurs on cooling a system from a molten to a solid state and for metals and crystalline thermoplastics the process is well understood. In thermoplastic-thermoset blends it is less clear how nucleation and growth can occur. It may be possible that molecules of a reacting phase could come together to form a nucleus as a result of the chemical reaction process. In this case a nucleus is likely to be a polymer particle in its glassy state (i.e. below its Tg). Once a nucleus has formed it can then grow by conventional downhill diffusion process as described earlier in this Chapter. It has also been proposed by Binder [27] that nucleation in polymer blends is a heterogeneous process where the starting nuclei are the highest molecular weight species in the molecular weight distribution of the system.

The nucleation and growth process in the case for amorphous thermoplastic-thermoset blends is therefore very different to conventional nucleation and growth processes where crystalline materials are cooling from a molten or liquid state.

Conventional nucleation and growth theory concerns the reduction in free energy if a spherical particle solidifies from the melt [16].

$$\Delta G = -\frac{4}{3}\pi r^3 \frac{\Delta H_m}{T_m}\Delta T + 4\pi r^2 \gamma_{sl} \qquad (34)$$

Here ΔH_m is the enthalpy of mixing, T_m is the melting point of the solid and γ_{sl} is the interfacial energy between the solid and the liquid.

This introduces a critical sized radius of nucleating particle that has to be attained before the particle is thermodynamically stable and can proceed to grow. The critical radius for nuclei, r_{crit} is therefore given by:

$$r_{crit} = \frac{2\gamma_{sl}T_m}{\Delta H_m \Delta T} \qquad (34)$$

where ΔT is the degree of undercooling. The free energy barrier to nucleation and growth ΔG^* is therefore given by:

$$\Delta G^* = \frac{16\pi}{3}\gamma_{sl}\left(\frac{T_m}{\Delta H_m}\right)^2 \frac{1}{\Delta T^2} \qquad (35)$$

The number of critical sized nuclei is proportional to $\exp\left(-\frac{\Delta G^*}{kT}\right)$

In a thermoset thermoplastic blend its is not possible to define a T_m but this could be envisaged as the Tg of the system which in a reactive system will be function of conversion. ΔT could therefore be the difference between the advancing Tg of the curing thermoset phase and the reaction temperature. Therefore nucleation may be possible if a situation occurs where the Tg of curing thermoset phase becomes higher than that of the temperature of the system. In this case the nucleated particles will be in the vitrified state. These particles could then begin to grow by standard downhill diffusion. In the case of thermoplastic-thermoset blends in the metastable region although there is a thermodynamic driving force for the blend to separate into α and β phases, it is difficult to define a process occurring in the system that can overcome the activation energy required for nucleation and growth to occur. Due to the dynamic nature of the phase diagram in a reactive thermoplastic-thermoset blend it is probably more likely that a metastable blend finds itself in the unstable region prior to nucleation occurring. This has also been observed by Inoue and co workers [28,29]. This would suggest that in the case of reactive thermoplastic-thermoset blends spinodal decomposition is the most likely mechanism of phase separation.

2.4 Phase Separation And The Effect On Microstructural Morphology.

The nature of the phase separation process will influence the final cured microstructural morphology of the polymer. This is important, as it will influence the global properties of the polymer blend system. This phenomenon will be discussed further in chapter 7 but here we will introduce how the different mechanisms of phase separation will influence the microstructural morphology of the blend.

2.4.1 Morphology Produced By Nucleation And Growth

Nucleation is a sporadic process that has no defined characteristic length scale associated with the morphology. The forming nuclei will be spherical in order to minimise the interfacial energy of the system. The growth process will occur by a downhill diffusion process. The nucleation and growth process will therefore produce a morphology that consists of randomly arranged spherical particles of a dispersed phase, α, in a continuous phase of β. This is shown in figure 2.4.1.1.

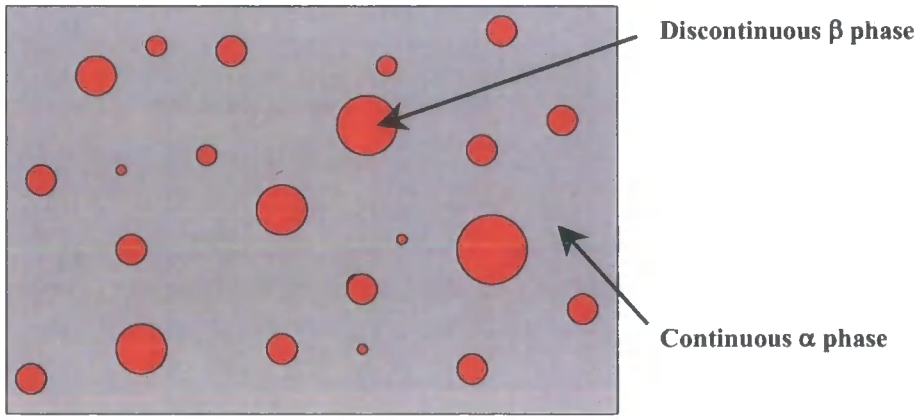

Figure 2.4.1.1 This figure shows a schematic diagram of a polymer blend that has undergone phase separation by a nucleation and growth process. This shows a morphology of randomly arranged particles of β in a continuous phase of α. There is no defined length scale to this type of structure.

2.4.2 Morphology Produced By Spinodal Decomposition

When a polymer blend phase separates by spinodal decomposition there is a characteristic length scale associated with the morphology. As described in section 2.3 above this is as a result of concentration fluctuations becoming thermodynamically stable and growing. This causes demixing of the polymer blend to produce what is termed a co-continuous morphology where both α and β phases are continuous percolating networks throughout the bulk of the material. Because this structure has a defined length scale its formation can be studied using scattering techniques. Scattering patterns with a well-defined peak therefore indicate a phase separation process by spinodal decomposition. This will be discussed further in chapters 5 and 6. Figure 2.4.2.1 below shows a typical morphology produced in a polymer blend undergoing phase separation by spinodal decomposition.

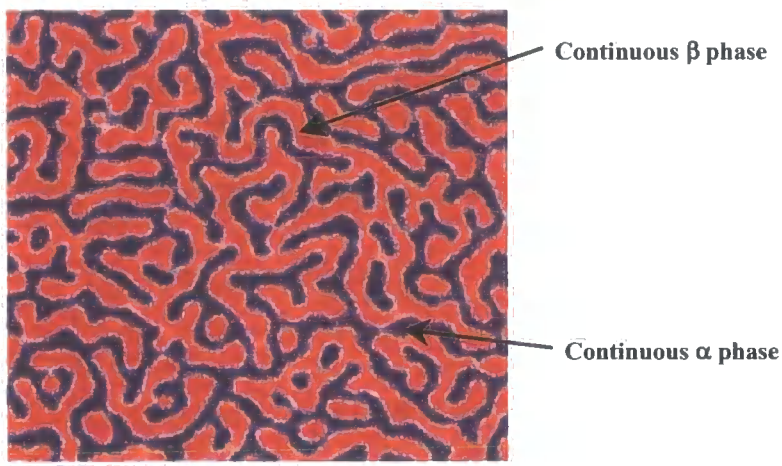

Figure 2.4.2.1 Schematic diagram of the morphology of a polymer blend that has undergone phase separation by spinodal decomposition. Both α and β phases are continuous percolating networks. The morphology posses a characteristic length scale, which can be identified through scattering experiments. (Picture courtesy of Prof R. Jones of Sheffield University)

2.4.3 Morphology Produced By Percolation To Cluster Transformations

Percolation to cluster transformations can occur when a polymer blend phase separates by spinodal decomposition. This produces a co-continuous morphology as described above. However the interfacial energy of the system may be reduced if one of the phases forms particulate spherical particles. This process was described in section 2.3.1 above. In such circumstances the morphology that forms will be particulate in nature but the morphology will still maintain its characteristic length scale produced by the spinodal decomposition process. Figure 2.4.3.1 below schematically shows the nature of the morphology that can occur when a polymer blend undergoes percolation to cluster transformations

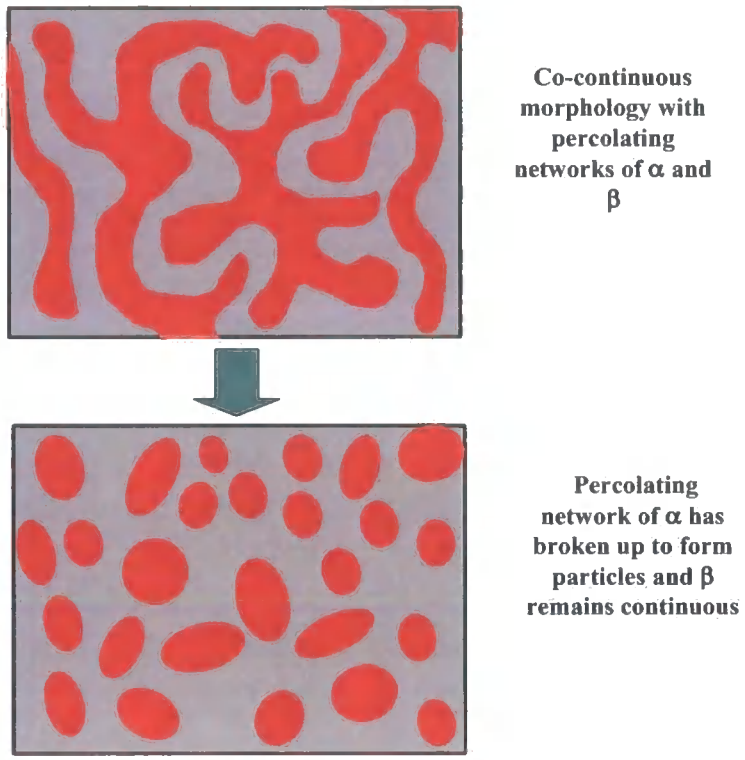

Figure 2.4.3.1 Schematic morphology formed when a percolation to cluster transformation occurs. The final morphology maintains the original spinodal length scale.

2.4.4 The effect of Secondary Phase Separations on the microstructure of the blend.

It was described in section 2.2.5 above how secondary phase separation can occur in reactive thermoplastic-thermoset blends. If the equilibrium formulations from a primary phase separation α and β cross a phase boundary they can themselves phase separate into formulation α_1 and β_1. This will have the effect of secondary structures occurring inside the boundaries of the primary phase separation. There are a number of different microstructures that may occur under such circumstances. Figure 2.4.4.1 below shows an example of microstructure that may occur as a result of secondary phase separations.

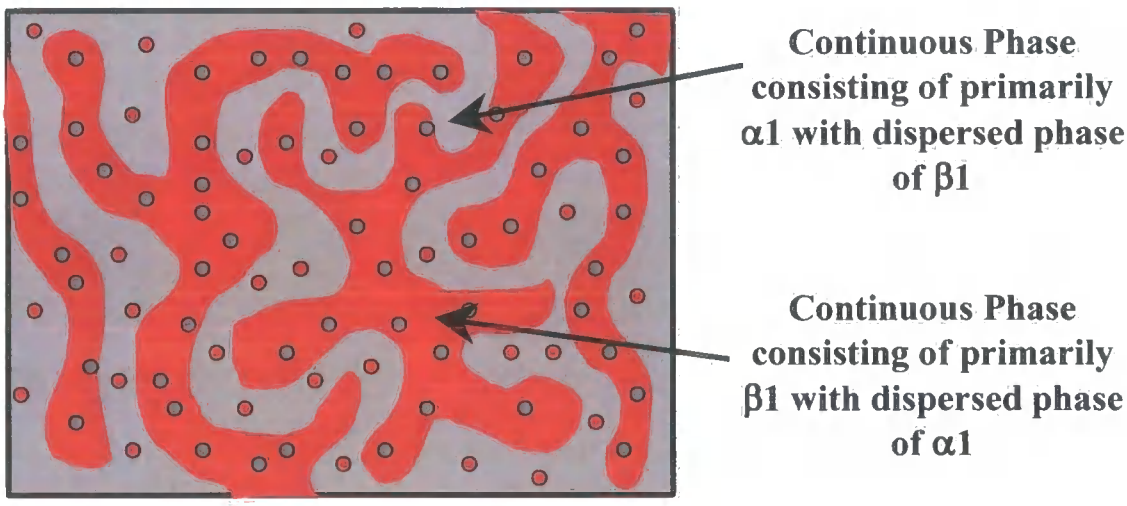

Figure 2.4.4.1 This shows a schematic example of a polymer blend morphology resulting due to both primary and secondary phase separations. Here the primary phase separation has occurred by spinodal decomposition which has defined the large scale morphology. Then secondary phase separation has occurred by spinodal decomposition followed by PCT.

With the possibility of secondary phase separations occurring a wide range of different morphologies can occur and such structures have been observed in practice [14].

2.5 Summary

In this chapter theories of both the thermodynamic and kinetic aspects of polymer blends have been introduced and discussed with particular reference to reactive thermoplastic-thermoset blends. From thermodynamic considerations it has been shown how the cure reaction in a thermoplastic-thermoset blend leads to changes in the $\Delta G°$ versus composition relationship that drives the phase separation process. Studying the $\Delta G°$ versus composition relationship in detail identifies regions of homogeneity, metastability and also instability of the blend. This defines the phase diagram for the particular polymer blend.

It has also been explained that from thermodynamic considerations the phase separation process can occur by either nucleation and growth, or spinodal decomposition. The kinetics of the spinodal decomposition process has been describe with the linerised Cahn Hilliard theory and it has been shown how this can be applied to early stage spinodal decomposition to estimate the uphill diffusion coefficient D_{app} and an amplification rate $R(q)_{max}$ for the dominant length scale for the developing morphology. In the later stages of spinodal decomposition other mechanisms contribute to the kinetics of the process and the linerised Cahn Hilliard theory is no longer applicable. In the later stages the kinetics of the process are approximated by the Lifshitz-Slyozov theory.

The concept of secondary phase separations has also been introduced and it has been shown how these can be predicted from phase diagrams of reactive thermoplastic-thermoset blends.

This chapter has also described phase separation by nucleation and growth and shown how it is difficult to envisage this process occurring in reactive thermoplastic-thermoset blends. Therefore it is predicted that phase separation in thermoplastic-thermoset blends under normal circumstances will occur by spinodal decomposition.

Finally it has been shown how the phase separation process can influence the cured microstructure of the thermoplastic-thermoset blend and this in turn will affect both the physical and chemical properties of the final cured structure.

In the following chapters the theories developed in this Chapter will be applied to a reactive polyethersulphone thermoplastic-epoxy thermoset blend.

2.6 References

1 Flory, P.J. *Principles of Polymer Chemistry*, Cornell University Press. Ithaca, NY.1953.

2 Flory, P.J. *J. Chem Phys.* 1941,9,660.

3 Huggins, M.L. *J. Chem Phys.* 1941,9, 440.

4 Olabisi O, Robertson LM, Shaw MT, *Polymer-Polymer Miscibility*, New York Acedemic Press 1979.

5 R.J.J. Williams et al. *Reaction Induced Phase Separation in Modified Thermosetting Polymers, Advances in Polymer Science No 128*, Springer ,1997

6 Tompa H, *Polymer Solutions*, Butterworth , London, 1956

7 Ellis B, *Chemisrty and Technology of epoxy resins, Chapman and Hall*, 1993

8 Hamerton I. *Chemistry and Technology of Cyanate Ester Resins*. Chapman and Hall, London 1994.

9 Stockmayer,W.H. *J. Chem Phys.*, 1949,17,588

10 Kamide,K. Thermodynamics of Polymer Solutions; Phase Equilibria and critical Phenomena: Elsevier: Amsterdam,1990

11 Cowie, J.M.G. *Polymers; Chemistry and Physics of Modern Materials*, 2nd edition, Chapman and Hall, NY,1991.

12 http://www.poco.phy.cam.ac.uk/teaching/A_Donald/

13 http://www.shef.ac.uk/uni/academic/NQ/phys/people/rjones/PHY369downloads.html

14 Clarke. N, McLiesh TCB, Jenkins S,D, *Macromolecules 28.* 4650, 1995

15 Delides CG, Hayward D, Pethrick RA, Vatalis, AS. *Journal of Applied Polymer Science.* 47:2037 1995

16 Kingery DS, *Introduction to Ceramics* (Book reference)

17 Honeycome, *Steels*, (Book reference)

18 Roe R-J, *Methods of X-ray and Neutron Scattering in Polymer Science*, OUP, NY. 2000

19 Cahn JW Hilliard JE ,*J. Chem Phys*, 1958,28,258

20 Cahn JW, *Trans Met Soc AIME* 1968,242,166

21 Cahn JW, *Acta Met*, 1971,19,151

22 Hill RG et al, *Polymer*, 1985,26,1708

23 Langer,J.S, Baron,M, Miller, H.D., *Physics Review A*, 11,1417,1975

24 Lifshitz, I.M, Slyozov,V.V. *J. Phys Chem.Solids*,19,35, 1961.

25 http://koken-db.kogaku.kyoto-u.ac.jp/1998/B/PC/98BPC32012.html.

26 http://koken-db.kogaku.kyoto-u.ac.jp/1997/B/PC/97BPC32003.html

27 Binder K, J. Chemical Physiscs, 79,6387,1983.

28 Inoue, T. Progressions in Polymer Science Series 20,119,1995

29 Yamanaka K, Takagi V, Inoue T. Polymer , 30,1839, 1989

Chapter 3

Epoxy Resin Reaction Chemistry And Network Formation

3.1 Introduction

This chapter briefly reviews the reaction chemistry of epoxy resin systems. It highlights the different reaction mechanisms possible in epoxy resins and discusses how this may influence phase separation behaviour and mechanical properties of epoxy blends. Also this chapter discusses the issue of network formation and introduces the gel point and vitrification phenomenon. There are several excellent reviews on both the reaction chemistry of epoxy resins and thermoset resin network formation that deal with these issues in great detail and several of these are referenced at the end of the chapter. This chapter is intended as a summary of these areas and how they may influence phase separation and mechanical properties in blended epoxy systems.

3.2 Epoxy Cure Chemistry

Epoxy resins can be cured by addition reactions or homopolymerisations.

The cure of epoxy resins can be envisaged as a three stage process. In the initial stage linear growth occurs with a gain in molecular weight[1,2]. In the second stage the chains begin to branch and eventually a gel point is reached when a sufficient

amount of these branches interconnect to form a continuous three-dimensional network which is insoluble. Supported in this insoluble gel network there will be a certain amount of extractable material that has not reacted with the network, this is termed the sol fraction. In the final stage of the cure reaction most of the remaining sol fraction is incorporated into the network.

As the cure progresses and the network forms, the Tg of the system also increases during the cure. While the cure temperature is above the glass transition of the system the rate of the chemical reaction is kinetically controlled. However as the cure progresses and the Tg of the network increases eventually the Tg approaches the cure temperature. Under these circumstances the reaction slows down dramatically, this is because the reaction rate becomes limited by the rate of diffusion of the un-reacted material. This phenomenon is referred to as vitrification. Once a curing epoxy system has reached vitrification, chemical reaction rates can become negligible which can result in the large amounts of un-reacted material being present resulting in a high extractable soluble fraction. This can have a deleterious effect on the cured properties of the epoxy system, so in order to complete cure and realise the full properties of the system a post cure above the Tg of the vitrified network is usually employed.

There are three main chemical mechanisms by which the cure of epoxy resins can proceed, these are:

1. Nucleophilic addition.
2. Cationic polymerisation.
3. Anionic polymerisation.

These processes are shown in figures 3.2.1.1, 3.2.1.2 and 3.2.1.3;

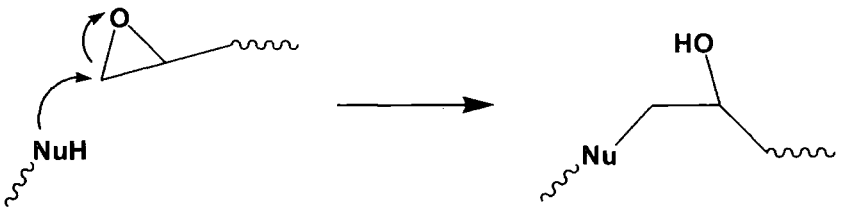

Figure 3.2.1.1 *This figure shows the reaction mechanism of an epoxy resin by nucleophilic addition of a hydrogen active nucleophile. This is typical of the reaction between an amine and an epoxy group.*

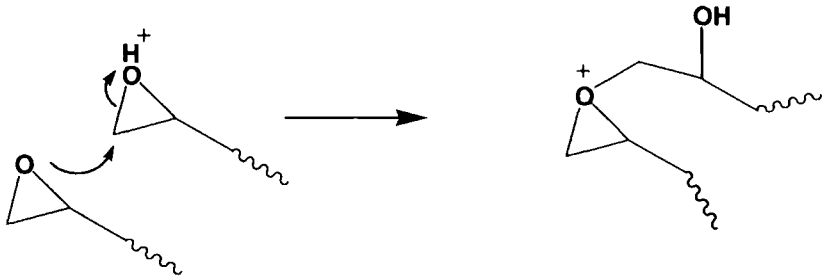

Figure 3.2.1.2 *This figure shows the reaction of an epoxy resin by cationic polymerisation.*

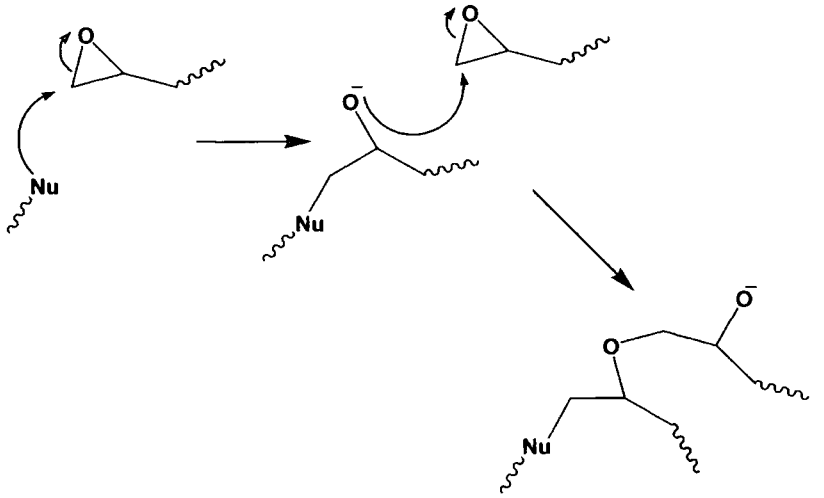

Figure 3.2.1.3 *This figure shows the anionic cure mechanism of an epoxy resin*

Epoxy resins can therefore be cured with a variety of functionalities containing active hydrogen's for example amines, phenols and carboxylic acids or through

etherification of the epoxy rings, which can be either cationic or anionic polymerisation.

In the previous chapter it was shown that the Flory-Huggins interaction parameter,χ , is related to the nature of the intermolecular forces of attraction between the molecular species. The change in χ , essentially alters the enthalpy of mixing of the blend and can cause the system to phase separate. It is interesting to note here that the different routes by which epoxy cure can take place result in different chemical structures. In the case of nucleophilic addition outlined in figure 3.2.1.1 above a polar hydroxyl group is formed, this will influence the interaction parameter χ as the reaction proceeds. In the case for anionic addition route less polar ether groups are formed so in this case the relationship between χ and the degree of cure will be different and this will also influence the nature of the phase diagram for the system. This indicates that the reaction mechanism for the epoxy resin will influence the phase behaviour in a blended system.

Cationic cured epoxy resins can be potentially radiation cured with light, electron beam or X-rays. For this to occur a radiation sensitive initiator is added to the formulation and when the system is exposed to radiation the initiator generates acid species that induce the cationic cure mechanism shown in 3.2.1.2 above. Such cationic reaction mechanisms effectively give the epoxy group a functionality of two hence they tend to produce networks that are highly crosslinked and therefore of low toughness. However the benefit of such systems is the rapid cure at low temperatures. Anionic cure of epoxy resins can occur when the resin is crosslinked using imadazole and these will be discussed later in this chapter. In this case the functionality of the epoxy ring is effectively 2 and the resulting network can be highly crosslinked and brittle in nature.

The epoxy ring can therefore be either mono- or di- functional depending on the reaction mechanism. In the case of nucleophilic addition at the ring, for example in the reaction between an epoxy and a primary amine, each epoxy group has a functionality of one. This is in contrast to cationic or anionic reaction mechanisms where etherification reactions occur in these circumstances the epoxy ring is di-functional. This has an influence on the mechanical properties of the cured system; generally speaking etherificated epoxy reactions produce brittle high modulus systems whereas nucleophilic addition reaction mechanisms produce tougher systems. The

chemistry of the resulting network is also dependent on the reaction mechanism occurring and in blended epoxy resins this can influence the interaction parameter,χ which will change the overall phase behaviour.

3.2.1 Amine Curing Agents

In this thesis all of the epoxy blend systems studied are cured by aromatic primary amines. In many practical applications of epoxy resins, aromatic amines are generally employed because they produce tough crosslinked epoxy networks with a high Tg and good thermal stability. The reaction rate of epoxy resins cured with aromatic primary amines is generally slow in comparison to imadazole or cationic cured epoxy resins. This is advantageous when curing large epoxy structures to avoid run away exothermic reaction occurring. This is why aromatic amines are commonly used as curing agents in epoxy matrix formulations for composite aerospace applications.

Active hydrogen compounds, such as primary aromatic amines undergo an addition reaction with the epoxy ring as shown in figure 3.2.1.1 when added in approximately stoichiometric ratio. However it has been observed that when there is an excess of epoxy groups present anionic etherification reaction is more likely to occur [3]. Primary amines react more rapidly than secondary amines and the ratio of secondary to primary amine reactivity generally increases as the reaction proceeds. A primary amine contains two active hydrogen's, it is therefore di-functional. Initially in the diamine cure, chain extension occurs more readily as the primary amines react with the epoxies to form secondary amine linkages. Reaction of these secondary amines then begins to dominate the cure, crosslinking the system. In the crosslinking reaction of a di-functional epoxy and a tetrafunctional diamine the gel point is reached at ~60% conversion and this is demonstrated using the Carothers equation detailed later in this chapter.

The reaction of a nucleophilic such as a primary amine and an epoxide ring is also accelerated by hydrogen bonding functionalities for example hydroxyl groups [4]. When a chemical functionality hydrogen bonds with the epoxy oxygen it decreases the electron density of the epoxy prior to ring opening and stabilises the alkoxide in the transition state[5]. The cure reaction therefore initially auto-accelerates due to the formation of the pendant hydroxyl groups from the opening of the epoxy. The degree

to which hydrogen bonding will accelerate the ring opening reaction increases with hydrogen bonding ability or the acidity of the proton. Hydrogen-bond acceptors, such as ethers and carbonyls, have been shown to slow down the amine/epoxy reaction [6]. Aromatic amines have a reduced electron density compared to aliphatic amines due to resonance with the adjacent aromatic ring [7]. This reduced electron density results in the nitrogen being a weaker, less reactive nucleophile. Networks cured with aromatic amines have improved solvent resistance and performance at elevated temperatures compared to the networks cured with aliphatic amines and imidazoles.

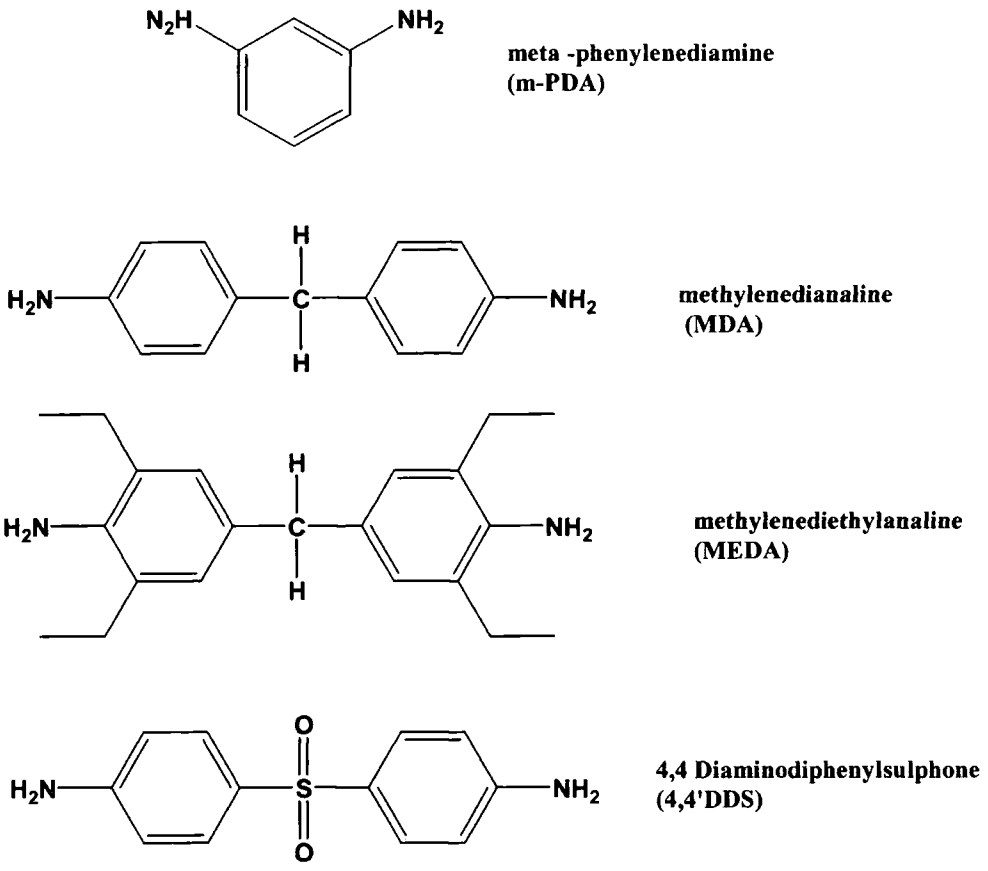

Figure 3.2.1.1 *Typical aromatic cure agents used in epoxy formulations*

Aromatic amines commonly used as epoxy cure agents are shown in figure 3.2.2.1 above. The different aromatic di-amines can significantly influence the chemical and physical properties of the resulting blend and can also impact the phase separation behaviour of the blend. For example the m-PDA shown in figure 3.2.2.1 produces epoxy resins, which have a high crosslinked density resulting in a high Tg brittle epoxy matrix. Epoxy resins prepared with 4,4' DDS have excellent thermal

performance, however the cure reaction is the slowest due to the electron withdrawing sulphone group [1,2]. Also in epoxy blends toughened with a PES thermoplastic the resulting epoxy network is highly compatible with the toughening thermoplastic. This produces only a minor change in the interaction parameter,χ, as the cure progresses and this produces a lower driving force for phase separation to occur. Phase separation of a polymer blend can have a significant impact on the toughness of a blend. It is generally advantageous to induce phase separation to produce a two-phase morphology as this usually produces a tougher cured blend.

3.2.2 Oxygen Containing Curing Agents

A variety of hydrogen active oxygen containing groups can be used as cure agents for epoxy resins these include carboxylic acids, anhydrides, alcohols and phenols which are all reactive with epoxy groups and are used industrially to prepare epoxy formulations [1,2]. This section will briefly review the reaction mechanisms of theses different cure agents

3.2.2.1 Carboxylic acid cure agents

Networks can form through two different mechanisms depending on the epoxy/carboxylic acid stoichiometry and the catalysts utilized. In both mechanisms the epoxide ring is di-functional and etherification reactions occur, producing highly crosslinked systems.

When a deficiency of carboxylic acid is used the acid hydroxyls initially react with epoxy rings. Crosslinking then proceeds through the subsequent etherification of the epoxy rings.

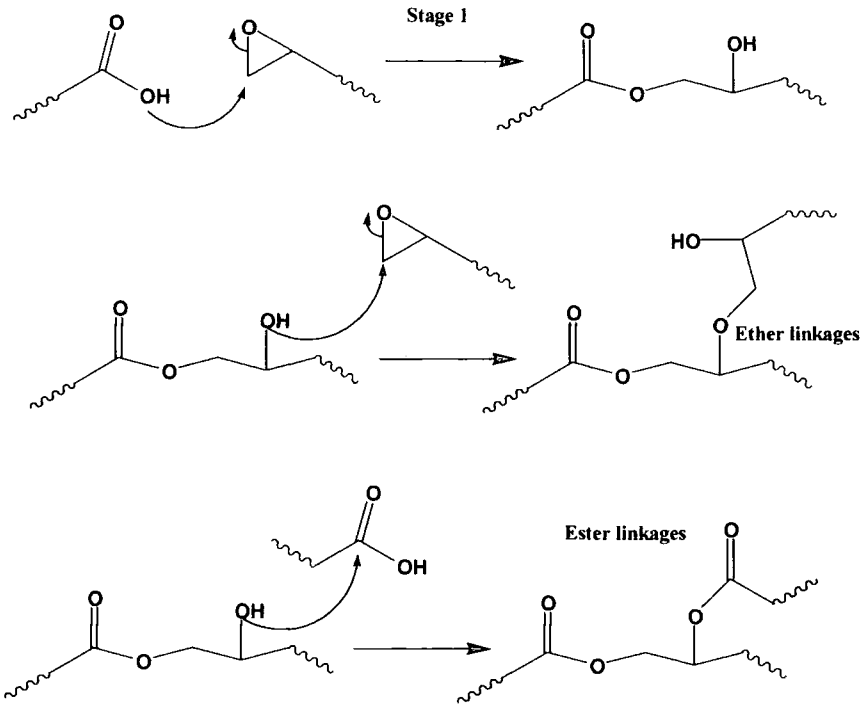

Figure 3.2.2.2 Reactions between carboxylic acids and epoxy resins

In the case of an excess of carboxylic acid, the first step is the same. Then the newly formed secondary hydroxyl condenses with another carboxylic acid functional group and water is produced as a by-product of the esterification. Often a base, such as a tertiary amine, is utilised to catalyse the epoxy-carboxy group reaction [1]. The base catalyses the reaction by deprotonating the carboxylic acid, thereby forming the carboxylate nucleophile. The amine accelerates the reaction and favours the carboxyl-epoxy reaction instead of the epoxy homopolymerisation reaction. Triphenylphosphine and ethyltriphosphonium iodide (ETPI) are commonly used and these too catalyse the carboxylic acid/epoxy reactions [8]. The phosphine ring opens the epoxy group. This produces a basic alkoxide anion, which then can abstract a proton from the carboxylic acid to yield the carboxylate anion.

3.2.2.1 Anhydride cured epoxy resins

Cycloaliphatic Anhydrides can be used to cross-link epoxy resins. The reactivity of anhydride cured systems is low, but this provides a good processing window. This is due to the necessity of a hydroxyl group to initially react with the anhydride and

because the carboxylate anion has reduced nucleophilicity compared to the amine curing agents [9]. The ring opening of the anhydride during cure leads to lower cure shrinkage than in other epoxy networks. Reduced water absorption is reported as another advantage of anhydride cured epoxy resins [9]. In the cure reaction, the anhydride reacts with a hydroxyl group to form an ester link and a carboxylic acid. The carboxylic acid formed in the first step reacts with an epoxy ring according to the carboxylic acid/epoxy mechanism shown in figure 3.2.3.2. When the epoxy ring opens, the hydroxyl can react with another anhydride or with another epoxy ring. Lewis acids or bases can be used to accelerate the cure reaction and this mechanism is shown in figure 3.2.3.3 below.

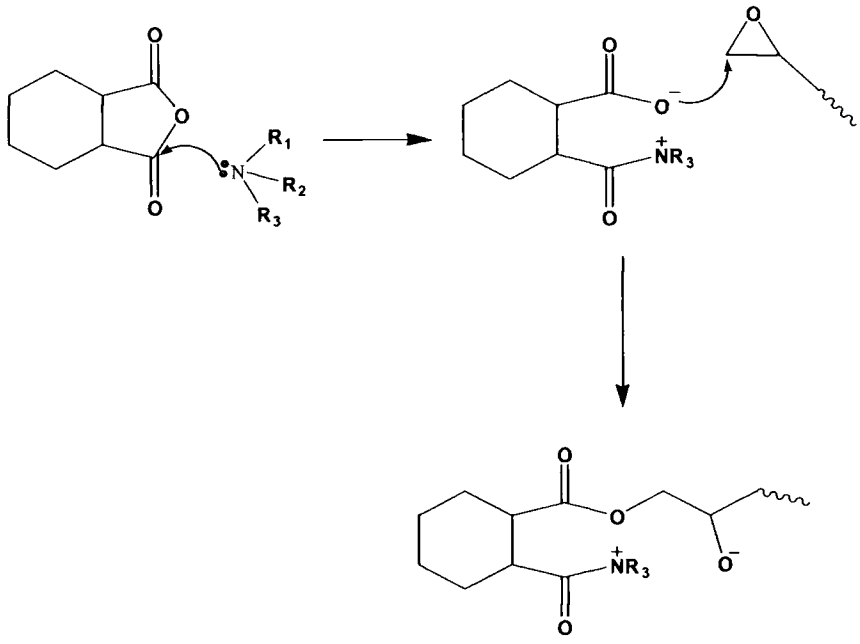

Figure 3.2.2.3 Reaction mechanism for a epoxy cure with an anhydride and catalysed by a tertiary amine base.

When acid catalysts are used, the epoxy ring is activated and the epoxy homopolymerisation is favoured. Due to the etherification reaction that occurs, optimum properties in an un-catalysed or acid catalysed system can be obtained with ~0.85 equivalents of anhydride [1]. Lewis bases used as accelerators for the anhydride/epoxy reaction activate the anhydride and produce a carboxylate anion that can open the epoxy ring as shown in figure 3.2.3.3. These materials, such as tertiary

amines and imidazoles, limit the amount of etherification and promote an alternating reaction between epoxy and anhydride, forming ester linkages [1,9].

Common anhydrides used to cure epoxy resins are phthalic anhydride hexahydrophthalic anhydride and methyl endomethylene tetra-hydrophthalicanhydride. These are shown in figure 3.2.3.4.

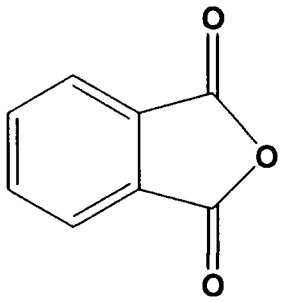

phtalic anhydride

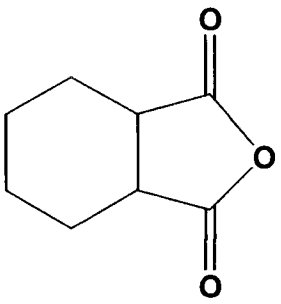

hexahydrophthalic anhydride

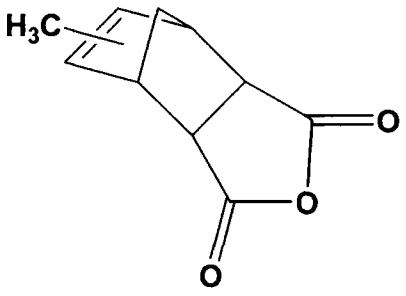

methyl endomethylene tetra-hydrophthalic anhydride

Figure 3.2.2.4 *Typical anhydrides used to cure epoxy resins*

3.2.2.1 Epoxy resins cured with hydroxyl functionality

Aliphatic hydroxyl groups react with epoxide resins at >200°C without the aid of catalysts. But the resins can also be cured at lower temperatures with an acid or base catalysts. Primary hydroxyl groups are more reactive than secondary hydroxyl groups. Tertiary alcohols are even less reactive due to steric hindrance and the reaction proceeds through homopolymerisation of the epoxies [1]. The more reactive diphenols and polyphenols are commonly used as crosslinking agents with Lewis base catalysts [1,8]. Di-phenols can be utilised with a 1/0.6 epoxy/phenol ratio to allow

crosslinking via the etherification reaction[1]. Initially, linear growth takes place as the phenol hydroxyls open the epoxy rings. Upon exhaustion of the phenol groups epoxy homopolymerisation occurs.

Figure 3.2.3.5 below shows a base catalysed hydroxyl/epoxide ring opening reaction.

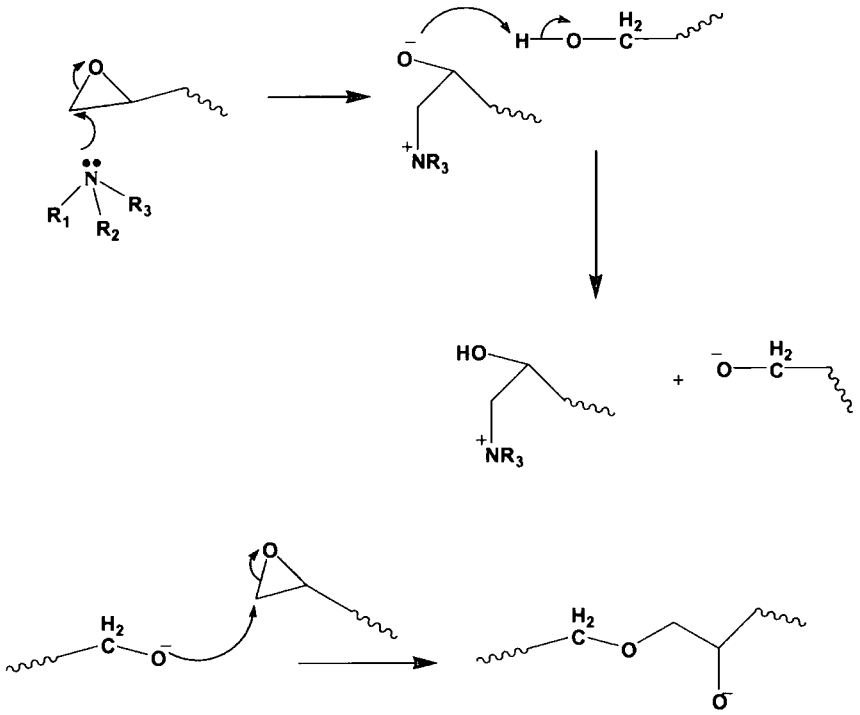

Figure 3.2.2.5 Reaction of epoxy and hydroxyl groups catalysed by a tertiary amine base

3.3 Epoxy Homopolymerisation

The homopolymerisation of epoxy resins is a chain reaction that can occur by either cationic or anionic initiators. As described above under these circumstances the functionality of the epoxy groups is 2 so each di-functional epoxy oligomer has a functionality of 4. Here homopolymerisation results in a highly crosslinked network formation. Cationic polymerisation of epoxy resins can be induced thermally by the addition of a Lewis acid or alternatively cationic homopolymerisation can be induced through radiation cure by the addition of a compound that generates super acids upon exposure to radiation. The radiation source could be light, electron beam or X ray.[2]

Anionic homopolymerisation can be induced in epoxy resins by the addition of a imadazole.

The most commonly used thermally induced cationic homopolymerisation catalysts are Lewis acids based on amine complexes of boron trifluoride [1]. Of these the monoethylamine complex has found the most use in epoxy curing because it is more light stable and less hygroscopic than other boron trifluoride compounds. The complex is strong because of the increased basicity of the amine resulting in the aforementioned advantages as well as a reduced rate of reaction with the epoxy group. These complexes serve as latent catalysts. The epoxy reaction is not catalysed until heated to ~95°C, at which temperature the boron complex dissociates to the catalytic species [10]. While boron trifluoride complexes are more often used as catalysts for aromatic amine and anhydride cured resins, the homopolymerized networks are used as adhesives and electrical varnishes [5].

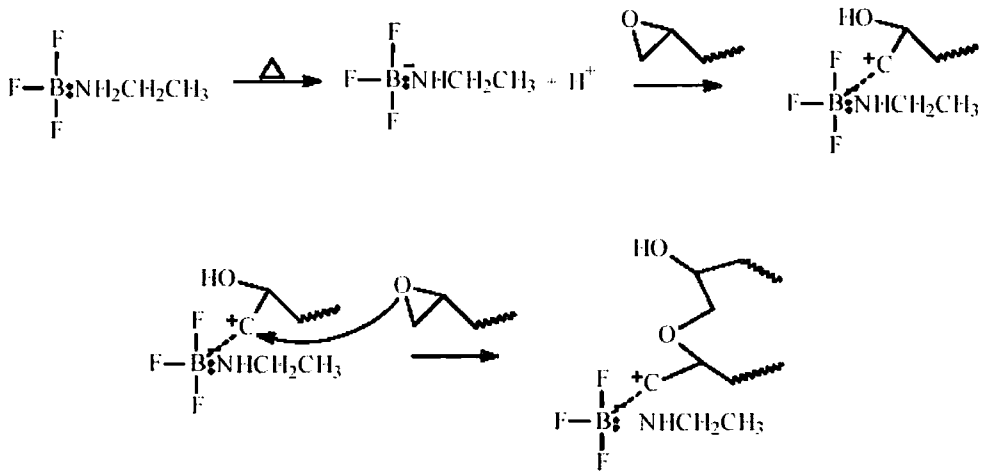

Figure 3.3.1.1 Cationic epoxy homopolymerisation using boron trifluoride monoethylamine1.

Photo curing can be achieved using UV sensitive salts, which generate cations that catalyse the epoxy etherification reaction [2]. The sensitivity of the initiator to photo and thermal energy is determined by the cation utilized, using a non-nucleophilic anion, boron tetrafluoride.

Diaryliodonium shown in figure 3.3.1.2 are more thermally stable and useful for cationic photo curing [2]. Diaryliodonium salts absorb strongly in the 220-250 nm UV region [11].

Upon irradiation, the salt degrades both homolytically and heterolytically to yield cationic and radical species.

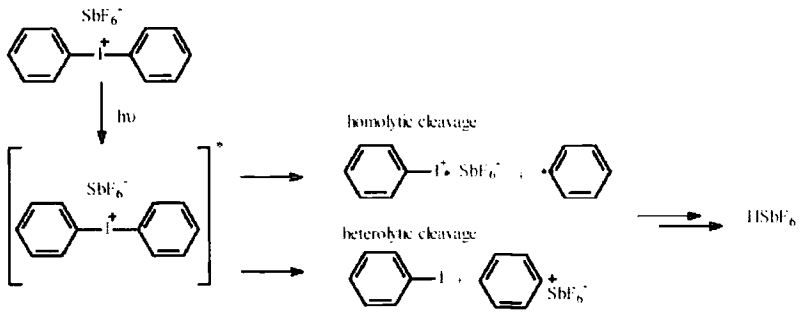

Figure 3.3.1.2 This figure shows the initiation mechanism for UV cationic cure of epoxy resins using Diaryliodonium cations

The highly reactive cations, both aryl and aryliodine radicals, react with the resin to yield protonic acids. Common counter ions include BF_4 , PF_6 , AsF_6 , and SbF_6, which generate acids. Protons from these superacids associate with the epoxy ring oxygen and initiate the cationic polymerisation. These produce very rapid cure epoxy systems that tend to be highly crosslinked. The selection of epoxy resin is also important for UV cured systems, cycloaliphatic epoxy resins are commonly used due to their low UV absorption characteristics. Another advantage is that unlike free radical photo curing, the cure is not sensitive to oxygen.

Imidazoles are commonly used to also initiate the anionic polymerisation of epoxy groups. These find application in many rapid thermal cured epoxy resins. Some typical examples are shown in figure 3.3.1.3 below

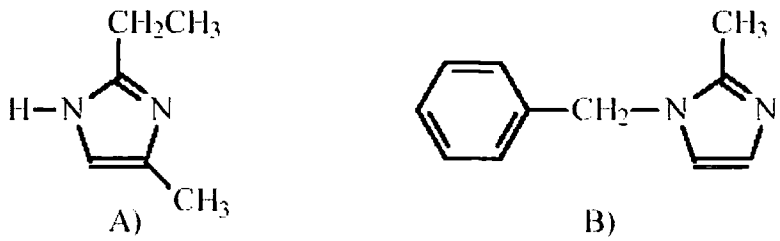

Figure 3.3.1.3 Commonly used imadazole cure agents for epoxy resins A) 2-ethyl-4-methylimidazole and B) 1-benzyl-2-methyl-imidazole.

In the first step of the reaction between an imadazole and an epoxy, the secondary amine nitrogen reacts with an epoxy via nucleophilic attack. The next step involves the reaction of the remaining nitrogen with a second epoxy ring that yields the alkoxide ion. Etherification proceeds with the terminal negative charge remaining near the positive nitrogen through bending of the chain

3.4 Thermoset Network Formation

3.4.1 Network Gelation

Epoxy resins undergo a stepwise polymerisation during cure. The characteristic of stepwise polymerisation is that high molecular weights are not achieved until a high degree of polymerisation has occurred [12.] This is in contrast to free radical chain growth polymerisation where high molecular weights can be achieved at low degrees of conversion. In stepwise polymerisation where the monomer functionality is greater than 2 crosslinking and gelation can occur. Gelation is defined as when a single molecule connected by covalent bonds percolates through the entire volume of the sample. A three dimensional molecular network is formed and this results in a rapid rise in viscosity of the system. This will also reduce the rate of any phase separation process occurring. After the gel point the cure continues resulting in the reduction of the sol fraction until at full conversion the weight fraction of the gel approaches 1. The gel point is therefore a critical point in the reaction of a thermosetting system. Carothers [13] suggested that the critical degree of conversion at which the gel point will occur in a reactive polymer system is given by :

$$p_{gel} = \frac{2}{f_{ave}} \qquad (1)$$

Where the f_{ave} is given by the following expression:

$$f_{ave} = \frac{\sum N_i f_i}{\sum N_i} \qquad (2)$$

Here N_i is the number of molecules with functionality of f_i. The summation is across all of different molecular species present in the system.

In a thermosetting epoxy system where the average functionality is given by f_{ave} as described in equation (2) above the number of reactive groups available for reaction can be given by $N_o f_{ave}$. Where N_o equals the average molecular weight of the unreacted monomers

$$\frac{N_o f_{ave}}{2} \qquad (3)$$

The Carothers equation (1) is only a general approximation and usually predicts higher p_{gel} values then observed in experiments [14]. This is because it does not take account of the formation of cyclic polymers and intramolecular reactions. The equation also does not consider steric hindrance effects that occur as the network develops. Several workers have carried out more detailed studies that yield more accurate predictions [15,16,17]of p_{gel} and a study of these works is outside the scope of this thesis.

The figure 3.4.1.1 below uses the Carothers equation to identify the gel point of three different epoxy formulations. In this example the epoxy is cured with a diamine having a functionality of 4. The formulations are mixed in a stoichiometric ratio and the ration of di-functional to tri-functional epoxy resin is varied. The gel point can be defined when the degree of polymerisation (DP) reaches infinity. It can be clearly seen that as more tri-functional epoxy resin is added to the formulation the extent of reaction required to reach the gel point is reduced.

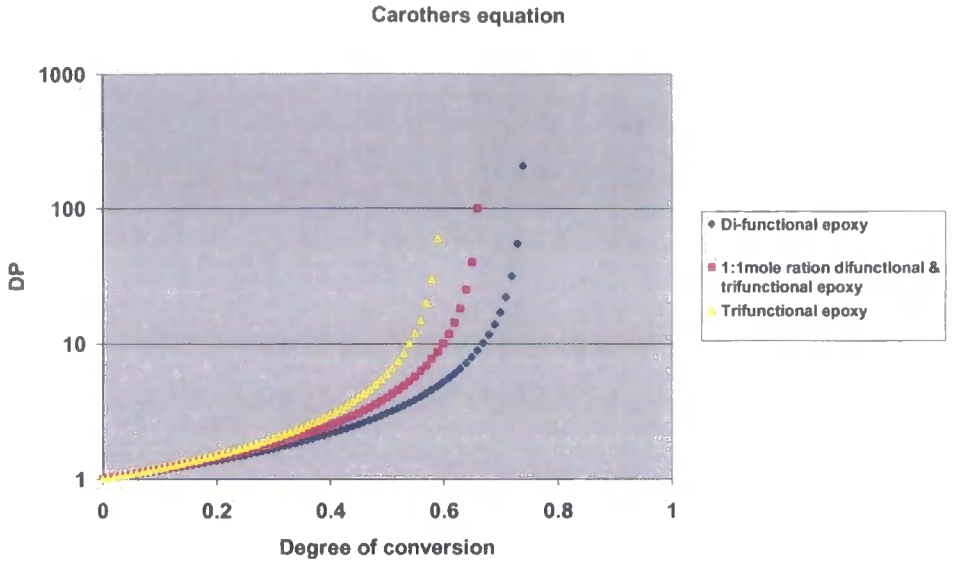

Figure 3.4.1.1 This figure shows a plot of DP versus degree of epoxy conversion for three different epoxy formulations containing different levels of tri-functional epoxy resin. This is for a stoichiometric ratio of epoxy to amine groups. The degree of conversion required for gelation to occur reduces as the tri-functional epoxy level is increased

3.4.2 Glass Transition Temperature And Vitrification

During the cure process as well as gelation occurring and preventing phase separation, vitrification can also occur. As the cure progresses the Tg of the forming network also increases. Vitrification will occur as the Tg of the emerging network approaches the temperature at which the cure is carried out. If the system vitrifies the network will change from being rubbery and mobile to becoming glass like and immobile.[14] This has the effect of severely reducing the cure reactions due to the immobile nature of the functional groups. Further chemical reaction of the network becomes diffusion controlled. Vitrification will also impede phase separation occurring. In the case of a thermoplastic-thermoset blend where a high Tg thermoplastic is used as the phase separation occurs it is possible that the thermoplastic rich phase very quickly vitrifies and prevents the thermodynamic equilibrium phase morphology from forming.

Vitrification may occur either before or after the gel point of the system. Both gellation and vitrification will impede cure reaction and phase separation.

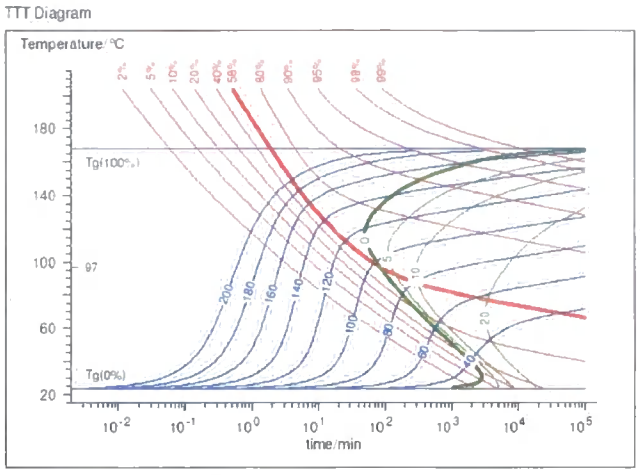

TTT diagram of an Epoxy Thermoset

red lines	temperature versus log(time) for given degree of reaction
thick red line	temperature vs. log(time) at degree of conversion in gel point (α = 58 %)
green lines	glass transition temperature Tg - temperature of curing
thick green line	glass transition temperature Tg - temperature of curing = 0
blue lines	glass transition temperature Tg vs. log(time) (curing temperature as parameter)

Figure 3.4.2.1 A TTT diagram for an epoxy cured with an aromatic diamine. This shows lines of gellation and vitrification for the network formation. (Courtesy of JK Gillam et al [18])

Figure 3.4.2.1 shows a typical TTT diagram for an epoxy cured with a aromatic diamine. This shows that the occurrence of the gel point and vitrification point is dependent on cure time and temperature. In this example cure temperatures below 97°C result in vitrification occurring prior to gellation.

3.5 Summary

In this section the chemical cure reactions of epoxy resins have been introduced. It has been shown that there are many different ways in which an epoxy resin can cure. The different cure reactions lead to epoxy networks with different chemical functionality and crosslinking density. These factors will influence the nature of the phase separation process by altering both the enthalpy of mixing (changing the interaction parameter,χ) and also influence the entropy of mixing. The chemistry of

the system will therefore have a significant influence on the phase separation behaviour.

Also in this chapter the important physical characteristics of the network formation have been discussed. The major stages of network formation in a stepwise cure process are gelation and vitrification. The occurrence of these processes during cure will also have a significant influence on the rates of chemical reaction and phase separation.

3.6 References

1 B Ellis, Chem & Tech of Epoxy Resins,. Chapman and Hall, 1993

2 Y. Tanaka and R. S. Bauer, Curing Reactions, Synthesis and Characteristics of Epoxides, Epoxy Resins:1986

Chemistry and Technology, C. A. May, Ed., 1988, Marcel Dekker, Inc. New York.

3U.M.Bokare and K. S. Gandhi, *J. Polym. Sci. Polym. Chem. Ed.*, 1980 18, 857-870.

4 C. A. May, Ed., Epoxy Resins: Chemistry and Technology, 1988, Marcel Dekker, Inc. New York.

5 W. R. Ashcroft, Curing agents for epoxy resins, Chemistry and Technology of Epoxy Resins, 1st edition,1998

B. Ellis, Ed., 1993, Chapman & Hall, New York, 37-71.

6 T. F. Mika and R. S. Bauer, Curing Agents and Modifiers, Synthesis and Characteristics of Epoxides,1998

Epoxy Resins: Chemistry and Technology, Ed. C. A. May, 1988, Marcel Dekker, Inc. New York.

7 H. Lee and K. Neville, Handbook of Epoxy Resins, 1967, McGraw-Hill, Inc., New York.

8 M.M Bobbitt Bump PhD Dissertation, Virginia Polytechnic Institute and State University 2001

9 T. D. Juska and P. M. Puckett, Matrix resins and fiber/matrix adhesion, Composites Engineering 1987

Handbook, P.K. Mallick, Ed., 1997, Marcel Dekker, Inc., New York, 101-165.

10 W. G. Potter, Epoxide Resins, 1970, Springer-Verlag, New York.

11 J. V. Crivello, *J. Polym. Sci.*, 1999, 37(A), 4241-4254.

12 PJ Flory, Polymer Chemistry Cornell University Press, 1952

13 Carothers WH, Trans Faraday Soc. 32,39-52, 1936

14 LH Sperling, Introduction to Physical Polymer Science, J.Wiley & Sons, 1992

15 Pinner S.H., J.Polymer Science, 21,153-157 1956

16 Elias H,G. Macromolecules Voll & Vol 2, Plenum Press. New York, p 606-614 1976

17 Billmeyer FW, Texbook of Polymer Science, Wiley, New York 1984

18 G. Wisanrakkit, J.K. Gillham: J. Coatings Techn. 62(1990) 35].

Chapter 4

Materials and Experimental Procedures

4.1 Introduction

This chapter describes the experimental methods and techniques used throughout this thesis. In order to study the phase separation behaviour in the thermoplastic-thermoset blends studied in this thesis a wide range of different experimental methods were employed. To study the phase separation behaviour a combination of small angle light scattering, DSC and optical microscopy were used. A large part of this project was in fact concerned with the design and manufacture of the small angle light scattering facility and subsequent data processing and this is described in detail in this chapter.

The mechanical properties of the cured thermoplastic-thermoset blends were evaluated by fracture mechanics and TEM evaluation of the fracture region to highlight the toughening mechanism occurring in phase separated morphologies. Finally the moisture uptake properties of the blends were studied using a dynamic moisture vapour sorption technique. All of these techniques will be described and discussed in this chapter.

4.2 Materials & Blend Preparation

4.2.1 Materials

The materials used this study are all detailed below. All of the epoxy resins and curing agents used in this study are commercially available.

4.2.1.1 Epoxy Resin PY306

The epoxy resin PY306 is available from Huntsman Chemical Corporation (formerly produced by Vantico) and this was used in its unmodified form. This material is a purified liquid bis phenol F epoxy resin and its structure is shown in the figure 4.2.1.1.

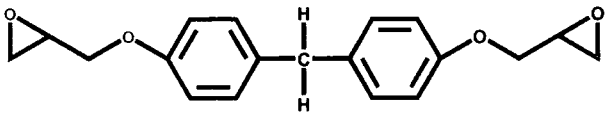

Figure 4.2.1.1 chemical structure of Epoxy resin PY306.

The molecular weight of this resin is 312 g mol^{-1} and has an epoxy equivalent weight(molecular weight of epoxy molecule / epoxy functionality) of 156 g mol^{-1} of epoxy.

This material is a low viscosity clear liquid at room temperature however on standing for prolonged periods of time the material crystallises and becomes a white solid. If this solid is warmed to 40-50°C it reverts back to a low viscosity clear liquid.

4.2.1.2 Epoxy Resin MYO510

The epoxy resin MYO510 is available from Shell Chemical Company (now Apollo) and was used in its unmodified form. This is a low viscosity amber liquid that does not crystallise. This is a trifunctional epoxy resin manufactured from para-amino phenol. The chemical structure of this resin is shown in figure 4.2.1.2.

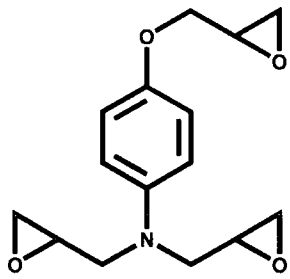

Figure 4.2.1.2 Chemical structure of epoxy resin MYO510

The epoxy resin MYO510 has a molecular weight of 277 g mol^{-1} and has an epoxy equivalent weight of 92.3 g mol^{-1} of epoxy groups.

4.2.1.3 Diamine cure agent MDEA.

The curing agent used in these studies is an aromatic diamine purchased from Lonza Chemical called Lonzacure MDEA[1]. Its structure is shown in figure 4.2.1.3.

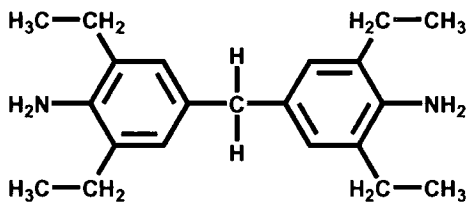

Figure 4.2.1.3 Chemical structure of the diamine cure agent MDEA.

The MDEA cure agent has a molecular weight of 310 g mol^{-1}. At room temperature this is a white non crystalline flaky powder. It is sparingly soluble in epoxy resins MYO510 and PY306 at ambient temperatures. At temperatures of 80°C and above the MDEA becomes readily soluble in the epoxy resins and a homogeneous transparent solution can be obtained.

4.2.1.4 PES:PEES Thermoplastic

The thermoplastic used in these studies was kindly provided by Cytec Industries. The polymer is a PES (polyether sulphone) based copolymer.

The polymer has the following generic structure:

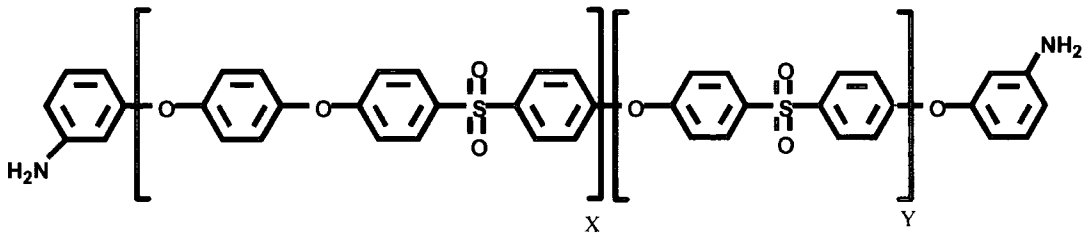

The ratio of X:Y is Cytec confidential information and the molecular weight is greater than 10000 g mol^{-1}.

4.2.2 Sample Preparation

The epoxy blends studied in this thesis were prepared using a hot melt technique. The epoxy resins and the thermoplastic were weighed into a small open necked glass jar. This mixture was then heated to 120°C in an air-circulating oven. The sample was held in the oven for approximately 15 minutes until the thermoplastic had fully dissolved in the liquid epoxy resin leaving a clear homogeneous solution. Next the solution was allowed to cool to below 100°C and the cure agent was added to the mixture and stirred. The mixture was then held at 100°C in an air-circulating oven for approximately 15 minutes until the cure agent had fully dissolved in the solution. This gave a light amber transparent solution. The formulation was then degassed in a vacuum oven at 100°C for approximately 30 minutes until all bubble formation in the sample had ceased. This degassing process was essential to prevent micro-void formation in the sample during the SALS experiment. For the light scattering experiments samples were placed between two glass cover slips and the samples were pressed lightly together using an optical microscope sample press. It was important that the two glass cover slips on either side of the specimen were parallel otherwise the laser beam was deflected off the central position during the SALS experiment and spurious readings could be achieved. The samples were approximately 500-700μm in thickness sandwiched between the two glass cover slips. It was found that sample preparation was extremely important in order to get good quality scattering patterns from the SALS experiments.

4.3 Small Angle Light Scattering

The small angle light scattering equipment used in this thesis was specifically designed and built for this study.

The system employs a 15mW, 523nm wavelength green laser supplied by Coherent Laser[2]. This is a continuous wave diode pumped single frequency laser. The footprint of the laser beam is 2 mm diameter at a distance of 2 meters.

The detection system is a specialised digital camera and frame grabber from Alrad Instruments [3]. This system has two specific features that make this camera suitable for this application. Firstly the camera has optimum sensitivity in the 523nm region and secondly the system has a specialised frame grabber that enables the image to be viewed and pictures to be taken simultaneously. The system also has a feature to take a series of pictures at a predetermined time period. Hence as the experiment proceeds the scattering profile can be observed and a series of 2D scattering profiles can be obtained as a function of time. This is ideal for capturing scattering profiles during dynamic curing experiments. The lens selected to use with this digital camera was a c-mount 16 m lens with adjustable aperture control manufactured by Tamron (code No. HF) [4].

In order to heat the sample during the scattering experiment an optical microscope hotstage manufactured by Linkam [5] the model THMS600 was used for these studies. This has both heating and cooling capabilities and a maximum temperature of 600°C. The hotstage has PC interface control and data logging facilities. The heating element is mounted in a silver block to ensure maximum heat transfer to the sample during the experiment. The hotstage was modified by removing both the glass windows and the quarts plug from the silver heating block. These were found to defect the path of the laser and give spurious scattering patterns

A schematic diagram of the SALS kit is shown in the figure 4.3.1.1.

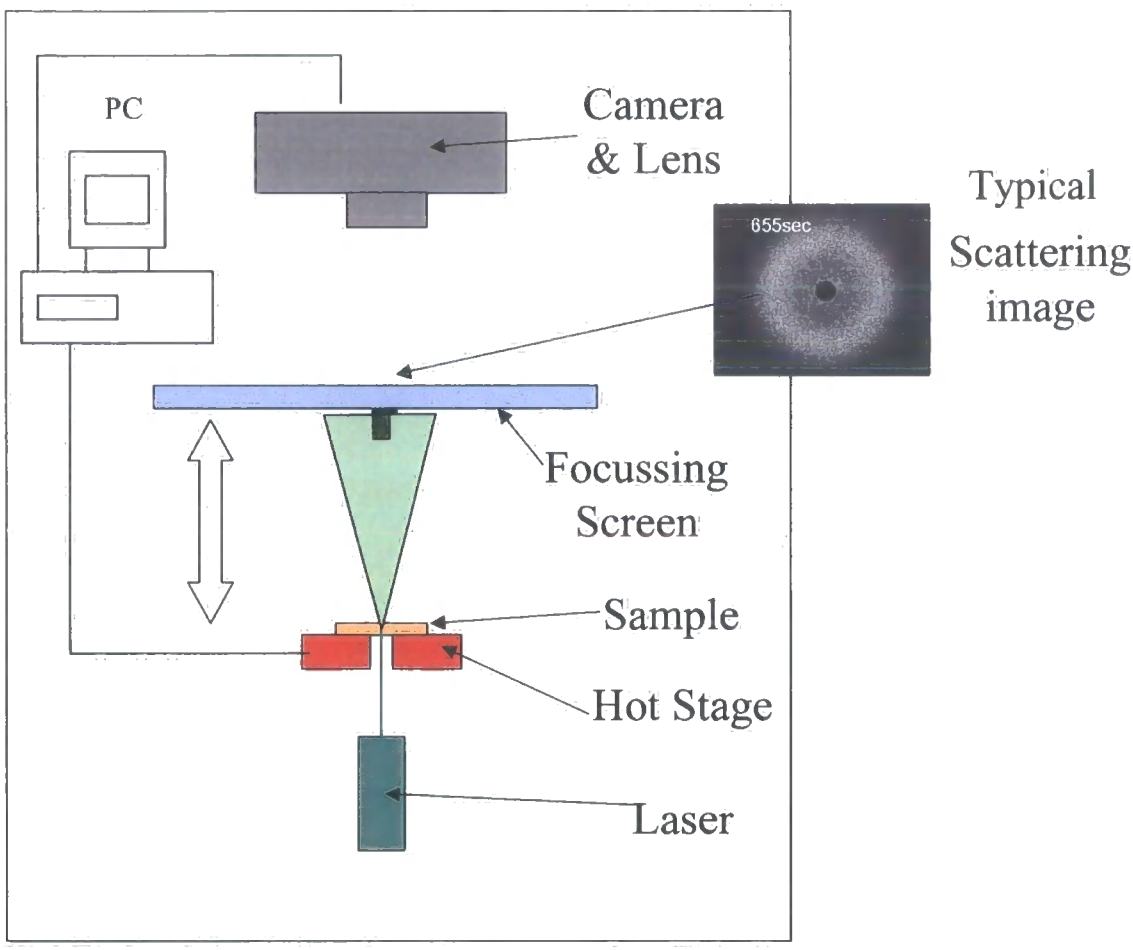

Figure 4.3.1.1 Schematic diagram of the light scattering equipment.

The equipment was designed with a motor controlled moveable focussing screen and camera. This greatly increases the q range that can be studied using the equipment. It also allows the scattering experiment to be focussed on a specific q range.

The focussing screen material was opaque tracing paper onto which a circular black dot was printed which acted as a beam stop. In order to prevent any spurious reflections from the laser beam a black metal cone was mounted on the beam stop spot.

The entire unit was mounted inside a black box that for safety reasons had interlocked doors that cut the power off to the laser when the doors were opened. All of the equipment could be operated remotely from outside of the box. An actual picture of the equipment is shown in the figure 4.3.1.2 .

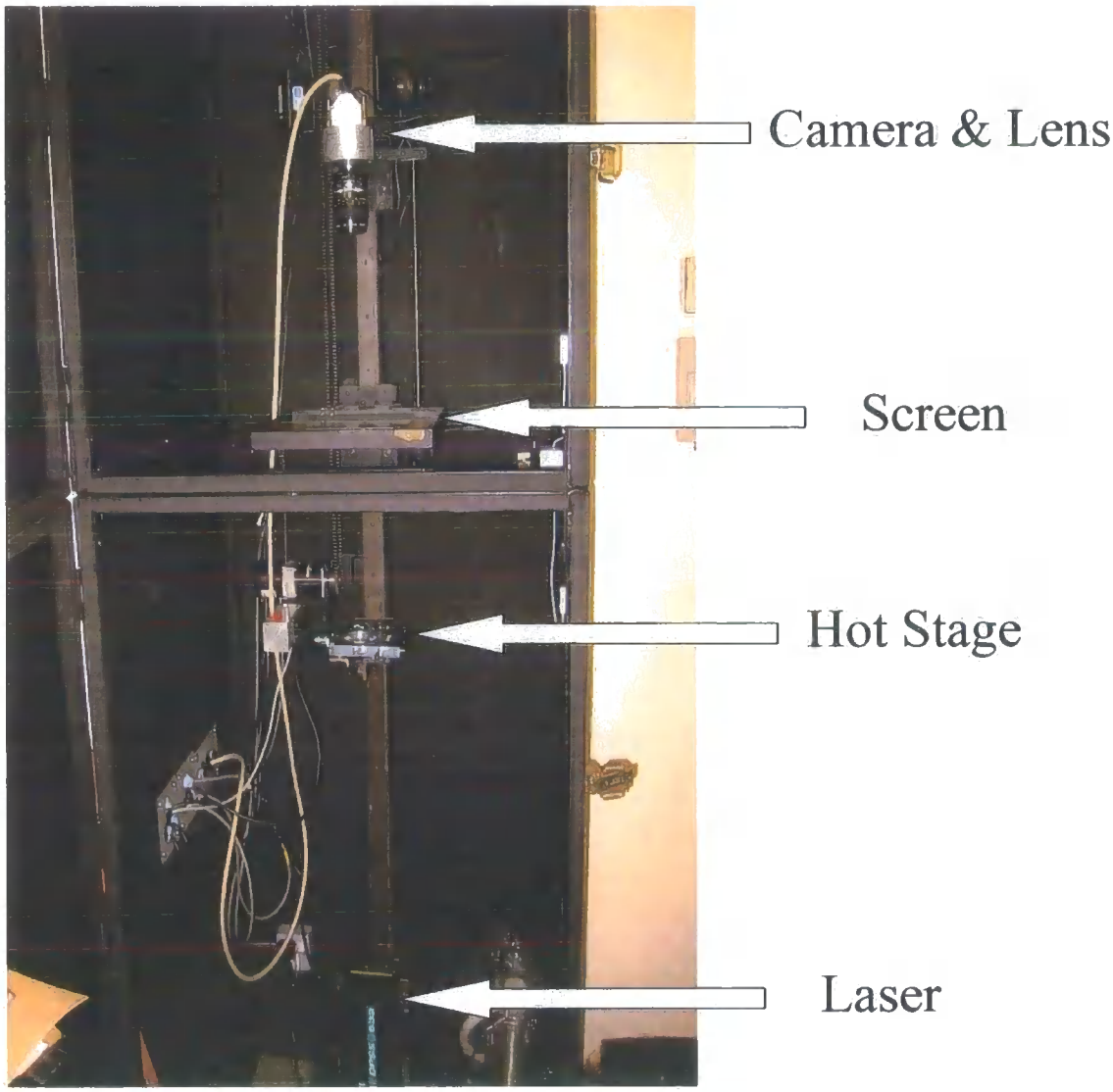

Figure 4.3.1.2 Picture of the SALS equipment used in these studies.

The system was calibrated by taking the scattering profile from a diffraction grating with a known spacing. This gives an interference pattern on the screen which can be interpreted to calibrate the q range for a specific sample to screen spacing. This removes the need to accurately measure the sample to screen distance.

The output from the SALS experiments is a series of digital jpeg images of the scattering pattern at different times. A typical series of scattering patterns is shown in figure 4.3.1.3.

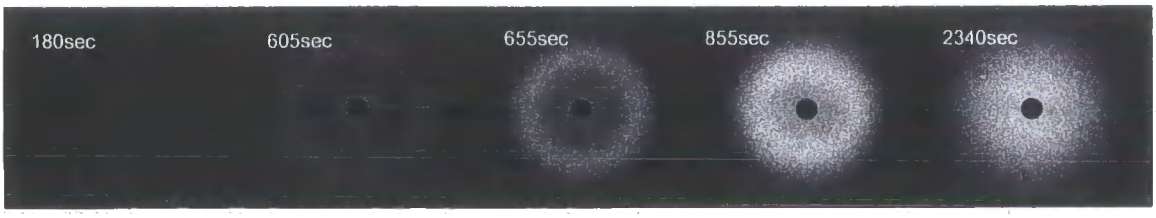

Figure 4.3.1.3 Typical series of scattering patterns at different cure times for a phase separating system

The jpeg images of the scattering patterns are next processed to give S(q) versus q plots for the data as a function of time. This was done by using the matrix mathematics processing software package Matlab. Within this package jpeg images can be imported and converted into a two dimensional matrix. This number matrix is essentially a plot of pixel intensity across the area of the jpeg. The first step in the processing is to identify the centre of the scattering pattern. This is done by a simple centre of mass type calculation. The Matlab code to do this calculation is shown in appendix 1 located at the end of this chapter. The second stage of the processing is to perform a radial average of the jpeg image from the centre point of the scattering pattern. The output from this processing is a matrix of intensity versus q for the scattering profile. The Matlab code to perform the radial average on the jpeg is also shown in appendix 1 of this chapter. This data can now be used to plot the S(q) versus q graph. An example of an S(q) versus q plot is shown in graph 4.3.1.1.

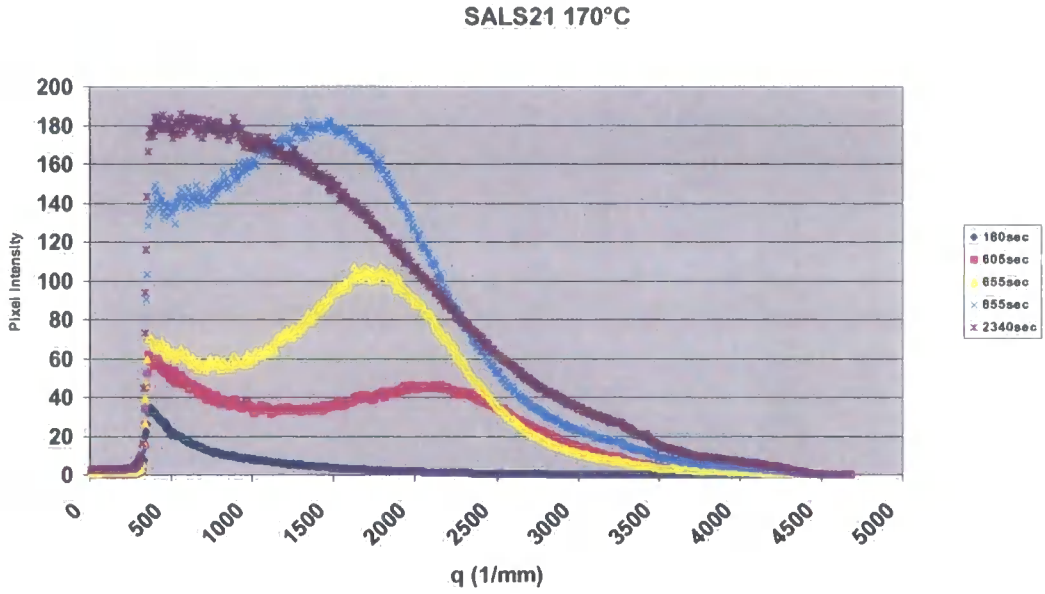

Graph 4.3.1.1 This shows a typical S(q) versus q plot obtained from a series of scattering images after different cure times.

In this study Cahn-Hilliard analysis was carried out on the scattering profiles and the details of this are described in chapter 2.

To calculate the rate of phase separation R(q) gradients were taken from the plots of ln S(q) versus time for each q. An example of an ln S(q) versus time plot is shown in graph 4.3.1.2. The gradient of this plot during the early stages of phase separation is taken to obtain the R(q) for each particular q value. This was done using linear regression analysis of the data in excel. The times between which the linear regression was chosen to coincide with the early stages of the spinodal decomposition. Also the error in the R(q) was also calculated from the linear regression data. Once the R(q) was calculated for each particular q then $R(q)_{max}$ was obtained from the plot of R(q) versus q. This is illustrated in graph 4.3.1.3.

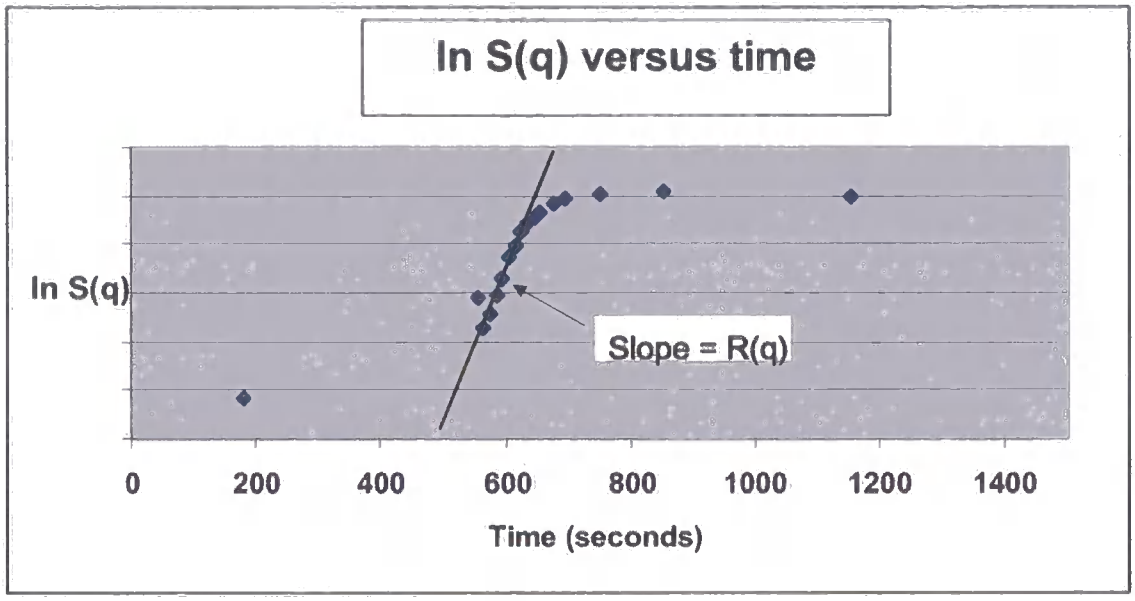

Graph 4.3.1.2 Graph of ln S(q) versus time for a particular q. The gradient of the line during the initial stages of phase separation is calculated to obtain R(q).

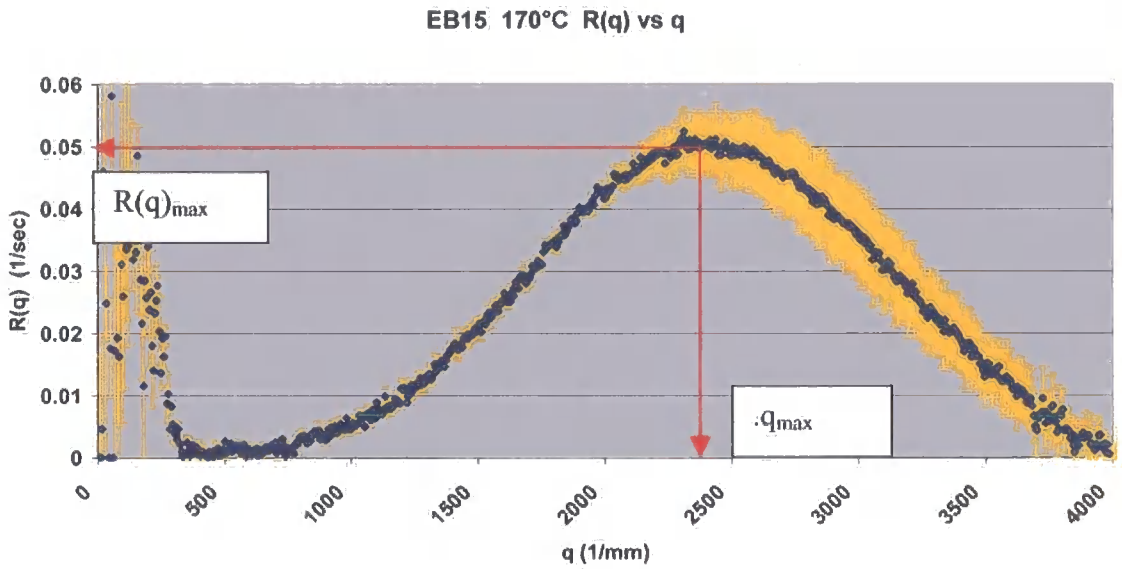

Graph 4.3.1.3 Example of a plot of R(q) versus q. From this plot the values of $R(q)_{max}$ and q_{max} may be obtained.

In order to calculate the apparent diffusion co-efficient, D^*_{app}, for the spinodal decomposition process a Cahn plot of $R(q)/q^2$ versus q^2 was obtained. The D^*_{app} was

obtained by extrapolation of the data to obtain the y axis intercept . According to Cahn-Hilliard theory the plot of $R(q)/q^2$ versus q^2 plot should be a straight line with a clear intercept on the y axis. Cahn –Hilliard theory was developed for spinodal decomposition processes in metal systems which do not undergo reaction and dynamic changes that can occur in reactive curing thermosetting polymer systems. As a consequence of this the $R(q)/q^2$ versus q^2 plots for the systems studied in this thesis did not give a clear straight line with a well defined intercept on the y axis. However the curves generally had a linear region at intermediate q values that could be extrapolated to extract a value of D^*_{app} from the data. An example of a typical $R(q)/q^2$ versus q^2 plot is shown in the graph 4.3.1.4.

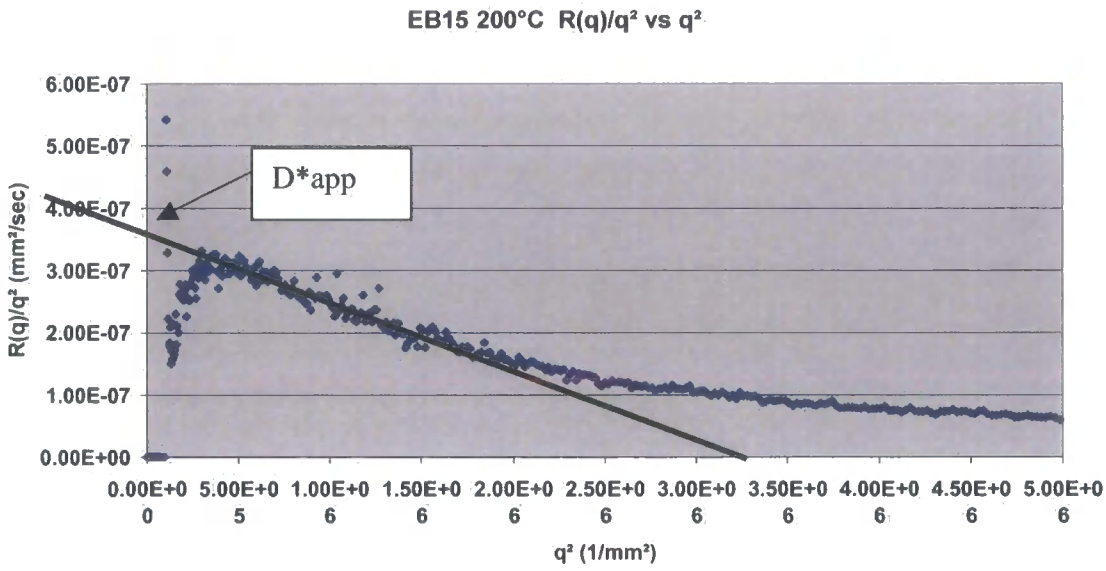

Graph 4.3.1.4 This graph shows a typical $R(q)/q^2$ versus q^2 plot for system undergoing spinodal decomposition. The D^*_{app} value is obtained by extrapolating the linear region of the graph back to the y axis intercept

4.4 Differential Scanning Calorimetry

Differential scanning Calorimetry was used in these studies to determine the degree of conversion as a function of time at four different isothermal cure temperatures. The equipment used for this study was a Mettler-Toledo DSC model 822e. Each epoxy blend was subjected to a range of isothermal DSC experiments as a function of time. A 10mg sample of the uncured epoxy resin was placed inside a standard DSC pan and

sealed. An empty pan was placed into the reference cell and the temperature of the heater block was set to the experiment temperature and allowed to equilibrate. Once at temperature the pan containing the epoxy sample was placed into the measurement cell. The DSC lid was then locked and the experiment was commenced. From this experiment a plot of the power to maintain the equilibrium temperature (in mW) versus time was obtained. An example of such a plot is shown in figure 4.4.1.1.

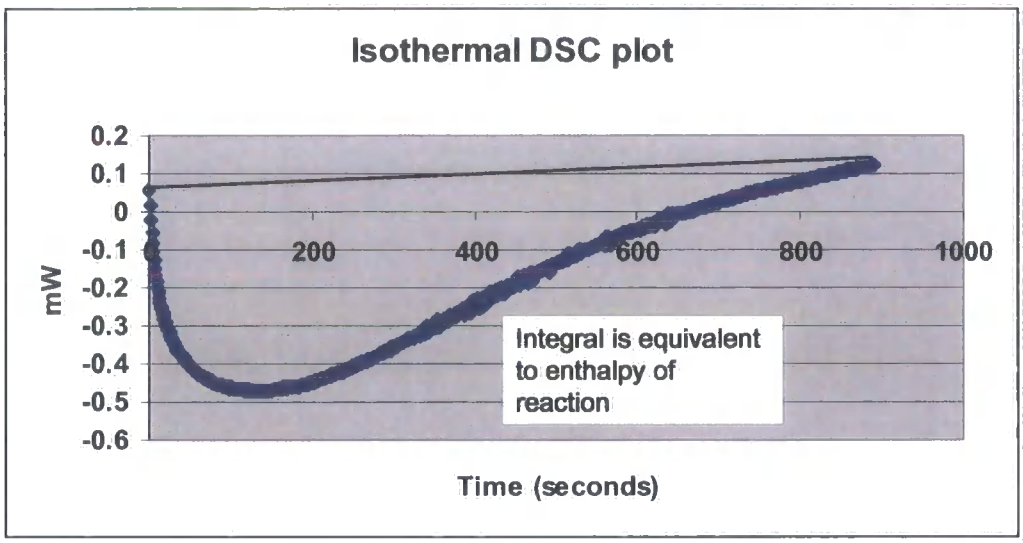

Figure 4.4.1.1 Example of an isothermal DSC plot of a curing epoxy blend.

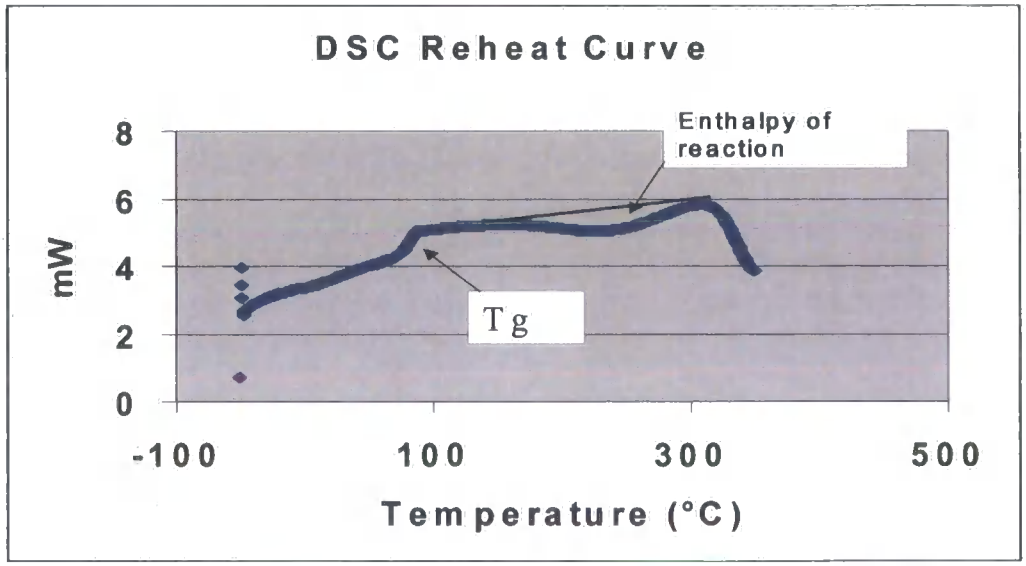

Figure 4.4.1.2 Example of a reheat DSC curve following an isothermal DSC experiment.

Following the isothermal experiment the sample was subjected to a temperature ramp DSC from -40°C to 350°C. This was done so that the level of residual cure following the isothermal DSC experiment could be determined. The isothermal plot was integrated with respect to time to calculate the amount of reaction exotherm as a function of time. The 100% conversion level was determined from both the exotherm from the isothermal and the temperature ramp experiments. From this the % conversion versus time for any given isothermal cure temperature can be obtained. The graph 4.4.1.1 shows a typical %conversion versus time for different isothermal cure experiments.

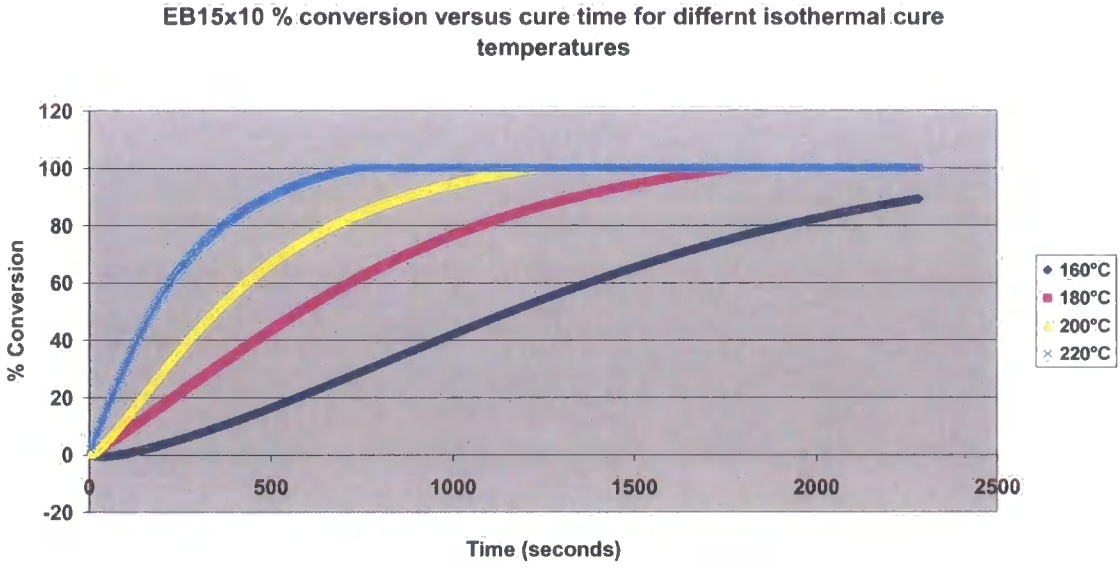

Graph 4.4.1.1 Graph showing a typical plot of conversion versus time for different isothermal cure temperatures.

4.5 Phase contrast optical Light Microscopy

The cured phase morphology of the samples following the isothermal SALS experimentation was examined using optical microscopy. For this an Olympus BX2 [6] optical microscope fitted with a digital camera and a phase contrast unit. The exact samples used in the SALS experiments were examined using optical microscopy to reveal the morphology. Transmission phase contrast optical microscopy was used in order to give enhanced contrast between the two separated phases, a full review of this technique can be found in reference 7. This technique is often useful when the two separated phases only have a small difference in refractive

index. One characteristic of phase contrast microscopy is a bright halo effect around dispersed particles in the system [7].

In order to calibrate the size scale of the micrographs photos of a 0.01 mm graticule were taken for each magnification used.

4.6 Mechanical Testing

Mechanical testing of the various thermoplastic-thermoset blends was carried out in order to assess how the phase separated morphology can influence the overall bulk properties of the system. One of the key characteristics of thermosetting systems is their brittleness or low fracture toughness. The general aim of formulating a thermoplastic-thermoset blend is to improve the fracture toughness without influencing other properties such as modulus and yield strength. In this study fracture toughness, modulus and yield strength of the thermoplastic-thermoset blends were characterised.

Also in order to investigate the mechanisms of toughening that occur in phase separated thermoplastic-thermoset blends a combination of fracture mechanics, sectioning and transmission electron microscopy was carried out. This section describes the experimental procedures used in this evaluation.

4.6.1 Sample preparation

To carry out the mechanical testing, panels were prepared that were approximately 150mm x 150mm x 3mm. This was done by preparing and degassing the thermoplastic-thermoset blend as described in section 4.2 above. After the blend was degassed the warm viscous liquid was transferred to a vertically mounted parallel plate mould. This was then placed in a programmable forced air oven and the sample was heated at 2°C/min to 180°C and held for 180mins. Following this the samples were removed from the mould and machined as necessary into the samples required for mechanical testing.

The mechanical properties of epoxy systems are very moisture sensitive, hence, samples were preconditioned. Some samples were tested 'dry' and this involved preconditioning the samples in an ultra dry nitrogen oven at 40°C for up to 1000hours until the weight of the samples had stabilised. Elevated heating of the samples to accelerate the drying was avoided to prevent any possible post curing effects on the

mechanical testing results. Samples were also tested after conditioning in a wet environment. This involved preconditioning the samples in an environmental chamber at 40°C and 85% relative humidity until the samples were fully saturated under those conditions. Saturation occurred in the samples after approximately 5 days. The samples were removed from the oven and tested immediately.

4.6.2 Fracture toughness testing.

Fracture toughness testing was carried out on pre-cracked single edge notched beam (SENB) specimens. The geometry of this test specimen is shown in figure 4.6.2.1.

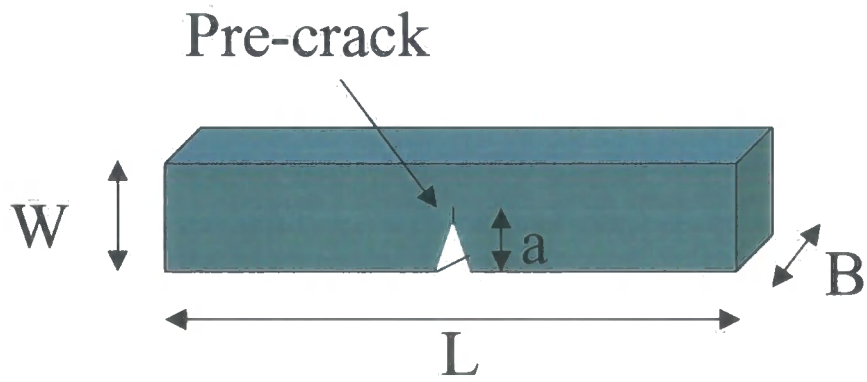

Figure 4.6.2.1 This figure illustrates the geometry of the SENB used to measure the fracture toughness of the thermoplastic-thermoset blends.

For the SENB specimens used in this study L = 60 mm, W =10 mm, B = 3 mm and a was nominally 5 mm but was accurately measured using a traversing microscope after pre-cracking the sample.

The edge notch was machined into the specimen using a high speed V profile diamond cutting blade driven by a milling machine. The pre-crack was introduced by using a razor tapping method. Here a single edged razor blade was held in the notch and given a firm strike with a hammer. The pre-crack was then examined under a microscope to ensure that the crack was straight to avoid any mixed mode effects.

The testing was carried out on an Instron Universal testing machine fitted with a 3 point bend testing fixture. Testing was carried out at 23°C +/- 2°C and a controlled humidity of 50% RH. A test speed of 1 mm min^{-1} was used for all the tests. This test

protocol satisfies the linearity and size criteria in the ESIS protocol [8] for Linear elastic fracture mechanics (LEFM) analysis.

This test measures the mode 1 energy release rate G_{IC} and the mode 1 critical stress intensity factor K_{IC}. G_{IC} is the stored elastic energy released from the sample (dU) when the crack grows an area of dA. For pure linear elastically deformed materials (LEFM) G_{IC} can be calculated using the following expression:

$$G_{IC} = \frac{U}{BW\phi}$$

where U is the energy of fracture obtained by integration of the force displacement curve up to the fracture point. ϕ is a geometry constant dependent upon the ratio of a/W where a is the crack length. This was generally between 0.275 and 0.32, a full table of geometry constants can be found in reference[8].

K_{IC} is obtained by the following expression,

$$K_{IC} = f\frac{P_Q}{BW^{0.5}}$$

Where P_Q is the load at the onset of fracture and f is a geometry constant dependent on the initial crack length to sample height, a/W. In these tests this value ranged from 9.14 to 12.57 depending on the pre-crack length.

The results were qualified using the 5% compliance rule to check for compliance with linear elastic fracture mechanics. A full review of the ESIS protocol on fracture mechanics of polymers used in this study is given in reference [8].

4.6.3 Modulus measurement

The modulus of the cured blends was measured in flexure using a 3 point bend test geometry. The test was carried out at a test speed of 1mm min^{-1} at 23°C and 50% relative humidity. The geometry of the test is shown in figure 4.6.3.1.

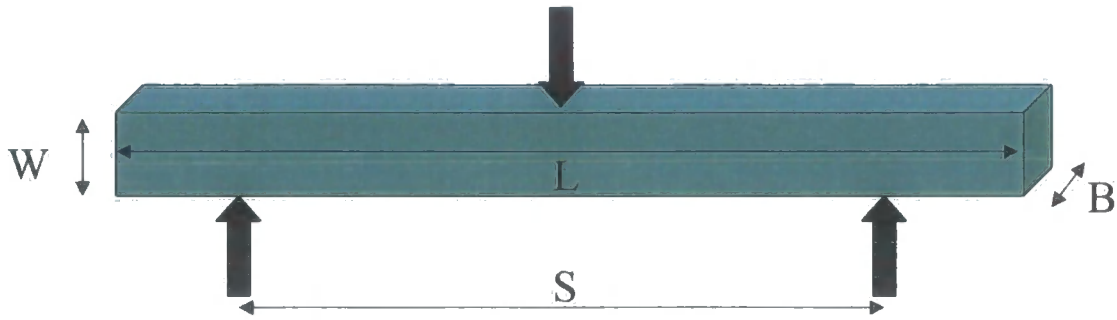

Figure 4.6.3.1 Diagram showing the geometry of the modulus test

For this test W =10 mm, B = 3 mm, L = 150 mm and S = 100 mm

The modulus of the sample was calculated using beam theory; the equation for modulus is given by[9]:

$$E = \frac{mS^3}{4BW^3}$$

where m is the initial slope of the stress strain curve.

4.6.4 Yield Strength Measurement.

Brittle materials such as thermosetting polymers generally do not exhibit a yield strength when tested in tension. Brittle failure usually occurs prior to any sample yielding occurring. Therefore in order to measure the yield strength of such materials they need to be tested in compression. By doing this the onset of any fracture process is effectively delayed because cracks and flaws in the material are subjected to compressive stresses and therefore do not grow. This then allows the material to yield during the test and a yield strength in compression can therefore be accurately measured. This can be converted into yield strength in tension by using simple elasticity theory. The geometry of the yield strength in compression test is shown in figure 4.6.4.1.

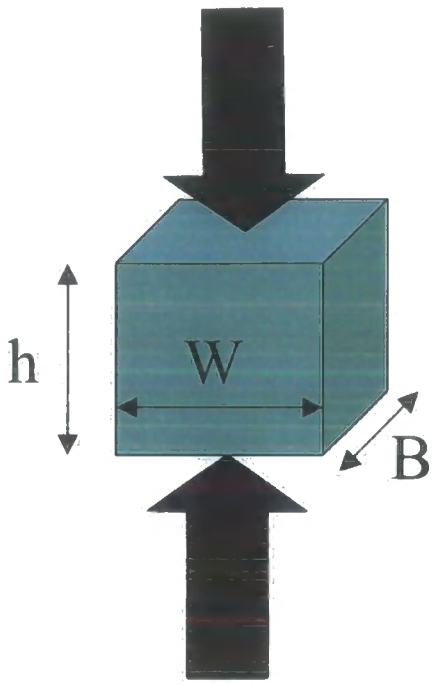

Figure 4.6.4.1 Diagram showing the geometry of the yield strength in compression test.

In the compression test h = 3 mm, W = 5 mm and B = 5 mm.

4.6.5 Evaluation Of Toughening Mechanisms

In order to investigate the toughening mechanisms that occur in phase separated thermoplastic-thermoset blends a combination of fracture mechanics, sectioning and TEM was carried out. Initially a fracture mechanics test was performed on the SENB sample as described in section 4.6.2. After testing the samples were sectioned and microtomed at 90° to the fractured surface of the specimen. The microtomed section was taken using a diamond knife microtome under liquid nitrogen. The thickness of the section was approximately 5 microns. It was found that for these samples there was enough atomic number contrast between the two phases to produce good well-defined TEM images of the samples without the need for staining.

The samples were carefully sectioned from the fractured SENB specimens so that the region close to the fracture surface could be observed. This was done to look for evidence of toughening mechanisms such as yielding or crazing in the bulk of the sample away from the fracture surface. The crack path could also be observed and the influence of the morphology upon both crack path and toughening mechanism could

be investigated. Figure 4.6.5.1 below details how the TEM samples were taken from the fractured SENB samples.

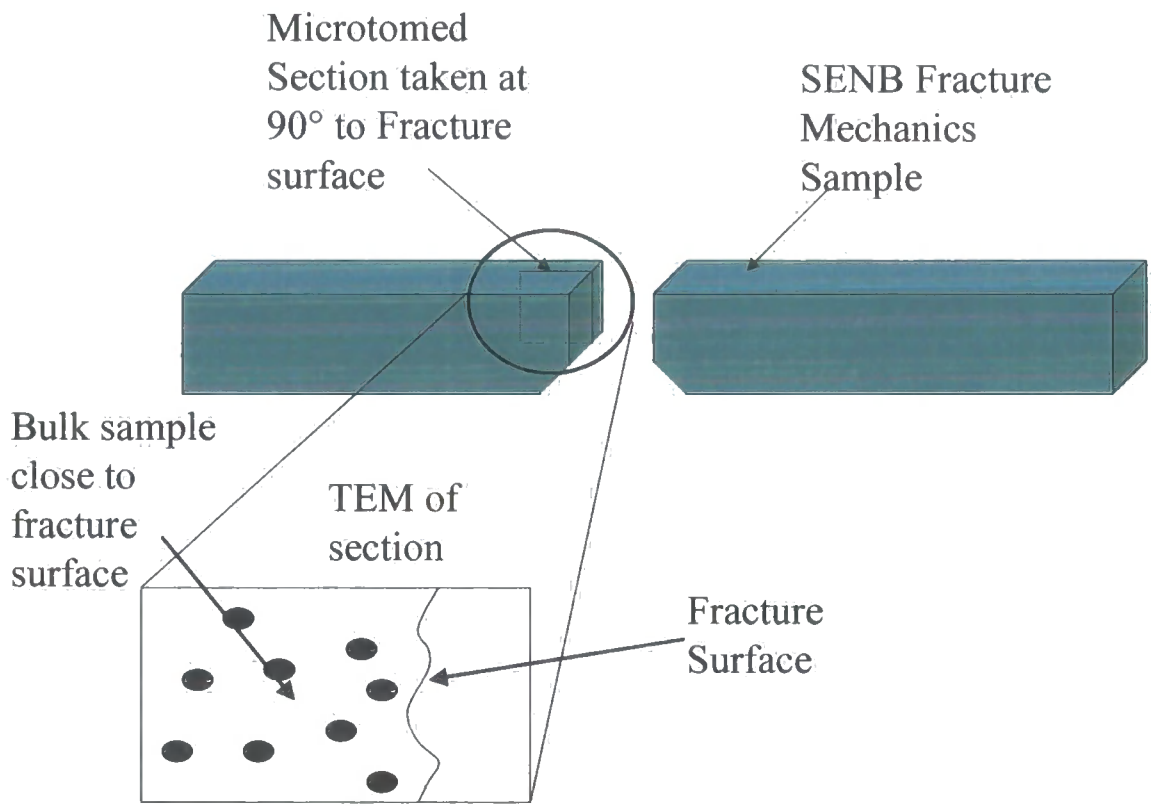

Figure 4.6.5.1 Diagram showing how TEM sections were taken from the fractured SENB specimens to elucidate the mechanisms of toughening in the blends.

4.6.6 Dynamic Mechanical Thermal Analysis (DMTA)

Dynamic mechanical thermal analysis evaluation was carried out using a Polymer Laboratories DMTA. For this test samples of the cured epoxy blend 10 mm x 50 mm x 2 mm were cut from the cured panel. Prior to testing, samples were dried in a dry nitrogen cabinet at 40°C until the weight had stabilised. This drying process took approximately 20-30 days. The samples were then removed from the drying cabinet and tested immediately. This technique applies a sinusoidal stress to the sample in three point bend mode and measures the phase shift between the stress amplitude and the sample deformation. This calculates the in phase modulus (or storage modulus) of the sample, E' and the out of phase modulus (loss modulus) E" of the sample. The

test carried out in this thesis were carried out with a sinusoidal stress frequency of 50 Hz. The tests were carried out as a function of temperature between 25°C and 250°C. From the plots, phase Tg's can be identified and also rubbery plateau modulus can be estimated.

4.7 Dynamic Vapour Sorption

One important factor in the performance of an epoxy based thermosetting system is the effect moisture has on the system. It is therefore important to look at how moisture diffuses into the epoxy resin blend. The thermoplastic-thermoset blends in this study were studied for moisture diffusion properties using dynamic vapour sorption apparatus manufactured by Scientific and Medical Systems Ltd [10]. This piece of equipment is essentially a very accurate microbalance where the environment around the sample can be controlled in terms of both temperature and relative humidity. Samples can for example be subjected to 80°C and 80% relative humidity and the sample weight can be accurately measured dynamically. This allows diffusion and saturation data to be obtained under a range of different conditions.

For this test a thin sample is cast approximately 0.5 mm in thickness, 15 mm square. This is supported in the weighing basket of the equipment. The equipment is then sealed and the experimental temperature set. The first stage of this experiment subjects the sample to a fully dry environment (0% RH). The sample weight is monitored until the sample weight becomes constant. This can take many hours depending on the sample thickness.

For this particular series of experiments 3 relative humidity values were selected for the isothermal temperature runs. These were 30% RH, 60% RH and finally 85% RH. In order to reduce the time of the experiment only elevated temperature isothermal experiments were performed. The temperatures chosen for this series of tests was 60°C and 85°C.

Once the sample had achieved an equilibrium weight under the dry, 0% RH conditions the equipment automatically sets the relative humidity to 30%. The mass of the sample is recorded until equilibrium is achieved. Once equilibrium is achieved at 30% RH the equipment then changes the RH to 60% and again monitors the sample weight until equilibrium is achieved. The next step sets the relative humidity to 85%

RH and the sample mass is monitored until equilibrium is achieved. This series of results is the adsorption isotherm.

The next stage of the experiment monitors the desorption isotherm. Here the relative humidity is sequentially reduced and the sample is allowed to equilibrate to constant weight at each stage. This is carried out at the same relative humidities performed on the adsorption isotherm. An example of the results from the adsorption and desorption isotherms is shown in graph 4.7.1.1.

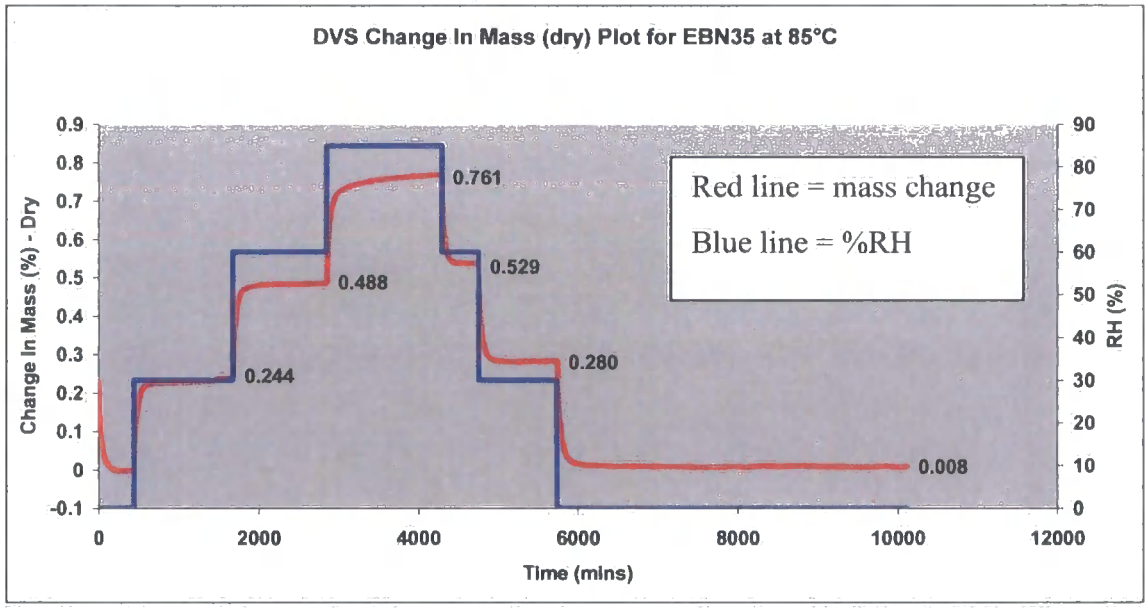

Graph 4.7.1.1 This graph shows an example of an adsorption and desorption isotherm produced from the DVS experiment. .

One advantage of measuring moisture uptake using this method is that diffusion coefficients can be calculated for each adsorption and desorption step of the experiment. Using Ficks law of diffusion, which appears to loosely apply to the thermoplastic-thermoset blends studied in this thesis, diffusion coefficients may be obtained for each step of the isotherm.

To calculate the diffusion coefficient the first step is to obtain a Fickian plot of Mt/Minf versus Square root of time/sample thickness. This can be done for all of the different adsorption and desorption steps of the isothermal experiment. The graph 4.7.1.2 below shows a typical adsorption Fickian plot by which a diffusion coefficient can be obtained.

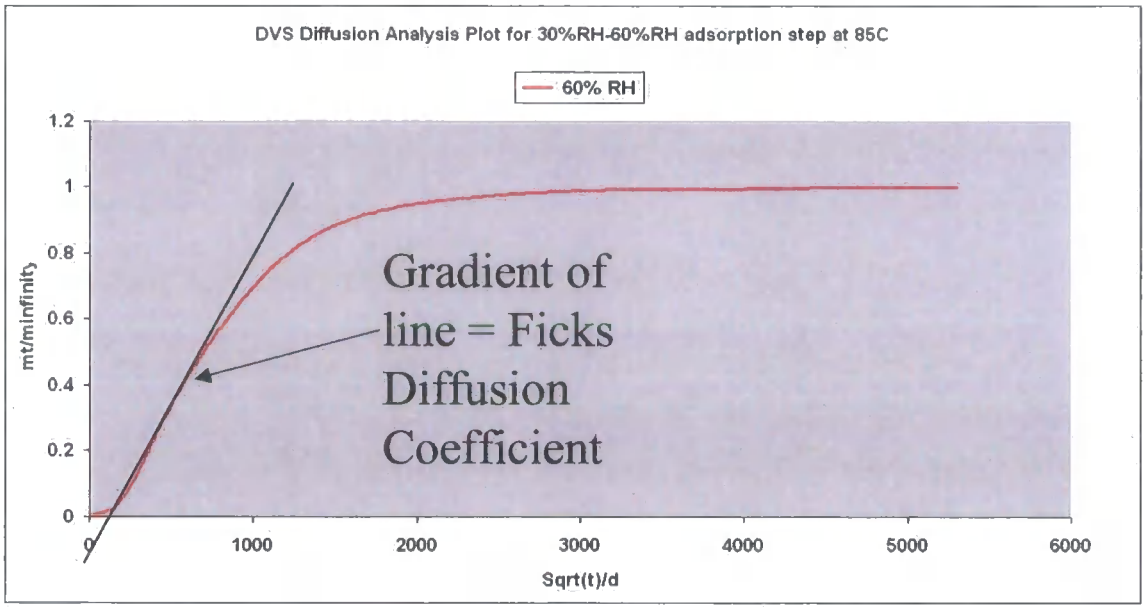

Graph 4.7.1.2 This Graph shows a typical Fickian diffusion plot for an adsorption isotherm step between 30%RH and 60%RH. The diffusion coefficient is obtained form the gradient of this plot.

The graph 4.7.1.2 above shows the typical shape of the Fickian diffusion plots for these materials. It can be seen that the very initial portion of the curve is not linear as would be expected from true Fickian diffusion; this suggests that non-Fickian diffusion may be occurring in the samples. However this region was ignored when calculating the gradient for the diffusion coefficient.

This can also be done for the desorption isotherm steps and a subsequent desorption coefficient can be calculated. From this data a comparison of saturation levels and diffusion coefficients on both adsorption and desorption may be carried out.

4.8 Appendix 1

Matlab code for processing the jpeg images into scattering profiles.

4.8.1 Matlab Code for calculating the radial average of a jpeg scattering pattern.

```
% Calculates the scattering pattern from a SALS pattern
% qcalc MUST first be run in order to set the appropriate q range
%

sals_file = input('SALS filename (incl. extension): ','s');
i=imread(sals_file);

idble=double(i);
clear S Srad;
clear kmcount;
kmcount(1:kmax)=0;
S(1:kmax,1)=0;
for m=1:sizeix
   for n=1:sizeiy
      k=sqrt(((m-cofmx).^2)+((n-cofmy).^2));
      km=round(k);
      if km > 0 & km < kmax+1
         S(km,1)=S(km,1)+idble(m,n);
         kmcount(km)=kmcount(km)+1;
      end
   end
end

Srad(1:kmax,1)=q;
Srad(1:kmax,2)=S(1:kmax,1);
for m=1:kmax
   if kmcount(m)>0
      Srad(m,2)=S(m,1)/kmcount(m);
   end
end

% asks for output filename
ow = 1;
out_file = input('Save data as: ','s');
%fid = fopen(out_file,'r');

file_exist = exist(out_file);

% checks whether file exists (fid not equal to -1), if so, should it be overwritten?
% '|' denotes 'or'
 while (file_exist == 2) & (ow == 1)
```

```
  overwrite = input('File exists. Overwrite y/n?: ','s');
  if (overwrite == 'y') | (overwrite == 'yes') | (overwrite == 'Y') | (overwrite == 'Yes')
    ow = 0;
  else
    out_file = input('Save data as: ','s');
    file_exist = exist(out_file);
  end
end


% clear some variables from the workspace
clear m n i idble kmcount k

save (out_file,'Srad','-ascii','-tabs');
```

4.8.2 Matlab Code for calculating the Centre point of the scattering profile

```
idble2=double(i);

idble3=idble2-40;

sizei=size(i);
sizeix=sizei(1);
sizeiy=sizei(2);

cofmx=0;
cofmy=0;
cofmm=0;
for m=1:sizeix
  for n=1:sizeiy
    if idble3(m,n)>0
      cofmx=cofmx+((idble3(m,n).*idble3(m,n).*idble3(m,n)).*m);
      cofmy=cofmy+((idble3(m,n).*idble3(m,n).*idble3(m,n)).*n);
      cofmm=cofmm+(idble3(m,n).*idble3(m,n).*idble3(m,n));
    end
  end
end

cofmx=cofmx/cofmm
cofmy=cofmy/cofmm

idble=double(i);
clear S;
clear kmcount;
kmcount(1:sizeix)=0;
S(1:sizeix)=0;
```

```
for m=1:sizeix
   for n=1:sizeiy
      k=sqrt(((m-cofmx).^2)+((n-cofmy).^2));
      km=round(k)+1;
      S(km)=S(km)+idble(m,n);
      kmcount(km)=kmcount(km)+1;
   end
end

Srad2=S;
for m=1:sizeix
   if kmcount(m)>0
      Srad2(m)=S(m)/kmcount(m);
   end
end
[C,J]=max(Srad2)
```

4.8.3 Matlab code for calculating the q range from a diffraction grating of known spacing.

```
Calculates the q scale from a diffraction grating scattering pattern
%

df_file = input('Diffraction grating filename (incl. extension): ','s');
ds = input('Diffraction grating spacing: ')

i=imread(df_file);
idble2=double(i);

idble3=idble2-40;

sizei=size(i);
sizeix=sizei(1);
sizeiy=sizei(2);

cofmx=0;
cofmy=0;
cofmm=0;
for m=1:sizeix
   for n=1:sizeiy
      if idble3(m,n)>0
%        cofmx=cofmx+((idble3(m,n).*idble3(m,n).*idble3(m,n)).*m);
%        cofmy=cofmy+((idble3(m,n).*idble3(m,n).*idble3(m,n)).*n);
%        cofmm=cofmm+(idble3(m,n).*idble3(m,n).*idble3(m,n));
         cofmx=cofmx+m;
         cofmy=cofmy+n;
         cofmm=cofmm+1;
```

```
      end
   end
end

cofmx=cofmx/cofmm
cofmy=cofmy/cofmm

kmax=round(0.5.*sqrt(sizeix.^2+sizeiy.^2));

idble=double(i);
clear S;
clear kmcount;
kmcount(1:kmax)=0;
S(1:kmax)=0;
for m=1:sizeix
   for n=1:sizeiy
      k=sqrt(((m-cofmx).^2)+((n-cofmy).^2));
      km=round(k);
      if km > 0 & km < kmax+1
         S(km)=S(km)+idble(m,n);
         kmcount(km)=kmcount(km)+1;
      end
   end
end

Srad=S;
for m=1:kmax
   if kmcount(m)>0
      Srad(m)=S(m)/kmcount(m);
   end
end

[Speak,kpeak]=max(Srad);

clear q
q(1:kmax,1)=0;
for m=1:kmax
   q(m,1)=2.*pi.*m./(ds.*kpeak);
end
```

4.9 References

1 http://www.lonza.com/highperf/en/mbis/polymerintermediates0.html

2 http://www.coherentinc.com/index.cfm

3 http://www.alrad.co.uk/

4 http://www.machine-vision.co.uk/optics.html

5 http://www.linkam.co.uk/THMS600.html

6 http://resources.olympus-europa.com//micro/catalogs/C12567B6003775C72A1AC57B12854D4C41256ABD005ECC5D_BX2M%5Foverview%20eng%2Epdf

7 Applied polymer light microscopy, Hemsley D.A. , Elsevier,1989, ISBN 1-85166-335-5.

8 Moore D.R, Pavan A, Williams J.G, ESIS publication 28, Fracture Mechanics Testing Methods for Polymers and Adhesives. Elsevier Press 2001..

9 LA Carsson , RA Pipes, Mechanical Characterisation of Materials , Dekker 1993

10 http://www.oconnor.com.sg/SScien.html

11 Hull D, Fractography Cambridge University Press 1999

Chapter 5

The Effect Of Temperature And Thermoplastic Loading On The Reaction Induced Phase Separation Process In A Thermoset -Thermoplastic Blend.

5.1 Introduction

This chapter will discuss the reaction induced phase separation process occurring in a di-functional epoxy system blended with an aromatic polyethersulphone.

Using time resolved small angle light scattering (SALS) both the nature and the kinetics of the phase separation process will be examined. Where appropriate the kinetics of the early stage reaction induced phase separation process will be analysed using Cahn-Hilliard approach detailed in Chapter 2.

Isothermal Differential Scanning Calorimetry (DSC) will be used to study the time-temperature-conversion level relationship for the epoxy blend and this information will be considered together with the SALS results to determine the nature of the phase diagram. Finally the results of the SALS experiments will be compared to the optical micrographs of the fully cured morphology of the thermoplastic-thermoset blends. This will give a comprehensive picture of the reaction induced phase separation process occurring in this particular thermoset-thermoplastic system.

5.2 The Theory of Reaction Induced Phase Separation in Polymer Blends

Phase separation in a thermoset-thermoplastic blend will occur when the reacting homogeneous blend crosses a phase boundary into a region of instability. The driving force for the phase separation process is the reduction in Gibbs free energy of mixing, ΔG°, of the blend. Chapter 2 discussed the Flory-Huggins theory and how this can be applied to polymer blends, it details the relationship of the ΔG° to blend characteristics. This can then be used to define the phase boundaries of the system and therefore outline the phase diagram. The Flory-Huggins relationship for ΔG° identifies two thermodynamic processes by which phase separation can occur these are nucleation and growth and spinodal decomposition. Phase separation by spinodal decomposition produces a morphology that has a characteristic length scale. This is in contrast to phase separation by nucleation and growth, which is a random process that has no such defined length scale. However it has been previously reported that under certain circumstances nucleation and growth may produce a maximum in the S(q) vs q plot due to coherent scattering from clustering of droplets [1].

This is the basis by which scattering experiments can be used to distinguish between spinodal decomposition and nucleation and growth phase separation processes. Generally in scattering experiments phase separation by spinodal decomposition will produce a peak at a scattering vector, q, which is directly related to the characteristic length scale.

Flory-Huggins theory can be used to describe the thermodynamic nature of the phase separation but it gives no indication of the kinetics of the process. Linerised Cahn-Hilliard theory outlined in Chapter 2 can be used to describe the kinetics of phase separation occurring by spinodal decomposition. As previously discussed Cahn-Hilliard theory was initially developed for studying phase separation in metallic alloys [2,3,4]. However for reactive polymer blends Cahn-Hilliard theory can in most circumstances be used to describe the kinetics of the initial stages of phase separation where the position of the spinodal peak in the scattering profile remains at a relatively constant q value. Generally in phase separating reacting polymer blend systems the position of the spinodal peak shifts to lower q as the phase separation process

advances and the kinetics of the later stages are generally defined by the Lifshitz – Slyozov equation detailed in Chapter 2[5].

In this Chapter Cahn-Hilliard theory described in chapter 2 will be used to analyse the results from the small angle light scattering results of a thermoset-thermoplastic blends with differing thermoplastic level loading and isothermal cure temperatures. This will yield information on phase separation rate $R(q)_{max}$, and the apparent diffusion constant D^*_{app} for the phase separation process. In circumstances where there is no well-defined early stage spinodal decomposition the approach taken by Alig et al [6] will be used to describe kinetics of the phase separation process. Here the value of $S(q)_{max}$ is taken as a function of time at different q values to account for the shifting position of $S(q)_{max}$ relative to q. From this a rate of phase separation by spinodal decomposition can be calculated.

5.3 Experimental

5.3.1 Thermoplastic-Thermoset blends

The blends studied in this chapter are detailed in table 5.3.1.1. The details of the raw materials used in this study are described in detail in Chapter 4.

	% Composition		
Reference Code	**Di-functional epoxy (PY306)**	**Cure Agent (MDEA)**	**Thermoplastic (PES:PEES)**
EB10	63.36	26.64	10
EB15	59.84	25.16	15
EB20	56.32	23.68	20
EB25	52.8	22.2	25

Table 5.3.1.1 Formulation of the epoxy blends. These compositions use a stoichiometric ratio of 1:0.77 (epoxy: amine cure agent). This is calculated neglecting the protons of the amine end groups on the PES: PEES thermoplastic.

These blends were prepared using a hot melt technique. The di-functional epoxy and thermoplastic were weighed into a small open necked glass jar. This mixture was then heated to 120°C in an air-circulating oven. The sample was held in the oven for approximately 15 minutes until the thermoplastic had fully dissolved in the liquid epoxy resin leaving a clear homogeneous solution. Next the solution was allowed to cool to below 100°C and the cure agent was added to the mixture and stirred. The mixture was then held at 100°C in an air-circulating oven for approximately 15 minutes until the cure agent had fully dissolved in the solution. This gave a light amber transparent solution. The formulation was then degassed in a vacuum oven at 100°C for approximately 30 minutes until all bubble formation in the sample had ceased. This degassing process was essential to prevent micro-void formation in the sample during the SALS experiment.

5.3.2 Time Resolved Small Angle Light Scattering

SALS experiments were carried out using the equipment and technique outlined in Chapter 4. The epoxy blend formulations were subjected to a series of temperature jump experiments in the range of 150°C to 220°C.

5.3.3 Differential Scanning Calorimetry

Time–temperature-conversion behaviour of the epoxy blend formulations were determined using a combination of isothermal and temperature ramp differential scanning Calorimetry (DSC). The experimental method and interpretation technique are described in detail in Chapter 4.

5.3.4 Optical Light Microscopy

Phase contrast polarised optical light microscopy was performed on the actual samples from the SALS experiments. This identified the nature of the morphology of

the epoxy blend formulations. The equipment and experimental technique used for this evaluation is described in detailed in Chapter 4.

5.4 Results & Discussion

5.4.1 Results for EB10

5.4.1.1 SALS S(q) versus q Results for EB10.

The series of graphs 5.4.1.1 to 5.4.1.7 below show the S(q) versus q plots obtained

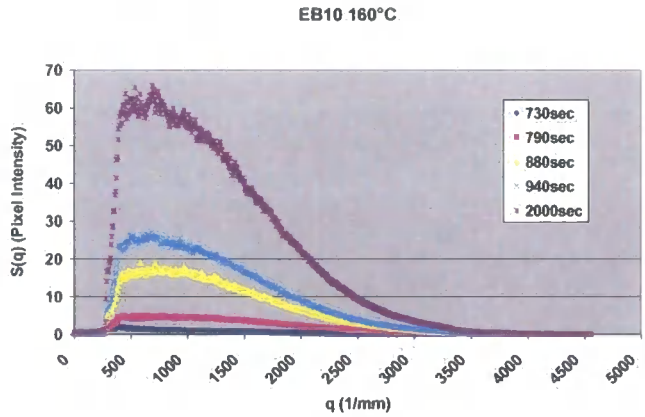

from Small angle light scattering (SALS) experiments for the system EB10 cured at temperatures between 160°C and 220°C.

Graph 5.4.1.1 S(q) versus q for EB10 cured at 160°C. This shows a broad spinodal peak that develops as cure progresses.

The graph 5.4.1.1 above shows the S(q) versus q plot for EB10 cured at 160°C. This shows a broad spinodal peak that develops at a q value of 900 mm^{-1} this corresponds to a spinodal length of 0.007 mm. This suggests that the blend has phase separated by spinodal decomposition. The phase separation begins at approximately 790 seconds into the cure.

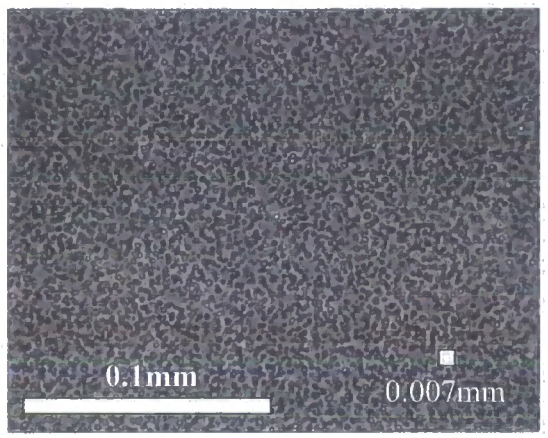

Figure 5.4.1.1 Optical micrograph of EB10 cured at 160°C. This shows a particulate morphology. The size of the dispersed particulates is very regular which suggest that the microstructure has formed by undergoing a percolation to cluster transformation. SALS experiments indicate that the spinodal length for this structure is 0.007mm.

Comparing the light scattering results in graph 5.4.1.1 and the corresponding micrograph in figure 5.4.1.1 it can be seen that although the mechanism of phase separation is spinodal decomposition the morphology of the cured blend is particulate in nature. The scattering from the sample after full cure still shows a peak at a q value of approximately 900 mm^{-1}. This suggests that this morphology has been produced by a spinodal decomposition undergoing a percolation to cluster transformation. From the micrograph in figure 5.4.1.1 it can be seen that there is a narrow size distribution to the dispersed phase, again this would suggest that this morphology has not formed by nucleation and growth. In the case of nucleation and growth it would be expected that there would be broad distribution of dispersed phase particle size with no characteristic length scale.

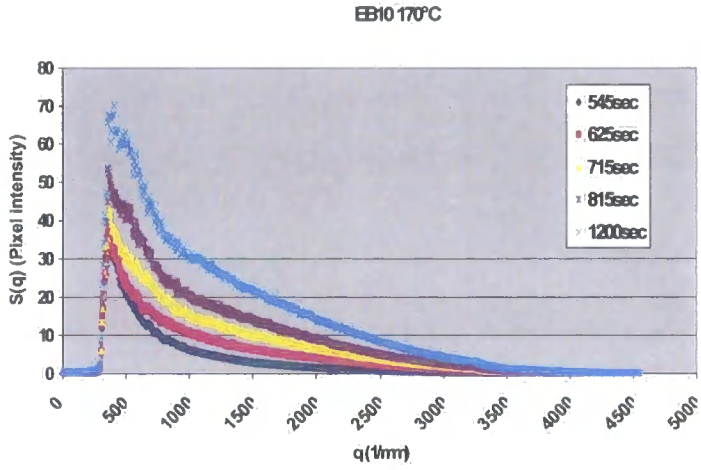

Graph 5.4.1.2 S(q) versus q for EB10 cured at 170°C. This scattering profile shows the tail end of a spinodal peak at low q.

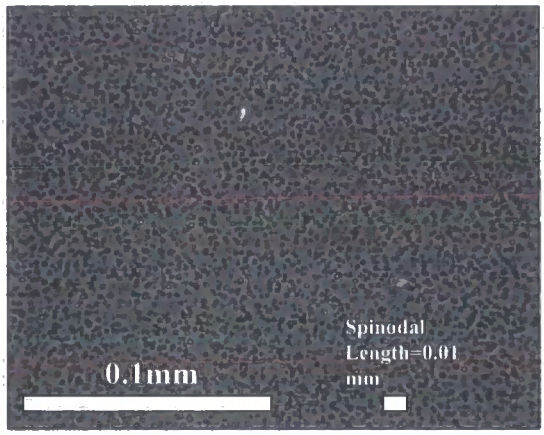

Figure 5.4.1.2 Optical micrograph of EB10 cured at 170°C. This shows a particulate morphology. The size of the dispersed particulates is very regular which suggest that the microstructure has formed by undergoing a percolation to cluster transformation. From SALS experiments this has an estimated spinodal length of approx 0.01mm

The graph 5.4.1.2 shows the S(q) versus q plot for EB10 cured at 170°C. This shows no obvious peak but may show the tail end of a spinodal peak occurring at a low q value. Unfortunately the peak occurred outside the q range used in the experiment. We can estimate that the peak may occur at a q value of approx 600 mm^{-1} which refers to a spinodal length of 0.0105 mm this is a larger spinodal length than that

observed in EB10 cured at 160°C. The figure 5.4.1.2 shows the optical micrograph of the fully cured EB10 sample cure at 170°C. This again shows a particulate morphology with a regular size distribution to the dispersed phase. This suggests that the morphology forms from a percolation to cluster transformation.

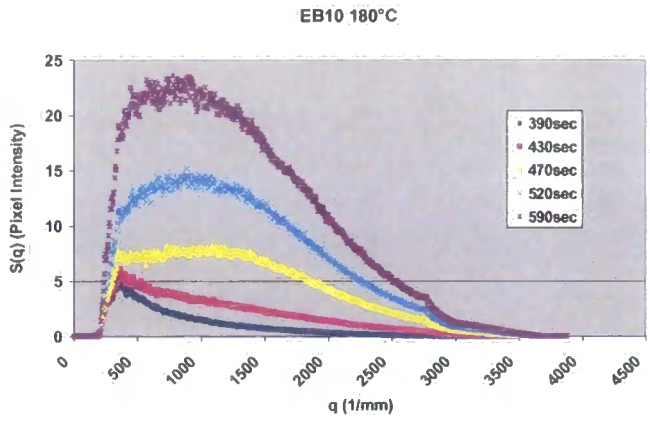

Graph 5.4.1.3 *S(q) versus q for EB10 cured at 180°C. This scattering profile shows a spinodal peak that develops as cure progresses.*

The Graph 5.4.1.3 above shows the S(q) versus q plot for EB10 cured at 180°C. This shows a broad spinodal peak occurring at a q value of around 1200 mm^{-1} after around 470 seconds into the cure cycle. This peak develops and slowly moves to a lower q value suggestion a coarsening of the morphology with time. The position of the peak after 590 seconds is at a q value of around 900 mm^{-1}, which corresponds to a spinodal length of 0.007 mm similar in size to, that observed in the EB10 system is cured at 160°C and 170°C. The optical micrograph of this morphology is shown in figure 5.4.1.3 below, this also shows a particulate morphology that suggests that this to has formed from a percolation to cluster transformation.

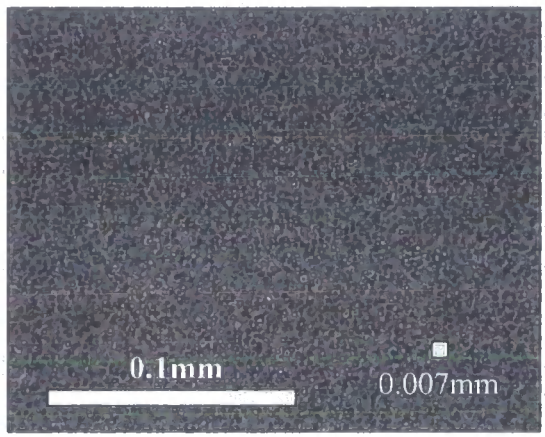

Figure 5.4.1.3 Optical micrograph of EB10 cured at 180°C. This shows a particulate morphology. The size of the dispersed particulates is very regular which suggest that the microstructure has formed by undergoing a PCT.

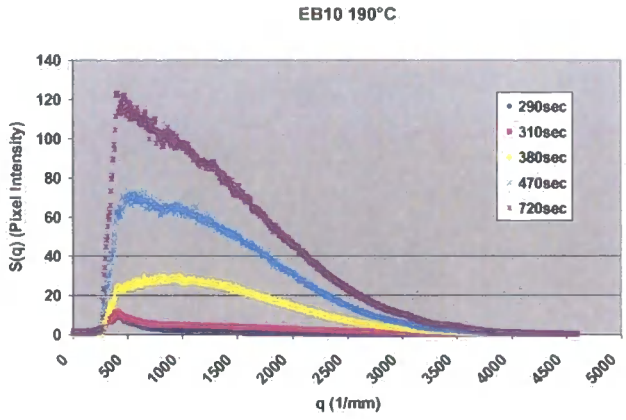

Graph 5.4.1.4 S(q) versus q for EB10 cured at 190°C. This shows the development of a spinodal peak that shifts to lower q as the cure progresses.

The graph 5.4.1.4 shows the S(q) versus q plot for EB10 cured at 190°C. This shows a broad spinodal peak occurring at a q value of around 1000 mm^{-1} after around 380 seconds into the cure cycle. This peak develops moves to a lower q value suggestion a coarsening of the morphology with time. The position of the peak after 720 seconds is at a q value of lower than 500 mm^{-1}. The optical micrograph of this morphology is shown in figure 5.4.1.4, this shows a particulate morphology that suggests that this has formed from a percolation to cluster transformation.

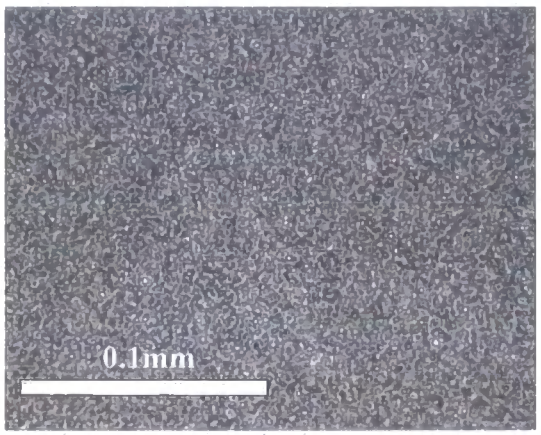

Figure 5.4.1.4 Optical micrograph of EB10 cured at 190°C. This shows a particulate morphology which has formed from a percolation to cluster transformation.

The graph 5.4.1.5 shows the S(q) versus q plot for EB10 cured at 200°C it shows a spinodal peak that forms at a q value of 700 mm^{-1} after approximately 175 seconds. This peak moves quickly to lower q and outside the range of the q range studied. The optical micrograph of this system is shown in figure 5.4.1.5 and shows a particulate morphology suggestion that this too has formed by a percolation to cluster transformation.

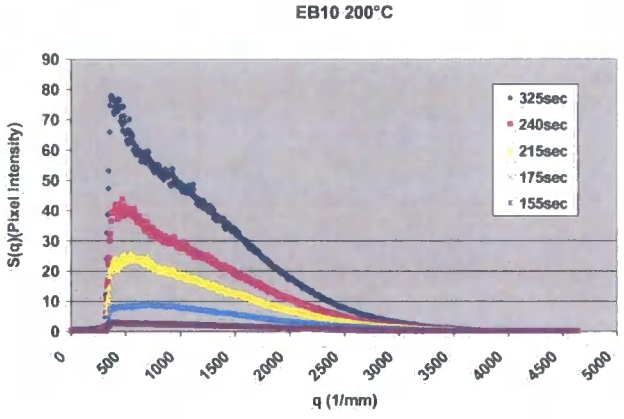

Graph 5.4.1.5 S(q) versus q for EB10 cured at 200°C. This shows the formation of a broad spinodal peak at low q that shifts to lower q as cure progresses.

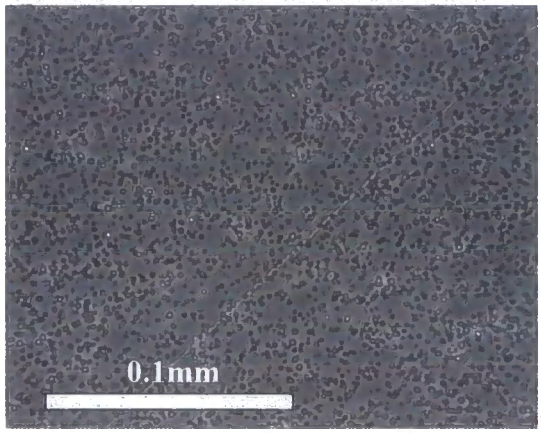

Figure 5.4.1.5 Optical micrograph of EB10 cured at 200 ℃. This shows a particulate morphology that has formed from a percolation to cluster transformation.

Graph 5.4.1.6 shows the S(q) versus q plot for EB10 cured at 210°C. This shows a broad spinodal peak that begins to form after 115 sec, which develops and shifts to lower q. There is evidence to suggest that this broad peak is composed of two separate peaks at different q values. After 360 seconds the broad peak has shifted to a q value outside the range of the experiment.

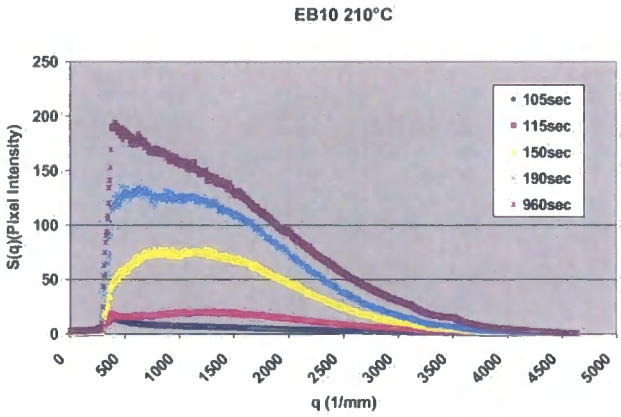

Graph 5.4.1.6 S(q) versus q for EB10 cured at 210°C. This scattering profile shows the formation of a broad spinodal peak that develops and shifts to lower q as the cure progresses.

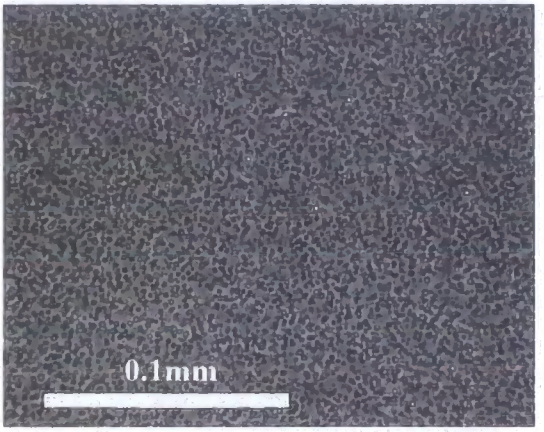

Figure 5.4.1.6 Optical micrograph of EB10 cured at 210°C. This shows a particulate morphology that has formed from a percolation to cluster transformation.

The graph 5.4.1.7 shows the S(q) versus q plot for EB10 cured at 220°C. This shows the formation of a spinodal peak that forms after approximately 80 seconds into the cure at a q value of around 500 mm-1. This peak shifts quickly to lower q and at the end of the experiment the peak position is outside the range of the experiment. Figure 5.4.1.7 shows the corresponding optical micrograph for EB10 cured at 220°C. This shows a particulate morphology that has formed from a percolation to cluster transformation.

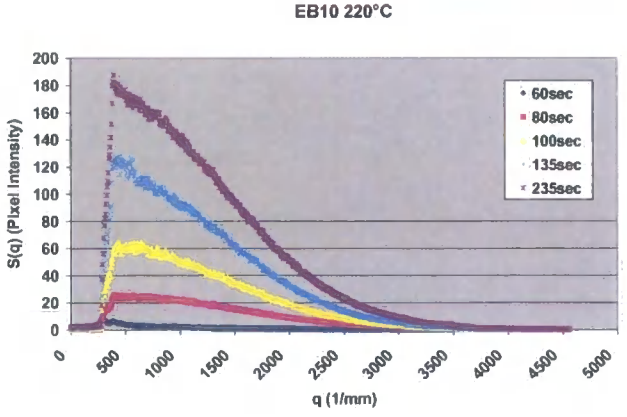

Graph 5.4.1.7 S(q) versus q for EB10 cured at 220°C. This scattering profile shows a spinodal peak that shifts to lower q as the cure progresses.

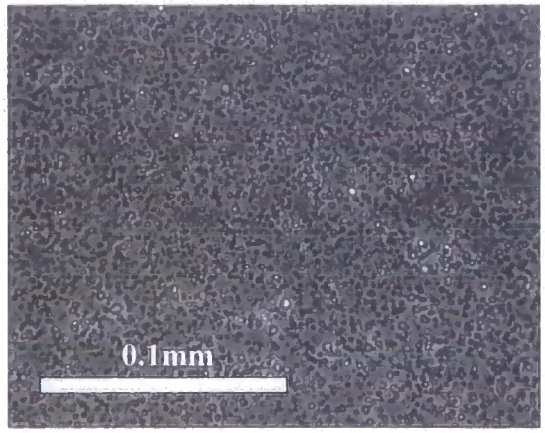

Figure 5.4.1.7 Optical micrograph of EB10 cured at 220℃ showing a particulate morphology that has formed from a percolation to cluster transformation

5.4.1.2 R(q) versus q data for EB10

R(q) versus q plots were obtained from the S(q) versus q data for the EB10 system cured at various isothermal cure temperatures. From this plot $R(q)_{max}$ and $q_{(max)}$ values were obtained. A typical R(q) versus q plot from this series is shown in graph 5.4.1.8. Table 5.4.1.2 documents the results from the EB10 system.

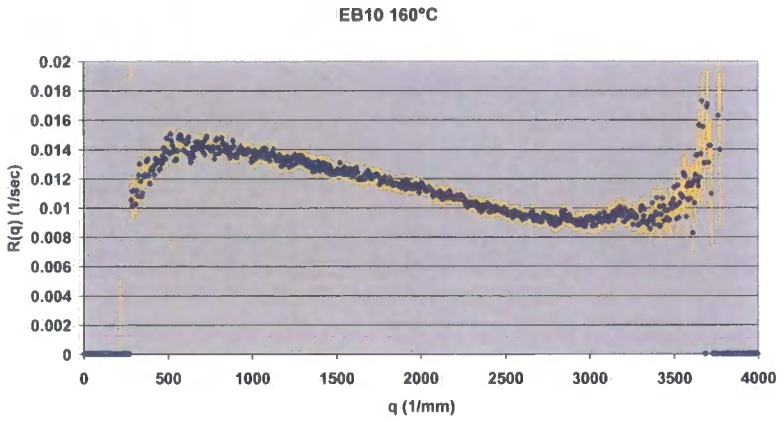

Graph 5.4.1.8 R(q) versus q for EB10 cured at 160°C. R(q) values were taken in between 790sec and 880sec into the cure.

EB10	160°C	170°C	180°C	190°C	200°C	210°C	220°C
$R(q)_{max}$ (sec^{-1})	0.0146		0.027	0.031	0.036	0.053	0.082
$q_{(max)}$ (mm^{-1})	610		1490	950	525	1500	1150

Table 5.4.1.2 R(q)max and q(max) values for EB10 cured at different isothermal temperatures.

5.4.2 Results for EB15

5.4.2.1 S(q) versus q Results for EB15

This section shows the S(q) versus q plots and optical micrographs obtained from the system EB15 cured isothermally at temperatures between 150°C and 220°C.

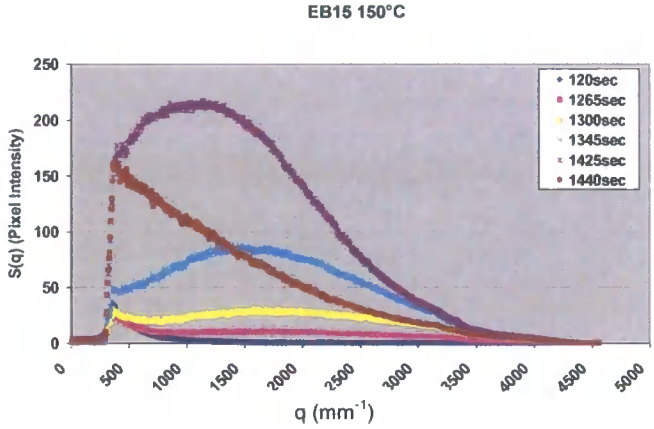

Graph 5.4.2.1 S(q) versus q for EB15 cured at 150°C. This scattering profile shows a broad spinodal peak that shifts to low q as the cure reaction progresses.

The graph 5.4.2.1 shows the S(q) versus q plot for EB15 cured at 150°C. This shows a well-defined spinodal peak that forms at around 1300 seconds at a q value of around 1900 mm^{-1}, this corresponds to a length scale of 0.003 mm. The peak develops and slowly moves to lower q values and after 1440 seconds into the cure the peak has shifted to a q value lower than 500 mm^{-1} and is outside the q range studied in this

experiment. In the early stages of the spinodal decomposition the peak position remains fairly constant.

Figure 5.4.2.1 shows the corresponding optical micrograph of EB15 cured at150°C. This shows a particulate morphology with wide distribution of dispersed particles. Due to the spinodal peak occurring in the light scattering trace from this sample this suggests that the morphology has formed from a percolation to cluster transformation.

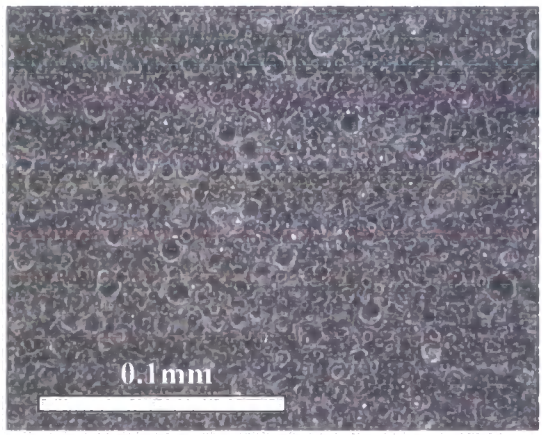

Figure 5.4.2.1 Optical micrograph of EB15 cured at 150°C. This shows a particulate morphology with a range of different particle sizes. The scattering profile from this sample shows a well-defined spinodal peak that suggests the morphology has formed by a percolation to cluster transformation.

The graph 5.4.2.2 shows the S(q) versus q plot for EB15 cured at 160°C. This shows a well defined spinodal peak that occurs at approximately 990 seconds at a q value of around 2100 mm^{-1} which corresponds to a length scale of 0.003 mm. This peak grows and shifts to lower q value as the cure progresses and after 2400 seconds the peak has shifted to a q value of around 600 mm^{-1} which corresponds to a length scale of 0.0105 mm. Although the peak shift position as cure progresses it remains relatively constant during the early stages of the spinodal decomposition.

The figure 5.4.2.2 shows the optical micrograph of EB15 cured at 160°C and this shows a particulate morphology that has formed from a percolation to cluster transformation.

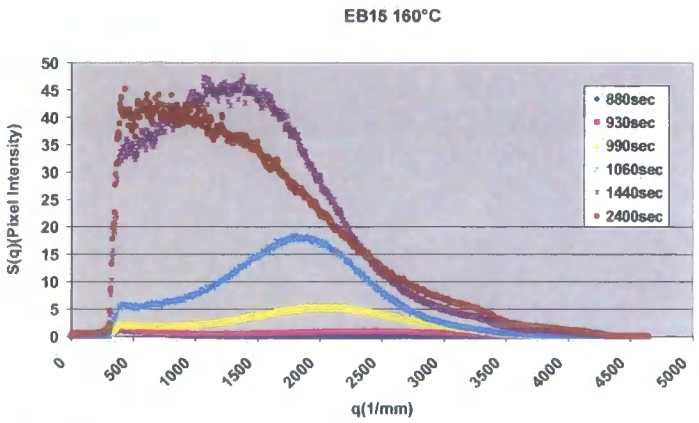

Graph 5.4.2.2 S(q) versus q for EB15 cured at 160°C. This scattering profile shows a broad spinodal peak that shifts to low q as the cure reaction progresses.

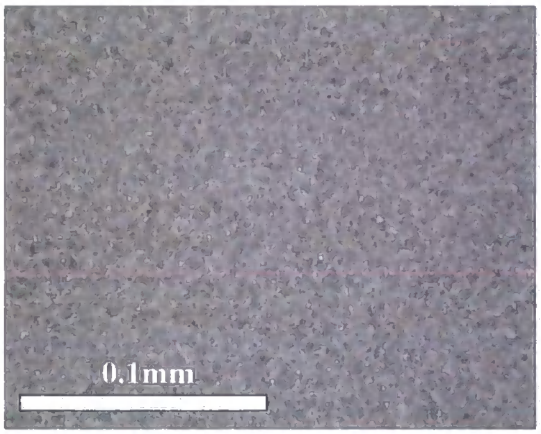

Figure 5.4.2.2 Optical micrograph of EB15 cured at 160°C. This shows a fine scale particulate morphology that has formed from a percolation to cluster transformation.

The graph 5.4.2.3 shows the S(q) versus q plot for EB15 cured at 170°C. This shows a well-defined spinodal peak that occurs at after approximately 600 seconds at a q value of around 2100 mm^{-1} that corresponds to a length scale of 0.003 mm. This peak grows and shifts to lower q value as the cure progresses and after 2400 seconds the peak has shifted to a q value of around 500 mm^{-1}, which corresponds to a length scale of 0.0126 mm. The peak begins to shift to lower q almost as soon as it forms and

there is only a limited region where the peak remains at a relatively constant q. Hence there is only a short period of early stage spinodal decomposition.

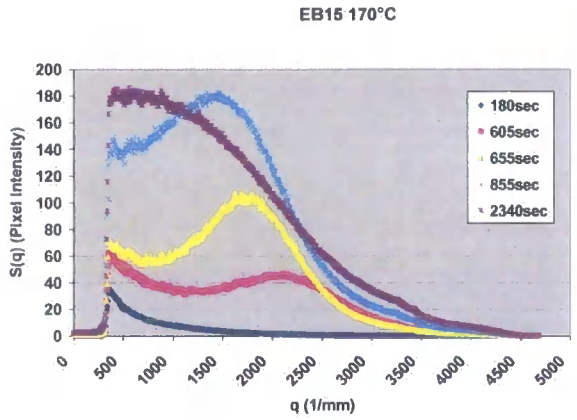

Graph 5.4.2.3 S(q) versus q for EB15 cured at 170°C. This scattering profile shows a well-defined spinodal peak that shifts to low q as the cure reaction progresses.

The Figure 5.4.2.3 shows the optical micrograph of EB15 cured at 170°C and this shows a particulate morphology that has formed from a percolation to cluster transformation.

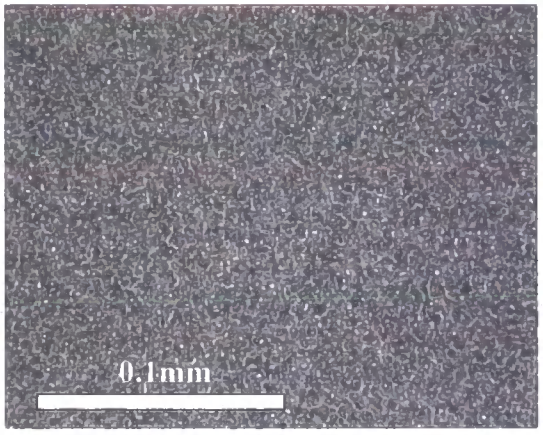

Figure 5.4.2.3 Optical micrograph of EB15 cured at 170°C. This shows a fine scale particulate morphology that has formed from a percolation to cluster transformation.

The Graph 5.4.2.4 shows the S(q) versus q plot for EB15 cured at 180°C. This shows a well-defined spinodal peak that occurs at after approximately 380 seconds at a q value of around 1750 mm^{-1} that corresponds to a length scale of 0.0036 mm

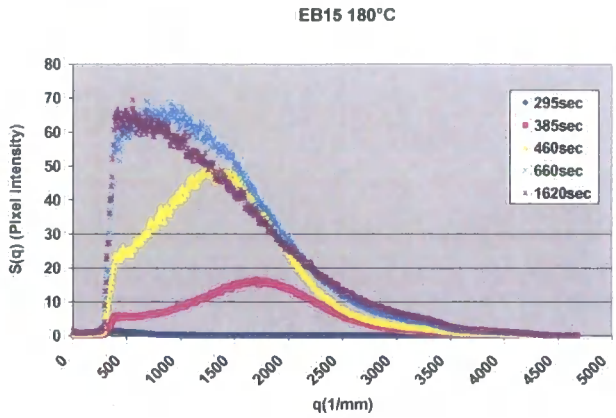

Graph 5.4.2.4 S(q) versus q for EB15 cured at 180°C. This scattering profile shows a broad spinodal peak that shifts to low q as the cure reaction progresses.

This peak grows and shifts to lower q value as the cure progresses and after 1620 seconds the peak has shifted to a q value less than 500 mm^{-1} outside of the q range of the experiment. The peak begins to shift to lower q almost as soon as it forms and there is only a limited region where the peak remains at a relatively constant q. Hence there is only a short period of early stage spinodal decomposition.

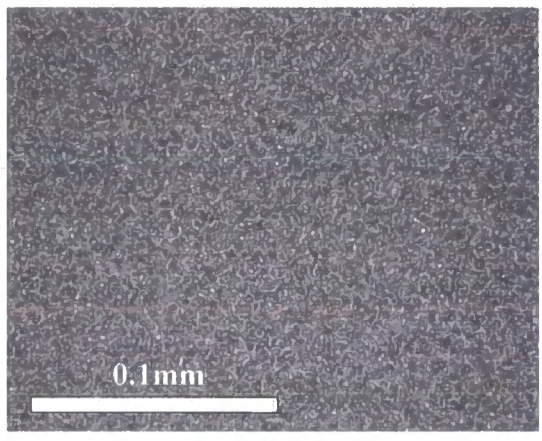

Figure 5.4.2.4 Optical Micrograph of EB15 cured at 180°C. This shows a fine scale particulate morphology.

Figure 5.4.2.4 shows the optical micrograph of EB15 cured at 180°C. This shows a fine scale particulate morphology that has formed by a percolation to cluster transformation.

The Graph 5.4.2.5 shows the S(q) versus q plot for EB15 cured at 190°C. This shows a well-defined spinodal peak that occurs at after approximately 255 seconds at a q value of around 2500 mm^{-1} that corresponds to a length scale of 0.0025 mm. This peak grows rapidly and shifts to lower q value as the cure progresses and after 430 seconds the peak has shifted to a q value less than 500 mm^{-1} outside of the q range of the experiment. The intensity of the peak rapidly falls off between 420 sec and 430 sec this may correspond to the percolation to cluster transformation occurring. The peak begins to shift to lower q almost as soon as it forms and there is only a limited region where the peak remains at a relatively constant q. Hence there is only a short period of early stage spinodal decomposition.

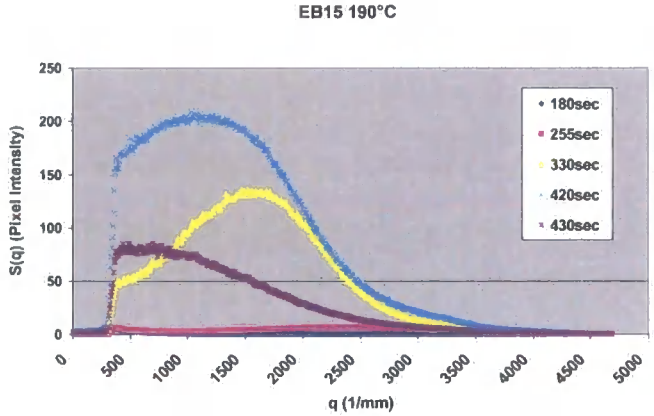

Graph 5.4.2.5 *S(q) versus q for EB15 cured at 190°C. This scattering profile shows a broad spinodal peak that shifts to low q as the cure reaction progresses.*

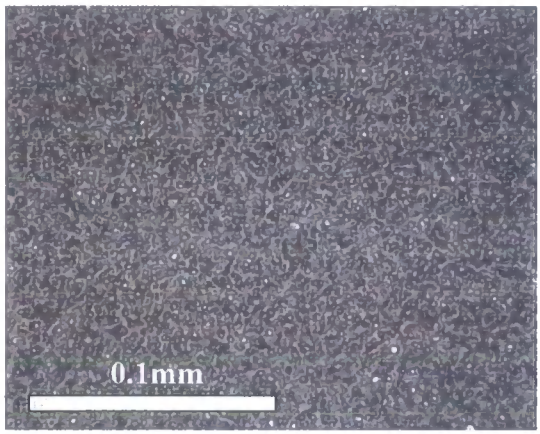

Figure 5.4.2.5 Optical micrograph of EB15 cured at 190°C. This shows a fine scale particulate morphology that has formed from a percolation to cluster transformation

The Graph 5.4.2.6 shows the S(q) versus q plot for EB15 cured at 200°C. This

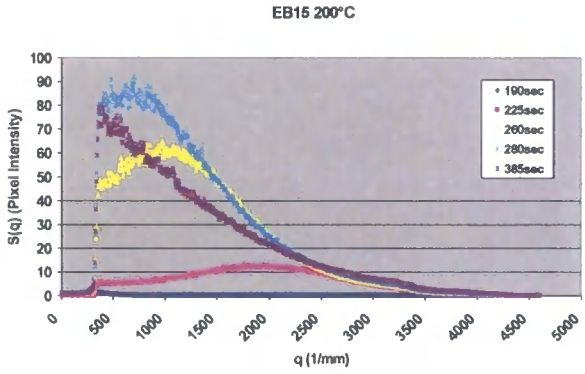

Graph 5.4.2.6 S(q) versus q for EB15 cured at 200°C. This scattering profile shows a broad spinodal peak that shifts to low q as the cure reaction progresses

shows a well-defined spinodal peak that occurs at after approximately 225 seconds at a q value of around 2000 mm^{-1} that corresponds to a length scale of 0.00315 mm. This peak grows rapidly and shifts to lower q value as the cure progresses and after 385 seconds the peak has shifted to a q value less than 500 mm^{-1} outside of the q range of the experiment. The peak begins to shift to lower q almost as soon as it forms and there is only a limited region where the peak remains at a relatively constant q. Hence there is only a short period of early stage spinodal decomposition.

Figure 5.4.2.6 shows the corresponding optical micrograph of EB15 cured at 200°C. This shows a particulate morphology that has formed by a percolation to cluster transformation. The size of the dispersed phase is noticeably larger than in the case of EB15 cured at temperatures below 200°C. This may be due to changes in the surface energy, γ , between the two phases at higher temperatures.

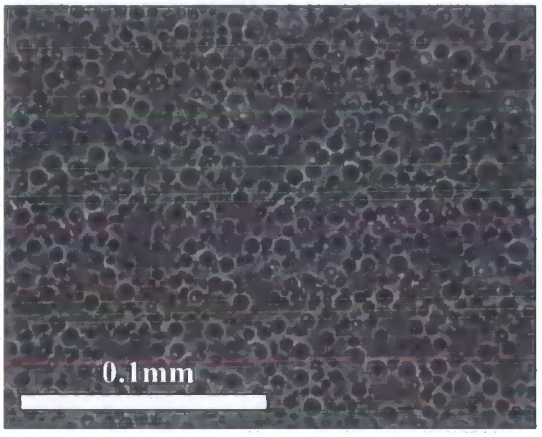

Figure 5.4.2.6 Optical micrograph of EB15 cured at 200°C. This shows a particulate morphology that has formed from a percolation to cluster transformation.

The Graph 5.4.2.7 shows the S(q) versus q plot for EB15 cured at 210°C. This shows a broad spinodal peak that occurs at after approximately 170 seconds at a q

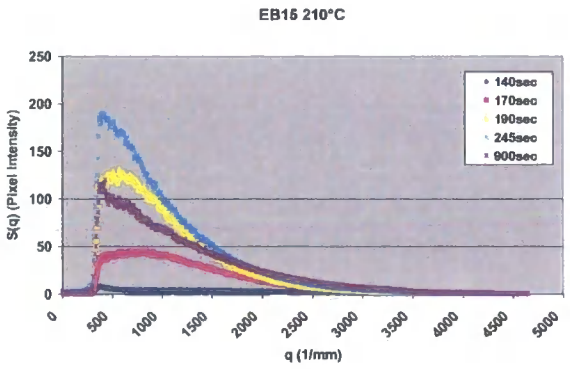

Graph 5.4.2.7 S(q) versus q for EB15 cured at 210°C. This scattering profile shows a broad spinodal peak that shifts to low q as the cure reaction progresses

value of around 800 mm^{-1} that corresponds to a length scale of 0.0079 mm. This peak grows rapidly and shifts to lower q value as the cure progresses and after 245 seconds the peak has shifted to a q value less than 500 mm^{-1} outside of the q range of the

experiment. The peak begins to shift to lower q almost as soon as it forms and there is only a limited region where the peak remains at a relatively constant q. Hence there is only a short period of early stage spinodal decomposition.

Figure 5.4.2.7 shows the corresponding optical micrograph of EB15 cured at 210°C. This shows a particulate morphology that has formed by a percolation to cluster transformation. The size of the dispersed phase is noticeably larger than in the case of EB15 cured at temperatures below 200°C.

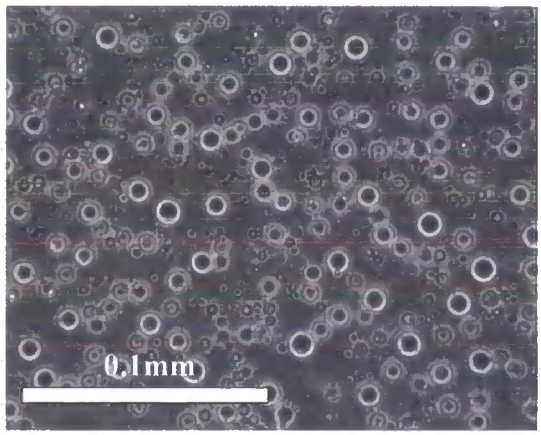

Figure 5.4.2.7 Optical micrograph of EB15 cured at 210°C. This shows a particulate morphology that has formed from a percolation to cluster transformation. Also in this micrograph there is evidence of the dispersed particles clustering together in lines suggesting that this has formed from the break up of a continuous network.

The Graph 5.4.2.8 shows the S(q) versus q plot for EB15 cured at 220°C

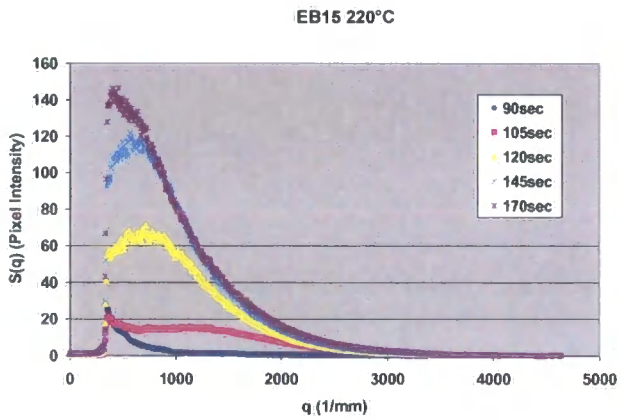

Graph 5.4.2.8 S(q) versus q for EB15 cured at 210°C. This scattering profile shows a broad spinodal peak that shifts to low q as the cure reaction progresses

This shows a well-defined spinodal peak that occurs at after approximately 105 seconds at a q value of around 1400 mm^{-1} that corresponds to a length scale of 0.0045 mm. This peak grows rapidly and shifts to lower q value as the cure progresses and after 245 seconds the peak has shifted to a q value less than 500 mm^{-1} outside of the q range of the experiment. The peak begins to shift to lower q almost as soon as it forms and there is only a limited region where the peak remains at a relatively constant q. Hence there is only a short period of early stage spinodal decomposition. Figure 5.4.2.8 shows the corresponding optical micrograph of EB15 cured at 220°C. This shows a particulate morphology that has formed by a percolation to cluster transformation.

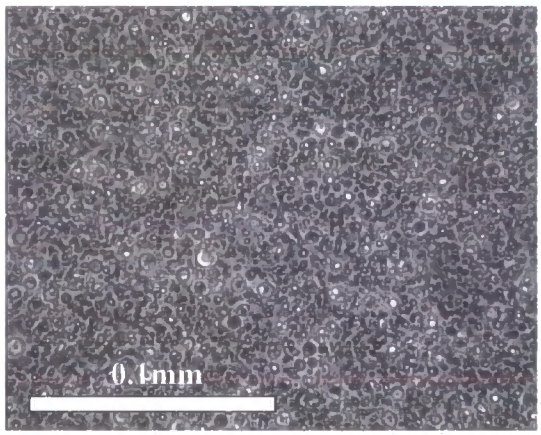

Figure 5.4.2.8 Optical micrograph of EB15 cured at 220°C. This shows a particulate morphology that has formed from a percolation to cluster transformation.

5.4.2.2 R(q) versus q plots for EB15

R(q) versus q plots were obtained for the EB15 system cured isothermally at temperatures between 150°C and 220°C. The R(q) values were obtained for the early stages of the spinodal decomposition process. These plots had a well defined peak from which a $R(q)_{max}$ and $q_{(max)}$ value could be obtained. A typical example a R(q) versus q plot for the EB15 system is shown in graph 5.4.2.9.

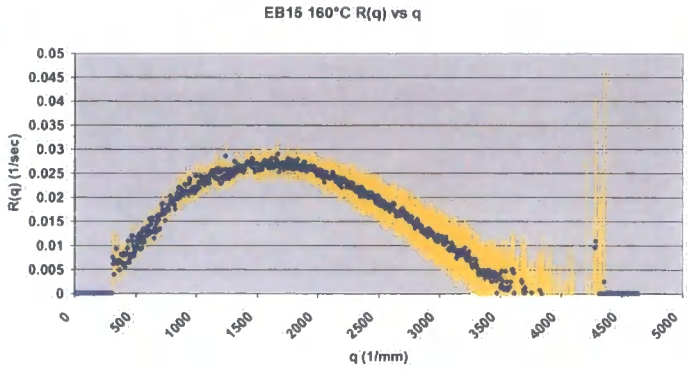

Graph 5.4.2.9 R(q) versus q for EB15 cured at 160°C. R(q) values were taken between 950sec and 990sec into the cure.

Table 5.4.2.2 below documents the $R(q)_{max}$ and $q_{(max)}$ values from the EB15 system.

EB15	**150°C**	**160°C**	**170°C**	**180°C**	**190°C**	**200°C**	**210°C**	**220°C**
$R(q)_{max}$ (sec^{-1})	0.029	0.027	0.05	0.086	0.124	0.31	0.08	0.15
$q_{(max)}$ (mm^{-1})	1500	1600	2450	1700	2100	1400	1000	1100

Table 5.4.2.2 $R(q)_{max}$ and $q_{(max)}$ values for EB10 cured at different isothermal temperatures.

The graph 5.4.2.9 shows the $R(q)_{max}$ of phase separation versus cure temperature for EB15

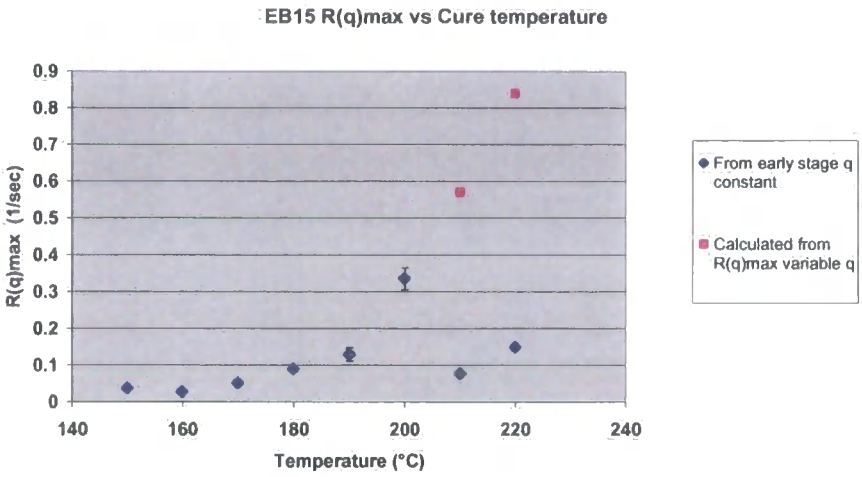

Graph 5.4.2.10 This graph shows the relationship between $R(q)_{max}$ and cure temperature for EB15.

The graph 5.4.2.9 above shows the relationship between $R(q)_{max}$ and cure temperature for EB15. If $R(q)_{max}$ values are taken from the early stages of the spinodal decomposition then at higher temperatures above 200°C the calculated value for R(q) is lower than expected. The reason for this is that above 200°C the position of the spinodal peak shifts rapidly to lower q. If the Rate is calculated from the $R(q)_{max}$ with shifting q then the rates at higher temperatures become greater and more in line with expected values (pink points on the chart). Above 200°C there is a rapid increase in the rate of phase separation perhaps due to the PES:PEES thermoplastic being above its Tg.

5.4.2.3 R(q)/q² versus q² results for EB15

Plots of $R(q)/q^2$ versus q^2 were obtained for EB15 cured isothermally at different temperatures. From Cahn-Hilliard theory outlined in Chapter 2 these should be straight lines with a clear intercept on the y axis. This is not the case for these plots due to the non-linear nature of the spinodal decomposition in these reactive blends.

Extrapolations have been made to extract a D^*_{app} value. The graph 5.4.2.10 below shows a typical example of a $R(q)/q^2$ versus q^2 plot from this series. This shows how extrapolations were taken.

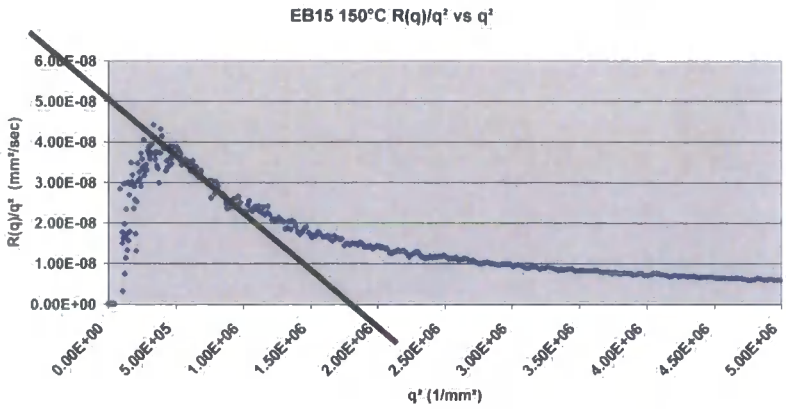

Graph 5.4.2.11 $R(q)/q^2$ versus q^2 for EB15 cured at 150°C

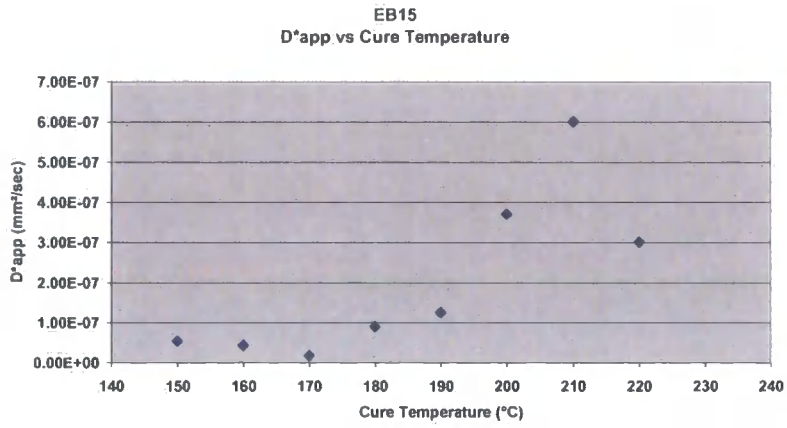

Graph 5.4.2.12 Apparent Diffusion coefficient D^*_{app} versus cure temperature for EB15. This shows rapidly increasing D^*_{app} with increasing cure temperature.

The graph 5.4.2.11 shows the apparent diffusion coefficient D^*_{app} versus cure temperature for EB15. This shows a rapidly increasing D^*_{app} above isothermal cure temperature of 190°C which may be as a result of the Tg of the thermoplastic polymer. The general upwards trend of the D^*_{app} with temperature suggests LCST.

5.4.2.4 DSC results from EB15

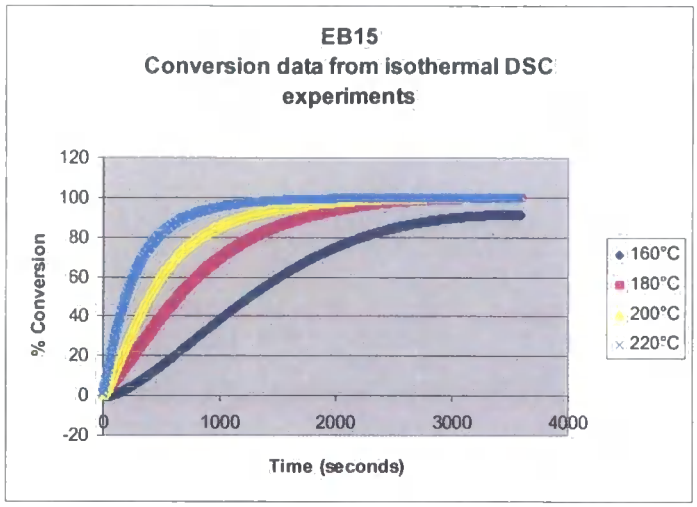

Graph 5.4.2.13 *This graph shows the % conversion versus cure time for EB15 cured at different temperatures. This data was obtained from isothermal DSC experiments.*

The DSC data shown in Graph 5.4.2.12 above shows how the % conversion varies with time at different cure temperatures. It can be seen that at a cure temperature of 160°C full conversion is not achieved after 3500 seconds.

5.4.2.5 Time to onset of phase separation for different isothermal cure temperatures for EB15

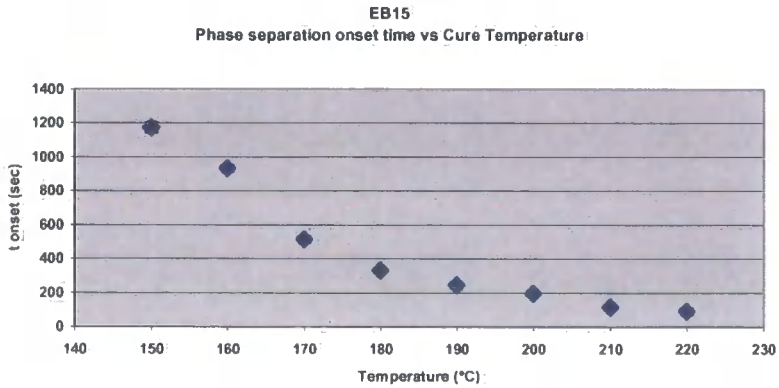

Graph 5.4.2.14 *Time to onset of phase separation versus cure temperature for EB15.*

Graph 5.4.2.13 above shows the relationship between the time to onset of phase separation for different isothermal cure temperatures. This information is obtained from the SALS experiments and shows decreasing onset time with higher cure temperatures

5.4.2.6 Conversion at the onset of phase separation versus Cure Temperature for EB15

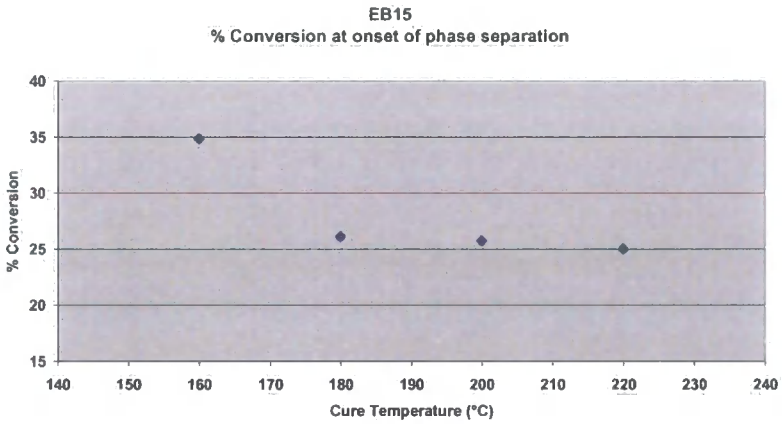

Graph 5.4.2.15 Graph showing the % conversion at the onset of phase separation for different isothermal cure temperatures for EB15. This shows falling % conversion at phase separation with increasing temperature suggesting LCST behaviour.

The graph 5.4.2.14 above shows the % conversion at the onset of phase separation for different isothermal cure temperatures. This information is obtained from a combination of SALS and DSC experimentation. It clearly shows that as temperature increases the level of conversion needed to drive the system to phase separate is reduced. Therefore as temperature increases the system has a greater tendency to phase separate. This suggests that the system exhibits lower critical solution temperature (LCST).

5.4.3 Results for EB20

5.4.3.1 SALS S(q) versus q Results for EB20

This section shows the S(q) versus q plots and optical micrographs obtained from SALS experiments for the system EB20 cured isothermally at temperatures between 160°C and 220°C.

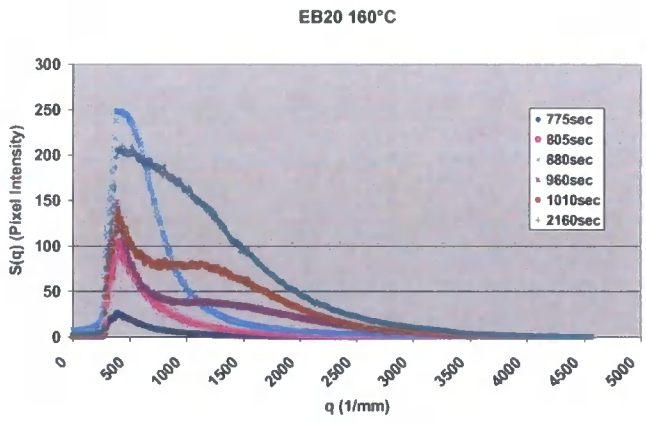

Graph 5.4.3.1 S(q) versus q for EB20cured at 160°C. This scattering profile shows two spinodal peaks. A primary spinodal peak begins to form after 775 seconds at low q, this develops and shifts to lower q. At 960 seconds into the cure a second spinodal peak forms at a q value of 1500 mm^{-1}. This secondary peak also shifts to lower q as the cure progresses.

The Graph 5.4.3.1 above shows the S(q) versus q plot for EB20 cured at 160°C. This shows the formation of a primary spinodal peak that occurs at a low q after approximately 775 seconds. As the cure progresses a secondary spinodal peak forms at a q value of around 1500 mm^{-1} that corresponds to a length scale of 0.0042 mm. This peak grows and shifts to a lower q value as the cure progresses and after 2160 seconds the peak has shifted to a q value less than 500 mm^{-1} outside of the q range of the experiment. This double spinodal peak behaviour has previous been observed by Alig et al in both reactive thermoplastic-thermoset blends and also in non reactive thermoplastic-thermoplastic blends quenched from the melt into the unstable region of the phase diagram [7]. Figures 5.4.3.1 and 5.4.3.2 show the corresponding optical micrographs of EB20 cured at 160°C.

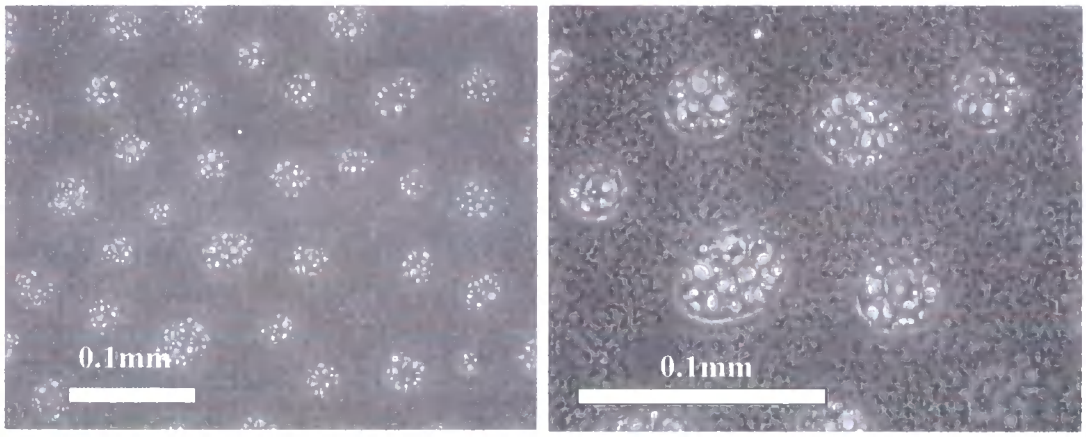

Figure 5.4.3.1 Optical micrographs of EB20 cured at 160℃. This morphology shows large discontinuous particles inside of which are particles from a secondary phase separation. The continuous phase also has small-scale dispersed particles resulting from a secondary phase separation.

The micrographs shown in figures 5.4.3.1 show the morphology of EB20 cured at 160°C. This shows a discontinuous phase that contains secondary particles that have resulted from secondary phase separation. Also the continuous phase has secondary phase separation discontinuous particles. It is likely that this morphology has arisen from primary and secondary spinodal decompositions occurring followed by percolation to cluster transformations. In figure 5.4.3.1 it can be seen that around the larger scale dispersed phase there is a region of the continuous phase that is relatively free from any secondary dispersed particles. This may have resulted during the percolation to cluster transformation occurring of the primary spinodal decomposition structure. As the primary spinodal decomposition continuous phase has become discontinuous it has left a region depleted in secondary phase separated particles in the continuous phase.

Graph 5.4.3.2 shows the S(q) versus q plot for EB20 cured at 170°C. This shows the formation of a primary spinodal peak that occurs at a low q after approximately 990 seconds

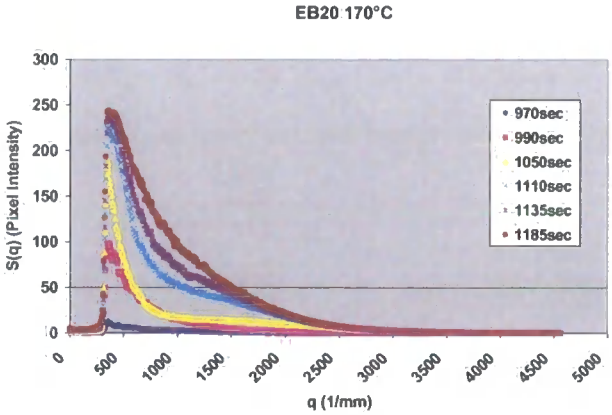

Graph 5.4.3.2 *S(q) versus q for EB20cured at 170°C. . This scattering profile shows two spinodal peaks. A primary spinodal peak begins to form after 990 seconds at low q, this develops and shifts to lower q. At 1110 seconds into the cure a second spinodal peak forms at a q value of 1500 mm-1.*

As the cure progresses a secondary spinodal peak forms at a q value of around 1500 mm^{-1} that corresponds to a length scale of 0.0042 mm. This peak grows and shifts to a lower q value as the cure progresses. Figure 5.4.3.2 shows the corresponding optical micrographs of EB20 cured at 170°C. This shows a similar morphology as that seen in EB20 cured at 160°C, this has arisen as a result of primary and secondary phase separation occurring followed by percolation to cluster transformations. The larger scale particles have formed as a result of the percolation to cluster transformation from the first spinodal peak occurring at low q in the S(q) versus q plot from the light scattering. The continuous phase has particulate sub-inclusions that have probably resulted from a percolation to cluster transformation from the secondary peak observed in the light scattering results.

The large dispersed phase also contains small scale sub-inclusion particles that have resulted from a percolation to cluster transformation from the secondary spinodal decomposition observed in the light scattering S(q) versus q plot.

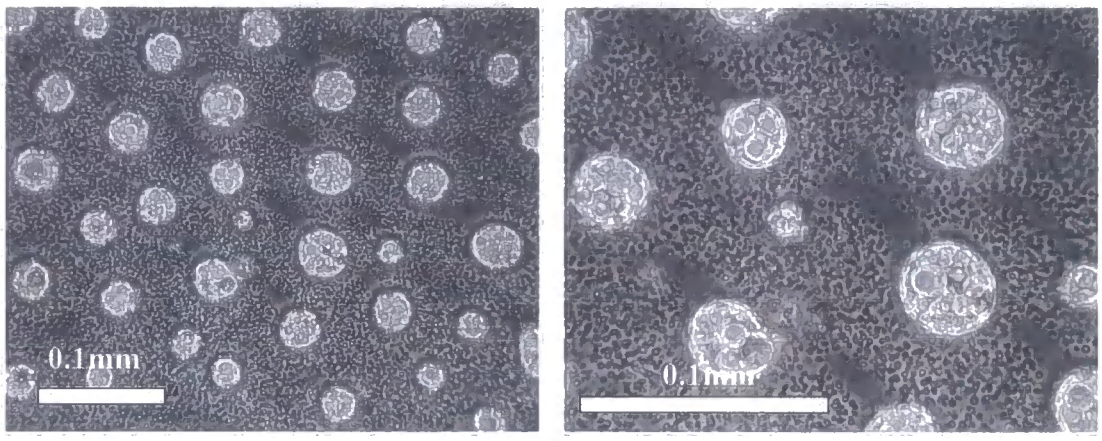

Figure 5.4.3.2 Optical micrographs of EB20 cured at 170°C. This morphology shows large discontinuous particles inside of which are smaller particles from a secondary phase separation. The continuous phase also has small-scale dispersed particles resulting from a secondary phase separation. This is likely to be the result of primary and secondary spinodal decompositions followed by percolation to cluster transformations.

Graph 5.4.3.3 shows the S(q) versus q plot for EB20 cured at 180°C. This shows the formation of a primary spinodal peak that occurs at a low q after approximately 450 seconds. As the cure progresses a secondary spinodal peak forms at a q value of

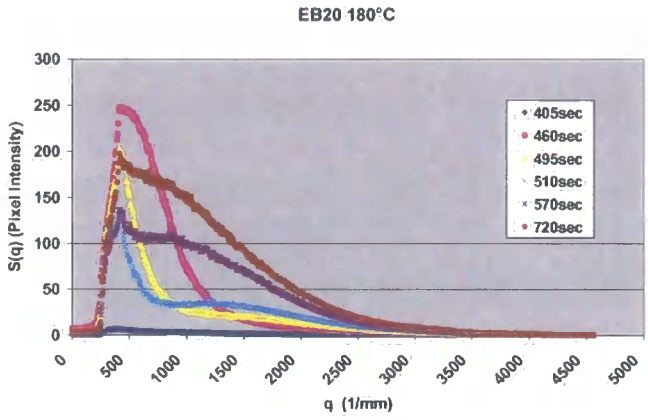

Graph 5.4.3.3 S(q) versus q for EB20 cured at 180°C.. This scattering profile shows two spinodal peaks. A primary spinodal peak begins to form after 410 seconds at low q, this develops and shifts to lower q. At 510 seconds into the cure a second spinodal peak forms at a q value of 1500 mm-1

around 1500 mm^{-1} that corresponds to a length scale of 0.0042 mm. This peak grows and shifts to a lower q value as the cure progresses. Figure 5.4.3.3 show the corresponding optical micrographs of EB20 cured at 180°C. This shows a morphology that has probably resulted from percolation to cluster transformation occurring from the two spinodal decompositions observed in the light scattering

profile from this sample. Within the large scale dispersed phase there appears to be one large sub-included particle surrounded by small secondary sub-included particles of a different composition. This structure is probably formed by a secondary percolation to cluster transformation. The continuous phase also contains a small-scale particulate phase likely to have resulted from secondary percolation to cluster transformation.

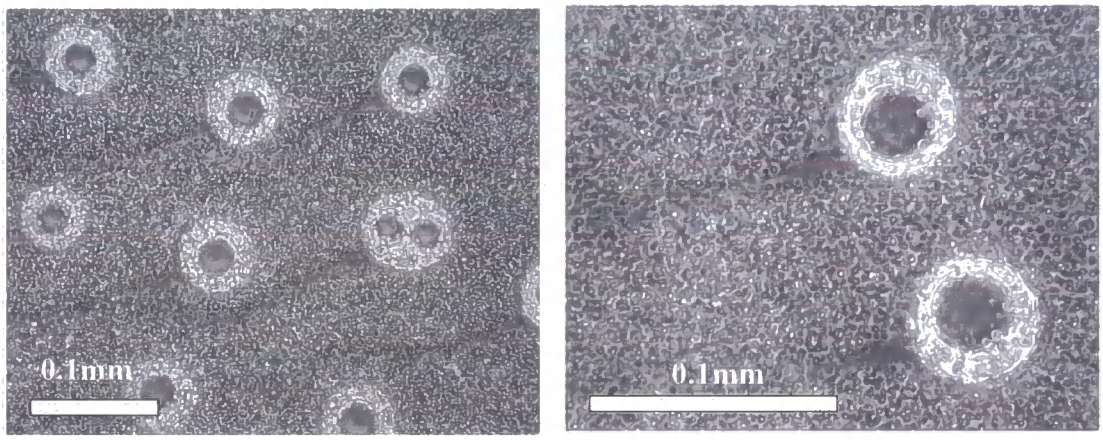

Figure 5.4.3.3 Optical micrograph of EB20 cured at 180 °C. This morphology shows large discontinuous particles inside of which are two different types of particles resulting from a secondary phase separation. The continuous phase also has small-scale dispersed particles resulting from a secondary phase separation. This is likely to be the result of primary and secondary spinodal decompositions followed by percolation to cluster transformations occurring.

Graph 5.4.3.4 shows the S(q) versus q plot for EB20 cured at 190°C. This shows the formation of a primary spinodal peak that occurs at a low q after approximately 255 seconds. As the cure progresses a secondary spinodal peak forms

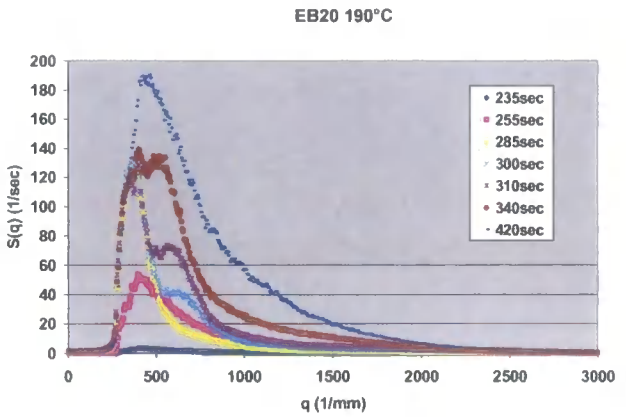

Graph 5.4.3.4 S(q) versus q for EB20 cured at 190°C. .. This scattering profile shows two spinodal peaks. A primary spinodal peak begins to form after 235 seconds at low q, this develops and shifts to lower q. At 255 seconds into the cure a second spinodal peak forms at a q value of 750 mm^{-1}

at a q value of around 700 mm^{-1} that corresponds to a length scale of 0.009 mm. This peak grows and slowly shifts to a lower q value as the cure progresses. Figures 5.4.3.4 below show the corresponding optical micrographs of EB20 cured at 190°C. These show a similar morphology to that seen in EB20 cured at temperatures below 190°C. This morphology is likely to occur due to primary and secondary spinodal percolation to cluster transformations occurring.

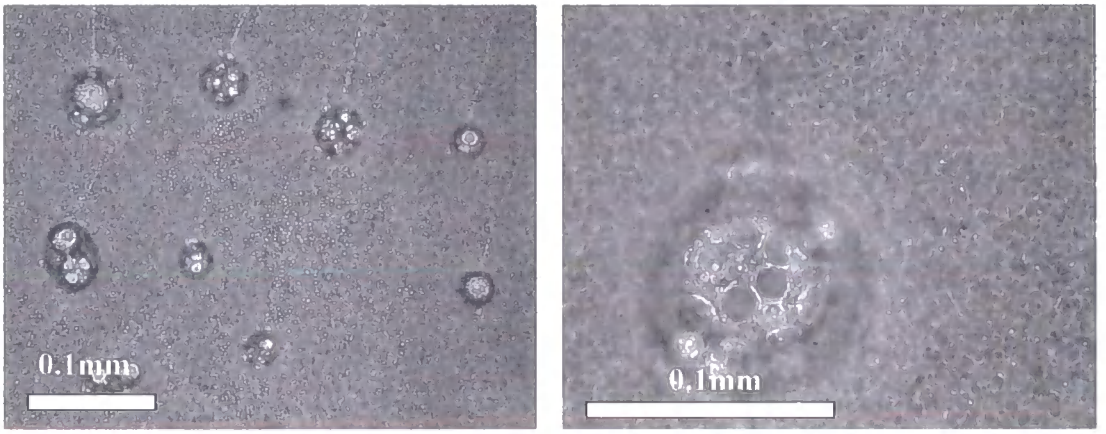

Figure 5.4.3.4 Optical micrographs of EB20 cured at 190°C. This morphology shows large discontinuous particles inside of which are two different phases resulting from a secondary phase separation. The continuous phase also has small-scale dispersed particles resulting from a secondary phase separation.

Graph 5.4.3.5 shows the S(q) versus q plot for EB20 cured at 200°C. This shows the formation of a primary spinodal peak that occurs at a low q after approximately 165 seconds. As the cure progresses a secondary spinodal peak forms

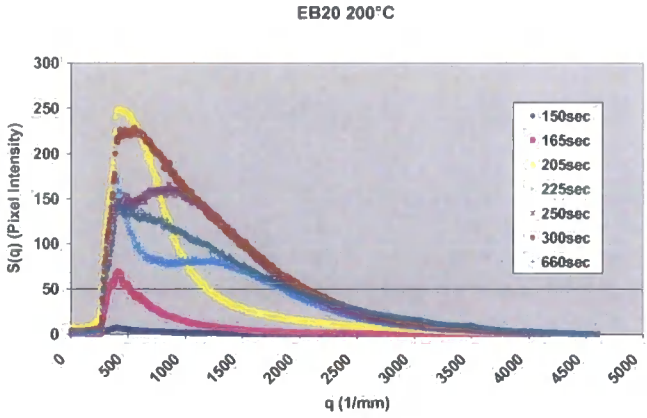

Graph 5.4.3.5 *S(q) versus q for EB20 cured at 200°C. This scattering profile shows two spinodal peaks. A primary spinodal peak begins to form after 165 seconds at low q, this develops and shifts to lower q. After 255 seconds into the cure a second spinodal peak forms at a q value of 1400 mm^{-1}, this peak shifts to lower q as the cure progresses*

at a q value of around 1500 mm^{-1} that corresponds to a length scale of 0.0042 mm. This peak grows and shifts to a lower q value as the cure progresses. Figures 5.4.3.5 below show the corresponding optical micrographs of EB20 cured at 200°C. This shows a morphology that has probably resulted from percolation to cluster transformation occurring from the two spinodal decompositions observed in the light scattering profile from this sample. The larger scale dispersed phase is less well defined in this sample it appears as if the primary dispersed phases have merged with the continuous phase resulting in fuzzy boundary between the phases.

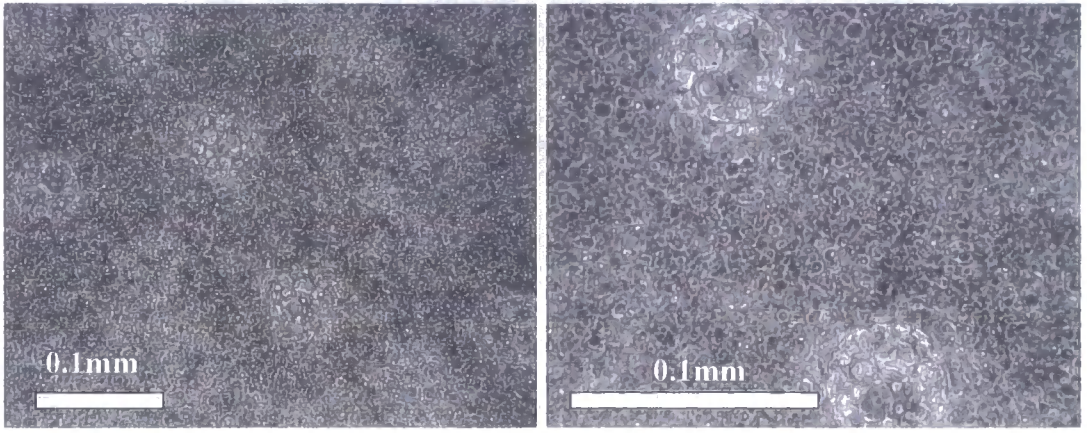

Figure 5.4.3.5 Optical micrographs of EB20 cured at 200℃. This morphology shows evidence of larger discontinuous particles inside of which are sub-included particles resulting from a secondary phase separation. These larger scale particles have a diffuse interface with the continuous phase which may suggest that they are beginning to merge with the continuous phase. The continuous phase also has small-scale dispersed particles resulting from a secondary phase separation.

Graph 5.4.3.6 shows the S(q) versus q plot for EB20 cured at 210°C. This shows the formation of a primary spinodal peak that occurs at a low q after approximately 125 seconds. As the cure progresses a secondary spinodal peak forms after 160 seconds at a q value of around 1500 mm^{-1} that corresponds to a length scale of 0.0042 mm. This peak grows and shifts to a lower q value as the cure progresses however after 900 seconds there is no evidence of any peak in the curve suggesting that the order resulting from spinodal decomposition has been lost.

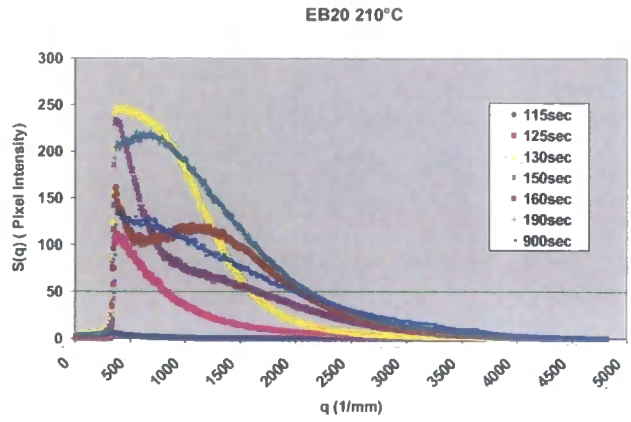

Graph 5.4.3.6 *S(q) versus q for EB20 cured at 210°C. . This scattering profile shows two spinodal peaks. A primary spinodal peak begins to form after 120 s, this develops and shifts to lower q. After 160 seconds a second spinodal peak forms, this peak also shifts to lower q as the cure progresses.*

Figure 5.4.3.6 shows the optical micrograph of EB10 cured at 210°C. This shows a fine scale particulate morphology, which has no evidence of any order resulting from a spinodal decomposition. Because the S(q) versus q plot from SALS experiment shown in graph 5.4.3.6 above clearly has two spinodal peaks it is postulated that this morphology has formed from primary and secondary spinodal percolation to cluster transformations followed by dissolution of the primary structure. This has resulted in a small scale particulate morphology with no long range order associated with spinodal decomposition.

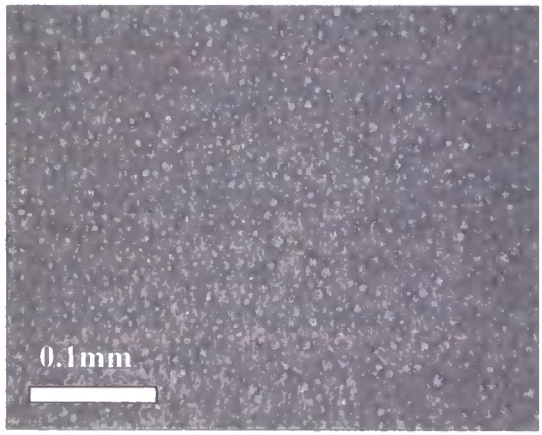

Figure 5.4.3.6 Optical micrograph of EB20 cured at 210C. This shows a small scale particulate morphology that has formed from primary and secondary percolation to cluster transformation followed by complete dissolution of the primary structure.

5.4.3.2 R(q) versus q data for EB20

This section reports the R(q) vs q data from the light scattering traces from EB20 cured at different isothermal temperatures. Because the S(q) versus q plots for EB20 show two spinodal peaks R(q) vs q plots were taken at two different times into the cure to capture the initial formation of each of the spinodal peaks. This allows $R(q)_{max}$ and D^*_{app} to be calculated for each spinodal decomposition occurring during cure. Because of the dynamic nature of the phase separation process occurring in these systems and the shifting q_{max} associated with the spinodal decomposition it is often difficult to obtain a single peak in the R(q) vs q plot. The graphs 5.4.3.7 and 5.4.3.8 show examples of R(q) versus q plots for both primary and secondary spinodal decomposition processes.

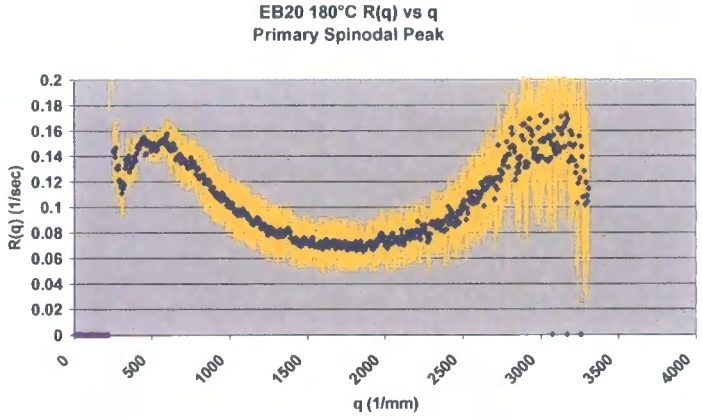

Graph 5.4.3.7 R(q) versus q for EB20 cured at 180°C for Primary spinodal peak. R(q) values were taken between 405sec and 420sec.

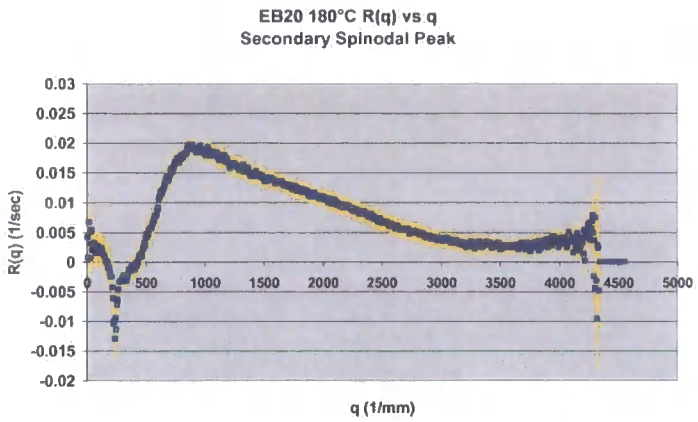

Graph 5.4.3.8 *R(q) versus q for EB20 cured at 180°C for Secondary spinodal peak. R(q) values were taken between 500sec and 570sec. This shows a well defined peak for the secondary phase separation.*

Table 5.4.3.1 below documents the $R(q)_{max}$ and $q_{(max)}$ values from the EB20 system.

EB20	**160°C**	**170°C**	**180°C**	**190°C**	**200°C**	**210°C**
Primary $R(q)_{max}$ (sec^{-1})	0.042	0.12	0.15	0.16	0.15	0.35
$q_{(max)}$ (mm^{-1})	500	350	500	300	700	1200
Secondary $R(q)_{max}$ (sec^{-1})	0.011	0.015	0.019	0.036	0.042	0.06
$q_{(max)}$ (mm^{-1})	1000	900	950	1400	1400	1400

Table 5.4.3.1 *$R(q)_{max}$ and $q_{(max)}$ values for EB20 cured at different isothermal temperatures.*

$R(q)_{max}$ versus cure temperature for EB20 for both primary and secondary phase separation processes is shown in graph 5.4.3.9. The rate of phase separation increases

with increasing temperature for both primary and secondary phase separations. Once again there is a rapid increase rate above 200°C that may correspond to the Tg of the thermoplastic

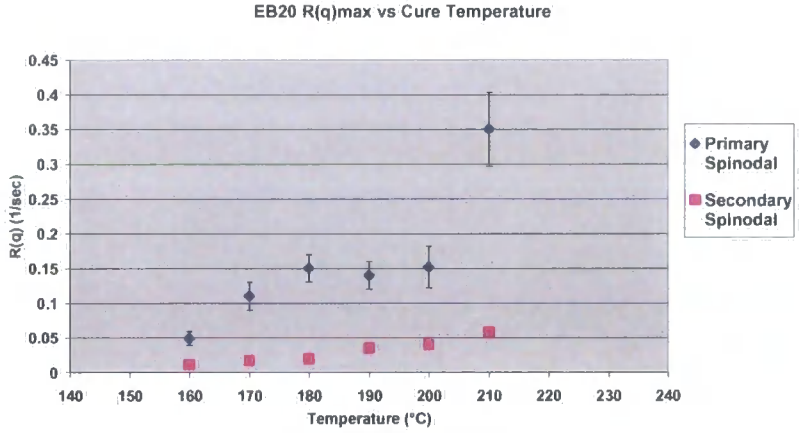

Graph 5.4.3.9 *This graph shows the relationship between $R(q)_{max}$ and cure temperature for EB20.*

5.4.3.3 R(q)/q² versus q² results for EB20

$R(q)/q^2$ versus q^2 plots for EB20 cured at different temperatures were obtained. From Cahn-Hilliard theory outlined in chapter 2 these should be straight lines with a clear intercept on the y-axis. This is not the case for these plots due to the non-linear nature of the spinodal decomposition in these reactive blends. Extrapolations have been made to extract a D^*_{app} value. The graph 5.4.3.10 shows an example of a $R(q)/q^2$ versus q^2 plot from this series.

The graph 5.4.3.11 shows the relationship between D^*_{app} and the cure temperature for EB20.

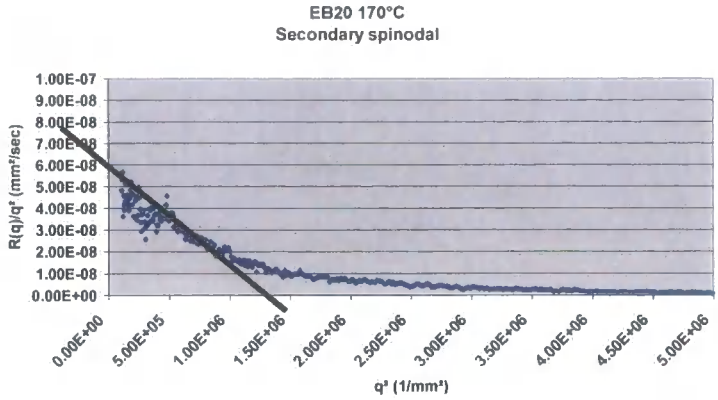

Graph 5.4.3.10 *R(q)/q² versus q² for EB20 cured at 170°C for Secondary Spinodal peak*

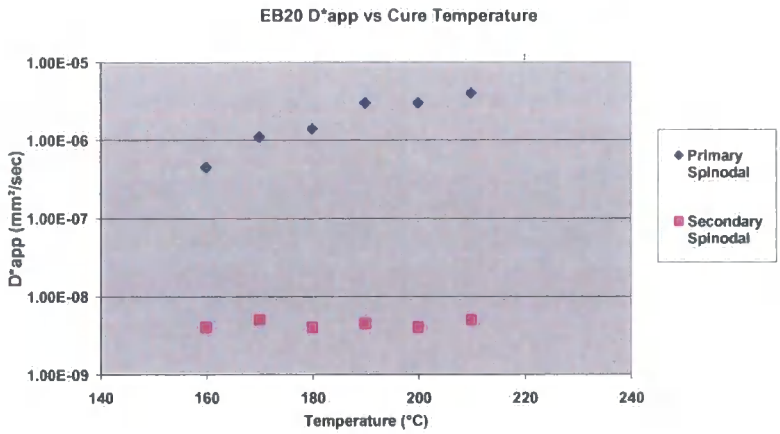

Graph 5.4.3.11 *Apparent Diffusion coefficient D^*_{app} versus cure temperature for EB20. This shows the D^*_{app} for both primary and secondary phase separations. The D^*_{app} for the primary phase separation increases rapidly with temperature however D^*_{app} remains constant with temperature for the secondary phase separation.*

The graph 5.4.3.11 above shows the relationship between D^*_{app} and the cure temperature for both primary and secondary phase separations. For the primary phase separation this shows a logarithmic increase in D^*_{app} with temperature this trend suggests LCST. The D^*_{app} for the secondary spinodal decomposition appears to remain constant with temperature.

5.4.3.4 DSC results from EB20

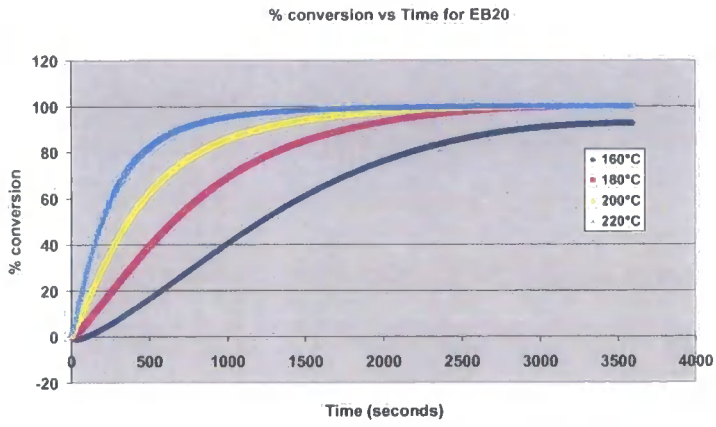

Graph 5.4.3.12 *This graph shows the conversion versus time relationship for EB20 cured at various temperatures. This data was obtained from isothermal DSC experiments.*

The data shown in Graph 5.4.3.12 above was obtained using the isothermal DSC method outlined in Chapter 4.

5.4.3.5 Time to onset of phase separation for different isothermal cure temperatures for EB20

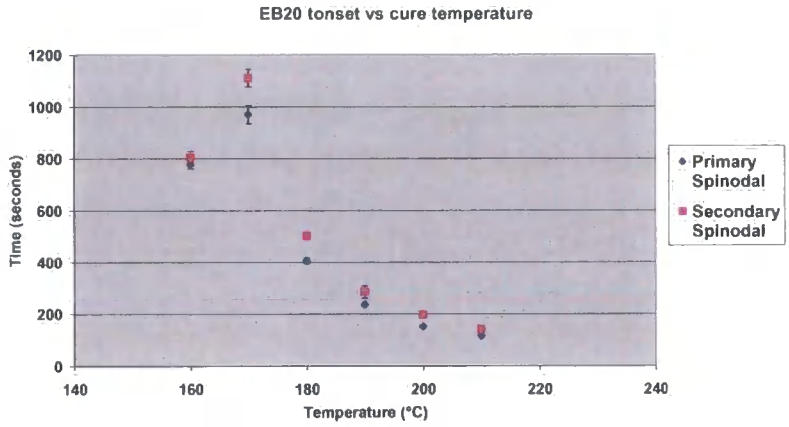

Graph 5.4.3.13 *Time to onset of phase separation versus cure temperature for primary and secondary spinodal decompositions inEB20.*

Graph 5.4.3.13 above shows the relationship between the time to onset of phase separation for different isothermal cure temperatures for both primary and secondary

spinodal decompositions. This information is obtained from the SALS experiments and shows decreasing onset time with higher cure temperatures.

5.4.3.6 Conversion at the onset of phase separation versus Cure Temperature for EB20

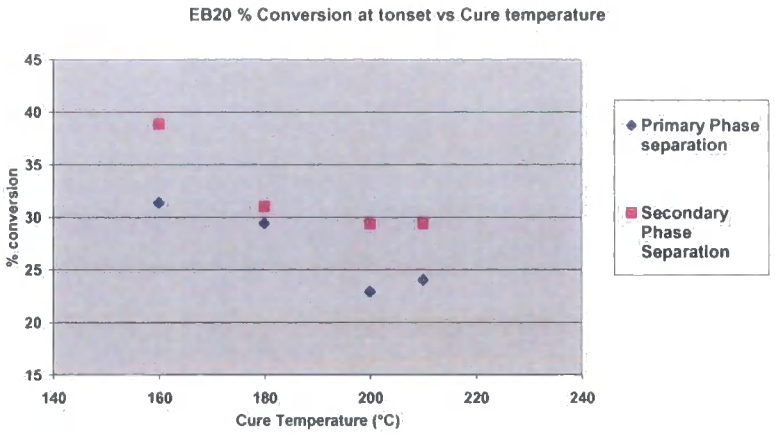

Graph 5.4.3.14 Graph showing the % conversion at the onset of phase separation for different isothermal cure temperatures for EB20. This shows falling % conversion at phase separation with increasing temperature for both primary and secondary spinodal peaks suggesting LCST behaviour.

The graph 5.4.3.14 above shows the % conversion at the onset of phase separation for different isothermal cure temperatures for both primary and secondary spinodal decompositions. This information is obtained from a combination of SALS and DSC experimentation. It clearly shows that as temperature increases the level of conversion required to drive the system to phase separate is reduced. Therefore as temperature increases the system has a greater tendency to phase separate. This suggests that the system exhibits lower critical solution temperature (LCST).

5.4.4 Results for EB25

5.4.4.1 S(q) versus q and optical microscopy results for EB25

The Graph 5.4.4.1 shows a single spinodal peak that begins to develop after approximately 1275 seconds into the cure cycle. This develops and shifts to lower q

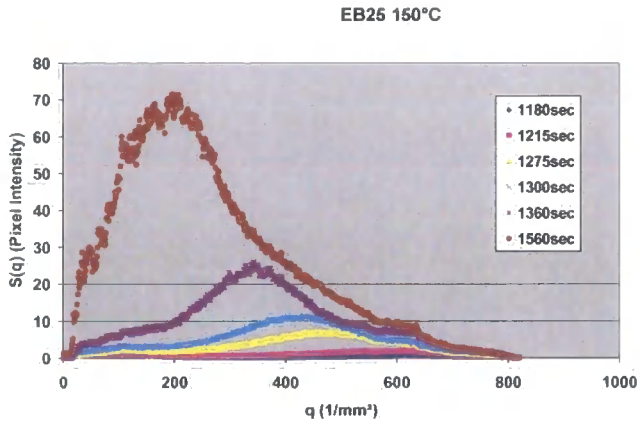

Graph 5.4.4.1 S(q) versus q for EB25 cured at 150°C. This scattering profile shows a single spinodal peak that begins to form around 1275 seconds. As the cure progresses the position of this peak shifts to lower q

as the cure progresses. The initial peak forms at a q value of around 500 mm^{-1} and shifts to 200 mm^{-1} which corresponds to a length scale of 0.0315 mm. The Figure 5.4.4.1 shows the corresponding optical micrograph of EB25 cured at 150°C. It shows a large scale two phase morphology with the minority phase being continuous. The majority phase consists of large irregular particles contains smaller sub included particles resulting from secondary phase separation. This morphology has probably formed from a percolation to cluster transformation from the initial spinodal decomposition. There is clear evidence of secondary phase separations occurring in the majority phase.

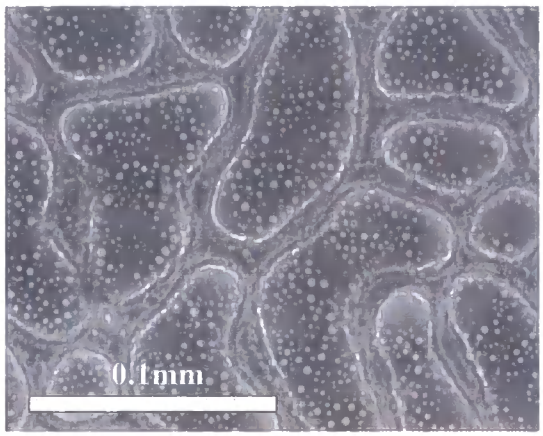

Figure 5.4.4.1 Optical micrograph of EB25 cured at 150°C. This morphology shows a continuous minor phase with a discontinuous majority phase containing sub- included particles from secondary phase separations.

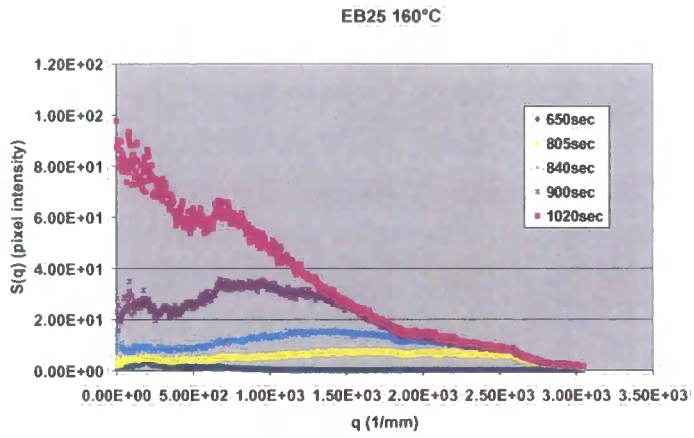

Graph 5.4.4.2 S(q) versus q for EB25 cured at 160°C. This scattering profile shows a single broad spinodal peak that develops around 805sec into the cure. The position of the peak shifts to lower q as the cure advances

The graph 5.4.4.2 shows the S(q) versus q plot for EB25 cured at 160°C and shows a single spinodal peak that begins to develop after approximately 800 seconds into the cure cycle. This develops and shifts to lower q as the cure progresses. The initial peak forms at a q value of around 2000 mm^{-1} and shifts to a low q value outside of the range of the experiment. The figure 5.4.4.2 below shows the corresponding optical micrograph of EB25 cured at 160°C. It shows a large scale two phase morphology with the minority phase being continuous and containing sub inclusion particles from secondary phase separation. The majority phase consists of large irregular particles contains smaller sub included particles resulting from secondary phase separation. This morphology has probably formed from a percolation to cluster transformation

from the initial spinodal decomposition. There is clear evidence of secondary phase separations occurring in both phases

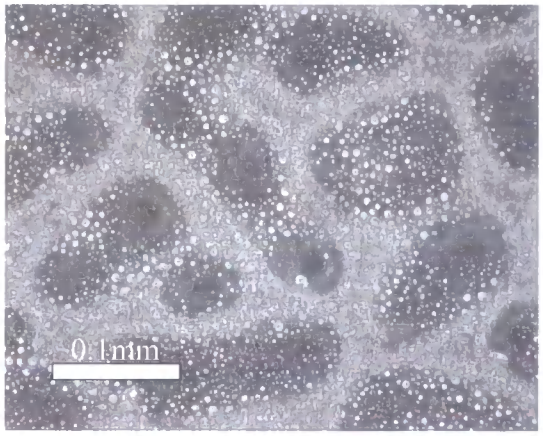

Figure 5.4.4.2 Optical micrograph of EB25 cures at 160°C. This shows a large two phase morphology that has formed from a percolation to cluster transformation. Both the phases contain sub included particles as a result of secondary phase separations.

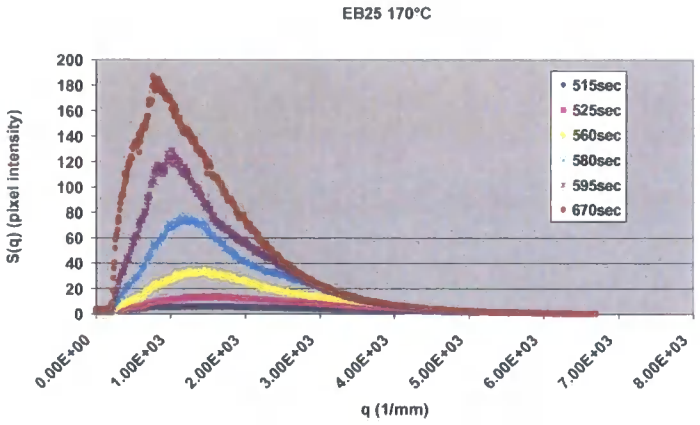

Graph 5.4.4.3 S(q) versus q for EB25 cured at 170°C. . This scattering profile shows a spinodal peak that begins to form after around 525 seconds this develops and shifts to lower q as the cure progresses.

The graph 5.4.4.3 shows the S(q) versus q plot for EB25 cured at 170°C. This shows a single spinodal peak occurring after approximately 525 seconds at a q value of 1400 mm^{-1} corresponding to a length scale of 0.0045 mm. There is also evidence of the formation of a secondary spinodal peak occurring at around 2500 mm^{-1} after 580 seconds. Figure 5.4.4.3 shows the corresponding cured micrograph of EB25 cured at

170°C. This shows a two-phase morphology with a large-scale discontinuous phase. The continuous phase contains sub-included particles from a secondary phase separation. The large-scale structure has formed from a percolation to cluster transformation from the primary spinodal decomposition.

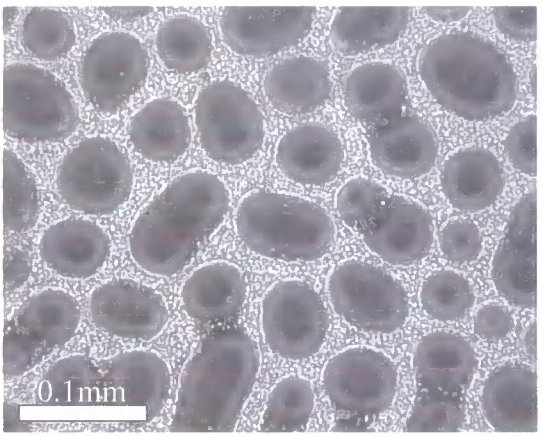

Figure 5.4.4.3 Optical micrograph of EB25 cured at 170°C. This shows a large two phase morphology that has formed from a percolation to cluster transformation. The continuous phase contains sub-included particles as a result of secondary phase separation.

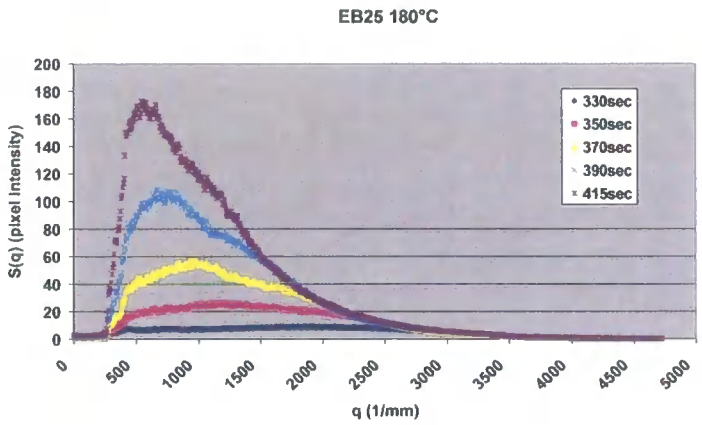

Graph 5.4.4.4 S(q) versus q for EB25 cured at 180°C. This scattering profile shows a spinodal peak that begins to form after around 330 seconds this develops and shifts to lower q as the cure progresses. There is also evidence of a secondary spinodal peak that begins to form after 370secs at a q value of 1750 mm-1.

The graph 5.4.4.4 above shows the S(q) versus q plot for EB25 cured at 180°C. This shows a spinodal peak occurring after approximately 350 seconds at a q value of 1250 mm^{-1} corresponding to a length scale of 0.005 mm. There is also a secondary spinodal peak occurring at around 1750 mm^{-1} after 370 seconds. Both peaks shift to lower q as the cure advances. Figure 5.4.4.4 below shows the corresponding cured micrograph of EB25 cured at 180°C. This shows a two-phase morphology with a large-scale discontinuous phase. The continuous and dispersed phases contain sub-included particles from a secondary phase separation. The large-scale structure has formed from a percolation to cluster transformation from the primary spinodal decomposition and the fine scale sub included particles have likely formed from percolation to cluster transformation of the secondary spinodal decomposition.

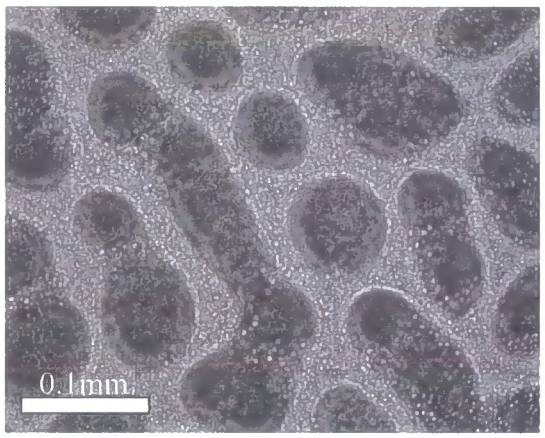

Figure 5.4.4.4 Optical micrograph of EB25 cured at 180°C. This shows a large two phase morphology that has formed from a percolation to cluster transformation. Both the continuous phase and dispersed phase contain sub-included particles as a result of secondary phase separation.

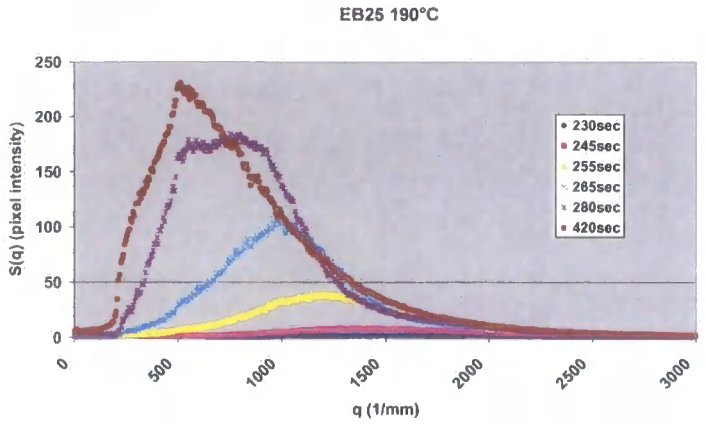

Graph 5.4.4.5 *S(q) versus q for EB25 cured at 190°C.. This scattering profile shows a single spinodal peak that begins to form at around 245seconds into the cure. The position of this spinodal peak shifts quickly to lower q as the cure progresses.*

The graph 5.4.4.5 shows the S(q) versus q plot for EB25 cured at 190°C. This shows a spinodal peak occurring after approximately 245 seconds at a q value of 1250 mm^{-1} corresponding to a length scale of 0.005 mm. The peak shifts to lower q as the cure advances. Figure 5.4.4.5 below shows the corresponding cured micrograph of EB25 cured at 190°C. This shows a two-phase morphology with a large-scale discontinuous phase. The continuous phase contains sub-included particles from a secondary phase separation. The large-scale structure has formed from a percolation to cluster transformation from the primary spinodal decomposition and the fine scale sub included particles have likely formed from a secondary phase separation process not picked up from the light scattering experiment.

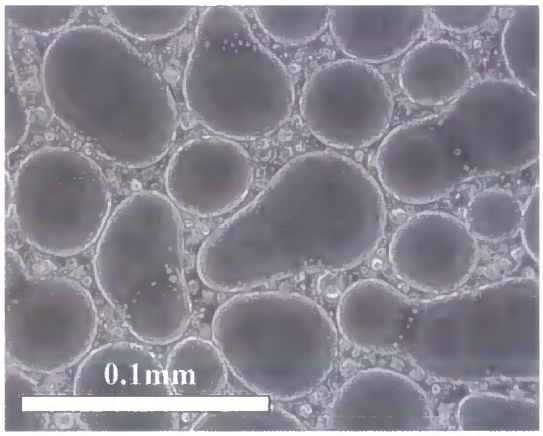

Figure 5.4.4.5 Optical micrograph of EB25 cured at 190°C. This shows a large scale two phase morphology that has formed from a percolation to cluster transformation. The continuous phase contains sub-included particles as a result of secondary phase separation.

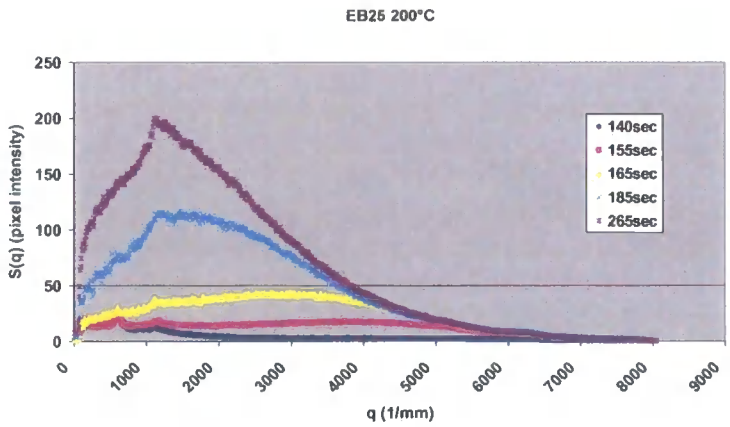

Graph 5.4.4.6 S(q) versus q for EB25 cured at 200°C. This scattering profile shows a single spinodal peak that begins to form at around 155 seconds into the cure.

The graph 5.4.4.6 shows the S(q) versus q plot for EB25 cured at 200°C. This shows a spinodal peak occurring after approximately 155 seconds at a q value of 3000 mm^{-1} corresponding to a length scale of 0.0021 mm. The peak shifts to lower q as the cure advances. Figure 5.4.4.6 below shows the corresponding cured micrograph of EB25 cured at 190°C. This shows a two-phase morphology with a large-scale discontinuous phase. Both the continuous phase and the discontinuous phase contain sub-included particles from a secondary phase separation. The large-scale structure has formed

from a percolation to cluster transformation from the primary spinodal decomposition and the fine scale sub included particles have likely formed from a secondary phase separation process not picked up from the light scattering experiment due to its size.

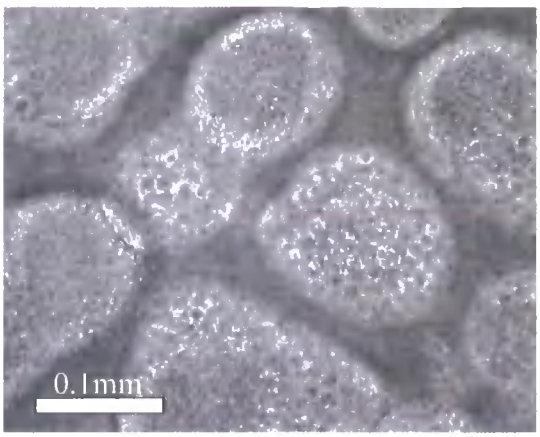

Figure 5.4.4.6 Optical micrograph of EB25 cured at 200°C. This shows a large scale two phase morphology that has formed from a percolation to cluster transformation. Both the phases contain sub-included particles as a result of secondary phase separation.

The graph 5.4.4.7 shows the S(q) versus q plot for EB25 cured at 210°C. This shows a broad spinodal peak occurring after approximately 90 seconds at a q value of 1500 mm^{-1} corresponding to a length scale of 0.0042 mm.

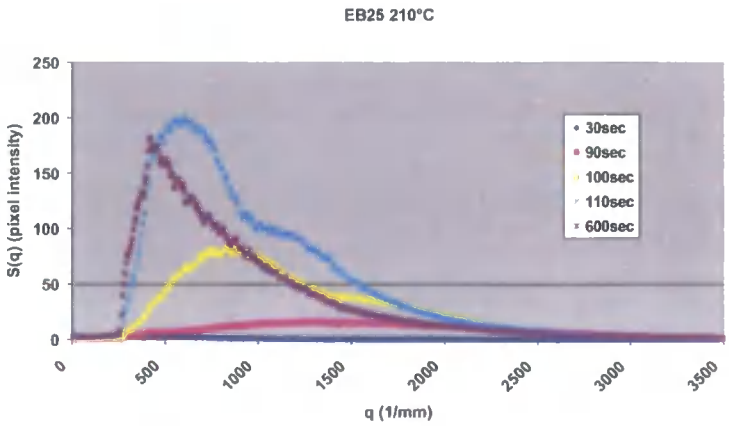

Graph 5.4.4.7 S(q) versus q for EB25 cured at 210°C. This scattering profile shows two spinodal peaks. A primary spinodal peak begins to form after 90 seconds at low q, this develops and shifts to lower q as the cure progresses. After 100 seconds into the cure a second spinodal peak forms at a q value of 1700 mm^{-1}, this peak also shifts to lower q as the cure progresses.

The peak rapidly shifts to lower q as the cure advances. A secondary spinodal peak forms at around 100 seconds at a q value of 1600 mm^{-1} and also shifts to lower q. After 600 seconds the peaks have shifted to a q value below 500 mm^{-1} outside the range of the experiment. Figure 5.4.4.7 shows the corresponding cured micrograph of EB25 cured at 210°C. This shows a two-phase morphology with a large-scale discontinuous phase. Both the continuous phase and the discontinuous phase contain sub-included particles from a secondary phase separation. The large-scale structure has formed from a percolation to cluster transformation from the primary spinodal decomposition and the fine scale sub included particles have formed from secondary percolation to cluster transformations.

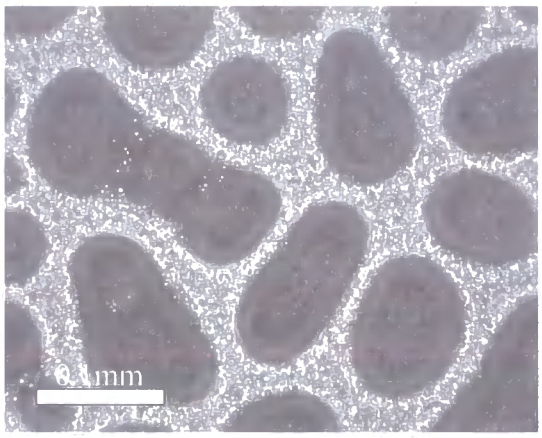

Figure 5.4.4.7 Optical micrograph of EB25 cured at 210°C. This shows a large-scale two-phase morphology that has formed from a percolation to cluster transformation. Both the phases contain sub-included particles as a result of secondary phase separations.

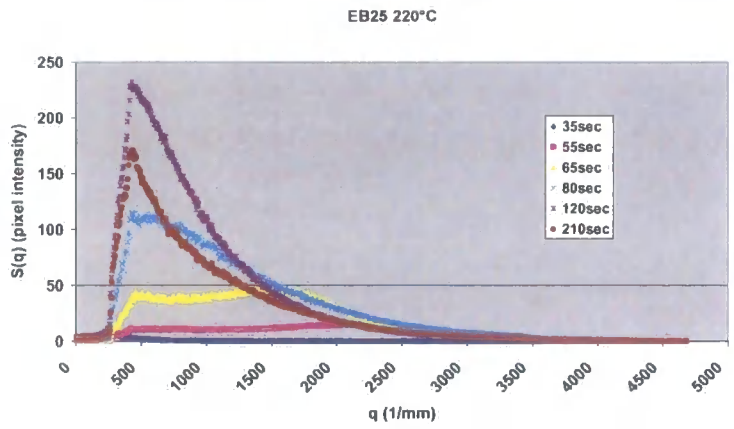

Graph 5.4.4.8 S(q) versus q for EB25 cured at 220°C. . This scattering profile shows a single spinodal peak that begins to form after 55sec and rapidly moves to lower q as the cure progresses

The graph 5.4.4.8 above shows the S(q) versus q plot for EB25 cured at 220°C. This shows a broad spinodal peak occurring after approximately 65 seconds at a q value of 1700 mm^{-1} corresponding to a length scale of 0.0037 mm. The peak rapidly shifts to lower q as the cure advances. After 210 seconds the peak has shifted to a q value below 500 mm^{-1} outside the range of the experiment. Figure 5.4.4.8 below shows the corresponding cured micrograph of EB25 cured at 220°C. This shows a two-phase morphology with a large-scale discontinuous phase. Both the continuous phase and the discontinuous phase contain sub-included particles from a secondary phase separation. The large-scale structure has formed from a percolation to cluster transformation from the primary spinodal decomposition and the fine scale sub included particles have formed from secondary percolation to cluster transformations

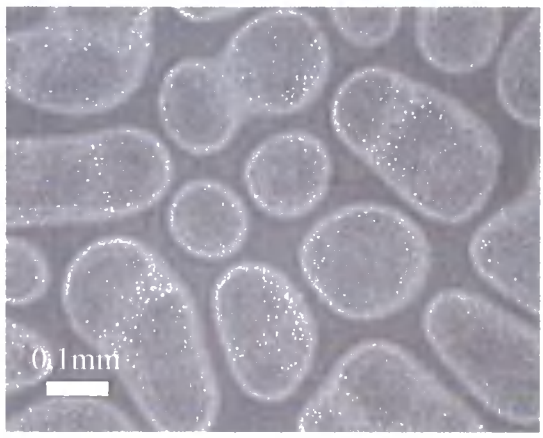

Figure 5.4.4.8 Optical micrograph of EB25 cured at 220°C. This shows a large scale two phase morphology that has formed from a percolation to cluster transformation. Both the phases contain sub-included particles as a result of secondary phase separations .

5.4.4.2 R(q) vs q plots for EB25

This section shows the R(q) vs q data for EB25 from the light scattering traces shown in section 5.4.4.1. R(q) versus q from this series show well defined peaks. An example of a R(q) versus q plot from this series is shown in graph 5.4.4.9

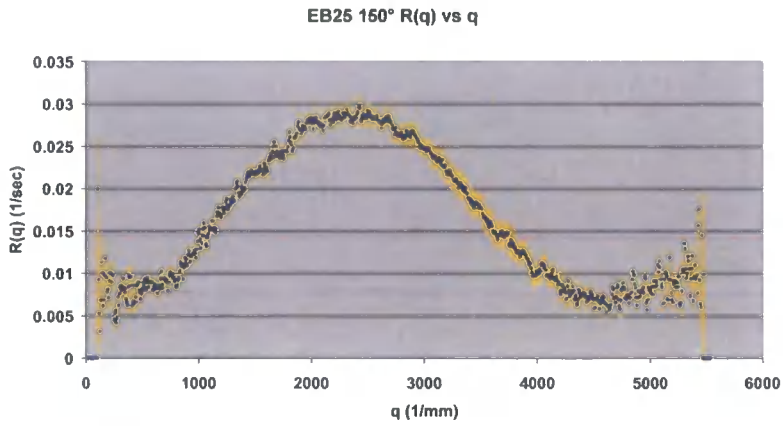

Graph 5.4.4.9 R(q) versus q for EB25 cured at 150°C R(q) values were taken between 1215 sec and 1300 sec.

The table 5.4.4.2 documents the $R(q)_{max}$ and $q_{(max)}$ results from EB25 and graph 5.4.4.10 represents this data graphically.

EB25	150°C	160°C	170°C	180°C	190°C	200°C	210°C	220°C
$R(q)_{max}$ (sec^{-1})	0.028	0.026	0.037	0.051	0.139	0.110	0.22	0.24
$q_{(max)}$ (mm^{-1})	2400	1000	1400	950	1050	3250	1060	1740

Table 5.4.4.2 *$R(q)_{max}$ and $q_{(max)}$ values for EB10 cured at different isothermal temperatures.*

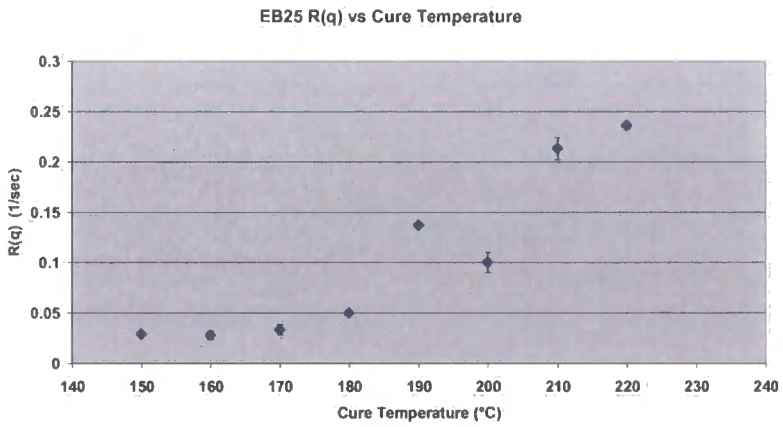

Graph 5.4.4.10 *This graph shows the relationship between $R(q)_{max}$ and cure temperature for EB25.*

5.4.4.3 $R(q)/q^2$ versus q^2 data for EB25

$R(q)/q^2$ versus q^2 plots were obtained for the EB25 cured at different isothermal temperatures. From Cahn-Hilliard theory outlined in Chapter 2 these should be straight lines with a clear intercept on the y axis. This is not the case for these plots due to the non-linear nature of the spinodal decomposition in these reactive blends. Extrapolations have been made to extract a D^*_{app} value. An example of a $R(q)/q^2$ versus q^2 plot from this series is shown in graph 5.4.4.11.

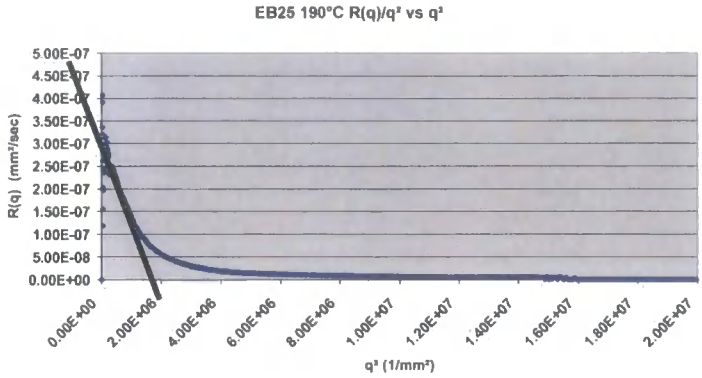

Graph 5.4.4.11 *R(q)/q² versus q² for EB25 cured at 190°C .*

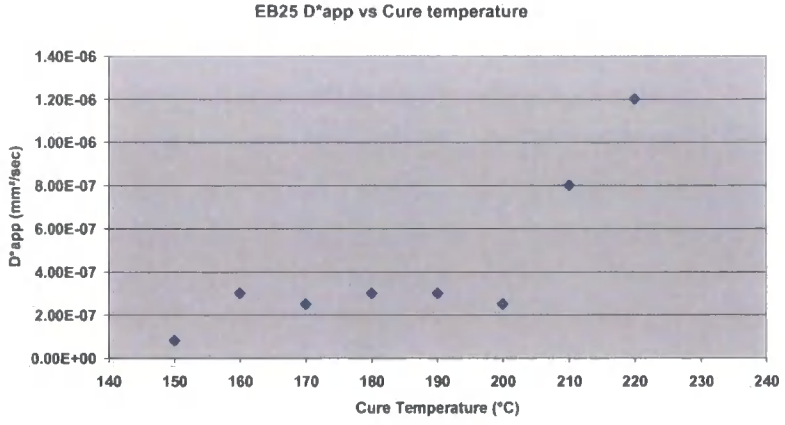

Graph 5.4.4.12 *D^*_{app} of phase separation versus cure temperature for EB25*

The graph 5.4.4.12 above shows the relationship between D^*_{app} and cure temperature for EB20. The rate of phase separation increases with increasing temperature suggesting LCST behaviour. Once again there is a rapid increase rate above 200°C, which may correspond to the Tg of the thermoplastic.

5.4.4.4 Time to onset of phase separation for different isothermal cure temperatures for EB25

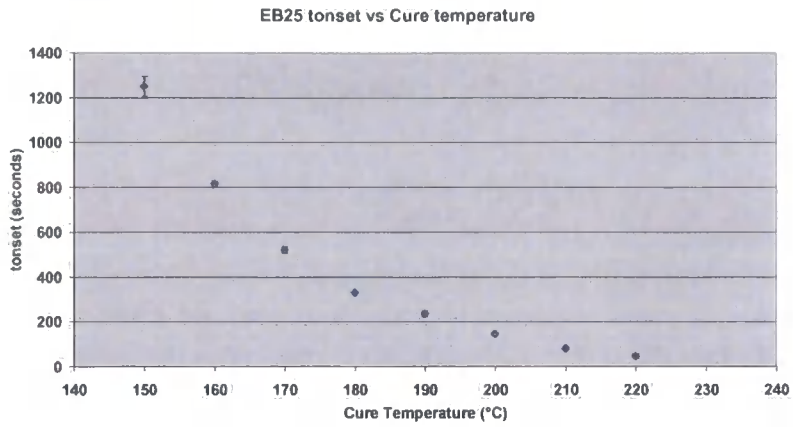

Graph 5.4.4.13 Time to onset of phase separation versus cure temperature for EB25.

Graph 5.4.4.13 above shows the relationship between the time to onset of phase separation for different isothermal cure temperatures. This information is obtained from the SALS experiments and shows decreasing onset time with higher cure temperature. This as expected shows decreasing time to onset of cure with increasing temperature.

5.4.4.5 Conversion at the onset of phase separation versus Cure Temperature for EB25

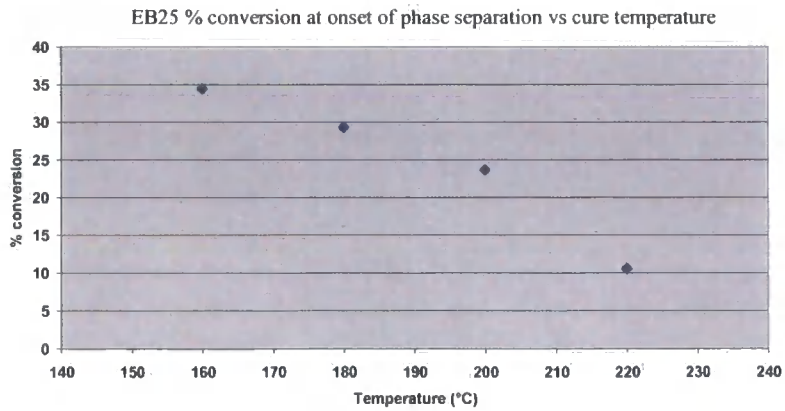

Graph 5.4.4.14 Graph showing the % conversion at the onset of phase separation for different isothermal cure temperatures for EB25.

The graph 5.4.4.14 above shows the % conversion at the onset of phase separation for different isothermal cure temperatures. This information is obtained from a combination of SALS and DSC experimentation. It clearly shows that as temperature increases the level of conversion required to drive the system to phase separate is reduced. Therefore as temperature increases the system has a greater tendency to phase separate. This suggests that the system exhibits lower critical solution temperature (LCST).

5.5 Discussion

5.5.1 Mechanism of Phase Separation.

From the results reported in the previous section from observations of the S(q) versus q plots in a majority of cases a spinodal peak is formed and in no cases was nucleation and growth observed. This is for all the blend formulations studied. Hence spinodal decomposition is the primary mechanism for phase separation in these systems. This is to be expected due to the unlikelihood of nucleation and growth occurring in thermoplastic-thermoset blends. It is difficult to envisage a process by which nucleation could occur in thermally cured reactive thermoplastic-thermoset blends. At high temperatures for nucleation to occur would require diffusion of material against concentration gradients, which for formulations outside of the unstable region is unlikely to occur.

It is interesting to compare the cured morphologies from the epoxy blends with the corresponding S(q) versus q plots. For the case of EB10 all of the final cured morphologies have a particulate morphology where dispersed particles of thermoplastic rich particles are contained in a continuous epoxy rich phase. One characteristic of the morphologies produced from the EB10 range is that for any particular cure temperature the dispersed particles are of a very uniform size.

From the light scattering it is clear that the EB10 formulations all exhibit a spinodal peak it therefore suggests that the morphology seen in EB10 forms from a percolation to cluster transformation. Such behaviour has been reported in other systems [8,9].

In EB15 we observe the same phenomenon, well defined spinodal peaks are observed in the S(q) versus q plots and the resulting morphology is particulate with

thermoplastic rich particles being dispersed in an epoxy rich matrix. The size of the dispersed particles appears to increase as the cure temperature is increased with the exception of EB15 cured at 220°C. The morphology in EB15 has therefore also likely to have arisen as a result of percolation to cluster transformation behaviour. Because the dispersed particle size increases with increasing cure temperature yet the spinodal length remains relatively consistent this coarsening of the morphology at higher temperatures may be as a result of particle coalescence in the later stages of the percolation to cluster transformation. It is clearly seen that there is a large increase in dispersed particulate size above 190°C. The Tg of the PES: PEES thermoplastic is 195°C, it could be postulated that particle coalescence cannot occur below Tg because the particles may be in a vitrified state. Coalescence may only be possible when the particles are above their Tg where molecular mobility permits the coalescence process to occur.

Phase separation in the EB20 formulations presents a very interesting case. Here across the temperature range both primary and secondary phase separations can be clearly observed from the S(q) versus q plots from light scattering experiments. The morphologies of these systems at cure temperatures below 210°C show the presence of large scale dispersed primary particles within which are smaller dispersed secondary sub-included particles. The continuous phase also contains a dispersed phase resulting from secondary phase separations. This morphology has formed from both primary and secondary spinodal decompositions undergoing percolation to cluster transformation. Similar morphologies to these have been reported previously in rubber toughened PMMA and Rubber modified Polystyrene [10,11] which result in blends with improved toughness. This increase in toughness is also observed with EB20 displaying this double percolation to cluster transformation morphology and this is reported in Chapter 6.

For EB20 cured at 200°C and 210°C it can be seen from the cured micrographs that the primary structure can further decompose until all that remains is a fine scale particulate morphology.

In the case of EB25 the S(q) versus q plots show spinodal decomposition and in some cases there is evidence of a secondary spinodal decomposition. The morphologies of the EB25 system cured at different temperatures show two phase morphology with secondary particles dispersed in both phases. It is postulated that in this morphology

the minority continuous phase is thermoplastic rich and the large majority dispersed particles are epoxy rich. This is so-called phase inverted morphology. This has arisen from percolation to cluster transformation of the primary spinodal decomposition process. Also secondary phase separations have occurred and these also are likely to be percolation to cluster transformations of secondary spinodal decompositions.

It can be concluded that the major process for phase separation in these blends is by spinodal decomposition followed by percolation to cluster transformation. Secondary phase separations also occur and it would appear that these too are by spinodal decomposition followed by percolation to cluster transformation. Dispersed phase morphologies are a common occurrence but nucleation and growth appears to be rare event.

5.5.2 Phase Diagram for EB system

The intention of this series of experiments was to elucidate the phase diagram for this particular blend of bisphenol F epoxy, MDEA cure agent and PES polymer. Across the range of compositions and temperatures studied all blends underwent a phase separation. This is indicated by both S(q) versus q plots and is confirmed by the optical micrographs of the cured blends. All of the formulations therefore have a tendency to phase separate on cure regardless of composition or cure temperature.

The mechanism of phase separation in all cases appears to be by spinodal decomposition followed by percolation to cluster transformation. Hence only a spinodal line can be predicted from these results.

The graph 5.5.1 below shows the spinodal lines in conversion and composition co-ordinates for this particular thermoplastic-thermoset blend. These are obtained from the time to onset of phase separation as indicated from the light scattering experiments and the degree of conversion is from the DSC experimentation.

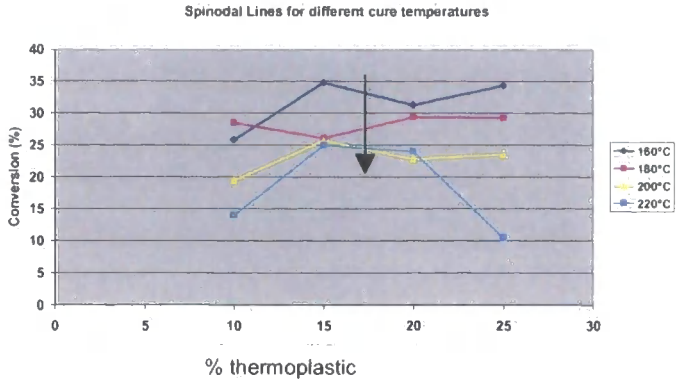

Graph 5.5.1 *This graph shows the phase diagram of this system as defined by the spinodal lines. This shows that this system shows lower critical solution temperature. This is indicated by the systems tendency to phase separate at lower % conversion at higher temperatures.*

This graph shows that as the cure temperature increases the % conversion at the onset of spinodal decomposition decreases. This indicates that the phase separation in this system is characterised by lower critical solution temperature (LCST). This is in agreement with several other researchers who have studied reaction induced phase separation in epoxy systems blended with aromatic thermoplastics. [12,13,14].

From graph 5.5.1 it can be seen that there is no obvious critical composition identified. The degree of conversion at the onset of phase separation appears to remain reasonably constant across the formulation range studied. The spinodal line obtained from isothermal cure experiments carried out at 220°C shows unusual behaviour. This appears to show a peak between 15% and 20% in the opposite direction to that expected. This may be as a result of the critical point shifting with respect to composition of thermoplastic level at higher temperatures. This behaviour needs further investigation to identify the nature of the effect.

5.5.3 The Kinetics Of Phase Separation.

In order to describe the kinetics of the phase separation process Cahn-Hilliard theory has been used to study the data from the light scattering experiments. Cahn-Hilliard theory is described in detail in chapter 2 but this theory is somewhat limited when applying to reactive polymer blends. The limiting factor with fitting Cahn-Hilliard theory to the polymer blends studied in this section is that the early stages of spinodal decomposition where the peak in the S(q) versus q plot remains constant is often not

apparent especially at higher cure temperatures. As soon as the peak forms in the S(q) versus q plot it begins to shift to lower q as the morphology begins to coarsen. Hence Cahn-Hilliard theory can in some cases only be fitted to short time scales immediately after the phase separation has begun. This makes calculating an accurate value for R(q) difficult but where possible Cahn-Hilliard theory was fitted to the data to calculate R(q) and D^*_{app} for the spinodal decomposition process.

5.5.4 The relationship between the Rate Of Phase Separation R(q) and Thermoplastic Content.

The rate of phase separation is useful to study because it gives an indication of the thermodynamic driving force for the phase separation process. The maximum rate of phase separation for the spinodal decomposition process occurs at a q value related to the dominant spinodal length scale. Hence plots of R(q) vs. q should produce a peak corresponding to the growth rate of the dominant wavelength of concentration fluctuation. The value of the R(q) max is a measure of the rate of phase separation of a spinodal decomposition.

The deeper into the unstable region of the phase diagram the greater is the thermodynamic driving force for the phase separation process and the higher the rate R(q)max will be.

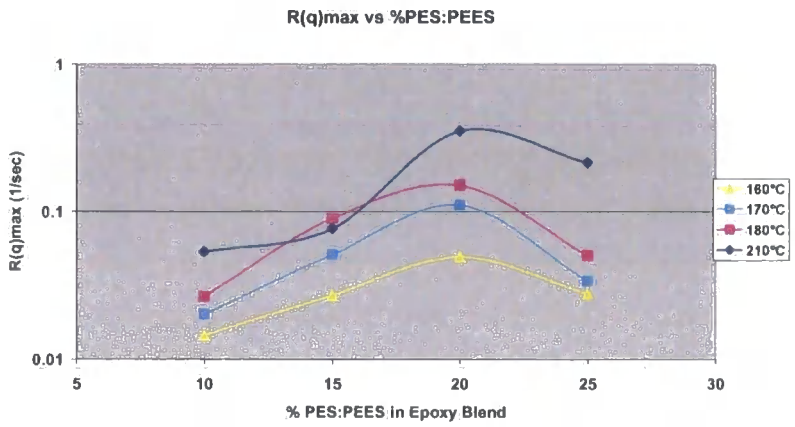

Graph 5.5.2 *R(q) versus PES:PEES loading for different cure temperatures.*

The Graph 5.5.2 above shows the relationship between $R(q)_{max}$ and the % thermoplastic loading in the blend for different isothermal cure temperatures. This shows that the rate increases with increasing temperature again confirming the LCST nature of the phase diagram. This graph also shows that there is a peak in the $R(q)_{max}$ versus % thermoplastic curve. This occurs at around 20 % thermoplastic loading for each different cure temperature. This suggests that the critical composition for this system is approximately 20 % thermoplastic. It is also worth noting that the $R(q)_{max}$ scale is logarithmic and at cure temperatures above 200°C there appears to be a large increase in the phase separation rate. This effect may be related to the glass transition temperature of the thermoplastic additive. The PES thermoplastic used in this study has a Tg of 195°C. When the spinodal decomposition begins the thermoplastic rich phase is likely to have a high Tg approaching that of the unmodified polymer. Therefore at cure temperatures below the Tg of the in the initial stages of spinodal decomposition the thermoplastic rich phase may become vitrified reducing the phase separation rate. However at temperatures above the Tg of the thermoplastic phase vitrification is not possible and the phase separation may proceed uninhibited.

This vitrification effect is likely to account for the greatly reduced region of early stage phase separation in samples cured above 195°C. Therefore the Tg of the toughening polymer is a key factor controlling the phase separation and subsequent final cured morphology. Altering the PES:PEES ration of the thermoplastic will therefore influence the phase separation process and the subsequent morphology

In this particular blend using a di-functional epoxy cured by a hindered aromatic diamine vitrification of the rich epoxy phase is less likely. However if multi functional epoxy resins are cured with non-hindered amines vitrification of the epoxy rich phase may also become a possibility and hinder the rate of phase separation.

5.5.5 The relationship between D^*_{app} and thermoplastic content

The D^*_{app} is the uphill diffusion coefficient for the spinodal decomposition process and is described in detail in Chapter 2. The driving force for the uphill diffusion process is the chemical potential difference of the thermoplastic in the different forming phases. The components will migrate against the concentration gradient to minimise the overall free energy of the blend. Hence studying the D^*_{app} of the

spinodal decomposition process can indicate the thermodynamic driving force for the phase separation process.

The graph 5.5.3 below shows the relationship between D^*_{app} and thermoplastic content for different isothermal cure temperatures. This shows a well-defined peak at 20% thermoplastic loading fof all cure temperatures. This suggests that there is a greater thermodynamic driving force for the spinodal decomposition at 20% thermoplastic that is indicative of the critical composition for this epoxy blend system. This is in good agreement with $R(q)_{max}$ data shown in section 5.5.4.

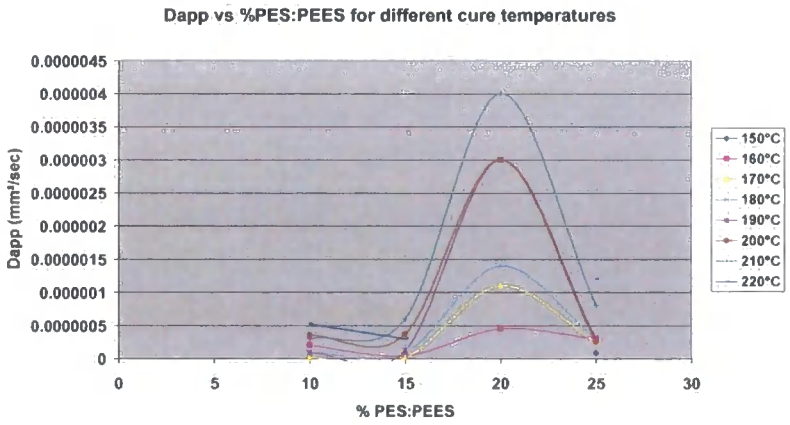

Graph 5.5.3 Graph of D^*_{app} versus % PES:PEES for different isothermal cure temperatures.

From graph 5.5.3 it can also be seen that there is a rapid increase in the D^*_{app} above 190°C for the critical composition. This again suggests that the Tg of the thermoplastic has a strong influence on the phase separation behaviour of the blend.

5.6 Conclusions

In this chapter the phase separation of this thermoplastic-thermoset blend has been studied using a combination of SALS, DSC and phase contrast optical microscopy. This study has shown that the predominant phase separation mechanism in the system is spinodal decomposition followed by percolation to cluster transformation. Nucleation and growth does not appear to occur in these systems under the conditions studied.

The investigations in this chapter have shown that this thermoplastic-thermoset blend exhibits lower critical solution temperature behaviour. Here higher cure temperatures favour phase separation of the blend. It has also been shown that the critical composition for this system is around 20% thermoplastic loading.

The critical formulation shows primary and secondary spinodal decompositions followed by percolation to cluster transformations for both spinodal networks. This produces very unique morphologies that have bimodal phase sizes that may have a significant impact on the mechanical properties of the cured blend.

It has also been shown that the Tg of the toughening thermoplastic has a strong influence on the rate and apparent diffusion coefficient for the spinodal decomposition that will influence the overall morphology of the system. Lowering the Tg of the thermoplastic polymer below the intended cure temperature will also help drive the system to undergo phase separation.

This work has also highlighted the difficulties in applying Cahn-Hilliard theory to non-linear reactive thermoplastic-thermoset blends.

5.7 References.

1 Elicabe G, Larrondo HA, Williams RJJ. *Macromolecules*, 1997,30,6550

2 Cahn JW Hilliard JE ,*J. Chem Phys*, 1958,28,258

3 Cahn JW, *Trans Met Soc AIME* 1968,242,166

4 Cahn JW, *Acta Met*, 1971,19,151

5 Lifshitz, I.M, Slyozov,V.V. *J. Phys Chem.Solids*,19,35, 1961.

6 Alig I, Rullman M, Holst M, Deutsches Kunststoff-Instiute,

7 Alig,I, Jenninger W, Schawe,J, Polymer 2000,41,1577.

8 http://koken-db.kogaku.kyoto-u.ac.jp/1998/B/PC/98BPC32012.html.

9 http://koken-db.kogaku.kyoto-u.ac.jp/1997/B/PC/97BPC32003.html

10 Bucknall CB, Partidge IK, Davis P. *Polymer 26*, 103. 1985

11 Bucknall CB, Partidge IK, Phillips MJ. *Polymer 32*, 786. 1991

12 R.J.J. Williams et al. *Reaction Induced Phase Separation in Modified Thermosetting Polymers, Advances in Polymer Science No 128*, Springer ,1997

13 Ellinardis S, PhD thesis, Imperial College London 1998

14 Clarke. N, McLiesh TCB, Jenkins S,D, *Macromolecules 28*. 4650, 1995

Chapter 6

The Influence Of Epoxy Functionality On Phase Separation In A Thermoplastic-Thermoset Blend

6.1 Introduction

Chapter 5 investigated the phase separation behaviour of a blend containing a di-functional epoxy, a di-functional amine cure agent and a reactive aromatic thermoplastic. This Chapter studies how adding a tri-functional epoxy resin to this system influences the phase separation behaviour and the final cured morphology of the blend. The investigation of the phase separation behaviour will be carried out using the same combination of SALS, DSC and phase contrast optical microscopy introduced in Chapter 4. Where appropriate Cahn-Hilliard theory of the kinetics of spinodal decomposition will be applied to the results from small angle light scattering. This will give an indication of how increasing the average epoxy functionality of the system will influence the overall phase diagram of the blend.

6.2 The Theory of Reaction Induced Phase Separation in Polymer Blends.

In Chapter 2 the Flory-Huggins theory of the thermodynamics of polymer blends was introduced. It was shown by considering Flory-Huggins theory how both entropic and enthalpic energies contribute to the overall free energy of mixing for a polymer blend. The thermodynamic driving force for an initially miscible thermoplastic-thermoset blend to phase separation is the reduction in overall free energy of the system, $\Delta G°$. In a thermoplastic-thermoset blend it was shown that as cure progresses the molar volume of the thermosetting epoxy V_E increase which causes an overall reduction in the $\Delta S°$ of the system which drives the system towards phase separation. In the blends studied in this Chapter the thermoplastic has reactive end groups enabling the molar volume of the thermoplastic to also increase during cure. This too causes a reduction in $\Delta S°$, which drives the system towards phase separation. Adding a tri-functional epoxy resin to the system may influence the relationship between the degree of conversion and the molar volume of the thermosetting epoxy.

Epoxy resins can be cured via addition reactions or homopolymerisations. During the cure of epoxy resins, there is initially linear growth with a gain in molecular weight. These chains begin to branch and eventually the gel point is reached when a sufficient amount of these branches interconnect to form a continuous three-dimensional network. The viscosity increases with conversion until the gel point is reached and the network becomes insoluble. The Tg also increases throughout the cure. When the Tg of the developing network reaches the cure temperature the system becomes vitrified and the reaction rate decreases dramatically and any further reaction is diffusion controlled.

When a tri functional monomer is present the network formation of the thermosetting epoxy will be altered [1]. There will be an increase in branching and cross-linking which will affect the entropy of the system, which in turn will change the free energy of mixing of the blend driving the system towards phase separation. It is predicted from Flory-Huggins theory that adding a tri-functional epoxy to the blend will increase the tendency of the blend to phase separate. The addition of a tri-functional epoxy will also influence the enthalpy of mixing, in particular the value of the

interaction parameter χ, is likely to change. Also the incorporation of a tri-functional epoxy monomer will lead to a state of gellation at lower % conversion this may prevent equilibrium phase structure from forming. The addition of a tri-functional epoxy may also increase the Tg of the epoxy phase for any particular level of conversion. This may lead to a state of vitrification occurring earlier in the cure cycle that could either prevent phase separation occurring or alternatively freeze in non-equilibrium morphologies.

6.3 Experimental

6.3.1 Thermoplastic-thermoset blends

The compositions of the formulations studied in this chapter are detailed in table 6.3.1

	% Composition by weight			
Blend Reference	**Di-functional epoxy resin (PY306)**	**Tri-functional epoxy resin (MYO510)**	**Di-functional amine (MDEA)**	**Thermoplastic (PES:PEES)**
EB10X5	60.25	3.09	26.65	10
EB15X5	56.91	2.92	25.17	15
EB20X5	53.56	2.75	23.69	20
EB25X5	50.21	2.58	22.21	25
EB10X10	57.13	6.19	26.68	10
EB15X10	53.96	5.85	25.19	15
EB20X10	50.78	5.50	23.71	20
EB25X10	47.61	5.16	22.23	25

Table 6.3.1.1 Table showing the composition of the formulations studied in this chapter. These formulations maintain a 1:0.77 molar ratio of epoxy : amine groups.

The nomenclature for these blends is as follows:

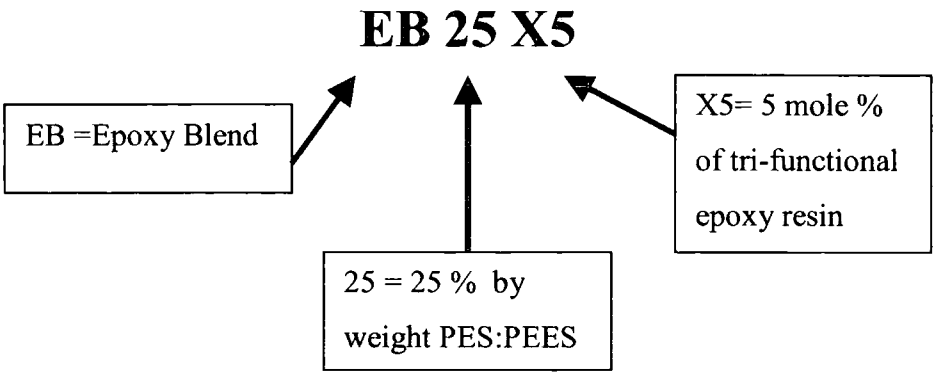

In these blends two different levels of tri functional epoxy have been added to the formulation these are 5 and 10 mole % with respect to the overall epoxy content of the system. The same stoichiometric ratio of epoxy to amine groups is maintained in all formulations at 77% deficiency of amine groups this is neglecting the amine group contribution from the PES:PEES end groups.

These blends were prepared using a hot melt technique. The epoxy resins and the thermoplastic were weighed into a small open necked glass jar. This mixture was then heated to 120°C in an air-circulating oven. The sample was held in the oven for approximately 15 minutes until the thermoplastic had fully dissolved in the liquid epoxy resin leaving a clear homogeneous solution. Next the solution was allowed to cool to below 100°C and the cure agent was added to the mixture and stirred. The mixture was then held at 100°C in an air-circulating oven for approximately 15 minutes until the cure agent had fully dissolved in the solution. This gave a light amber transparent solution. The formulation was then degassed in a vacuum oven at 100°C for approximately 30 minutes until all bubble formation in the sample had ceased. This degassing process was essential to prevent micro-void formation in the sample during the SALS experiment

6.3.2 Time Resolved Small Angle Light Scattering

SALS experiments were carried out using the equipment and technique outlined in Chapter 3. The epoxy blend formulations were subjected to a series of temperature jump experiments in the range of 160°C to 220°C.

6.3.3 Differential Scanning Calorimetry

Time–temperature-conversion behaviour of the epoxy blend formulations were determined using a combination of isothermal and temperature ramp differential scanning Calorimetry (DSC). The experimental method and interpretation technique are described in detail in Chapter 3.

6.3.4 Optical Light Microscopy.

Phase contrast polarised optical light microscopy was performed on the actual samples from the SALS experiments. This identified the nature of the morphology of the epoxy blend formulations. The equipment and experimental techniques used for this evaluation are described in detailed in Chapter 4.

6.4 Results and Discussion.

6.4.1 Results from system EB10X5

This section describes the results from the epoxy blend system EB10X5. In this system 5 mole % of the epoxy resin is tri-functional. The system contains 10 % PES:PEES thermoplastic. The precise formulation is detailed in table 6.3.1.

6.4.1.1 S(q) versus q results for EB10X5

This section discusses the light scattering results from system EB10X5 cured at different isothermal cure temperatures. It also compares the polarised optical micrographs of the cured samples to the scattering profiles.

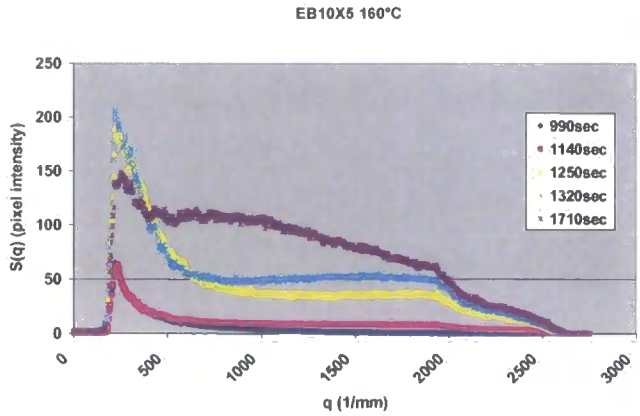

Graph 6.4.1.1 *This graphs shows the scattering profile S(q) versus q for EB10X5 cured at 160°C. This shows evidence of two spinodal peaks; a primary spinodal peak that occurs at low q outside the range of the experiment and a second broad spinodal peak that develops later in the cure process.*

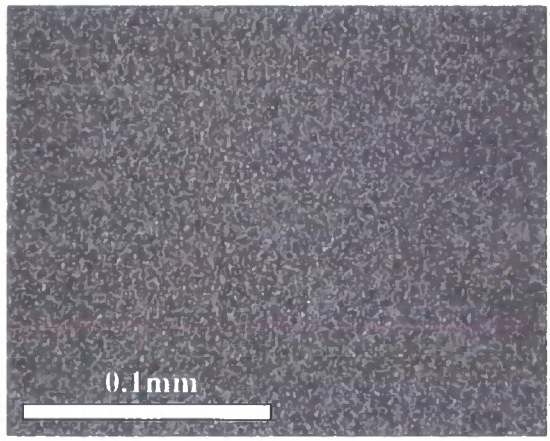

Figure 6.4.1.1 *Optical micrograph of EB10X5 cured isothermally at 160°C. This shows a small-scale particulate morphology.*

The graph 6.4.1.1 shows the SALS scattering profile for EB10X5. This appears to show double spinodal peak behaviour. There is evidence that early in the cure process a spinodal peak forms at low q, unfortunately this is outside the range of the experiment and only the tail end of the peak is observed. This primary peak appears to grow in magnitude. There is also a secondary peak that begins to form at around 1250 seconds this develops into a very broad flat peak. The micrograph shown in figure 6.4.1.1 shows the final cured morphology for EB10X5 and this clearly shows a fine scale particulate morphology. This suggests that this morphology has formed from a percolation to cluster transformation.

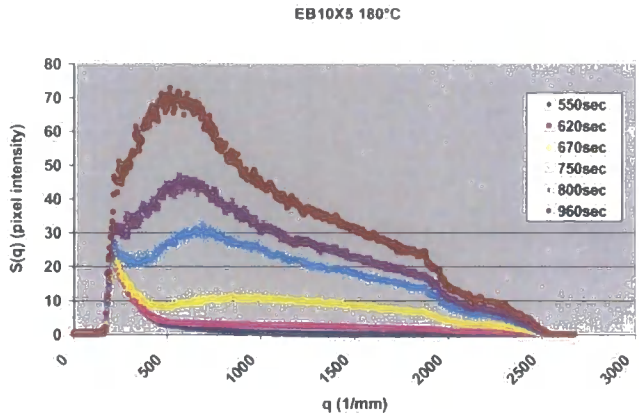

Graph 6.4.1.2 This shows the S(q) versus q plots for EB10X5 cured at 180℃. This shows the formation of a single spinodal peak that shifts to lower q as the cure progresses.

The Graph 6.4.1.2 shows the SALS S(q) versus q scattering profiles for EB10X5 cured at 180°C. This shows the initial formation of a broad peak that forms after around 670 seconds. This peak shifts to a lower q value as the cure progresses and increases in intensity. The figure 6.4.1.2 below shows the cured morphology of this sample. This shows a clear particulate morphology that has formed from a spinodal decomposition, which again suggests percolation to cluster transformation behaviour in this system.

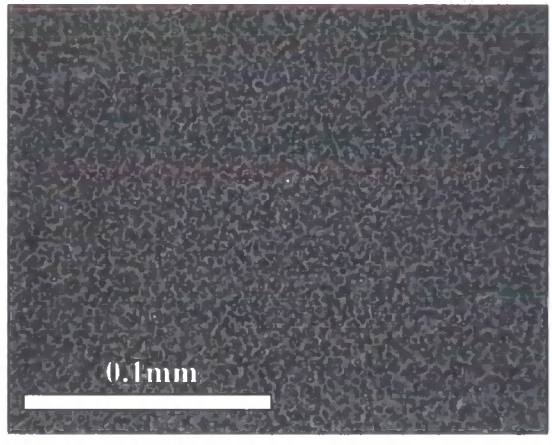

Figure 6.4.1.2 Optical micrograph of EB10X5 cured isothermally at 180℃. This shows a small scale particulate morphology

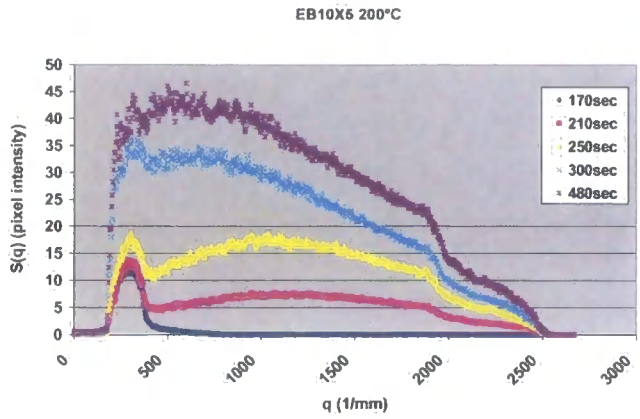

Graph 6.4.1.3 This shows the S(q) versus q plots for EB10X5 cured at 200℃. This shows evidence of the formation of two spinodal peaks.

The graph 6.4.1.3 shows the S(q) versus q plot for EB10X5 cured isothermally at 200°C. This seems to show the formation of two peaks, a very sharp primary peak that occurs early in the cure cycle and later in the cure cycle a broad peak develops and shifts to lower q as cure progresses. The primary peak here is unusual in its shape and definition and may be an artefact of the experiment. Its position relative to q remains constant which is unusual and not consistent with other primary spinodal peaks observed in these experiments. This could possibly be associated light diffraction around the beam stop. It is also possible that a spinodal process is occurring at a q value lower than that examined in this experiment.

The secondary peak that develops has a broad profile. The position of this peak shifts to lower q during the cure process

The figure 6.4.1.3 shows the final cured morphology of the EB10X5 cured at 200°C. This shows small scale particulate morphology, due to the peak formation in the S(q) versus q plot for this system it is likely this has formed by a percolation to cluster transformation.

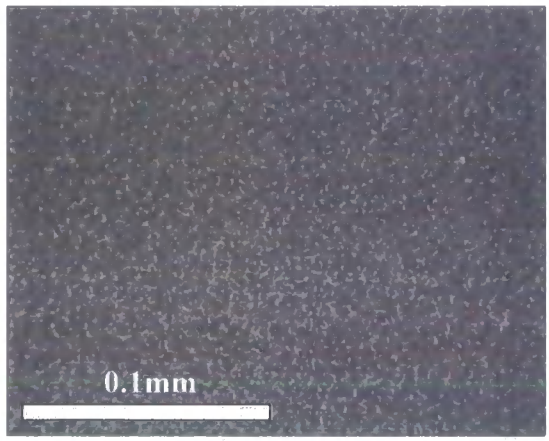

Figure 6.4.1.3 Optical micrograph of EB10X5 cured isothermally at 200℃. This shows a small scale particulate morphology

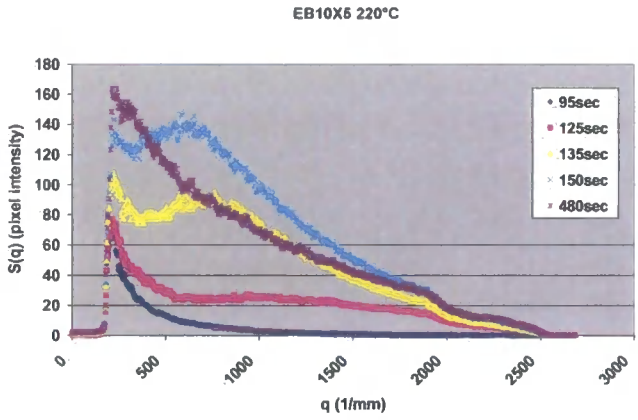

Graph 6.4.1.4 This shows the S(q) versus q plots for EB10X5 cured at 220℃. This shows the formation of a spinodal peak that shifts to lower q as the cure progresses. There is also evidence of a spinodal peak forming at low q outside the range of the experiment.

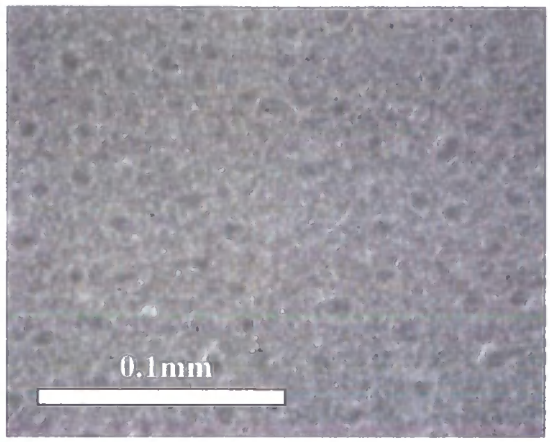

Figure 6.4.1.4 Optical micrograph of EB10X5 cured isothermally at 220℃. This shows particulate morphology that has a bimodal size distribution. This is likely to be the result of a percolation to cluster transformation

Graph 6.4.1.4 shows the SALS S(q) versus q plot for EB10X5 In this trace there appears to be two spinodal processes occurring. In the trace at 95 seconds there may be evidence of a peak occurring at a q value below 250 mm^{-1}. A major peak begins to form after around 125 seconds into the cure. This peak is broad but becomes well defined and shifts to lower q as the cure progresses.

The optical micrograph of the cured morphology for EB10X5 is shown in figure 6.4.1.4 and this shows a particulate morphology that appears to have a bimodal size distribution to the dispersed phase. It is likely that this has resulted from percolation to cluster transformations of the two spinodal separation that are indicated in the S(q) vs q plot for this formulation.

6.4.1.2 R(q) vs q data for EB10X5.

R(q) vs q plots were obtained for EB10X5 at the different isothermal cure temperatures. This data is obtained from the S(q) vs q plots shown in the previous section. Where possible R(q) vs q plots were taken for both primary and secondary phase separations. The times between which the R(q) values are taken was restricted to the early stage formation of the peak where the peak max remains relatively constant with respect to q. The plots all showed a well defined peaks for the observed

spinodal decomposition process. A typical example of a R(q) versus q plot from this series is shown in graph 6.4.1.5. From these plots $R(q)_{max}$ and $q_{(max)}$ values were obtained for the series. This data is shown in table 6.4.1.1

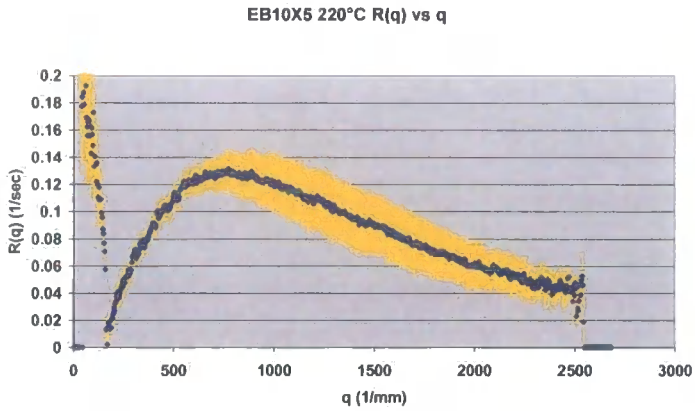

Graph 6.4.1.5 R(q) vs q plot for EB10X5 cured at 220°C. This shows a single well-defined peak. R(q) values were taken between 120 and 150 seconds during the early stages of the spinodal decomposition

EB10X5	**160°C**	**180°C**	**200°C**	**220°C**
R(q)max primary (1/sec)	N/A	0.0158	0.09	0.13
$q_{(max)}$ (1/mm)	600	750	850	850
R(q)max Secondary (1/sec)	0.0033	N/A	N/A	N/A
$q_{(max)}$ (1/mm)	970	N/A	N/A	N/A

Table 6.4.1.1 Table of $R(q)_{max}$ values for EB10X5 for different isothermal cure temperatures

The table 6.4.1.1 above shows the $R(q)_{max}$ values for EB10X5 cured at different isothermal cure temperatures. It can be observed that at cure temperatures above 180°C there is a rapid rise in the phase separation rate, $R(q)_{max}$ which is likely to due the cure temperature being above the Tg to the PES:PEES thermoplastic. This will effectively prevent vitrification of the thermoplastic rich phase and increase the phase separation rate.

6.4.1.3 R(q)/q² vs q² plots for EB10X5

R(q)/q² vs q² plots for EB10X5 were obtained for the different isothermal cure temperatures. An example of such a plot from the EB10X5 series is shown in graph 6.4.1.6. Cahn -Hilliard theory for spinodal decomposition predicts this plot should yield a straight line with a clear intercept on the y-axis. However the plots obtained for this series were not straight lines as can be seen in figure 6.4.1.6. To obtain D^*_{app} from these plots the curve was extrapolated and an intercept on the y-axis taken.

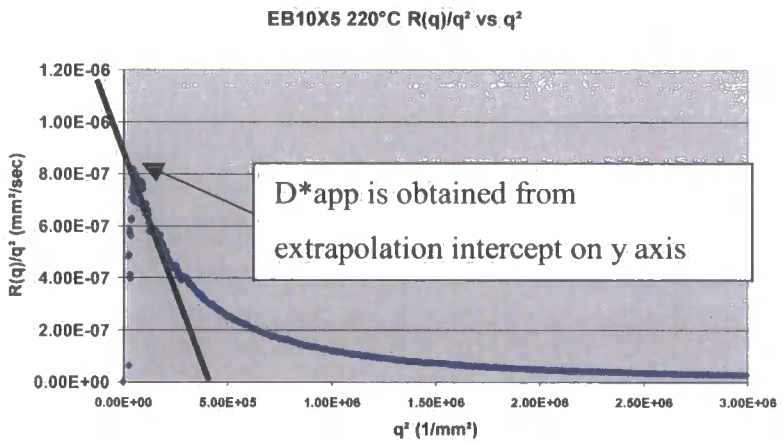

Graph 6.4.1.6 R(q)/q² vs q² for EB10X5 cured isothermally at 160 ℃. This plot is for the primary spinodal peak observed in this system.

The fact that these R(q)/q^2 versus q^2 plot are not linear suggests that Cahn-Hilliard theory does not fully describe the spinodal decomposition occurring in these reaction induced phase separation processes.

EB10X5	**160°C**	**180°C**	**200°C**	**220°C**
D^*_{app} primary (mm²/sec)	N/A	8.5E-8	3.25E-7	8.4E-7*
D^*_{app} secondary (mm²/sec)	8E-9	N/A	N/A	N/A

Table 6.4.1.2 Table showing D^*_{app} for EBX10 cured at different isothermal temperatures. (the value at 220 ℃ may be a secondary spinodal decomposition).*

The table 6.4.1.2 above shows the apparent diffusion coefficients for the spinodal process in EB10X5 cured at different cure temperatures. This shows that as the cure temperature increases the apparent diffusion coefficient for the spinodal phase separation process increases. It is uncertain as to whether the value quoted for 220°C is for a primary or secondary phase separation. It is very possible that this is a secondary phase separation with the primary phase separation process being outside the q range of the experimental range.

6.4.1.4 % Conversion versus cure time for EBX10X5

In this section the % conversion versus cure time for all the different isothermal cure temperatures is reported. This information is calculated from isothermal cure experimentation outlined in chapter 4.

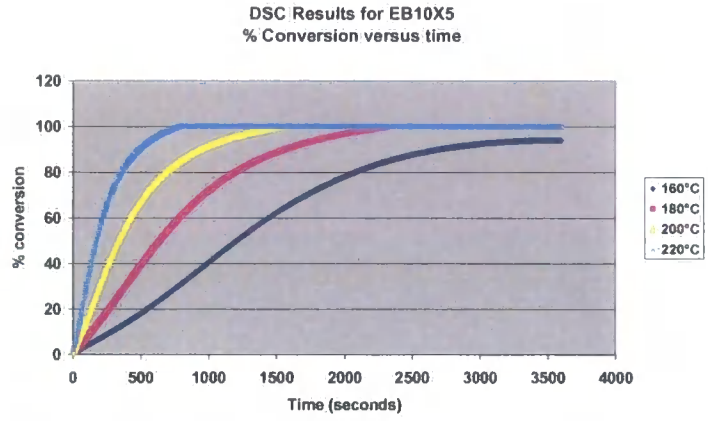

Graph 6.4.1.7 EB10X5 % conversion versus cure time for different isothermal cure temperatures.

The graph 6.4.1.7 shows the % conversion versus time for the different isothermal cure temperatures for EB10X5. This information was obtained from isothermal DSC method outlined in chapter 4.

6.4.1.5 Discussion on results for EB10X5.

The results in the previous section show that the mechanism of phase separation for EB10X5 at all isothermal cure temperature is spinodal decomposition followed by percolation to cluster transformation. This is indicated by the peaks observed in the S(q) versus q plots and from the micrographs of the final cured morphology.

It can also be observed that in some cases there is clear evidence that double spinodal decomposition occurs. Unfortunately it appears that a primary phase separation may be occurring at a very low q value that is outside the q range studied in these experiments. This obviously makes a true Cahn-Hilliard analysis of the spinodal processes occurring somewhat difficult because the primary spinodal peak is not fully observed.

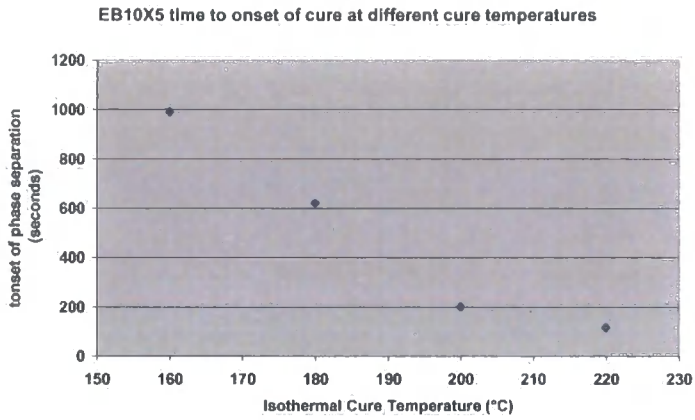

Graph 6.4.1.8 This graph shows the time to onset of phase separation for the different cure temperatures.

The graph 6.4.1.8 above shows the relationship between the cure temperature and the time to onset of the phase separation process as observed by light scattering. As expected the time to onset of phase separation decreases with increasing isothermal cure temperature. Using this information and the % conversion versus cure time relationship shown in graph 6.4.1.5 shows the % conversion at phase separation at the various isothermal cure temperatures can be established.

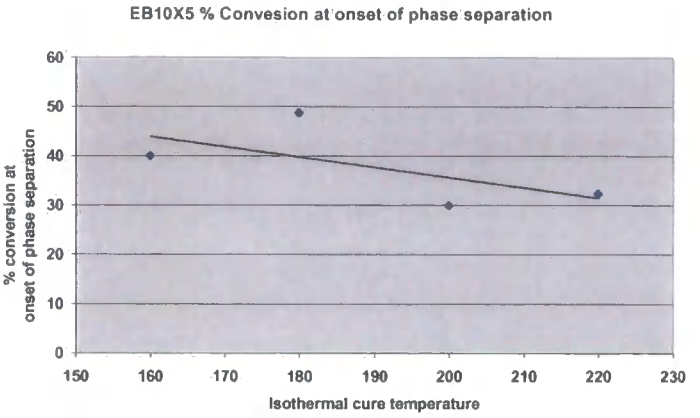

Graph 6.4.1.9 *This graph shows the % conversion of the thermosetting system EB10X5 at phase separation for the different isothermal cure temperatures.*

The graph 6.4.1.9 shows the relationship between the % conversion at the onset of phase separation and the isothermal cure temperature for the EB10X5 system. This shows a general decreasing trend with increasing temperature. This suggests that the system exhibits LCST behaviour. LCST behaviour is also shown in the epoxy system EB10 shown in the previous chapter. It is interesting to compare EB10 and EB10X5. Both these systems show LCST however the % conversion at the onset of phase separation is higher in the case of EB10X5 (see graph 5.4.1.8 in the previous chapter). This applies for all isothermal cure temperatures. This suggests that when the tri-functional epoxy is present in the system the thermoplastic is more compatible with the forming epoxy network and the phase separation process is delayed.

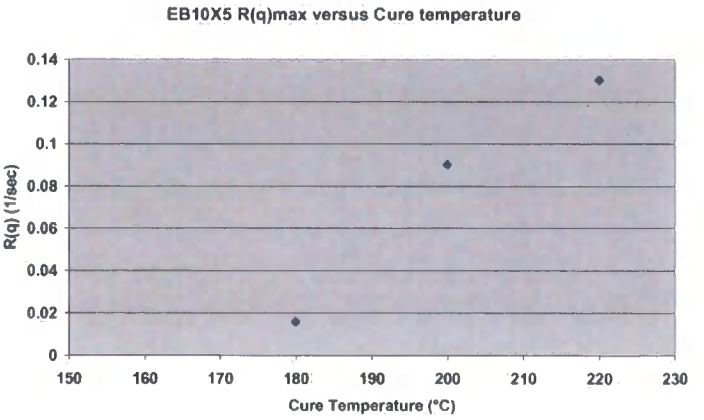

Graph 6.4.1.10 *This graph shows the R(q)max for the different cure temperatures. This is for the observed primary phase separation.*

The graph 6.4.1.10 above shows the relationship between the $R(q)_{max}$ for the primary spinodal peak versus the isothermal cure temperature. It is debatable to whether the $R(q)_{max}$ value is for a primary or secondary spinodal process however it is clear that the trend here is for an increasing rate of phase separation with increasing cure temperature. This again suggests LCST behaviour because a higher $R(q)_{max}$ suggests that there is a higher thermodynamic driving force for separation process. This can only suggest that at higher temperatures the system is deeper into the spinodal region and this is characterised by LCST behaviour. One complicating factor in this assumption is that the Tg of the PES:PEES copolymer is 195°C. Therefore in the case of the 200°C and 220°C experiments the Tg of the thermoplastic is exceeded and it is unlikely that the thermoplastic rich phase vitrifies in the early stages of the phase separation. However it may be possible that at lower cure temperatures (160°C and 180°C) the forming thermoplastic rich phase may instantly vitrify and greatly reduce the rate of phase separation despite the high thermodynamic driving force for the phase separation process.

It is interesting to compare the $R(q)_{max}$ values obtained in both EB10 and EB10X5. (see graph 5.4.1.9 in the previous chapter). This shows that the $R(q)_{max}$ values are slightly higher at all cure temperatures compared to EB10. This may suggest that the addition of MYO510 has a two-fold effect on the system. Firstly the MYO510 tri-functional epoxy acts as an effective solvent for the PES:PEES thermoplastic and stabilises the system and delays the onset of phase separation. However the formation of the more highly branched thermoset network as a result of the presence of the tri-functional epoxy produces a phase separation process which has a higher $R(q)_{max}$. This suggests that the PES:PEES copolymer is much less compatible with the more highly branched epoxy network.

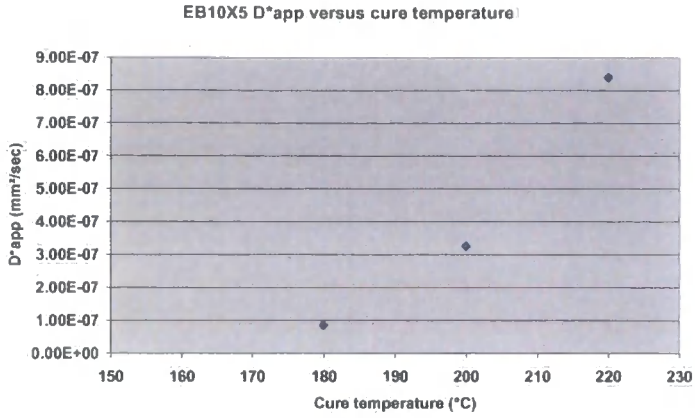

Graph 6.4.1.11 *This graph shows the relationship between D^*_{app} and the isothermal cure temperature for the primary spinodal decomposition peak. Note that it is not clear from these experiments if the 220℃ value is for a primary or secondary spinodal process.*

The Graph 6.4.1.11 above shows the relationship between D^*_{app} and the isothermal cure temperature for the primary spinodal decomposition process observed in the SALS S(q) versus q plots. It is debatable if the 220°C data is a primary or secondary peak but the general trend is for a higher D^*_{app} for higher cure temperature. This again supports the theory that this formulation shows LCST behaviour. It is interesting to note that the D^*_{app} values for EB10 and EB10X5 are very similar in magnitude (see graph 5.4.1.10 in the previous chapter) however the D^*_{app} values are slightly higher in the case for EB10X5 but this may just be experimental scatter.

6.4.2 Results from system EB15X5

This section describes the results from the epoxy blend system EB15X5. In this system 5 mole % of the epoxy resin is tri-functional. The system contains 15 % PES:PEES thermoplastic. The precise formulation is detailed in table 6.3.1.1 above

6.4.2.1 SALS results form system EB15X5

This section discusses the light scattering results from system EB10X5 cured at different isothermal cure temperatures. It also compares the polarised optical micrographs of the cured samples to the scattering profiles.

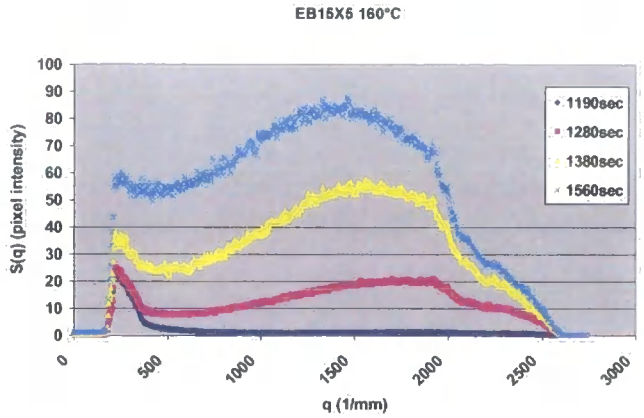

Graph 6.4.2.1 S(q) versus q plot for EB15X5 cured at 160 ℃

Graph 6.4.2.1 above shows the SALS S(q) versus q plot for EB15X5 cured at 160°C. This shows a broad spinodal peak forming after around 1200 seconds. However the traces may suggest that some event is occurring at low q. This may be just spurious scattering around the beam stop but due to the fact that this event occurs outside of the range of the experiment it is difficult to determine accurately.

There is also an unusual shape to the forming major spinodal peak at high q. This may be the overlapping of two peaks.

The micrograph of the cured morphology for EB15X5 is shown in figure 6.4.2.1 below. This shows a small-scale particulate morphology with a dispersed thermoplastic rich dispersed phase. Because there is clear evidence of a peak formation in the S(q) versus q plot for this sample it is clear that this morphology has arisen as a result of a percolation to cluster transformation .

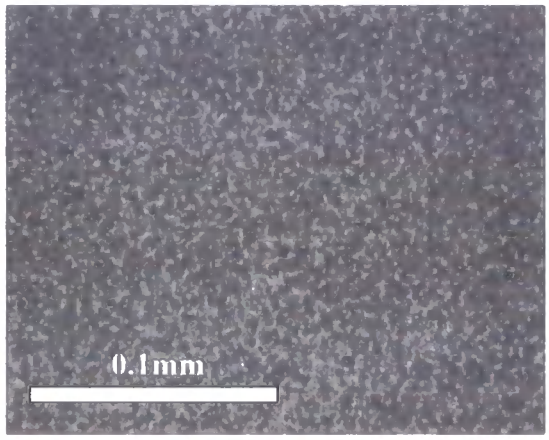

Figure 6.4.2.1 *Optical micrograph of EB15X5 cured at 160°C. This shows a small-scale particulate morphology that has formed from a percolation to cluster transformation.*

The graph 6.4.2.3 shows the S(q) versus q plot for EB15X5 cured at 180°C. This shows the formation of a broad peak after around 450 seconds and moves to lower q . There is an unusual shape to the peak at high q values similar to that observed for this sample-cured at160°C. This may suggest that there may be secondary phase separation process occurring at high q.

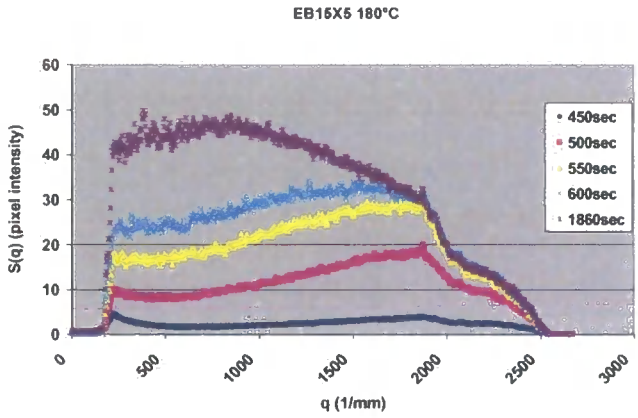

Graph 6.4.2.2 *S(q) versus q plot for EB15X5 cured at an isothermal temperature of 180°C This shows a peak formation with an unusual shape at higher q values.*

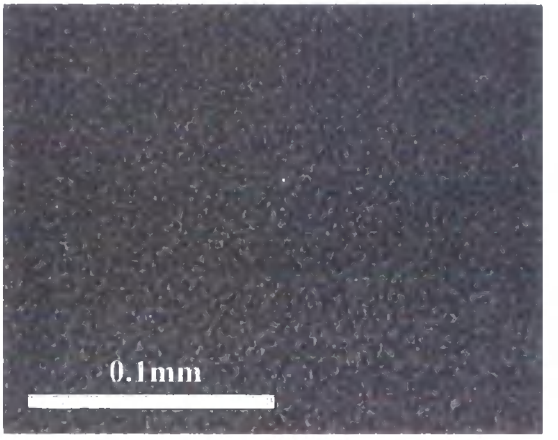

Figure 6.4.2.2 Optical micrograph of the cured morphology of EB15X5 cured at 180℃. This shows a particulate morphology with a dispersed thermoplastic rich phase.

The optical micrograph of the final cured morphology of EB15X5 cured at 180°C is shown in figure 6.4.2.2. This shows a clear particulate morphology with a thermoplastic rich dispersed phase. Due to the formation of a peak in the S(q) versus q plot for this sample during cure it is likely that this has formed as a result of a percolation to cluster transformation.

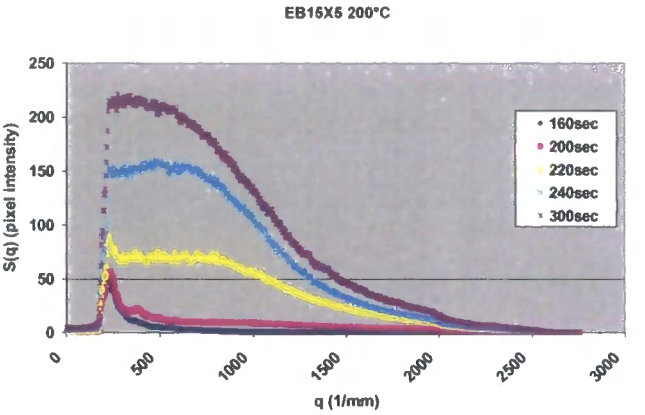

Graph 6.4.2.3 This graph shows the S(q) versus q plot for EB15X5 cured at200℃ This shows the formation of a single spinodal peak.

The graph 6.4.2.3 shows the S(q) versus q plot for EB15X5 and this shows the formation of a single spinodal peak. The peak position shifts slightly to lower q as the cure progresses. The final cured morphology for this system is shown in figure 6.4.2.3 and this also shows a particulate morphology. Due to the peak in the S(q)

versus q plot this morphology has probably formed by a percolation to cluster transformation

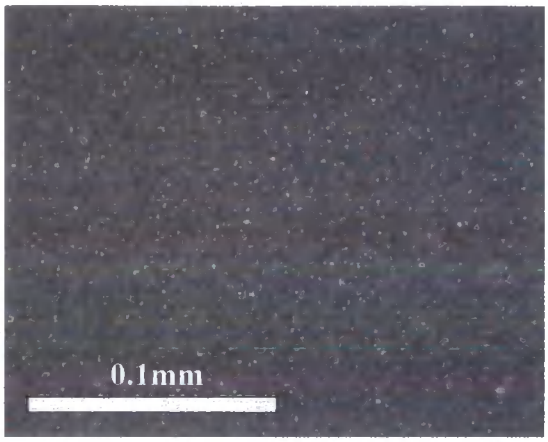

Figure 6.4.2.3 This figure shows the cured morphology of EB15X5 cured at 200℃. This shows a particulate morphology that has formed from a percolation to cluster transformation.

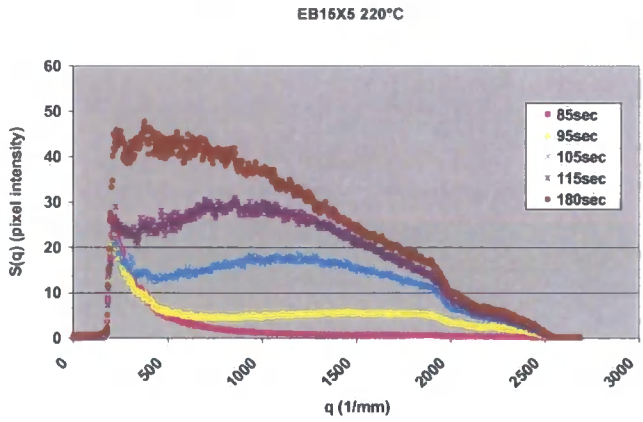

Graph 6.4.2.4 This graph shows the S(q) versus q plot for EB15X5 cured at 220℃ This shows the formation of a spinodal peak which shifts to lower q as the cure advances. There may also be evidence of spinodal peak occurring at low q outside of the range of the experiment.

The graph 6.4.2.4 shows the S(q) versus q plot for EB15X5 cured at 220°C. This shows the formation of a broad spinodal peak that occurs after around 90 seconds into the cure this develops and shifts to lower q as the cure progresses. In the early stages of the cure there is also some evidence that an event is occurring at low q outside the range of the experiment. This may be a spinodal peak but equally it may also be spurious scattering that sometimes occurs around the beam stop.

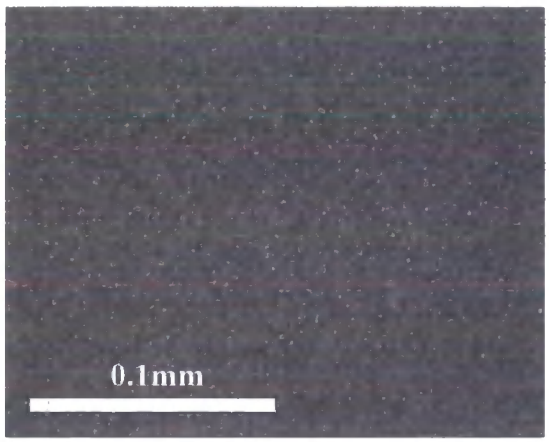

Figure 6.4.2.4 This micrograph shows the final cured morphology of EB15X5 cured at 220°C. This shows a small scale particulate morphology that has occurred through a percolation to cluster transformation

The figure 6.4.2.4 shows the optical micrograph of the final cured morphology of EB15X5 cured at 220°C. This shows a small-scale particulate morphology with a dispersed thermoplastic phase. Due to the formation of a peak in the S(q) versus q plot for this system it is likely that this morphology has arisen from a percolation to cluster transformation

6.4.2.2 R(q) versus q plots for EB15X5 cured at different isothermal temperatures.

This section shows the R(q) versus q results for the EB15X5 formulation cured at different isothermal cure temperatures. The R(q) values were taken for the major peak formed in the S(q) versus q plots in the early stages of the peak formation. $R(q)_{max}$ values were taken from the peak value in theses plots. Graph 6.4.2.5 shows an example of a R(q) versus q plot from this series and the table 6.4.2.1 documents

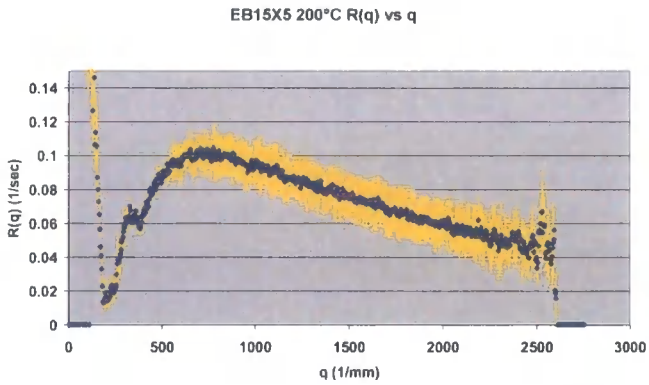

the overall results.

Graph 6.4.2.5 R(q) versus q plot for EB15X5 cured at 200 ℃. This shows a well defined peak occurring at a q value of around 1450 mm^{-1}.

EB15X5	**160°C**	**180°C**	**200°C**	**220°C**
R(q)max (sec^{-1})	0.049	0.033	0.11	0.17
$q_{(max)}$ (mm^{-1})	870	960	760	1248

Table 6.4.2.1 Table showing the R(q)max values for EB15X5 cured at different cure temperatures.

6.4.2.3 R(q)/q² versus q² for EB15X5 cured at different isothermal cure temperatures

This section shows the R(q)/q² versus q² results for different isothermal cure temperatures. This series of plots were not straight lines with a clear intercept on the y axis suggesting that Cahn-Hilliard theory does not fully describe the spinodal decomposition process in these systems. However from these plots extrapolations were taken and D^*_{app} values were taken from the extrapolated intercept on the y axis.

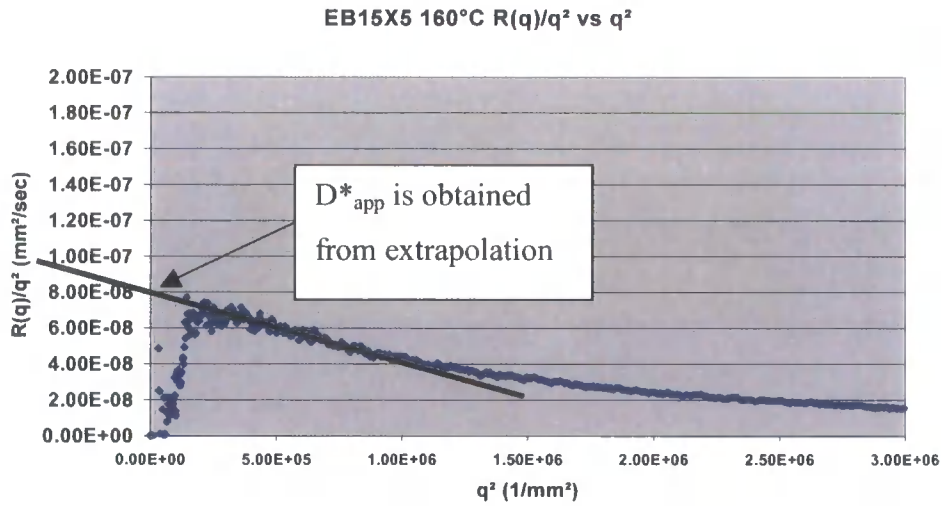

Graph 6.4.2.6 R(q)/q² versus q² plot for EB15X5 cured at 160 °C.

Graph 6.4.2.6 shows an example of a R(q)/q² versus q² plot from this series and also shows how the value of D^*_{app} was obtained from these plots. The table 6.4.2.2 below shows the D^*_{app} results from this series.

EB15X5	**160°C**	**180°C**	**200°C**	**220°C**
D^*_{app} (mm^2/s^{-1})	8E-08	5.1E-07	5.6E-07	3.0E-7

Table 6.4.2.2 This table shows the calculated D^*_{app} values for EB15X5 cured at different isothermal cure temperatures.

6.4.2.4 % Conversion versus time for different isothermal cure temperatures.

The graph 6.4.2.7 shows the relationship between % conversion of the thermoset versus cure time for EB15X5 this data was obtained for isothermal DSC experiments. The method used to obtain this data is detailed in Chapter 4.

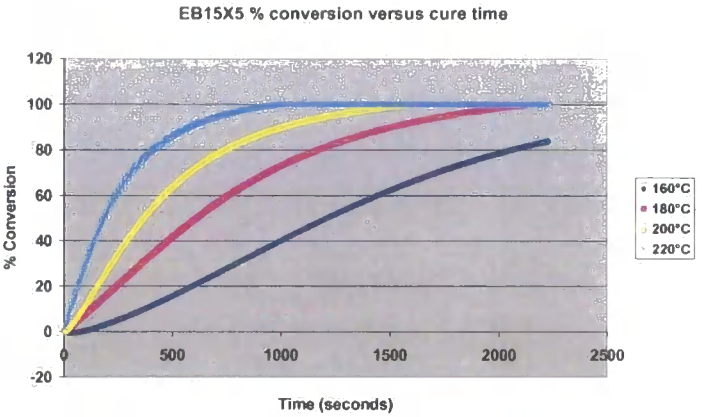

Graph 6.4.2.7 % Conversion versus cure time for different isothermal cure temperatures for EB15X5.

6.4.2.5 Discussion on results form EB15X5.

From the S(q) versus q plots from EB15X5 it can be seen that in all cases a spinodal peak is observed to form during the cure process. In some cases there is some evidence of peaks forming at low q outside the range of the experiment. However at all isothermal cure temperatures the optical micrographs of the final cured morphology show particulate morphology with a dispersed thermoplastic rich phase. This suggests that this morphology has formed from a percolation to cluster transformation. This is very similar to behaviour of EB15 studied in the previous chapter. EB15X5 differs from EB15 only in the fact that it contains 5 mole % of the tri-functional epoxy resin MYO510.

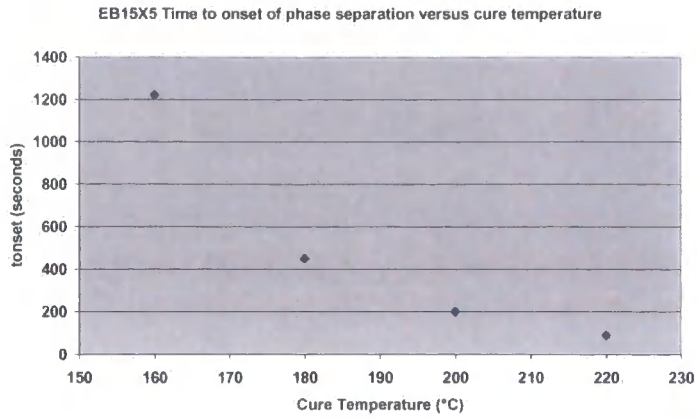

Graph 6.4.2.8 *This graph shows the time to onset of phase separation versus cure temperature for EB15X5.*

The graph 6.4.2.8 shows how the time to onset of phase separation varies with the cure temperature. This as expected shows a decrease in time to phase separation with increasing cure temperature. It is interesting to compare this result with that obtained from the EB15 system (see graph 5.4.2.13 in the previous chapter). From this comparison it can be clearly seen that the time to onset of phase separation is greater for EB15X5 at all cure temperatures.

Using this information together with the % conversion versus cure time shown in graph 6.4.2.7 above the % conversion at the onset of phase separation can be established. This information is shown in the graph 6.4.2.9 below and this clearly shows a decreasing % conversion at the onset of cure as the cure temperature increases. This suggests that the system is exhibiting LCST behaviour. This is a general characteristic of these thermoplastic-thermoset blends.

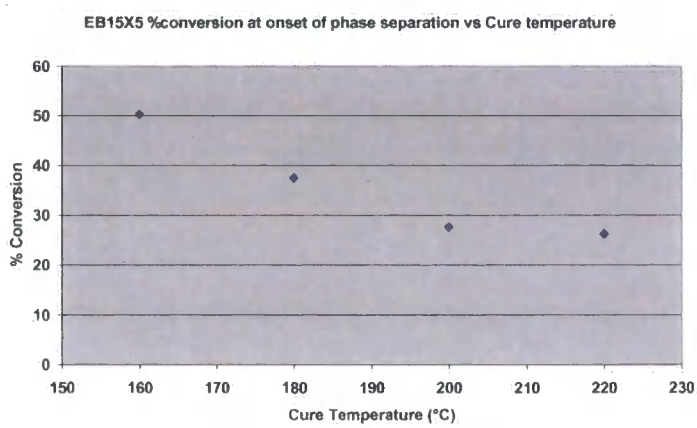

Graph 6.4.2.9 *This graph shows the relationship between the % conversion at the onset of phase separation and the isothermal cure temperature. This indicates LCST behaviour.*

Comparing the % conversion at onset of phase separation for both EB15 and EB15X5 (see graph 5.4.2.14) it can be seen that the level of conversion at which phase separation occurs is significantly greater in the EB15X5 formulation. This suggests that the addition of the epoxy MYO510 to the blend acts to compatibilise the PES:PEES thermoplastic with the thermosetting epoxy network and therefore delays the onset of phase separation.

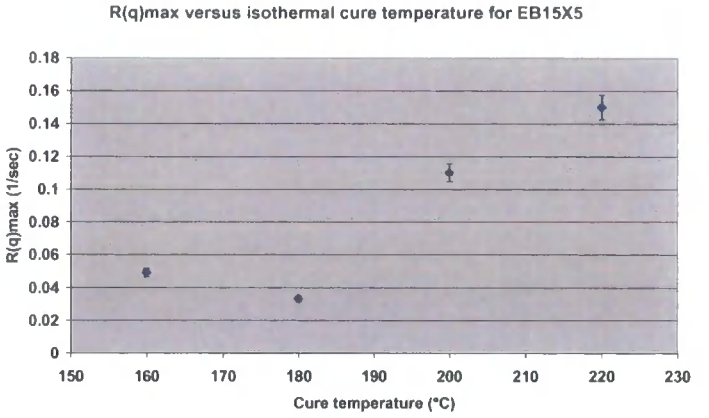

Graph 6.4.2.10 *This graph show the relationship between $R(q)_{max}$ and the isothermal cure temperature for EB15X5. This shows a general increasing trend with increasing cure temperature that suggests LCST behaviour.*

The graph 6.4.2.10 above shows the $R(q)_{max}$ relationship with isothermal cure temperature for EB15X5. This shows an increasing trend with increasing cure temperature. This again confirms that the system shows LCST behaviour. Comparing this result to that from EB15 (Graph 5.4.2.9) it can be seen that the rate of phase separation is lower for EB15X5, this suggests that the presence of MYO510 acts to compatibilise the thermoplastic with the epoxy network and retard the phase separation process.

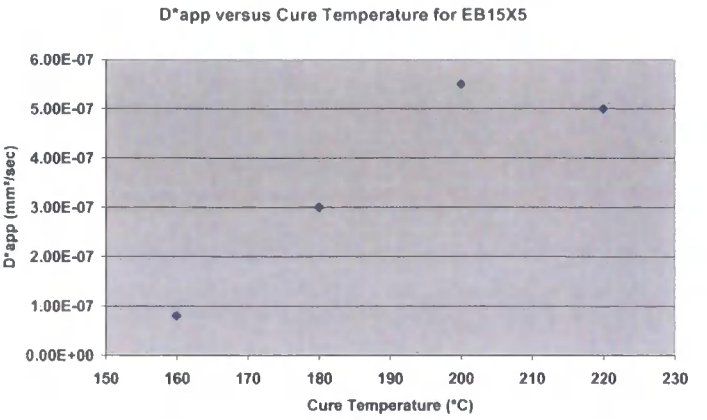

Graph 6.4.2.11 This Graph shows the relationship between D^*_{app} and the isothermal cure temperature for EB15X5.

The graph 6.4.2.11 above shows the relationship between D^*_{app} and the isothermal cure temperature for the EB15X5 system. As expected this shows an increasing trend with increasing temperature, this is further evidence that this system shows LCST behaviour. If this is compared with EB15 the formulations that differs from EB15X5 in that it does not contain any tri-functional epoxy resin (See figure 5.4.2.11) it can be seen that the D^*_{app} values for EB15X5 are greater in magnitude at all temperatures.

6.4.3 Results from system EB20X5

This section describes the results from the epoxy blend system EB20X5. In this system 5 mole % of the epoxy resin is tri-functional. The system contains 20 % PES:PEES thermoplastic. The precise formulation is detailed in table 6.3.1.1 above.

6.4.3.1 SALS results from EB20X5

This section discusses the light scattering results from system EB10X5 cured at different isothermal cure temperatures. It also compares the polarised optical micrographs of the cured samples to the scattering profiles.

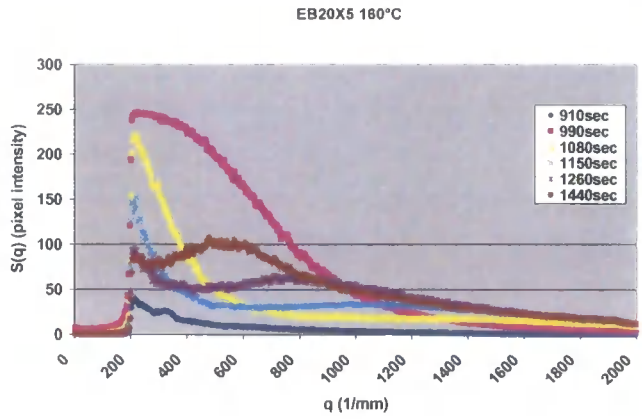

Graph 6.4.3.1 *This graphs shows the scattering profile S(q) versus q for EB20X5 cured at 160°C. This shows evidence of two spinodal peaks; a primary spinodal peak that occurs rapidly after 950sec and moves to low q outside the range of the experiment and a second broad spinodal peak that develops later in the cure process and also shifts to lower q as cure progresses.*

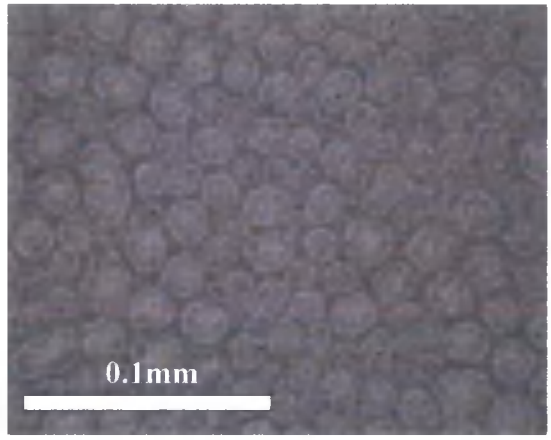

Figure 6.4.3.1 *Optical micrograph of EB20X5 cured at 160°C showing a minor continuous phase and a major dispersed phase. It is likely that the continuous darker phase is the thermoplastic rich phase.*

The graph 6.4.3.1 shows the S(q) versus q plot for EB20X5 this clearly shows the formation of two spinodal peaks that develop and shift to lower q as the cure process progresses. The primary peak begins to form after around 950 seconds and develops very rapidly and shifts to a lower q outside the range of the experiment. The secondary spinodal peak begins to form after around 1150 seconds at a q value of around 1100 mm^{-1}. This is a broad peak that develops and shifts to lower q. This peak remains after the system has fully cured.

The figure 6.4.3.1 shows the final cured morphology of this sample. It can be seen that there is a clear two phase morphology with a dark continuous minority phase which is likely to be the thermoplastic rich phase with a dispersed epoxy rich phase. Due to the spinodal peaks that are observed during the cure of this sample it is clear that the dispersed epoxy rich phase has undergone a percolation to cluster transformation to give this final morphology. In such morphologies it has been previously reported to have high fracture toughness [2]. A closer look at this morphology also shows evidence of secondary phase separation inside the dispersed particles. This may be secondary phase separation process observed in the S(q) versus q plot for this sample.

The graph 6.4.3.2 shows the S(q) versus q plot for EB20X5 cured at 180°C this shows a clear spinodal peak that forms at low q and shifts to lower q outside the q range studied in this experiment. There is also some evidence that there is the formation of a second peak forming after 600 seconds, which manifests itself as a shoulder on the 600 second curve. The optical micrographs for this sample are shown in figure 6.4.3.2. This shows a very interesting morphology, which appears to be a sub-included, or salami type morphology previously seen in rubber modified thermoplastics such as HIPS [3].
Such structures have been reported to have exceptional fracture toughness at low rubber loadings. In this instance this morphology has in fact formed from a double percolation to cluster transformation process.

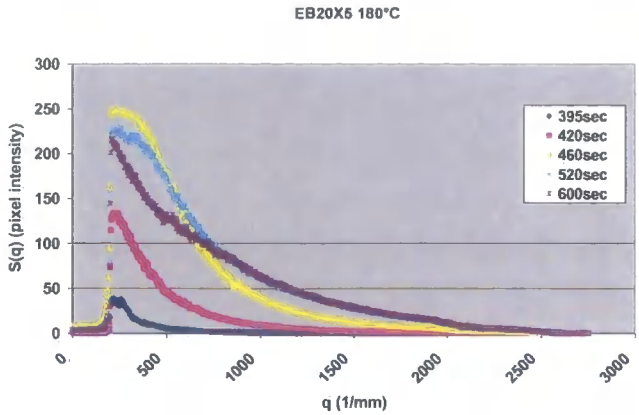

Graph 6.4.3.2 This graph shows the S(q) versus q plot plot for EB20X5 cured at 180℃. This shows the formation of a spinodal peak at low q and evidence of a secondary peak occurring at 600sec.

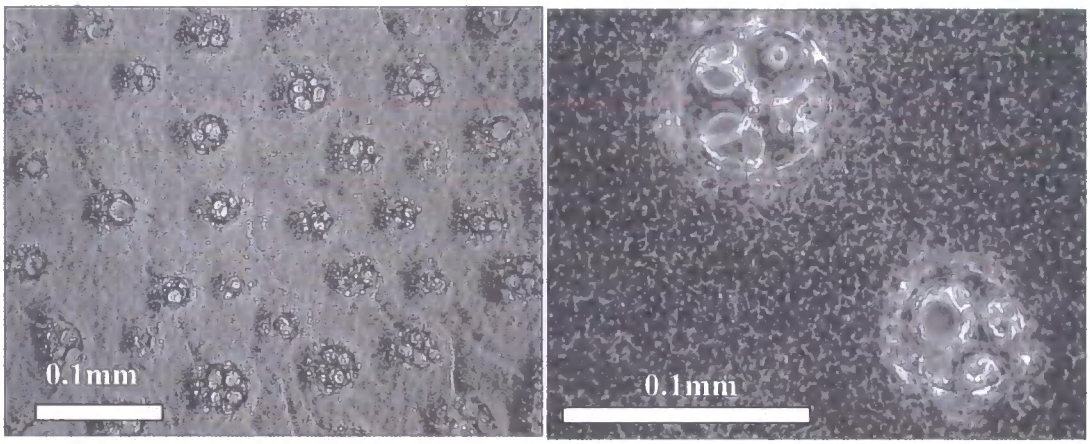

Figure 6.4.3.2 This figure shows the optical micrographs of the EB20X5 sample cured at 180℃. This shows a sub-included dispersed morphology this has likely resulted from a percolation to cluster transformation of two spinodal processes.

A closer look at the higher magnification micrograph in figure 6.4.3.2 it can be seen that in the continuous phase there is also a small scale particulate morphology, this is likely to consist of thermoplastic rich particulates in an epoxy rich matrix, whereas the dispersed salami particles are likely to consist of a continuous thermoplastic rich phase with a dispersed epoxy phase. This is a most unusual morphology for a thermoplastic-thermoset blend and its properties should be further investigated.

The graph 6.4.5.3 shows the S(q) versus q plot for EB20X5 cured at 200°C, This appears to show the formation of a single spinodal peak that unfortunately occurs slightly outside of the q range of the experiment.

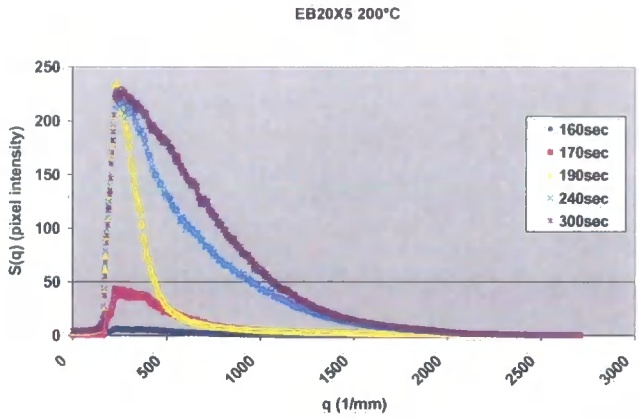

Graph 6.4.3.3 This graph shows the S(q) versus q plot for EB20X5 cured at 200 ℃. This shows the formation of a spinodal peak at low q

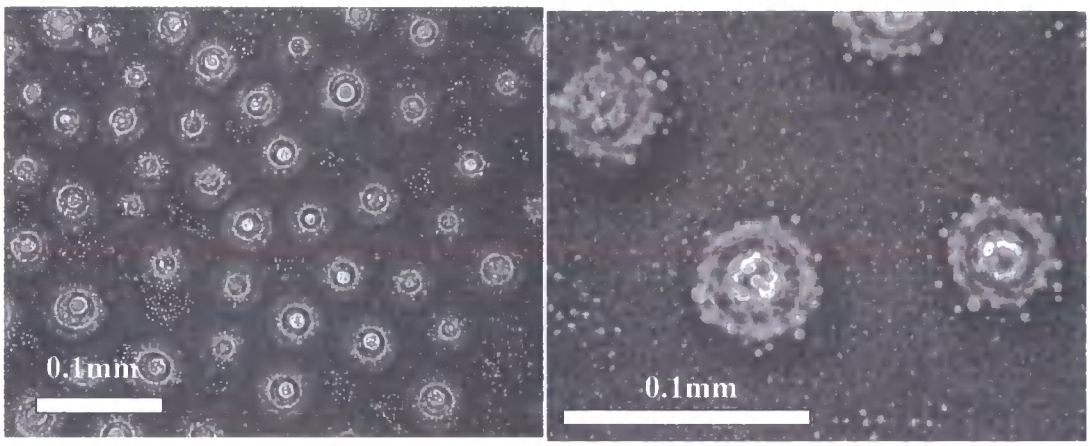

Figure 6.4.3.3 This figure shows the optical micrographs of the EB20X5 sample cured at 200 ℃. This shows a sub-included dispersed morphology this has likely resulted from a percolation to cluster transformation

Optical micrographs for EB20X5 cured at 200°C are shown in figure 6.4.3.3. These show a similar morphology to that seen in the sample cured at 180°C. It shows a sub-included salami type morphology that has likely formed from a percolation to cluster transformation. There is evidence in these micrographs that at some stage the salami particles begin to disperse into the continuous phase to produce a multi type particulate morphology. This has resulted in epoxy rich particles and thermoplastic rich particles dispersed in a continuous epoxy rich phase.

The S(q) versus q plot show in graph 6.4.3.4 is for the EB20X5 system cured at 220°C. This clearly shows the formation of two spinodal peaks. A primary peak that forms early in the cure process at low q, this peak appears to either demise or shift outside the q range of the experiment. A secondary peak forms after around 130 seconds. This peak also shifts to lower q as the cure progresses but the feature remains in the final cured morphology

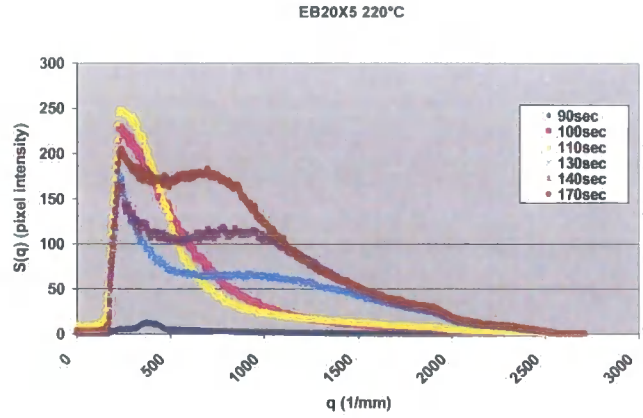

Graph 6.4.3.4 *This graph shows the S(q) versus q plot plot for EB20X5 cured at 220℃. This shows the formation of a two spinodal peaks, one at low q early in the cure process and a secondary peak occurring after 130sec*

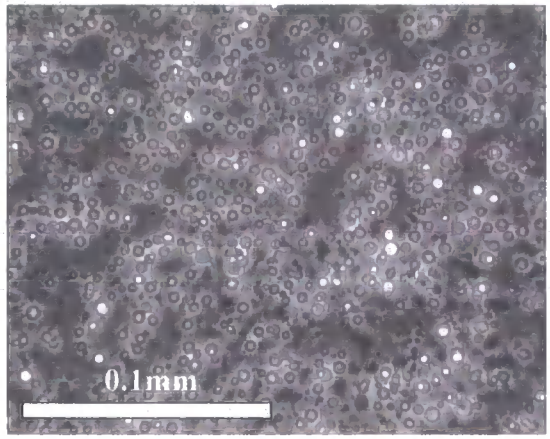

Figure 6.4.3.4 *This figure shows the cured morphology of EB20X5 cured at 220℃. This shows an irregular particulate morphology*

The micrograph of the cured morphology for EB20X5 cured at 220°C is shown in figure 6.4.3.4. This shows an irregular particulate morphology which has probably formed from the complete percolation to cluster transformation of the two spinodal

processes observed in the S(q) versus q plot for this sample. It is possible that this morphology evolved from a sub-included salami morphology from which the sub-included particles dispersed into the continuous phase.

6.4.3.2 R(q) versus q plots for EB20X5 cured at different isothermal temperatures

R(q) versus q plots were obtained for the early stages of the observed spinodal decomposition process in the S(q) versus q plots reported in the previous section. From these plots the $R(q)_{max}$ and $q_{(max)}$ values are obtained. An example of an R(q) versus q plot from this series is shown in graph 6.4.3.5.

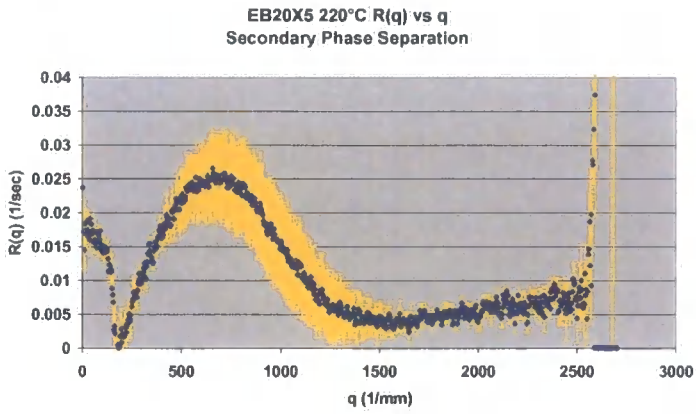

Graph 6.4.3.5 R(q) versus q plot for the secondary spinodal decomposition observed in EB20X5 cured at 220℃.

Table 6.4.3.1 shows the $R(q)_{max}$ and $q_{(max)}$values for the EB20X5 system.

EB20X5	160°C	180°C	200°C	220°C
R(q)max Primary Spinodal (s^{-1})	0.035	0.045	0.14	0.2
$q_{(max)}$ (mm^{-1})	660	490	540	550
$R(q)_{max}$ Secondary Spinodal (1/sec)	0.007	N/A	N/A	0.025
$q_{(max)}$ (1/mm)	790			760

Table 6.4.3.1 This table shows the $R(q)_{max}$ values for both primary and secondary spinodal processes observed in EB20X5 cured at different isothermal temperatures.

6.4.3.3 R(q)/q² versus q² plots for EB15X5 cured at different isothermal cure temperatures

R(q)/q² versus q² plots were obtained for the different isothermal cure temperatures for EB20X5. Where appropriate D*app values are calculated for both primary and secondary processes. These plots were generally not linear as predicted by Cahn-Hilliard theory, However extrapolations were taken from the data to obtain the D^*_{app} value for the system. An example of a $R(q)/q^2$ versus q^2 plot from this series is shown in 6.4.3.6 and the D^*_{app} values are shown in table 6.4.3.2.

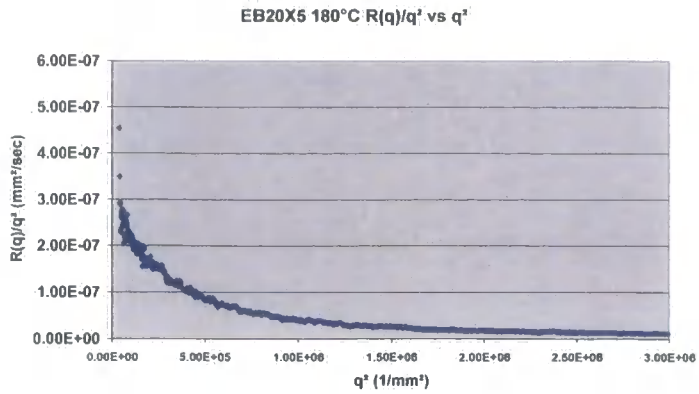

Graph 6.4.3.6 R(q)/q² versus q² plot for the primary spinodal peak for EB20X5 cured at 180°C

EB20X5	160°C	180°C	200°C	220°C
D^*_{app} (mm²/sec) Primary	6E-07	3E-07	6E-06	1E-05
D^*_{app} (mm²/sec) Secondary	2E-08	N/A	N/A	1.38E-08

Table 6.4.3.2 This table shows the calculated D^*_{app} for the primary and secondary spinodal decomposition processes

6.4.3.4 EB20X5 % Conversion versus time for different isothermal cure temperatures

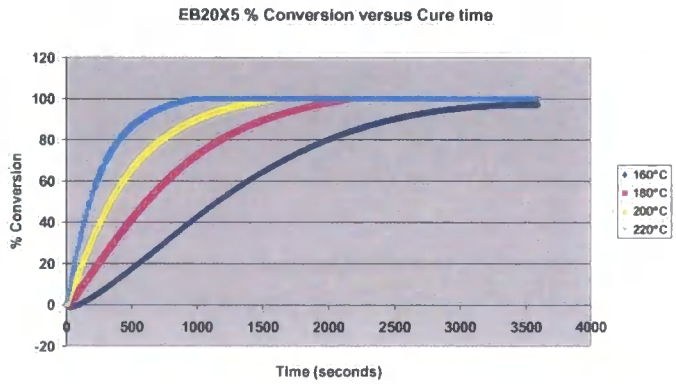

Graph 6.4.3.7 EB20X5 % conversion versus cure time for different isothermal cure temperatures

The graph 6.4.3.7 shows the relationship between % conversion of the thermoset versus cure time for EB20X5 this data was obtained for isothermal DSC experiments. The method used to obtain this data is detailed in Chapter 4.

6.4.3.5 Discussion of results from EB20X5

The previous section showed the S(q) versus q plots for EB20X5 cured at different isothermal cure temperatures. From these it is clear to see that the mechanism for phase separation in this blend at all temperatures is spinodal decomposition. In some cases two spinodal processes can be clearly observed. At 160°C a percolation to cluster transformation has occurred which has resulted in a continuous thermoplastic rich phase and a discontinuous epoxy rich phase. There is also evidence of secondary phase separations in the dispersed phase. The morphologies in the system cured at 180°C and 200°C show a very interesting morphology which is a sub-included or so called salami morphology. This has formed from a double percolation to cluster transformation. It is possible that these morphologies have interesting mechanical properties. The morphologies observed in the EB20X5 are very similar than that observed in EB20 system reported in the previous chapter.

The graph 6.4.6.1 below shows the time to onset of phase separation for the different isothermal cure temperatures. The graph show the onset times for both primary and secondary phase separation processes.

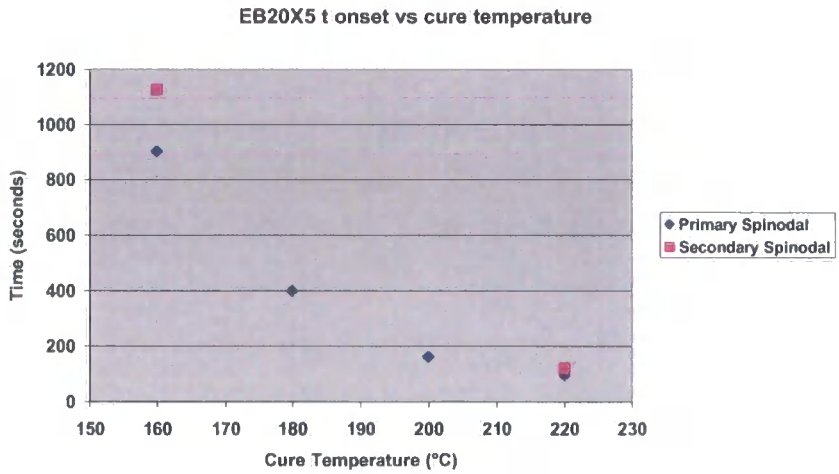

Graph 6.4.3.8 This graph shows the relationship between the time to onset of phase separation and the isothermal cure temperature for both primary and secondary phase separation processes.

Comparing this data from EB20X5 with EB20 (see chapter 5) it can be seen that the onset times for EB20X5 are increased. The onset of phase separation is delayed with the addition of the tri-functional epoxy resin.

This information can be used in conjunction with the % conversion versus time data from DSC studies to give the % conversion at the onset of phase separation for the different isothermal cure temperatures. This is shown in the graph 6.4.6.2 for both primary and secondary phase separation processes.

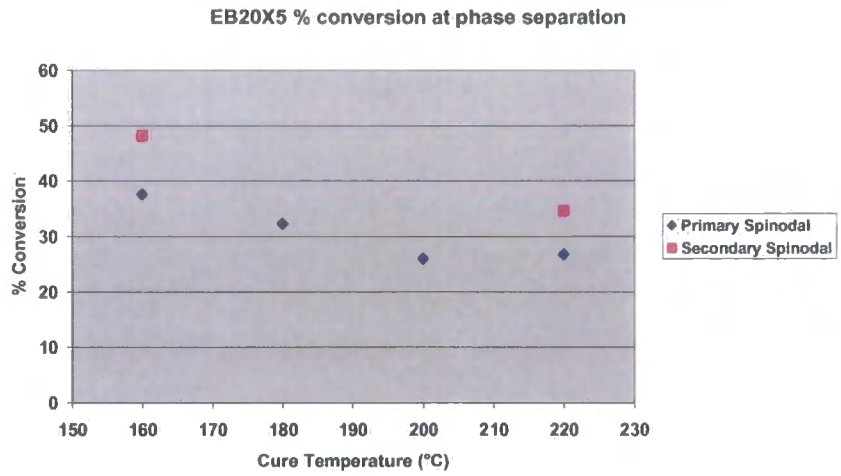

Graph 6.4.3.9 *This graph shows the % conversion of the thermosetting system EB20X5 at the onset of phase separation for the different isothermal cure temperatures Data is shown for both primary and secondary spinodal processes.*

The data in graph 6.4.3.9 above suggests that the system behaves in a LCST fashion. This is characteristic of these epoxy blend systems. Comparing EB20X5 with EB20 it can be seen that in for EB20X5 the % conversion at the onset of phase separation is higher at all cure temperatures. Again this suggests that the incorporation of the tri-functional epoxy MYO510 compatibilises the thermoplastic with the epoxy network. It is therefore likely that the MYO510 epoxy is a more effective solvent for the thermoplastic that the di-functional PY306 epoxy.

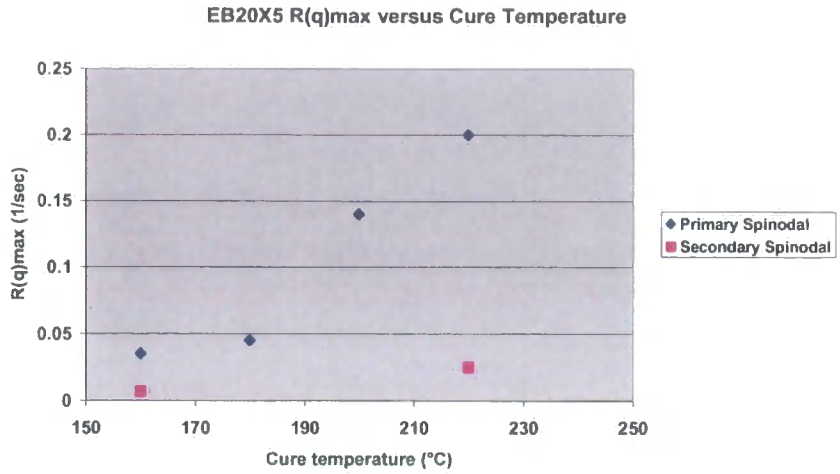

Graph 6.4.3.10 *This graph show the relationship between $R(q)_{max}$ and the isothermal cure temperature for EB20X5. This shows a general increasing trend with increasing cure temperature that suggests LCST behaviour*

The Graph 6.4.3.10 above shows how the $R(q)_{max}$ values for both primary and secondary phase separations change with isothermal cure temperature. This shows an increasing trend with increasing cure temperature. There appears to be a significant increase in the $R(q)_{max}$ value above 180°C which may reflect the Tg of the thermoplastic phase. This suggests that the sub 180°C cured systems are hindered by vitrification of the emerging thermoplastic rich phase. Comparing this data with the $R(q)_{max}$ values form EB20 (see chapter 5) it can be clearly seen that $R(q)_{max}$ values for EB20X5 are lower than in EB20. This suggests that the tri-functional epoxy is a better solvent for the thermoplastic and reduces the tendency for the system to phase separate. It could also be proposed that the phase separation process is hindered by the higher level of branching in the epoxy network due the presence of the tri-functional epoxy.

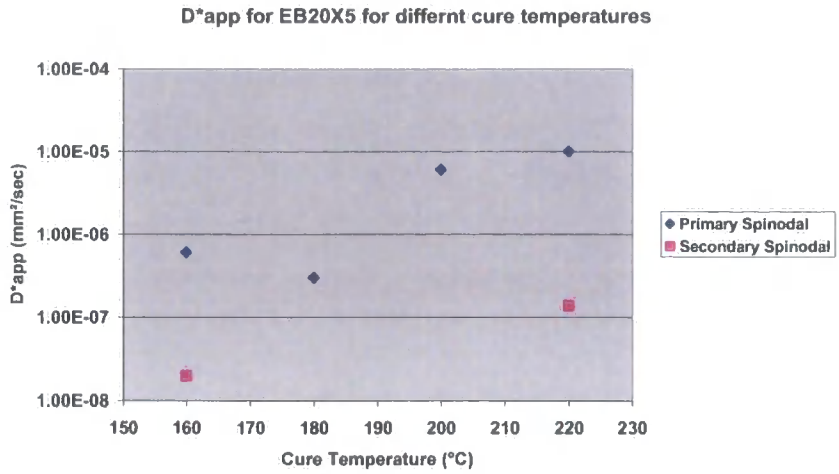

Graph 6.4.3.11 *This Graph shows the relationship between D^*_{app} and the isothermal cure temperature for EB20X5 for both primary and secondary phase separation processes.*

The graph 6.4.3.11 above shows how the D^*_{app} varies with isothermal cure temperature for both primary and secondary phase separations. This shows a strong increasing trend with increasing cure temperature for both primary and secondary processes. This further confirms the LCST behaviour. Comparing this result with that from EB20 (see previous chapter) it can be seen that the values of the D^*_{app} are similar in magnitude for the individual isothermal cure temperatures.

6.4.4 Results from system EB25X5

This section describes the results from the epoxy blend system EB25X5. In this system 5 mole % of the epoxy resin is tri-functional. The system contains 25 % PES:PEES thermoplastic. The precise formulation is detailed in table 6.3.1.1 above.

6.4.4.1 SALS results from EB25X5

This section discusses the light scattering results from system EB10X5 cured at different isothermal cure temperatures. It also compares the polarised optical micrographs of the cured samples to the scattering profiles.

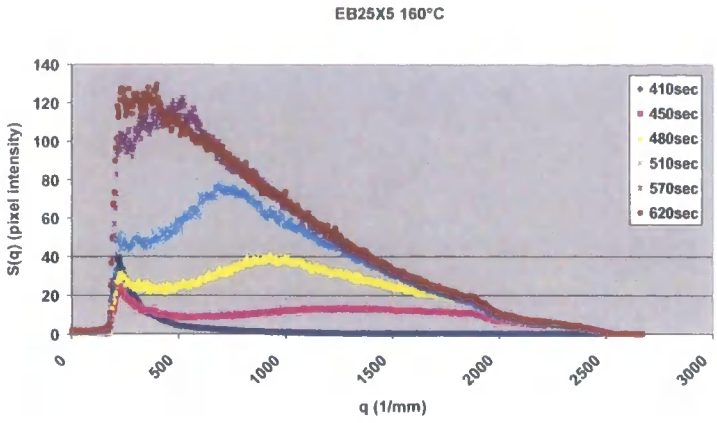

Graph 6.4.4.1 S(q) versus q plot for EB25X5 cured at 160°C. This shows a well defined peak that forms after 420 s. The peak develops and shifts to a lower q as the cure advances.

The graph 6.4.4.1 shows the S(q) versus q plot for EB25X5 cured at 160°C. This shows a single spinodal peak forming after 420 seconds. This peak becomes well defined and shifts to lower q as the cure progresses. There is no obvious region in the early stages of the phase separation process where the peak position remains at a constant q as soon as the peak forms its position begins to shift to lower q. This suggests that there is an increase in spinodal length of the forming morphology. The figure 6.4.4.1 shows the optical micrograph of the EB25X5 system cured at 160°C and this shows a particulate morphology. Due to the strong peak observed in the S(q) versus q plot for this system this morphology has formed from a percolation to cluster transformation. It is possible that in this system the dispersed phase in the epoxy rich phase with a continuous thermoplastic rich phase. This morphology is termed phase inverted and is commonly observed in thermoplastic-thermoset blends with super critical thermoplastic loadings.

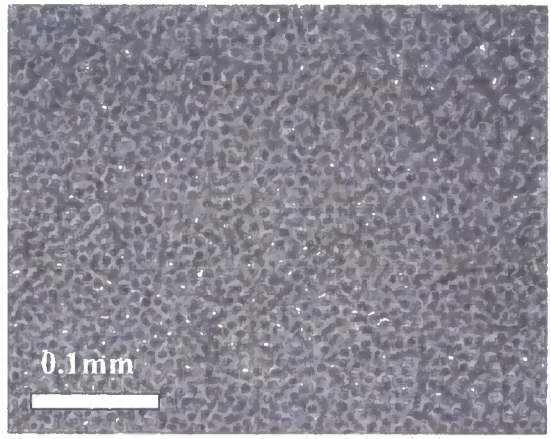

Figure 6.4.4.1 *This figure shows the optical micrograph of EB25X5 cured at 160℃. This shows a particulate morphology which has formed from a percolation to cluster transformation.*

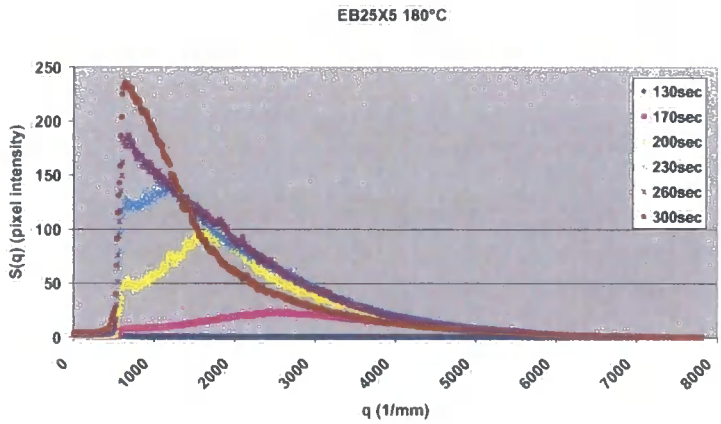

Graph 6.4.4.2 *S(q) versus q plot for EB25X5 cured at 180℃. This shows a well defined peak that forms after 170 s. The peak develops and shifts to a lower q as the cure advances*

The graph 6.4.4.2 above shows the S(q) versus q plot for EB25X5 cured at 180°C. This shows a trend very similar to that seen in this system cured at 160°C. A single peak forms after around 170 seconds. There is no obvious early stage to the spinodal decomposition and the peak instantly begins to shift to lower q. As the cure progresses the position of the peak shifts outside the q range of the experiment.

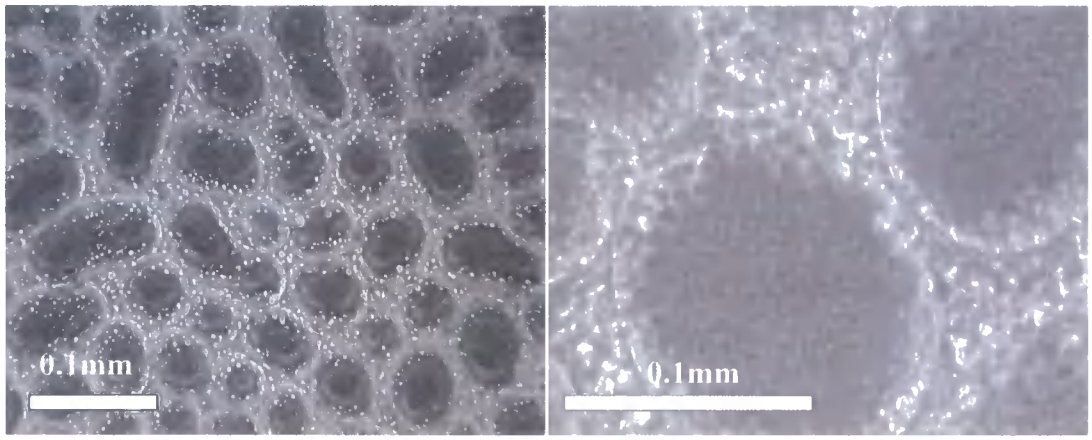

Figure 6.4.4.2 This figure shows the optical micrographs of EB25X5 cured at 180°C. This shows a large scale particulate morphology which has secondary sub-included particles in both phases which has formed from a percolation to cluster transformation

The figure 6.4.4.2 shows the optical micrograph of the final cured morphology of EB25X5 cured at 180°C. This shows a large scale particulate morphology that has formed from a percolation to cluster transformation of the spinodal decomposition observed in the S(q) versus q plot. Within each of the large scale phases there are sub-included particles that have resulted from secondary phase separation. From the S(q) versus q plot of this system there is no obvious evidence of any secondary phase separations occurring. It is likely that this small-scale phase separation has occurred at a q value higher than that studied in the experiment. It is also possible that this small-scale phase separation is smaller that the wavelength of light used in the SALS experiment and therefore would not be detected.

The minority phase in this morphology is the continuous phase and it is likely that this is the thermoplastic rich phase. It is interesting to note that on closer inspection of the large discontinuous particles the sub-included secondary particles concentrated in the centre of the larger particles. This produces a secondary phase depleted zone around the edges of the large-scale dispersed phase. This could be as a result of the coarsening of the spinodal morphology observed in the S(q) versus q plot for this system.

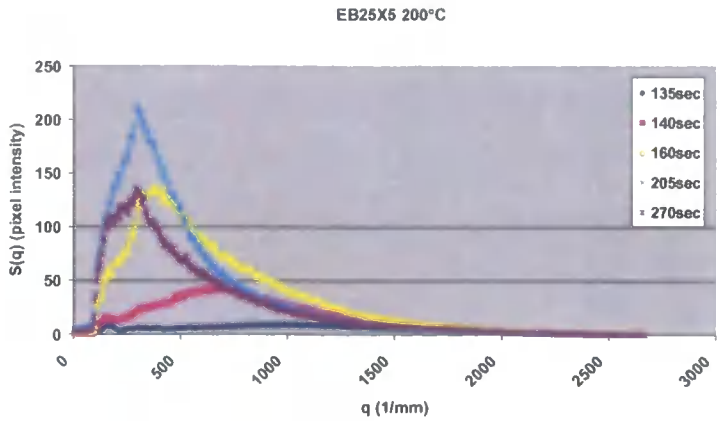

Graph 6.4.4.3 S(q) versus q plot for EB25X5 cured at 200°C. This shows the formation of a well-defined peak that begins to form after 135 s. The peak develops and shifts to a lower q as the cure advances

The graph 6.4.4.3 above shows the S(q) versus q plot for EB25X5 cured at 200°C. This shows the formation of a single peak that shifts to lower q with no obvious early stage spinodal decomposition. The peak rapidly shifts to a low q outside the range of the experiment. The unusual shape of the peak at 205 and 270 seconds is likely due to spurious scattering effects around the beam stop. The figure 6.4.4.3 below show the cured morphology of this system cured at 200°C. This shows a similar morphology to that seen in EB25X5 cured at 180°C.

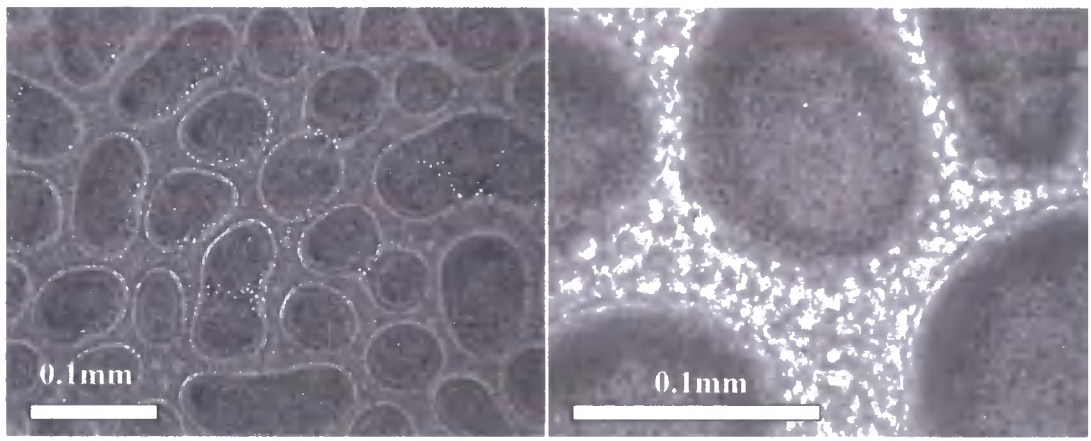

Figure 6.4.4.3 This figure shows the optical micrograph of EB25X5 cured at 200°C. This shows a large scale particulate morphology which has secondary sub-included particles in both phases.

The figure 6.4.4.3 shows the cured morphologies of BB25X5 cured at 200°C and this shows a large scale particulate morphology with evidence of secondary phase separations occurring in both large scale phases. There is also evidence to the

percolation to cluster transformation occurring where large scale discontinuous particles are dividing. The secondary phase separation were not detected in the S(q) versus q plot for this system probably due to the small size of these particles.

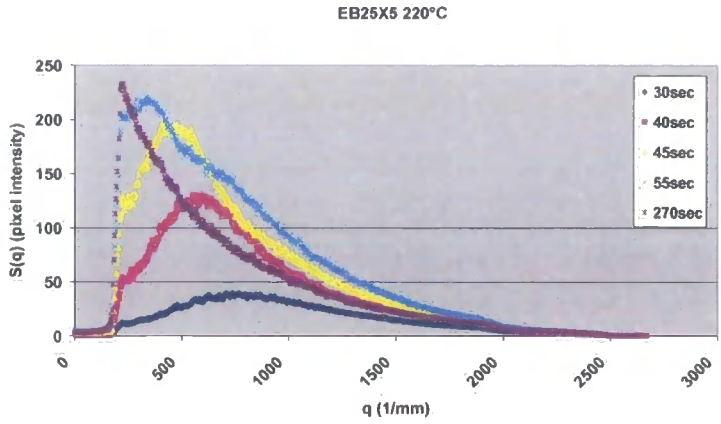

Graph 6.4.4.4 S(q) versus q plot for EB25X5 cured at 220°C. This shows the formation of a well-defined peak that begins to form after 20sec. The peak develops and shifts to a lower q as the cure advances

The graph 6.4.4.4 above shows the S(q) versus q plot for the EB25X5 system cured at 220°C. This again shows the formation of a single peak occurring and shifting to lower q during the cure process. There is no obvious early stage spinodal decomposition in this system. The position of the peak shifts to a lower q than the range of the experiment. The cured morphology of this system is shown in the figure 6.4.4.4. These show a large-scale particulate morphology with evidence of secondary phase separations occurring in both large-scale phases. There is also evidence to the percolation to cluster transformation occurring where large-scale discontinuous particles are dividing. The secondary phase separation were not detected in the S(q) versus q plot for this system probably due to the small size of these particles.

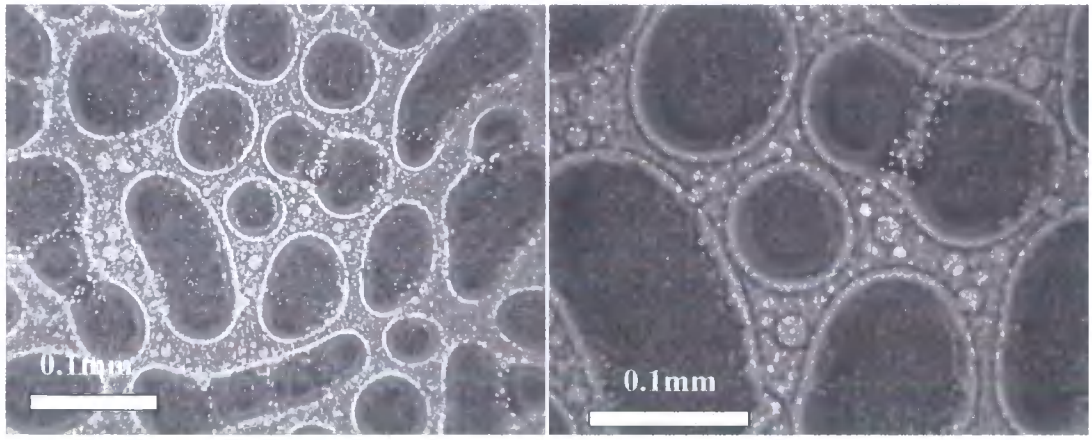

Figure 6.4.4.4 This figure shows the optical micrographs of EB25X5 cured at 220℃. This shows a large scale particulate morphology which has secondary sub-included particles in both phases which has formed from a percolation to cluster transformation. There is evidence of the break down of the percolating network to give large scale dispersed particles.

6.4.4.2 R(q) versus q plots for EB25X5 cured at different isothermal temperatures

R(q) versus q plots for the early stages of the observed spinodal decomposition process in the S(q) versus q plots were obtained for the EB25X5 series cured at different isothermal temperatures.. From these plots the $R(q)_{max}$ and $q_{(max)}$values are obtained to give information on the nature of the phase separation process.

An example of an R(q) versus q plot from this series is shown in graph 6.4.4.5. These plots showed a characteristic peak from which $R(q)_{max}$ and $q_{(max)}$ were obtained. The table 6.4.4.1 documents the results from this series.

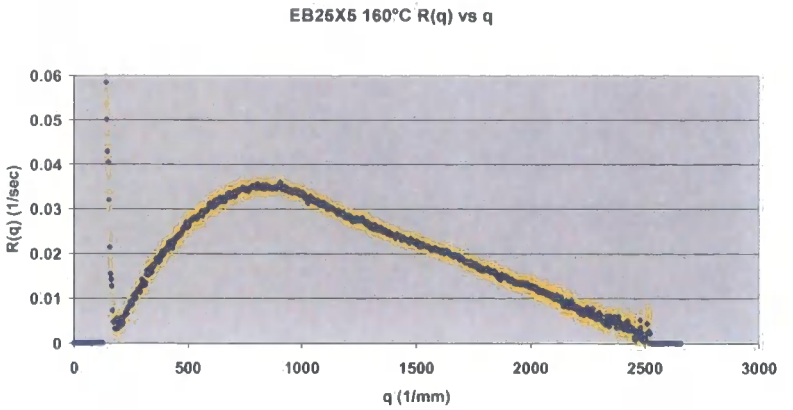

Graph 6.4.4.5 *R(q) versus q plot for the spinodal decomposition observed in EB25X5 cured at 160°C. This shows a well-defined peak for the early stages of the phase separation.*

EB25X5	**160°C**	**180°C**	**200°C**	**220°C**
$R(q)_{max}$ (sec^{-1})	0.035	0.1	0.26	0.16
$q_{(max)}$ (mm^{-1})	860	1970	650	450

Table 6.4.4.1 *Table showing the $R(q)_{max}$ values for EB25X5 cured at different cure temperatures.*

The table 6.4.4.1 above shows the $R(q)_{max}$ values for EB25X5 at different isothermal cure temperatures. It can be seen that this shows an increasing trend with increasing temperature, which suggests LCST. This is with the exception of the sample cures a 220°C the value here may be misleadingly low because the spinodal peak shifts very rapidly to lower q and this gives falsely lower value.

6.4.4.3 R(q)/q² versus q² plots for EB25X5 cured at different isothermal cure temperatures

$R(q)/q^2$ versus q^2 plots were obtained for EB25X5 cured at different isothermal cure temperatures. These plots were not linear as predicted form Cahn-Hilliard theory however extrapolations were made in order to estimate a D^*_{app} value for the spinodal

process. Graph 6.4.4.6 shows an example of a $R(q)/q^2$ versus q^2 plot from this series and the table 6.4.4.2 documents the results from this series.

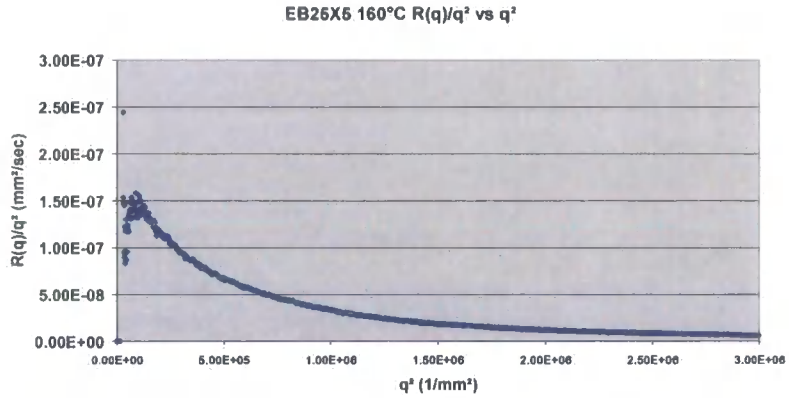

Graph 6.4.4.6 $R(q)/q^2$ versus q^2 plot for the spinodal peak observed in EB25X5 cured at 160℃

EB25X5	**160°C**	**180°C**	**200°C**	**220°C**
D^*_{app}	1.75E-7	3.5E-7	4.0E-6	1.0E-5

Table 6.4.4.2 This table shows the calculated D^*_{app} for the spinodal decomposition processes observed in EB25X5 cured at different isothermal cure temperatures.

The table 6.4.4.2 above shows the D^*_{app} values for EB25X5 at different cure temperatures. This shows a increasing trend with increasing temperature which suggests LCST behaviour. There is a rapid increase in D^*_{app} above 180°C which may be related to the Tg of the thermoplastic.

6.4.4.4 EB25X5 % Conversion versus time for different isothermal cure temperatures

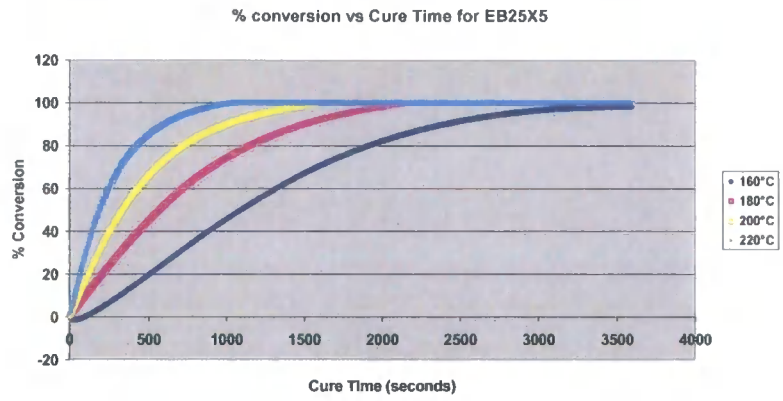

Graph 6.4.4.7 Conversion versus cure time for different isothermal cure temperatures for EB25X5.

The graph 6.4.4.7 above shows the relationship between % conversion of the thermoset versus cure time for EB25X5 this data was obtained for isothermal DSC experiments. The method used to obtain this data is detailed in Chapter 4

6.4.4.5 Discussion of results from EB25X5

From the light scattering results and optical micrographs of the cured morphologies reported in the previous section from EB25X5 it could be seen that the mechanism of phase separation is spinodal decomposition. Following the spinodal decomposition it would appear that the continuous epoxy rich phase then undergoes a percolation to cluster transformation. This produces what is termed a phase inverted morphology where the minority thermoplastic rich phase is a continuously percolation network which contains dispersed thermoset (epoxy) rich phase. A closer look at the optical micrographs of the final cured morphology of the EB25X5 systems cured at different isothermal cure temperatures clearly show that there are secondary phase separations occurring in both phases. There was no direct evidence of this in the light scattering experiments. This could be due to the small length scale associated with the secondary phase separation. It is possible that this is too small to be resolved by light scattering.

If the results from EB20X5 are compared with the system EB25 reported in the previous chapter it can be seen that the final cured morphologies are very similar in both cases. It would appear that the tri-functional epoxy has little influence on the final cured morphology. However a closer look at the kinetics of the phase separation process shows that there are clear differences.

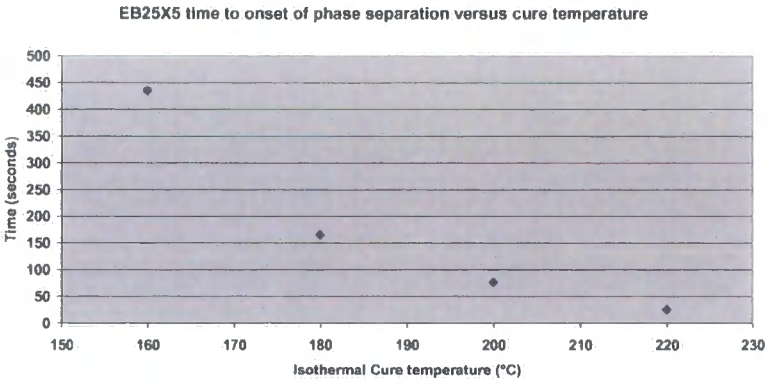

Graph 6.4.4.8 *This shows the relationship between the time to onset of phase separation and the isothermal cure temperature for EB25X5.*

The graph 6.4.4.8 shows the relationship between the time to onset of phase separation and the isothermal cure temperature for EB25X5. This shows the usual decreasing trend with increasing cure temperature. If this is compared with the EB25 system in the previous section it can be clearly seen that the time to onset of phase separation is considerably lower in the case for EB25X5. This suggests that the increase in branching of the forming network reduces the solubility of the thermoplastic in the system and promotes phase separation of the system. This is also reflected in the % conversion at the onset of phase separation for the different isothermal cure temperatures shown in graph 6.4.4.9. This shows a decreasing % conversion at the onset of phase separation with respect to isothermal cure temperature. This indicates that the system shows LCST behaviour.

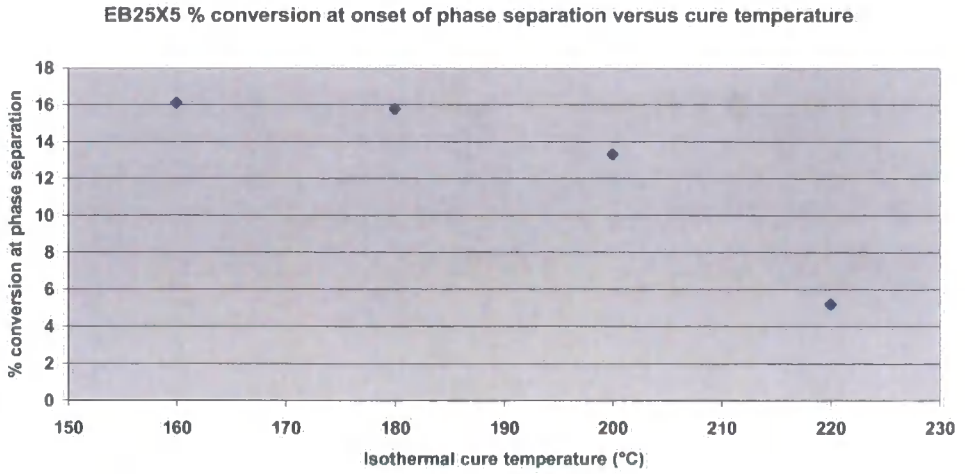

Graph 6.4.4.9 *This shows the relationship between % conversion at the onset of phase separation versus the isothermal cure temperature. This indicates LCST behaviour.*

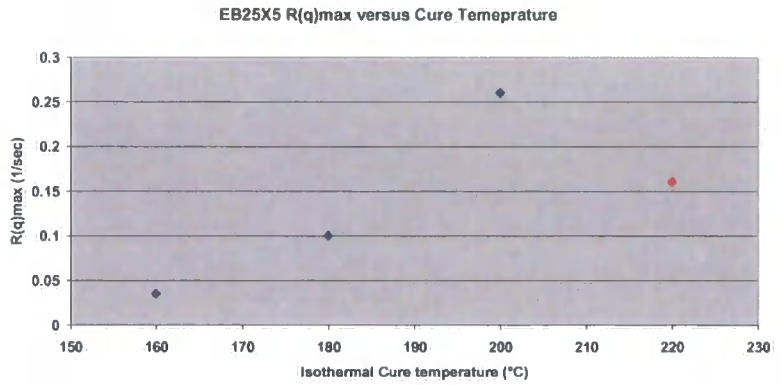

Graph 6.4.4.10 *$R(q)_{max}$ versus isothermal cure temperature for EB25X5. This shows an increasing trend with increasing cure temperature. The point at 220℃ is artificially low due to the rapidly shifting position of the forming spinodal peak.*

The graph 6.4.4.10 shows how the $R(q)_{max}$ value changes with the cure temperature. This increasing trend of this graph suggests LCST behaviour. A comparison of this data with EB20 (see chapter 5) reveals that the rates of phase separation are higher in the case of EB20X5 where the tri-functional epoxy is present. This again suggests that the thermoplastic is less soluble in the more highly branched network resulting from the incorporation of the tri-functional epoxy

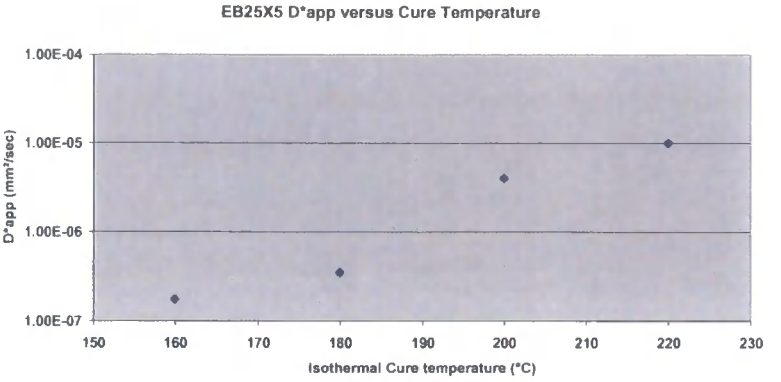

Graph 6.4.4.11 Apparent Diffusion Coefficient, $D^*_{app,}$ versus isothermal cure temperature for EB25X5. This shows a rapidly increasing trend with increasing temperature. There is a significant increase in D^*_{app} above 180°C which may be related to the Tg of the thermoplastic phase.

The graph 6.4.4.11 shows the relationship between D^*_{app} and the isothermal cure temperature. This shows a strong increasing trend with increasing temperature. There also appears to be a very significant increase in the value of D^*_{app} for the phase separation process above 180°C. This may correspond to the Tg of the thermoplastic. This suggests that below 180°C the phase separation process is kinetically hindered by vitrification of the thermoplastic phase. For cure temperatures above the Tg of the thermoplastic phase vitrification is not possible and the D^*_{app} increases rapidly as a function of cure temperature.

6.4.5 Results from system EB10X10

This section describes the results from the epoxy blend system EB10X10. In this system 10 mole % of the epoxy resin is tri-functional. The system contains 10 % PES:PEES thermoplastic. The precise formulation is detailed in table 6.3.1.1 above

6.4.5.6 SALS results from EB20X5

This section discusses the light scattering results from system EB10X5 cured at different isothermal cure temperatures. It also compares the polarised optical micrographs of the cured samples to the scattering profiles

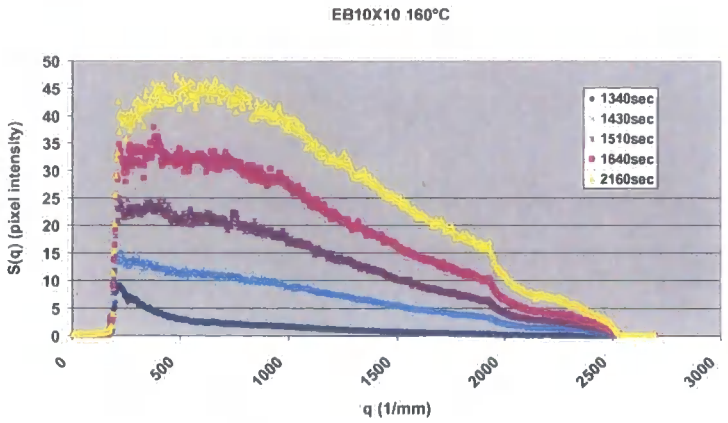

Graph 6.4.5.1 S(q) versus q plot for EB10X10 cured at 160 ℃

The graph 6.4.5.1 shows the S(q) versus q plot for EB10X10 cured at 160°C. This shows the development of a single broad spinodal peak that develops as the cure progresses. The figure 6.4.5.1 shows the cured morphology for EB10X10 cured at 160°C and this shows a particulate morphology, which has likely formed from a percolation to cluster transformation.

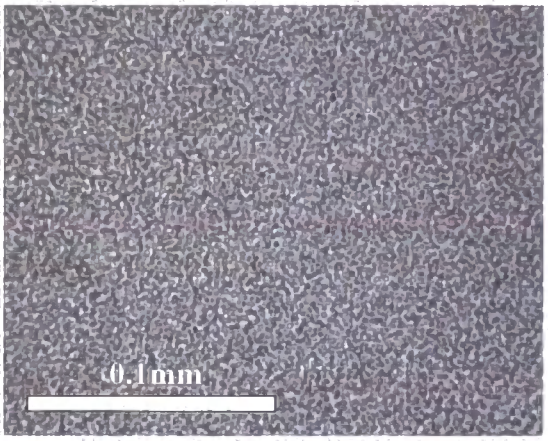

Figure 6.4.5.1 This shows the optical micrograph of the final cured morphology of EB10X10 cured at 160 ℃.

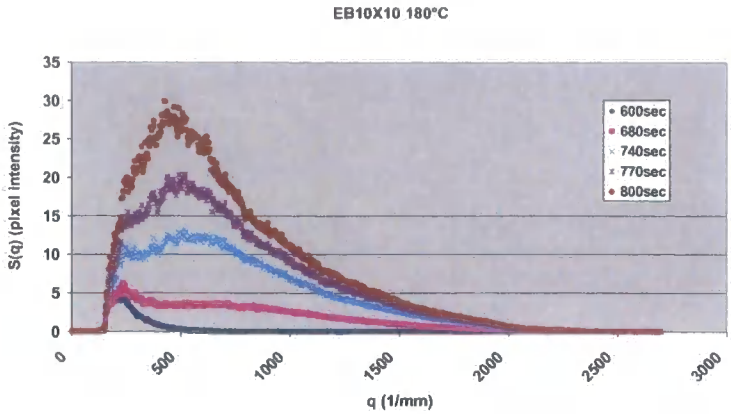

Graph 6.4.5.2 S(q) versus q plot for EB10X10 cured at 180℃ showing a single well defined spinodal peak.

Graph 6.4.5.2 shows the S(q) versus q plot for EB10X10 and this shows the formation of a clear spinodal peak that begins to form after around 680 seconds. This peak shifts to lower q as the cure progresses. The cured morphology of this sample is shown in figure 6.4.9.2 and this reveals a particulate morphology, which has occurred as a result of a percolation to cluster transformation of the thermoplastic rich phase.

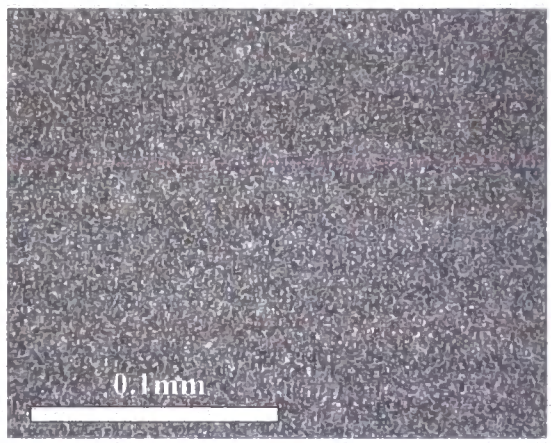

Figure 6.4.5.2 This shows the optical micrograph of the final cured morphology of EB10X10 cured at 180℃

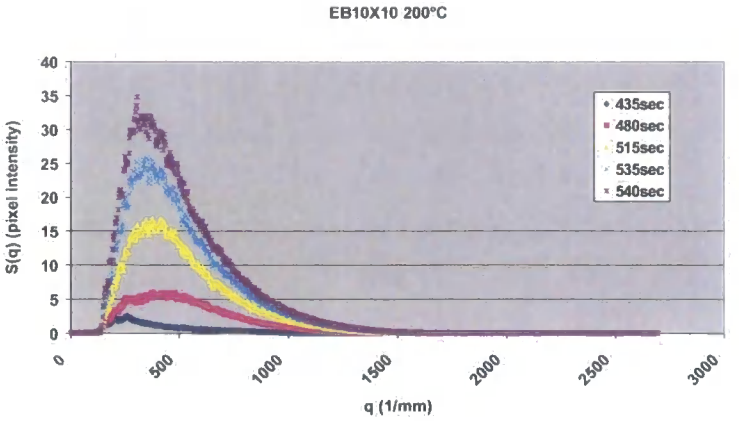

Graph 6.4.5.3 S(q) versus q plot for EB10X10 cured at 200℃

The graph 6.4.5.3 shows the S(q) versus q plot for EB10X10 cured at 200°C which shows the formation of a single spinodal peak which forms after around 480 seconds and begins to shift to lower q as the cure advances. The final cured morphology of the system in shown in figure 6.4.5.3. This too shows a particulate morphology, which has likely formed from a percolation to cluster transformation.

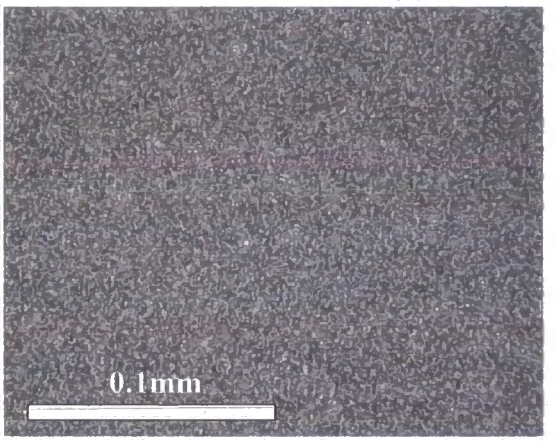

Figure 6.4.5.3 This shows the optical micrograph of the final cured morphology of EB10X10 cured at 200℃

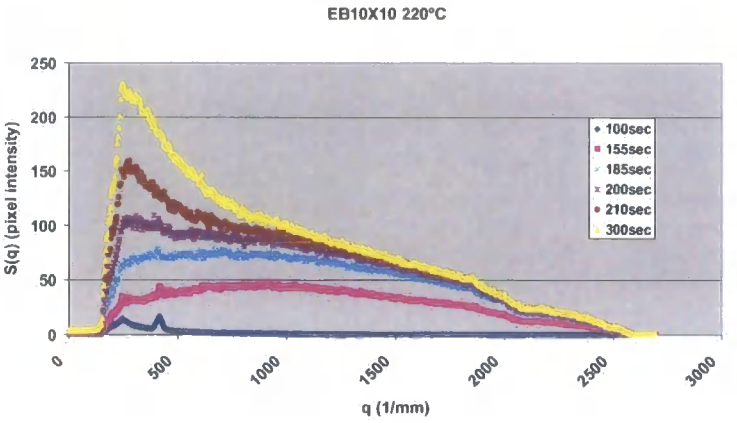

Graph 6.4.5.4 S(q) versus q plot for EB10X10 cured at 220℃

The graph 6.4.5.4 shows the S(q) versus q plot for EB10X10 cured at 220°C. This shows the formation of a broad peak that begins to form after around 155 seconds. After around 200 seconds it appears that a peak forms at low q outside of the range of the experiment. The final cured morphology of EB10X10 cured at 220°C is shown in figure 6.4.5.4 and this shows a particulate morphology that appears to have a bimodal distribution to the particle size. It is likely that this morphology has formed from a percolation to cluster transformation.

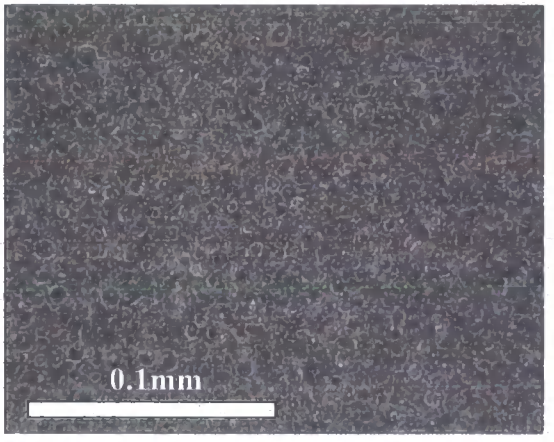

Figure 6.4.5.4 This shows the optical micrograph of the final cured morphology of EB10X10 cured at 220℃

6.4.5.7 R(q) versus q plots for EB10X10 cured at different isothermal temperatures

R(q) versus q plots for the early stages of the observed spinodal decomposition process in the S(q) versus q plots were obtained for the EB10X10 series cured at different isothermal temperatures. From these plots the $R(q)_{max}$ and $q_{(max)}$values are obtained to give information on the nature of the phase separation process.

An example of an R(q) versus q plot from this series is shown in graph 6.4.5.5. These plots showed a characteristic peak from which $R(q)_{max}$ and $q_{(max)}$ were obtained. The table 6.4.5.1 documents the results from this series.

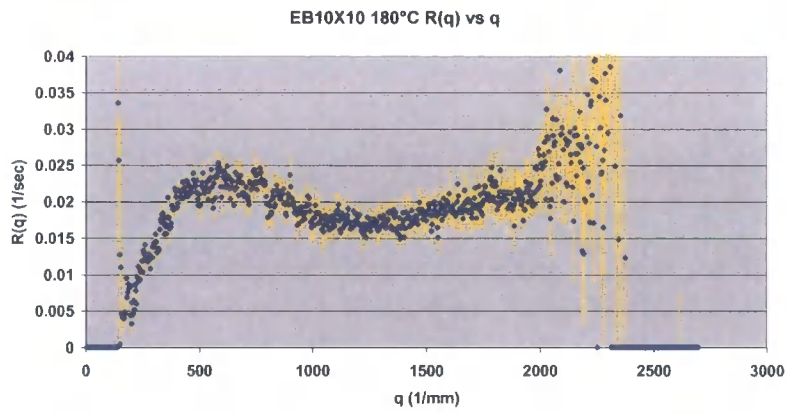

Graph 6.4.5.5 R(q) versus q plot of EB10X10 cured at 180 °C

EB10X10	**160°C**	**180°C**	**200°C**	**220°C**
$R(q)_{max}$ (sec^{-1})	0.0105	0.024	0.038	0.174
$q_{(max)}$ (mm^{-1})	1000	680	490	1400

Table 6.4.5.1 Table showing the variation of $R(q)_{max}$ with isothermal cure temperature for EB10X10

The table 6.4.5.1 shows the relationship between $R(q)_{max}$ and the isothermal cure temperature for EB10X10.

It can be seen that $R(q)_{max}$ increases as the cure temperature increases and this indicates LCST behaviour

6.4.5.8 R(q)/q² versus q² plots for EB10X10 cured at different isothermal cure temperatures

R(q)/q² versus q² plots were obtained for EB10X10 cured at different isothermal cure temperatures. These plots were not linear as predicted by Cahn-Hilliard theory however extrapolations were made to obtain D^*_{app} values from this data. The table 6.4.5.2 documents the D^*_{app} values obtained from the EB10X10 system. This generally shows an increasing trend with increasing cure temperature that indicates LCST

EB10X10	**160°C**	**180°C**	**200°C**	**220°C**
D^*_{app} ($mm^2\ sec^{-1}$)	9E-8	1.7E-7	5.4E-7	4.6E-7

Table 6.4.5.2 This table shows the variation of D^*_{app} with isothermal cure temperature for EB10X10.

6.4.5.9 EB10X10 % Conversion versus time for different isothermal cure temperatures

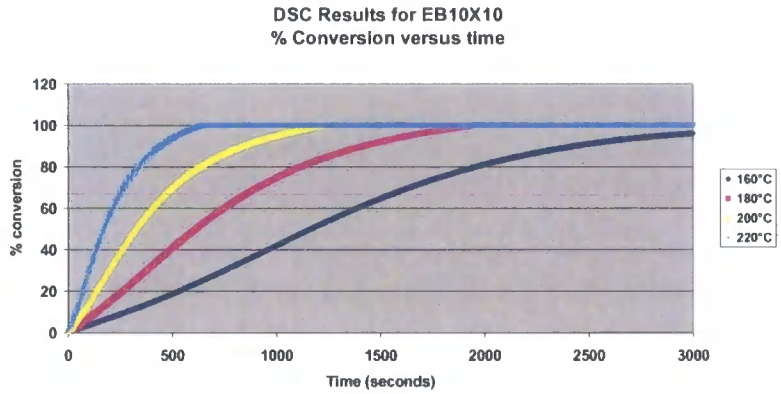

Graph 6.4.5.6 % Conversion versus cure time for different isothermal cure temperatures for EB10X10.

The graph 6.4.5.6 above shows the relationship between % conversion of the thermoset versus cure time for EB10X10 this data was obtained for isothermal DSC experiments. The method used to obtain this data is detailed in Chapter 4.

6.4.5.10 Discussion of results from EB10X10

The S(q) versus q plots for the EB10X10 series cured at different isothermal cure temperatures all show evidence of phase separation by spinodal decomposition. The micrographs from this series are all particulate morphologies. This suggests that the morphology in these samples has resulted from spinodal decomposition followed by percolation to cluster transformation. This is typical of the behaviour seen in the EB10 and EB10X5 systems. It appears that the addition of the multifunctional epoxy has little influence on the actual mechanism of phase separation.

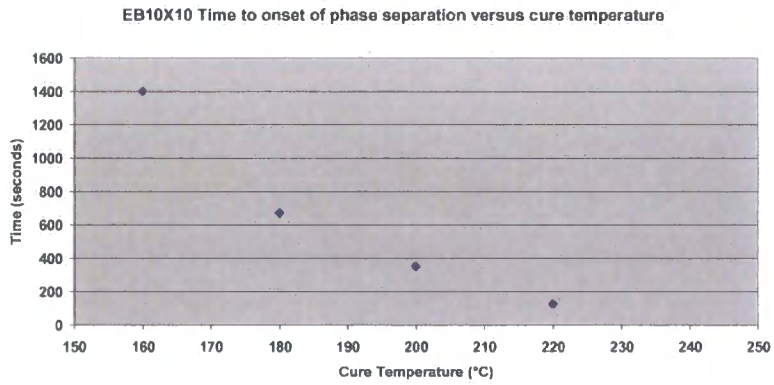

Graph 6.4.5.7 This graph shows the relationship between the time to onset of phase separation and the isothermal cure temperature for EB10X10.

Graph 6.4.5.7 shows the relationship between time to onset of phase separation and the isothermal cure temperature. This as usual shows a decreasing trend with increasing temperature. The onset times for this sample are higher than in the case of EB10X5, there appears to be an increase in time to phase separation as the level of tri-functional epoxy increases. This suggests the tri-functional epoxy compatiblises the blend and delays the onset of phase separation

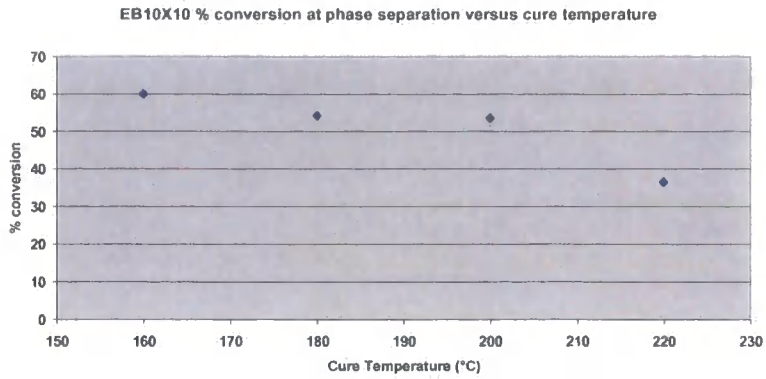

Graph 6.4.5.8 This graph shows the relationship between the % conversion and the isothermal cure temperature for EB10X10

The Graph 6.4.5.8 shows the relationship between the % conversion at the onset of phase separation and the cure temperature for EB10X10. This clearly shows a decreasing trend with increasing temperature, which suggests LCST behaviour.

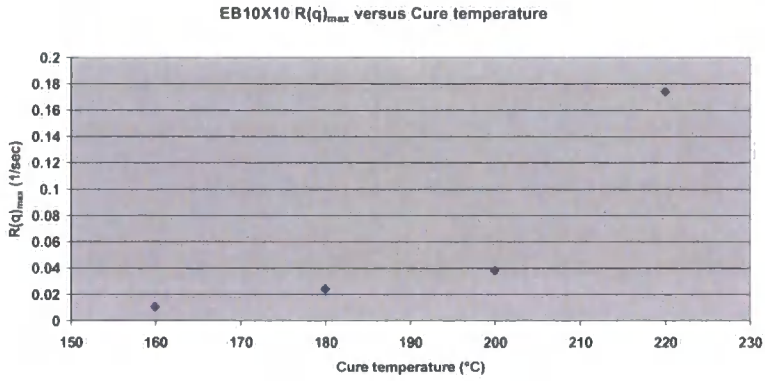

Graph 6.4.5.9 Graph of $R(q)_{max}$ versus isothermal cure temperature for EB10X10

The graph 6.4.5.9 shows the relationship between $R(q)_{max}$ and the isothermal cure temperature for EB10X10. This shows an increasing trend with increasing temperature that is representative of LCST behaviour.

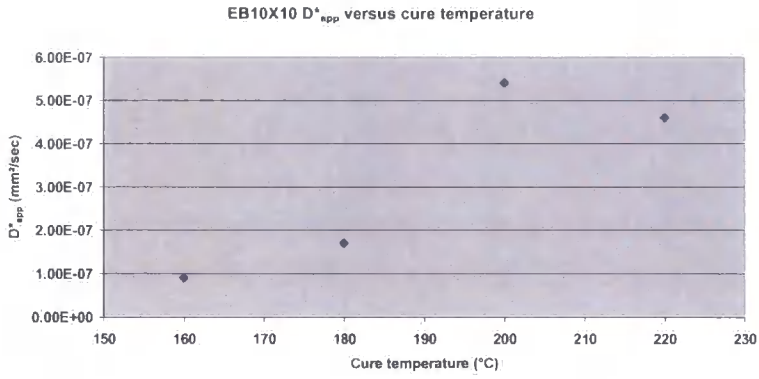

*Graph 6.4.5.10 Graph of D*app versus isothermal cure temperature for EB10X10*

The graph 6.4.5.10 shows the relationship between D^*_{app} and the isothermal cure temperature for EB10X10. This shows an increasing trend with increasing temperature. It can be also be observed that there is a rapid increase in D^*_{app} above 180°C which could be related to the Tg of the thermoplastic

6.4.6 Results from system EB15X10

This section describes the results from the epoxy blend system EB15X10. In this system 10 mole % of the epoxy resin is tri-functional. The system contains 15 %(w/w) PES:PEES thermoplastic. The precise formulation is detailed in table 6.3.1.1 above

6.4.6.1 S(q) versus q plot and optical micrographs for EB15X10

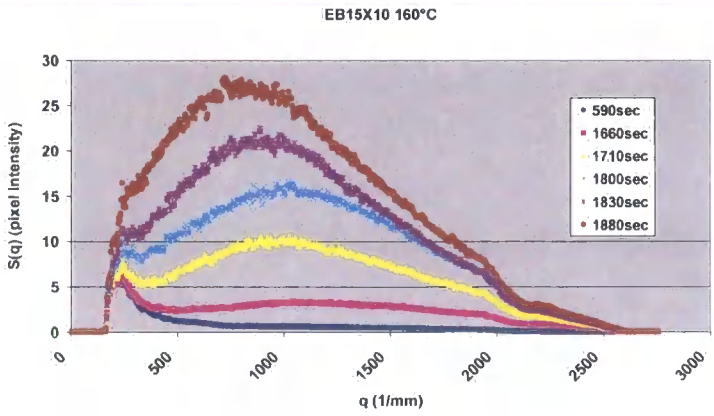

Graph 6.4.6.1 S(q) versus q plot for EB15X10 cured at 160°C

The graph 6.4.6.1 shows the S(q) versus q plot for EB15X10 cured at an isothermal cure temperature of 160°C. This shows the formation of a single spinodal peak. The position of q_{max} for this peak remains relatively constant during the cure process. This indicates that the mechanism of phase separation in this sample is by spinodal decomposition. The figure 6.4.6.1 shows the optical micrograph of the final cured morphology of this system and this shows a particulate morphology with a dispersed thermoplastic rich phase. Because of the spinodal peak seen in the S(q) versus q plot for this system it is likely that this morphology has formed from a percolation to cluster transformation of the thermoplastic rich phase during cure.

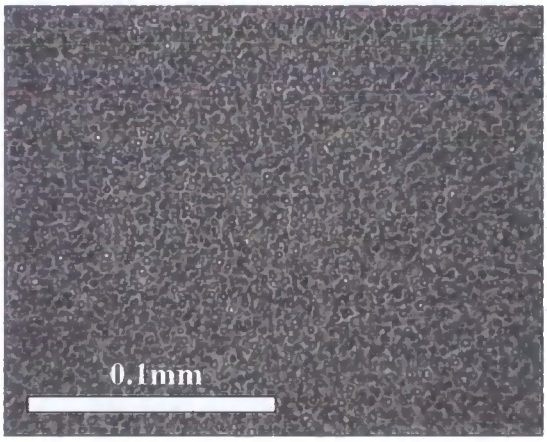

Figure 6.4.6.1 Optical micrograph of the cured morphology of EB15X10 cured at 160℃

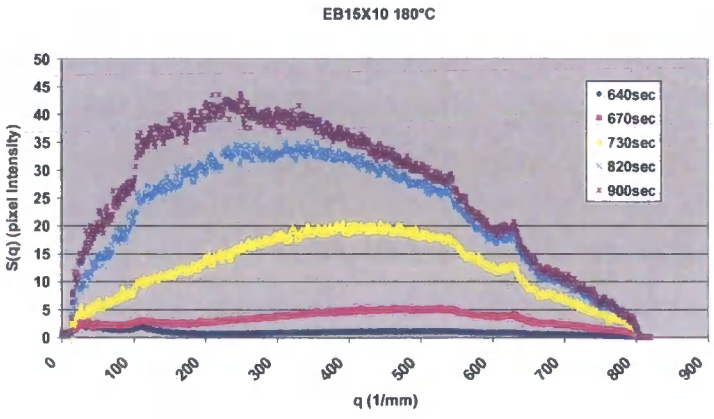

Graph 6.4.6.2 S(q) versus q plot for EB15X10 cured at 180℃

The graph 6.4.6.2 shows the S(q) versus q plot for EB15X10 cured at 180°C. This shows the formation of a spinodal peak in which the q_{max} shifts slowly to lower q as the cure progresses suggesting the mechanism of phase separation is spinodal decomposition. The cured morphology of this sample is shown in figure 6.4.6.2 below. The morphology of this sample is particulate with a dispersed thermoplastic rich phase. This has likely formed from a percolation to cluster transformation of the thermoplastic rich phase following the spinodal decomposition.

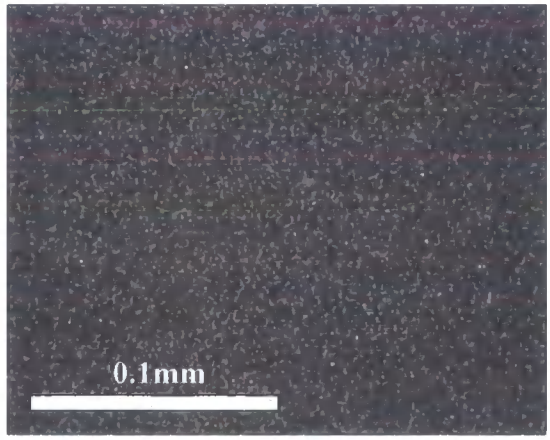

Figure 6.4.6.2 Optical micrograph of the cured morphology of EB15X10 cured at 180℃

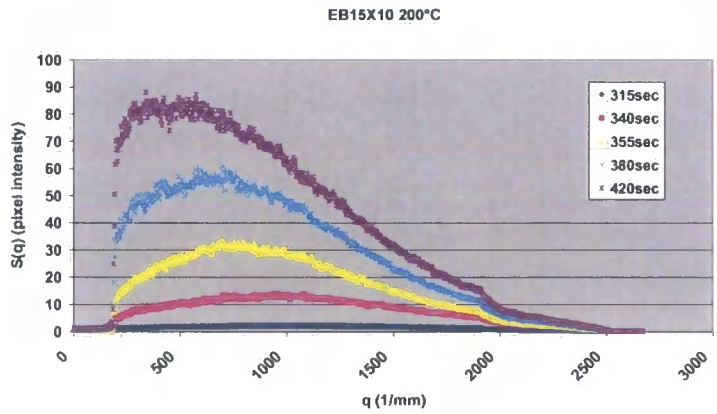

Graph 6.4.6.3 S(q) versus q plot for EB15X10 cured at 200℃

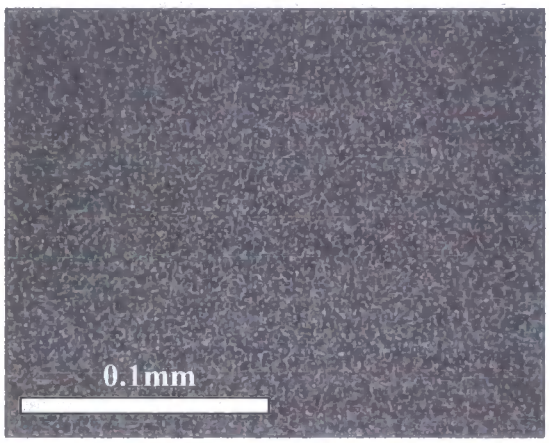

Figure 6.4.6.3 Optical micrograph of the cured morphology of EB15X10 cured at 200℃

The graph 6.4.6.3 shows the S(q) versus q plot for EB15X10 cured at 200°C. This shows the formation of a spinodal peak whose q_{max} shifts slightly to lower q as the cure progresses. This indicates that the phase separation mechanism for this sample is spinodal decomposition. The optical micrograph of this system is shown in figure 6.4.6.3 above and this reveals a particulate morphology that has a dispersed thermoplastic rich phase. This has therefore formed from the percolation to cluster transformation of the thermoplastic rich phase following the spinodal decomposition.

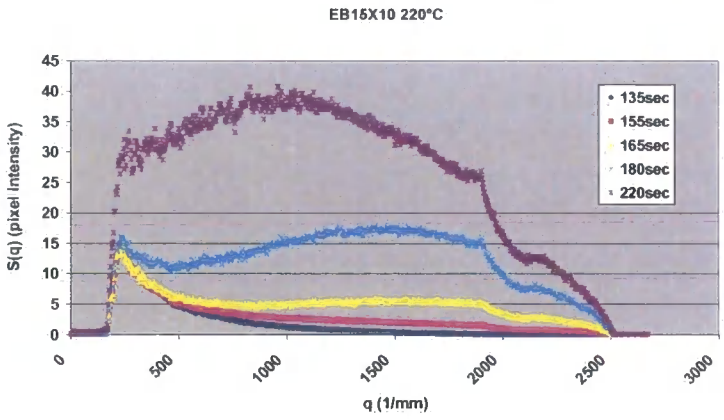

Graph 6.4.6.4 S(q) versus q plot for EB15X10 cured at 220℃

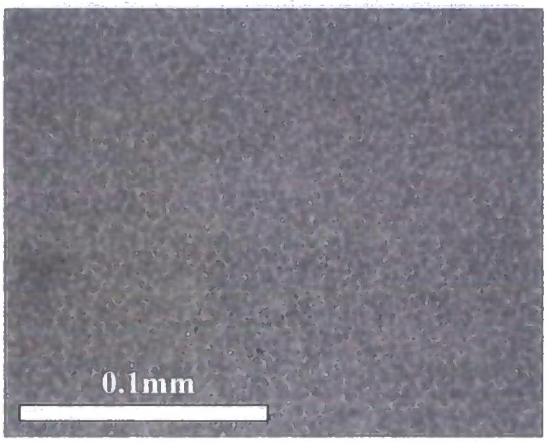

Figure 6.4.6.4 Optical micrograph of the cured morphology of EB15X10 cured at 220℃

The graph 6.4.6.4 above shows the S(q) versus q plot for EB15X10 cured at 220°C this shows the formation of a broad peak which shifts to lower q as the cure advances. This peak has an unusual shape at higher q values this may indicate a small-scale transition occurring in the samples. It is also possible that this may just be an artefact of the scattering experiment. The formation of the major peak indicates that spinodal decomposition is the mechanism of phase separation. The final cured morphology of this system is shown in the optical micrograph in figure 6.4.6.4 and this indicates a particulate morphology with a dispersed thermoplastic rich phase. This has therefore formed as a result of a percolation to cluster transformation of the thermoplastic rich phase following the initial spinodal decomposition.

6.4.6.2 R(q) versus q plots for EB15X10 cured at different isothermal temperatures

R(q) versus q plots were obtained for EB15X10 series during the early stages of the observed spinodal decomposition process in the S(q) versus q plots reported in the previous section. An example of such a plot is shown in 6.4.6.5 and table 6.4.6.1 documents the results.

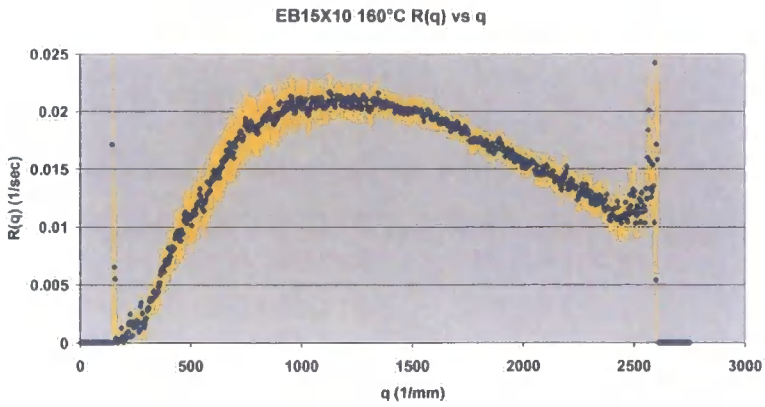

Graph 6.4.6.5 R(q) versus q plot of EB10X10 cured at 160°C

EB15X10	**160°C**	**180°C**	**200°C**	**220°C**
$R(q)_{max}$ (sec^{-1})	0.021	0.05	0.09	0.11 est
$q_{(max)}$	1240	1100	650	1500

Table 6.4.6.1 Table showing $R(q)_{max}$ values for EB15X10 at different isothermal cure temperatures.

The table 6.4.6.1 shows the $R(q)_{max}$ values for EB15X10 cured at different isothermal cure temperatures. The value at 220°C is an estimate because the peak in the R(q) versus q plot for this sample appears to occur slightly outside the q range of the experiment. This may explain the unusual nature of the S(q) versus q plot at high q for the EBX10 system cured at 220°C. In general the $R(q)_{max}$ value increases with increasing temperature which suggests LCST behaviour.

6.4.6.3 R(q)/q² versus q² plots for EB15X10 cured at different isothermal cure temperatures

The $R(q)/q^2$ versus q^2 plots for the EB15X10 did not exhibit linear behaviour however extrapolations were taken to estimate the D^*_{app} value for the process. The table documents the results from this series.

EB15X10	160°C	180°C	200°C	220°C
D^*_{app} ($mm^2\ sec^{-1}$)	5.2E-8	9E-8	8E-7	1.4E-7

Table 6.4.6.2 This table shows the values of D^*_{app} at different isothermal cure temperatures for EB15X10.

6.4.6.4 EB15X10 % Conversion versus time for different isothermal cure temperatures

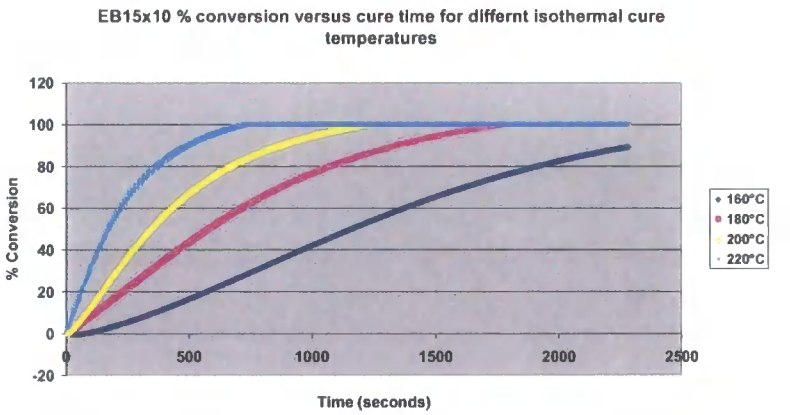

Graph 6.4.6.6 % Conversion versus cure time at different isothermal cure temperatures for EB15X10.

The graph 6.4.6.6 shows the relationship between the % conversion of the thermoset versus cure time for EB15X10 this data was obtained for isothermal DSC experiments. The method used to obtain this data is detailed in Chapter 4.

6.4.6.5 Discussion of results from EB15X10

From the S(q) versus q plots for EB15 cured at different isothermal cure temperatures reported in the previous section it can be seen that the mechanism of phase separation at all cure temperatures is spinodal decomposition. The final cured morphologies at all the different isothermal cure temperatures are particulate with a dispersed thermoplastic rich phase. This forms as a result of a percolation to cluster transformation of the thermoplastic rich phase following the spinodal decomposition.

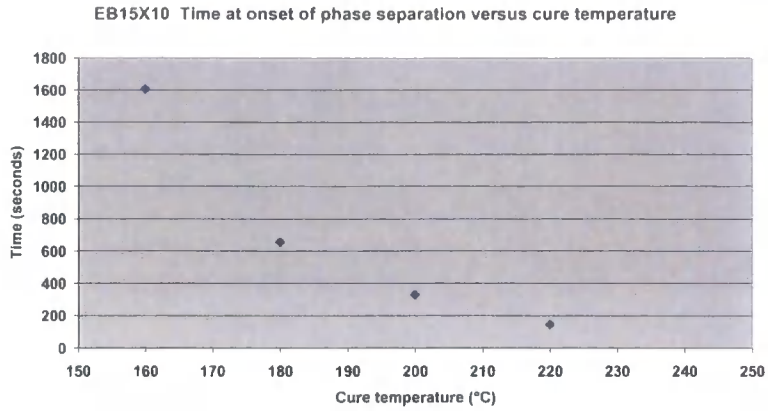

Graph 6.4.6.7 *This graph shows the relationship between the isothermal cure temperature and the time to onset of phase separation for EB15X10.*

The graph 6.4.6.7.shows the relationship between the isothermal cure temperature and the time to onset of phase separation for EB15X10. This shows a decreasing trend with increasing cure temperature. This data can be used in conjunction with the isothermal DSC data shown in graph 6.4.6.6 to estimate the % conversion at the onset of phase separation. This information is shown in graph 6.4.6.8.

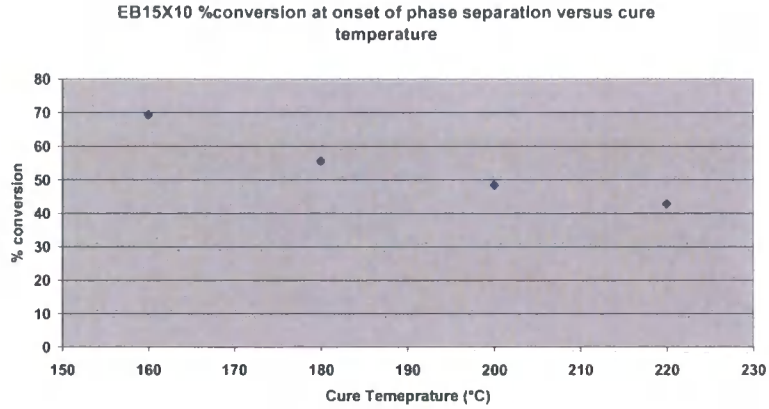

Graph 6.4.6.8 *This graph shows the relationship between the isothermal cure temperature and the % conversion at the onset of phase separation for EB15X10. The decreasing conversion with increasing cure temperature suggests LCST behaviour.*

The graph 6.4.6.8 shows the relationship between the isothermal cure temperature and the % conversion at the onset of phase separation for EB15X10 this clearly shows a decreasing % conversion at the onset of phase separation with increasing cure temperature. This is typical of the systems studies in this chapter and suggests that the overall phase diagram for the system shows lower critical solution behaviour.

This is also indicated in the $R(q)_{max}$ versus isothermal cure temperature plot for EB15X10 shown in graph 6.4.6.9. This shows an increasing trend of $R(q)_{max}$ with increasing cure temperature. This indicates that there is an increased thermodynamic driving force for the phase separation process at higher temperatures that further confirms the LCST behaviour of this blend.

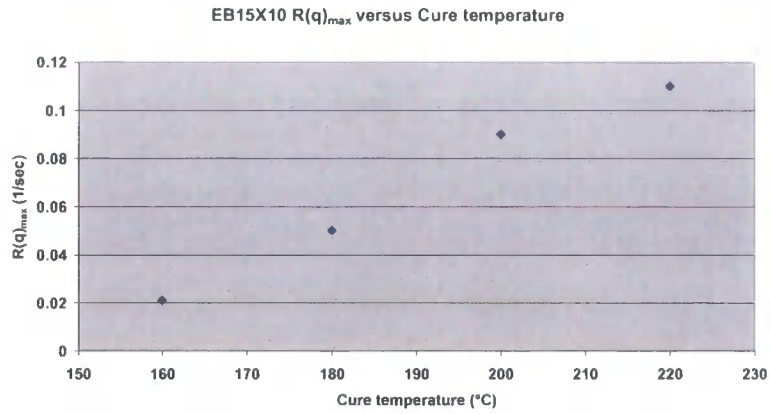

Graph 6.4.6.9 *$R(q)_{max}$ versus isothermal cure temperature for EB15X10.*

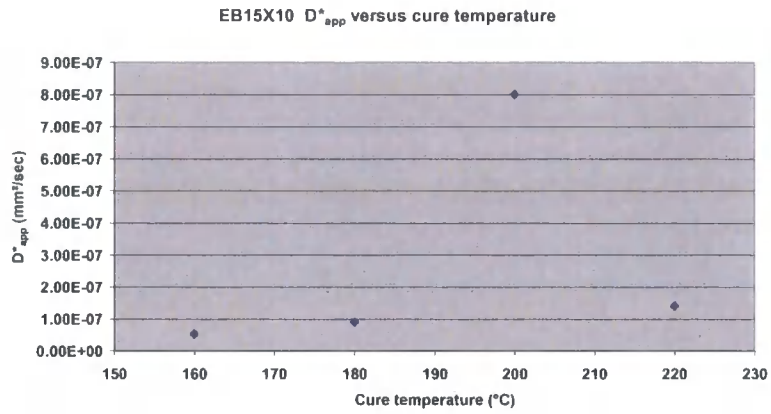

Graph 6.4.6.10 *D^*_{app} versus isothermal cure temperature for EB15X10.*

The graph 6.4.6.10 shows the variation of D^*_{app} with isothermal cure temperature. This generally shows an increasing trend with increasing temperature. This is with the exception of the D^*_{app} value at 220°C. This value may be artificially low due to the rapidly changing $q_{(max)}$ during the phase separation process for this sample.

6.4.7 Results from system EB20X10

This section describes the results from the epoxy blend system EB20X10. In this system 10 mole % of the epoxy resin is tri-functional. The system contains 20 % PES:PEES thermoplastic. The precise formulation is detailed in table 6.3.1.1 above

6.4.7.1 S(q) versus q plots and optical micrographs for EB20X10

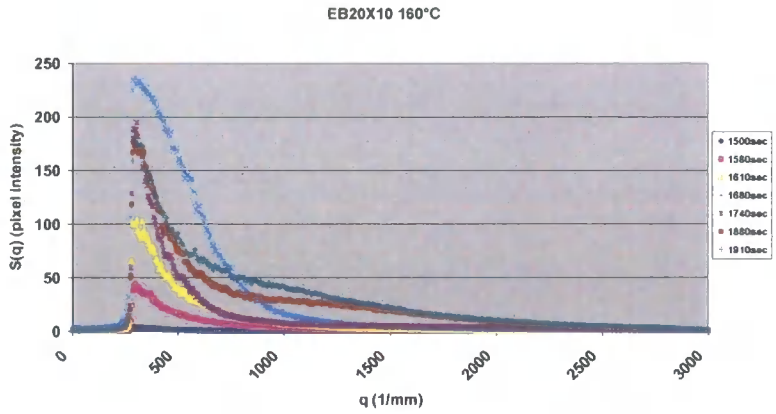

Graph 6.4.7.1 S(q) versus q plot for EB20X10 cured at 160 °C. This shows evidence of a primary spinodal peak occurring at a low q outside the range of the experiment. Then a secondary peak begins to form after around 1880sec.

The graph 6.4.7.1 above shows the S(q) versus q plot for EB20X10 cured at 160°C. This shows the formation of a primary spinodal peak at very low q followed by the formation of a secondary peak after around 1880 seconds into the cure. This indicates that the method of phase separation is primary and secondary spinodal decomposition. The figure 6.4.7.1 shows the cured morphology of EB20X10 and this appears to show a phase inverted morphology with a continuous minority thermoplastic rich phase with dispersed epoxy rich particles. This has likely formed for the percolation to cluster transformation of the epoxy rich phase following the spinodal decomposition phase separation process. There is no clear evidence in the micrograph of any secondary process occurring in this sample.

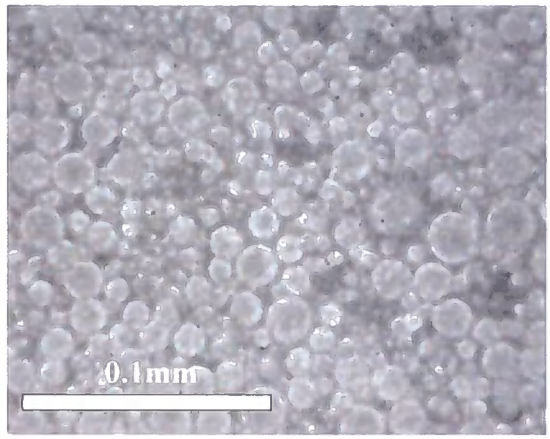

Figure 6.4.7.1 This shows the optical micrograph of the final cured morphology of EB20X10 cured at 160℃

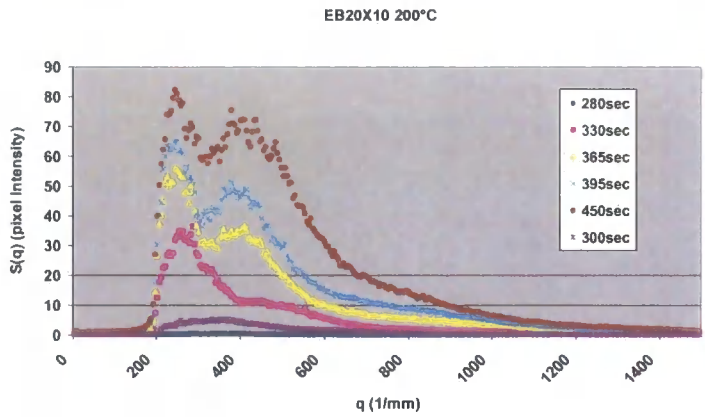

Graph 6.4.7.2 S(q) versus q plot for EB20X10 cured at 200℃. This shows a primary spinodal peak occurring at a low q which forms and shifts to lower q. A secondary peak forms after 330 seconds

The graph 6.4.7.2 shows the S(q) versus q plot for EB20X10 cured at 200°C. This shows the formation of two spinodal peaks. A primary peak forms after around 300 seconds and this peak moves very quickly to low q outside the range of the experiment. After around 330 seconds a secondary peak begins to form. This secondary peak develops and its position remains relatively constant with respect to q. This S(q) versus q plot indicates that phase separation in this sample is by a double spinodal decomposition. The optical micrograph for this sample is shown in figure 6.4.7.2. This shows a large-scale particulate morphology, which appears to have a bimodal size distribution. This has probably formed from a percolation to cluster transformation following spinodal decomposition. This is very different to the EB20X5 morphology shown above. It would appear that the addition of higher levels

of the tri-functional epoxy promote the break up of the spinodal networks by percolation to cluster transformation.

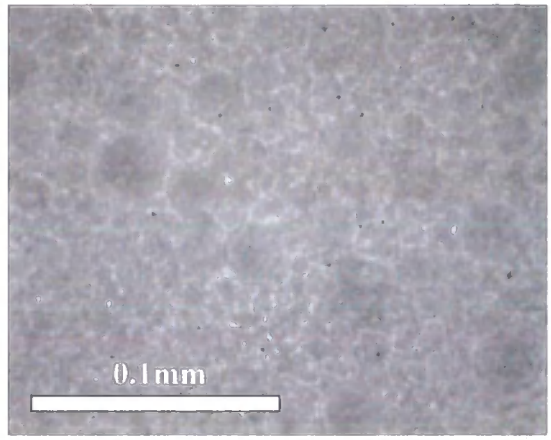

Figure 6.4.7.2 This figure shows the cured morphology of EB20X10 cured at 200℃

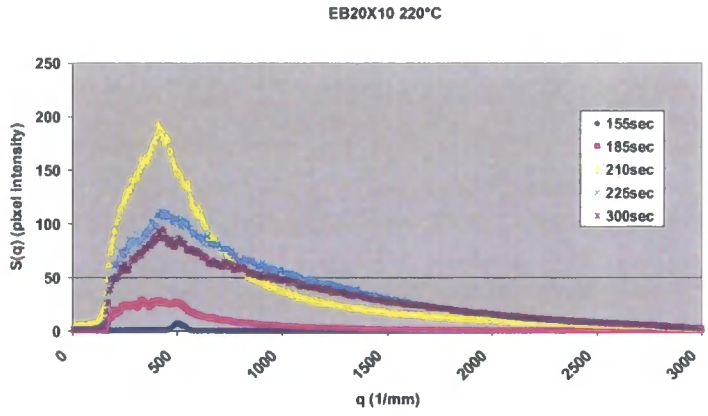

Graph 6.4.7.3 S(q) versus q plot for EB20X10 cured at 220℃. This shows the formation of a peak at low q.

The graph 6.4.7.3 shows the S(q) versus q plot for EB20 cured at 220°C this shows the formation of a peak after 185 seconds. This peak grows quickly but it has an unusual shape. This may be due to a spinodal decomposition occurring at a very low q outside the q range of the experiment. This may give unusual diffraction patterns around the beam stop. If this is the case then the observed peak in this experiment may be a secondary spinodal peak.

The final cured morphology of this sample is shown in figure 6.4.7.3. This shows a large-scale particulate morphology that has probably formed from a percolation to cluster transformation.

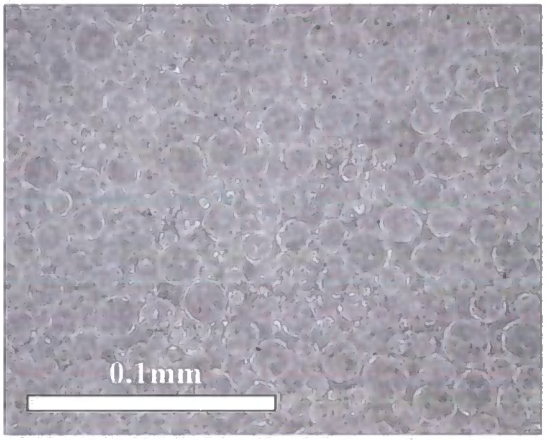

Figure 6.4.7.3 This figure shows the optical micrograph of the final cured morphology of EB20X10 cured at 220℃.

6.4.7.2 R(q) versus q plots for EB20X10 cured at different isothermal temperatures

The $R(q)_{max}$ and $q_{(max)}$ values obtained from the R(q) versus q plots for EB20X10 are shown in the table 6.4.7.1

EB20X10	**160°C**	**180°C**	**200°C**	**220°C**
Primary Spinodal $R(q)_{max}$ (1/sec)	0.026	N/A	0.08	0.09est
q(max) (1/mm)	600	N/A	375	750
Secondary Spinodal $R(q)_{max}$ (1/sec)	0.009	N/A	0.022	N/A
q(max) (1/mm)	1150	N/A	800	N/A

Table 6.4.7.1 Table of $R(q)_{max}$ values for both primary and secondary phase separations observed in EB20X10 cured at different isothermal cure temperatures.

6.4.7.3 $R(q)/q^2$ versus q^2 data for EB20X10 cured at different isothermal cure temperatures

The $R(q)/q^2$ versus q^2 plots from the EB20X10 series did not yield a linear relationship with a clear intersection on the y axis as predicted by Cahn-Hilliard theory. However, best fit extrapolations were taken to obtain an approximate D^*_{app} value for the spinodal process. The results are documented in table 6.4.7.2 .

EB20X10	160°C	180°C	200°C	220°C
Primary Spinodal D*app (mm^2/sec)	4.0E-7	N/A	3.5E-6	3E-6
Secondary Spinodal D*app (mm^2/sec)	1.6E-8	N/A	8E-8	N/A

*Table 6.4.7.2 This table shows the D*app values for the spinodal decompositions observed in EB20X10 cured at various different isothermal cure temperatures.*

6.4.7.4 EB20X10 % Conversion versus time for different isothermal cure temperatures

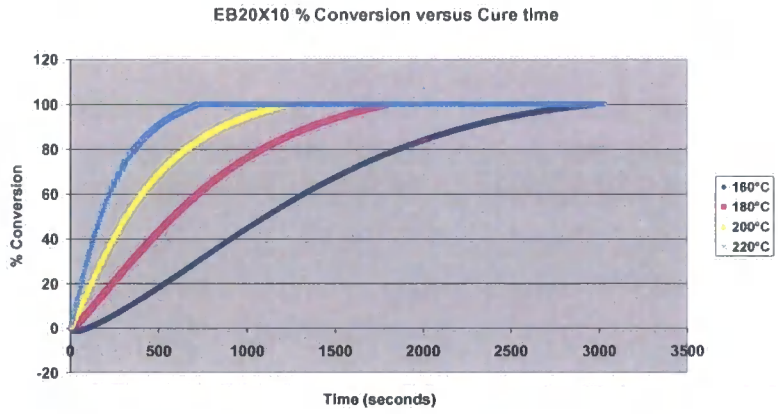

Graph 6.4.7.4 % Conversion versus cure time at different isothermal cure temperatures for EB20X10

The graph 6.4.7.4 shows the relationship between the % conversion of the thermoset versus cure time for EB20X10 this data was obtained for isothermal DSC experiments. The method used to obtain this data is detailed in Chapter 4.

6.4.7.5 Discussion of results from EB20X10

Section 6.4.7.1 shows the S(q) versus q plots and optical micrographs of EB20X10 cured at different isothermal cure temperatures. In all cases there is evidence of primary and secondary spinodal decompositions occurring. For the case of where EB20X10 is cured at 220°C there is only a single peak observed however the unusual shape of this peak may suggest that there is a primary larger scale spinodal decomposition occurring that is outside the q range of the experiment. Comparing the S(q) versus q plots with the optical micrographs it can be seen that percolation to cluster transformations have occurred in all cases. All of the morphologies seen in EB20X10 show particulate type morphologies. This differs from EB20 and EB20X5 it appears that at 10 mole % tri functional epoxy has promoted the percolation to cluster transformation process. This has resulted in the large scale particulate morphology observed in EB20X10. This suggests that the tri functional epoxy, MYO510 may act to increase the interfacial energy between the two phases. This causes the destabilisation of the co-continuous state occurring immediately following the spinodal decomposition. The system can then lower its overall energy by forming a larger scale particulate morphology that will reduce the area of interface between the two phases. This results in the large scale particulate morphology observed in these systems.

The graph 6.4.7.5 shows the relationship between the time to onset of phase separation and the isothermal cure temperature. This is shown for both primary and secondary phase separations observed in this system. This can then be used in conjunction with the DSC data on this system to establish the % conversion at the onset of cure. This information is shown in graph 6.4.7.6 below.

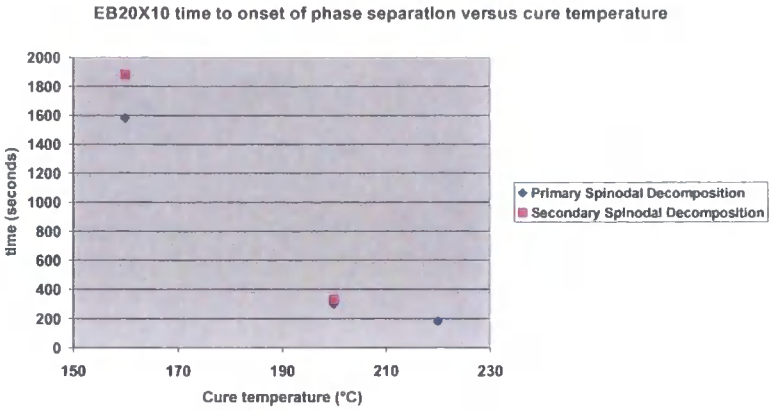

Graph 6.4.7.5 This graph shows the relationship between the time to onset f phase separation and the isothermal cure temperature for EB20X10

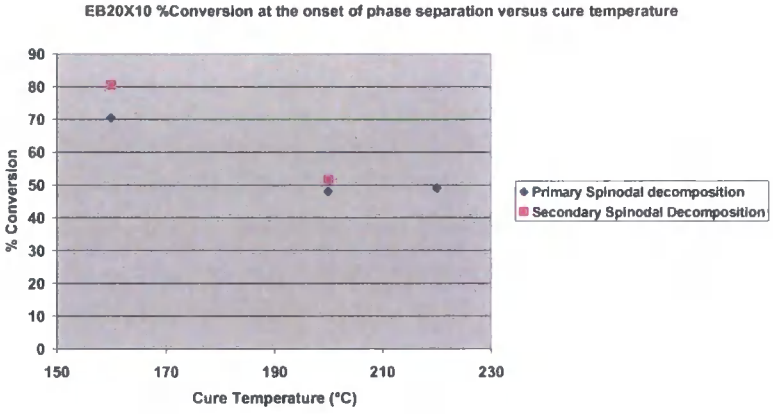

Graph 6.4.7.6 This graph shows the relationship between the degree of conversion at the onset of phase separation and the isothermal cure temperature for EB20X10

The graph 6.4.7.6 shows how the % conversion at the onset of phase separation varies with the isothermal cure temperature. It can be seen that the % conversion at phase separation decreases with increasing isothermal cure temperature. This is indicative of LCST, which is generally observed in these systems. It is also interesting to observe that the onset of phase separation occurs at relatively high % conversion when compared to EB20 and EB20X5. It appears that the tri-functional epoxy does act to compatibilise the thermoplastic with the epoxy network. It could be the case that the tri-functional epoxy, MYO510, preferentially reacts with the amine end groups of the thermoplastic. This essentially forms an ABA tri-block copolymer that due to its epoxy end blocks is more soluble in the epoxy network. This delays the onset of phase separation until higher levels of conversion are achieved. When phase

separation does occur it is likely that the adhesion between the two phases is high which could impart good toughness to the system. This highlights the importance of the end group chemistry of the toughening thermoplastic in such reactive blends.

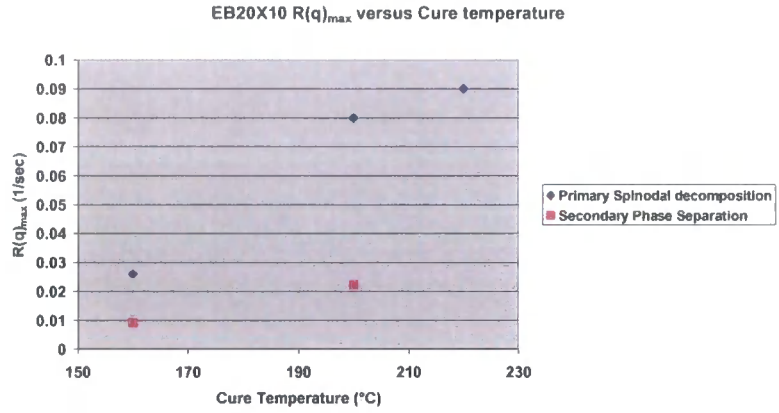

Graph 6.4.7.7 *This graph shows the relationship between $R(q)_{max}$ and the isothermal cure temperature for both primary and secondary phase separations observed in EB20X10.*

The graph 6.4.7.7 shows the relationship between $R(q)_{max}$ and the isothermal cure temperature for EB20X10. It can be seen that the $R(q)_{max}$ for the primary phase separation is always significantly larger than $R(q)_{max}$ for the secondary phase separation. This is likely to be as a result of the secondary phase separations will have a lower thermodynamic driving force compared with the primary phase separation. Another contributing factor to the slower rate of the secondary phase separation could be that it occurs at higher levels of conversion and therefore closer to the gel point. This may hinder the overall rate of the secondary phase separation.
$R(q)_{max}$ increase with increasing cure temperature this again is evidence that the system shows LCST behaviour.

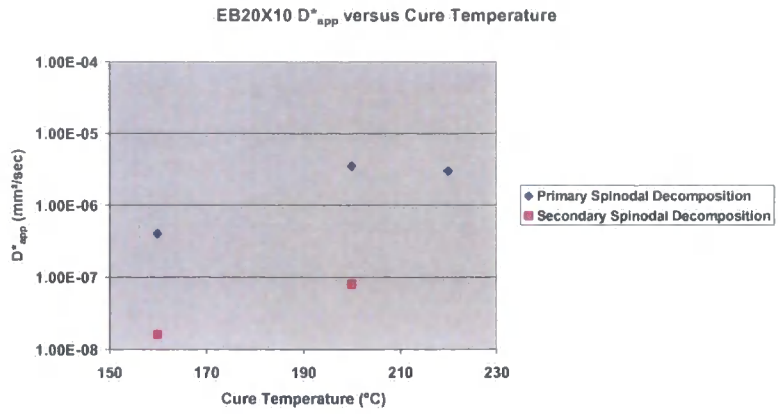

*Graph 6.4.7.8 D*app versus isothermal cure temperature for both primary and secondary phase separations in EB20X10.*

The graph 6.4.7.8.above shows the relationship between D^*_{app} and the isothermal cure temperature for EB20X10 cured at different isothermal cure temperatures. The graph shows D^*_{app} for both primary and secondary phase separations. The D^*_{app} for the secondary phase separations is always lower that that observed in the primary phase separation and this is likely to be due to the reasons mentioned above for $R(q)_{max}$ where there is likely to be less of a thermodynamic driving force for the secondary phase separation and that it occurs at higher levels of conversion.

6.4.8 Results from system EB25X10

This section describes the results from the epoxy blend system EB25X10. In this system 10 mole % of the epoxy resin is tri-functional. The system contains 25 % PES:PEES thermoplastic. The precise formulation is detailed in table 6.3.1.1 above

6.4.8.1 S(q) versus q plots and optical micrographs for EB20X10

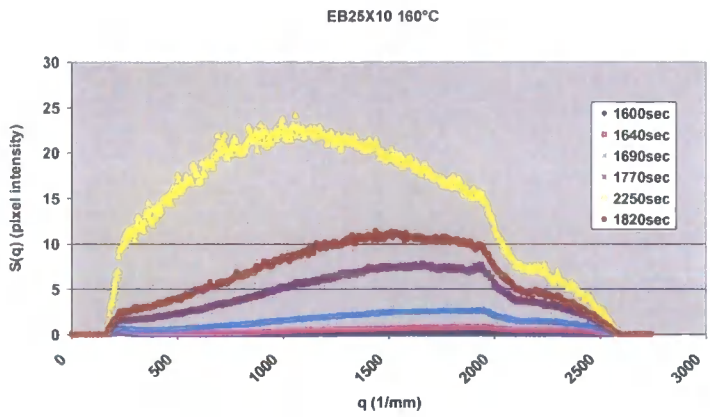

Graph 6.4.8.1 S (q) versus q plot for EB25X10 cured at 160 °C. This shows the formation of a broad spinodal peak. At high q this has an unusual shape to the curve, which may indicate that some secondary small-scale phase separation event is occurring.

The graph 6.4.8.1 above shows the S(q) versus q plot for EB25X10 cured at 160°C. The major feature of this plot is a broad spinodal peak that develops and shifts to lower q as the cure progresses. There is an unusual shape to this plot at higher q values. It appears as if a secondary peak forms at a q value of around 2300 mm^{-1}. This may be evidence of small-scale secondary phase separation occurring in the system. The figure 6.4.8.1 shows the final cured morphology of this system and this shows a small-scale particulate morphology. This is very small scale and difficult to interpret accurately by optical micrography. It is expected that this may be a phase-inverted morphology with a continuous phase of a thermoplastic rich phase and a dispersed epoxy rich phase. In order to confirm this electron microscopy would need to be carried out on this sample.

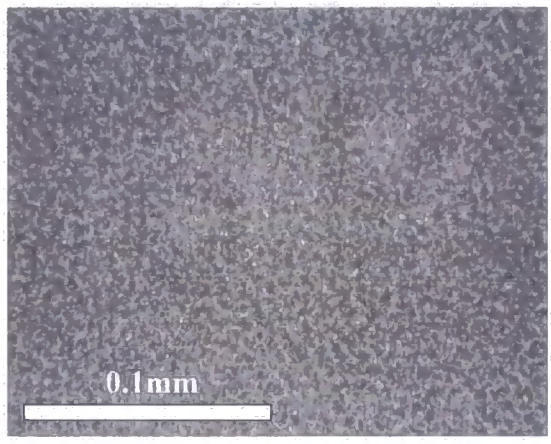

Figure 6.4.8.1 This figure shows the optical micrograph of the final cured morphology of EB25X10 cured at 160°C.

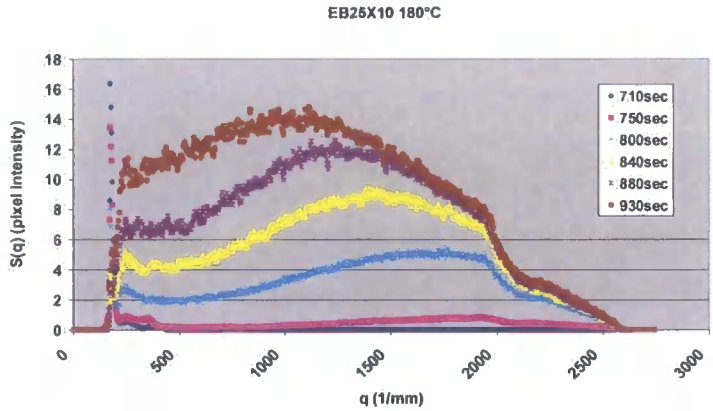

Graph 6.4.8.2 S(q) versus q plot for EB25X10 cured at 180°C

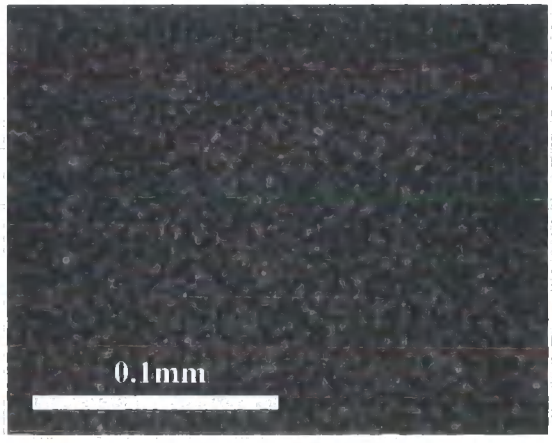

Figure 6.4.8.2 Optical micrograph of the final cured morphology of EB25X10 cured at 180°C

The graph 6.4.8.2 shows the S(q) versus q plot for EB25X10 cured at 180°C. This shows very similar behaviour to the S(q) versus q plot for this system cured at 160°C

shown above. At high q there appears to be some secondary small scale phase separation occurring in the system. The major feature is a broad spinodal peak that forms and shifts to lower q as the cure progresses. The micrograph of the final cured morphology for this system is shown in figure 6.4.8.2 this also shows a small scale particulate type morphology and it is likely that this is a phase inverted morphology with a continuous thermoplastic rich phase and a dispersed epoxy rich phase.

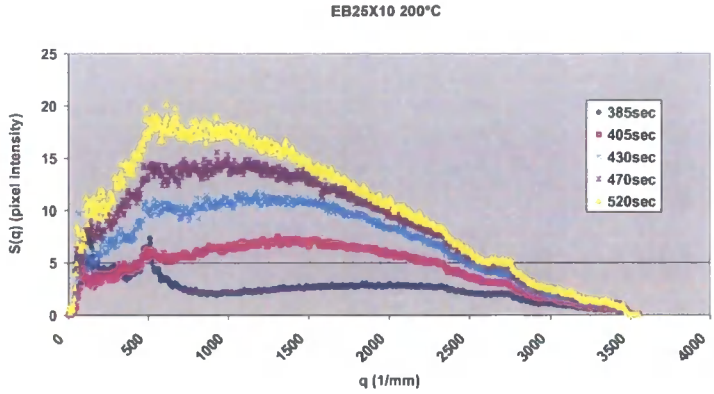

Graph 6.4.8.3 S (q) versus q plot for EB25X10 cured at 200℃. This shows the formation of a broad spinodal peak.

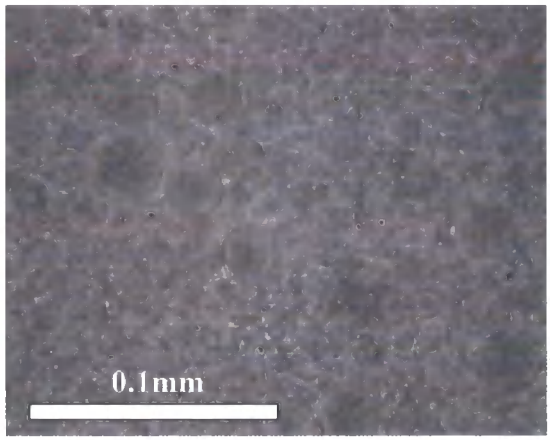

Figure 6.4.8.3 Optical micrograph showing the cured morphology of EB25X10 cured at 200℃.

The graph 6.4.8.3 shows the S(q) versus q plot for EB25X10 cured at 200°C. This shows the formation of a spinodal peak that shifts slowly to lower q as the cure progresses. This trace also has an unusual shape at high q which may indicate some small scale secondary event occurring. The final cured optical micrograph of this system is shown in figure 6.4.8.3 and this shows a large scale particulate morphology. There appears to be a broad size distribution to the dispersed particles in this morphology. It also appears that the minority phase is the continuous phase and this is likely to be thermoplastic rich. Due to the spinodal peak seen in the S(q) versus q plot for this system it is likely that this morphology has formed from a percolation to cluster transformation

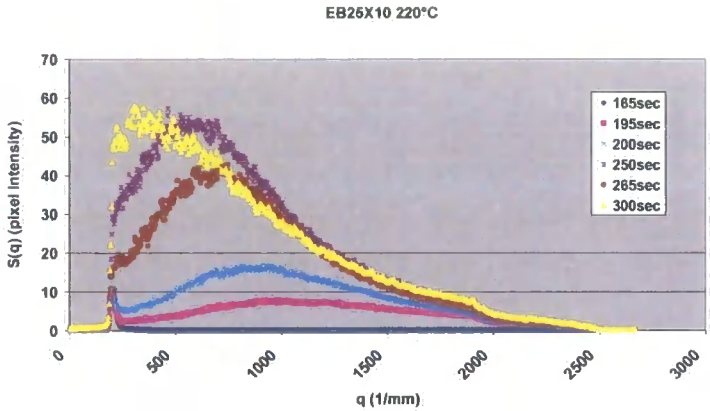

Graph 6.4.8.4 S(q) versus q plot for EB25X10 cured at 220°C. This shows the formation of a broad spinodal peak

The graph 6.4.8.4 shows the S(q) versus q plot for EB25X10 cured at 220°C this show the formation of a single spinodal peak which develops and shifts slowly to lower q in the later stages of the cure process. The final cured morphology of this sample is shown in figure 6.4.8.4 and this indicates a particulate morphology has formed. It is likely that this is a phase-inverted morphology with continuous thermoplastic rich phase and dispersed epoxy rich phase.

The graph 6.4.8.3 shows the S(q) versus q plot for EB25X10 cured at 200°C. This shows the formation of a spinodal peak that shifts slowly to lower q as the cure progresses. This trace also has an unusual shape at high q which may indicate some small scale secondary event occurring. The final cured optical micrograph of this system is shown in figure 6.4.8.3 and this shows a large scale particulate morphology. There appears to be a broad size distribution to the dispersed particles in this morphology. It also appears that the minority phase is the continuous phase and this is likely to be thermoplastic rich. Due to the spinodal peak seen in the S(q) versus q plot for this system it is likely that this morphology has formed from a percolation to cluster transformation

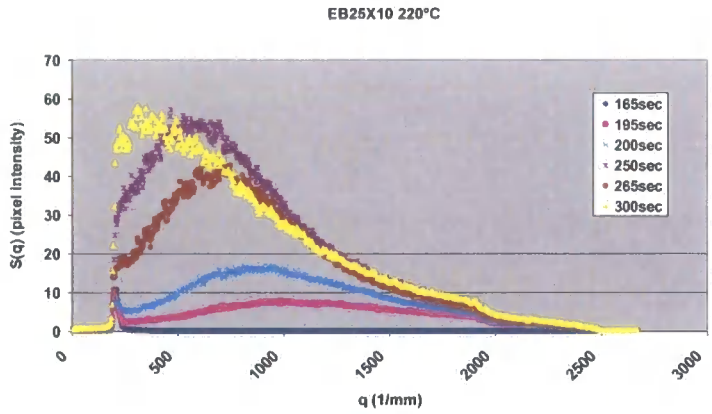

Graph 6.4.8.4 S(q) versus q plot for EB25X10 cured at 220°C. This shows the formation of a broad spinodal peak

The graph 6.4.8.4 shows the S(q) versus q plot for EB25X10 cured at 220°C this show the formation of a single spinodal peak which develops and shifts slowly to lower q in the later stages of the cure process. The final cured morphology of this sample is shown in figure 6.4.8.4 and this indicates a particulate morphology has formed. It is likely that this is a phase-inverted morphology with continuous thermoplastic rich phase and dispersed epoxy rich phase.

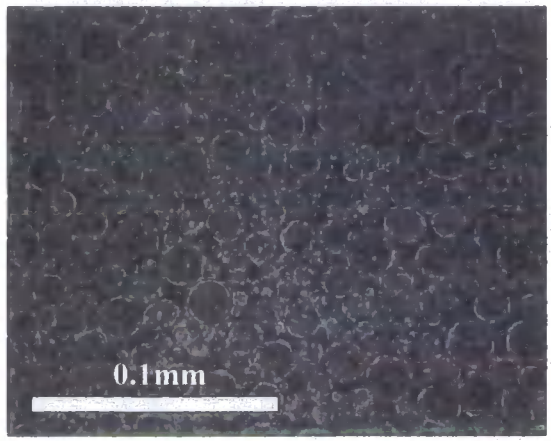

Figure 6.4.8.4 Optical micrograph showing the cured morphology of EB25X10 cured at 220℃

6.4.8.2 R(q) versus q plots for EB25X10 cured at different isothermal temperatures

R(q) versus q plots for EB25X10 were obtained for the early stages of the spinodal decomposition processes. From these plots the $R(q)_{max}$ and q_{max} values were obtained.

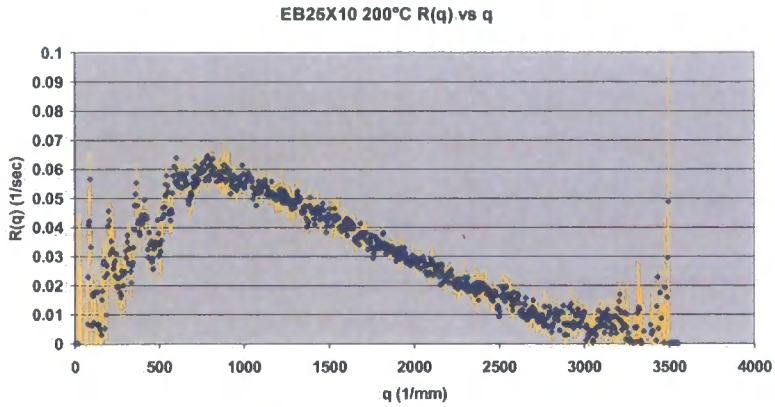

Graph 6.4.8.5 R(q) versus q plot of EB25X10 cured at 220℃

Graph 6.4.8.5 shows an example of a R(q) versus q plot from this series.

EB25X10	160°C	180°C	200°C	220°C
$R(q)_{max}$ (sec^{-1})	0.07	0.09	0.06	0.176
$q_{(max)}$ (mm^{-1})	690	680	670	590

Table 6.4.8.1 This table shows the $R(q)_{max}$ values from EB25X10 cured at different isothermal cure temperatures

The table 6.4.8.1 above shows the $R(q)_{max}$ and $q_{(max)}$values for EB25X10 at different isothermal cure temperatures. It can be seen that this shows a general increasing trend with increasing temperature, which suggests LCST.

6.4.8.3 R(q)/q² versus q² data for EB25X10 cured at different isothermal cure temperatures

This section shows the $R(q)/q^2$ versus q^2 data for different isothermal cure temperatures for EB25X10. These curves did not produce a linear relationship however extrapolations were made to estimate the D^*_{app} fro the spinodal decomposition process.

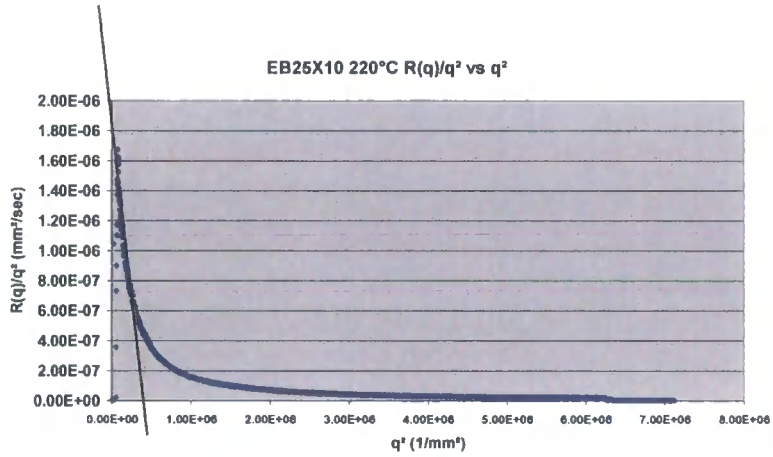

Graph 6.4.8.6 $R(q)/q^2$ versus q^2 plot for the spinodal peak for EB25X10 cured at 220 ℃

The graph 6.4.8.6 shows an example of a $R(q)/q^2$ versus q^2 plot from the EB25X10 series. This shows a non-linear relationship however the plot was extrapolated to

obtain D^*_{app}. The table 6.4.8.2 documents the D^*_{app} values for this EB25X10 system cured at different cure temperatures.

EB25X10	160°C	180°C	200°C	220°C
D*app (mm^2 sec^{-1})	3.5E-07	4E-07	3E-07	1.8E-06

Table 6.4.8.2 This table shows the D^*_{app} values for EB25X10 cured at different isothermal cure temperatures.

6.4.8.4 EB25X10 % Conversion versus time for different isothermal cure temperatures

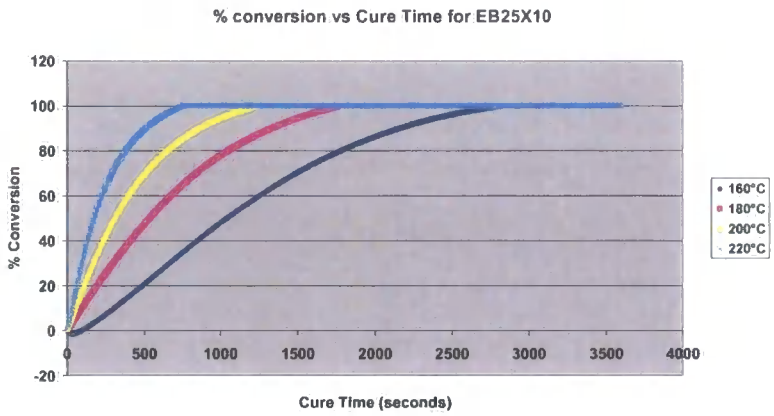

Graph 6.4.8.7 This graph show the % conversion versus cure time relationship between at different isothermal cure temperatures for EB25X10

The graph 6.4.8.7 shows the relationship between the % conversion of the thermoset versus cure time for EB25X10 this data was obtained for isothermal DSC experiments. The method used to obtain this data is detailed in Chapter 4

6.4.8.5 Discussion of Results from EB25X10

The S(q) versus q plots for the EB25X10 system cured at a range of different isothermal cure temperatures all show phase separation by spinodal decomposition. This is demonstrated by the formation of a peak in the S(q) versus q plot data for these systems. All of the morphologies formed with this system show particulate

morphology that suggests that percolation to cluster transformations occurs. It is expected that the morphology is a phase-inverted morphology where there is a continuous thermoplastic rich phase percolation through the bulk of the system. This suggests that the percolating epoxy rich phase has transformed to a particulate system following phase separation by spinodal decomposition.

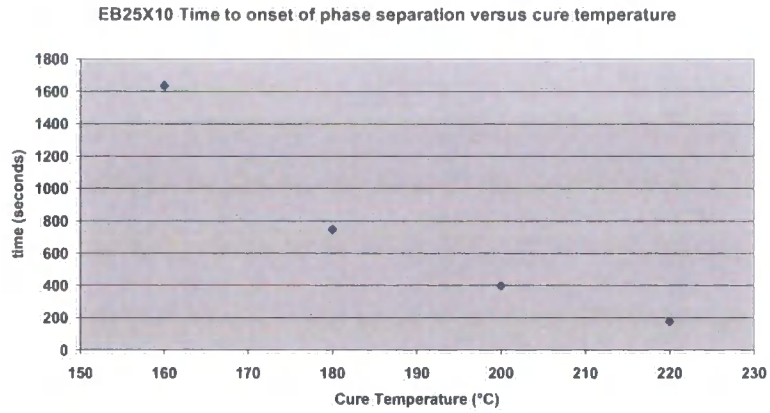

Graph 6.4.8.8 This graph shows the relationship between time to onset of phase separation versus the isothermal cure temperature for EB25X10

The graph 6.4.8.8 above shows the time to onset of phase separation changes with the isothermal cure temperature for EB25X10. As expected this shows a decreasing trend with increasing temperature. This information can be combined with the DSC data in graph 6.4.8.7 to calculate the % conversion at the onset of phase separation. This data is shown in graph 6.4.8.9. This shows a definite decreasing % conversion with increasing cure temperature. This indicates LCST behaviour for this system. One interesting point to note here is the high degree of conversion at which the onset of phase separation occurs. It is likely that this is close to the gel point for this system.

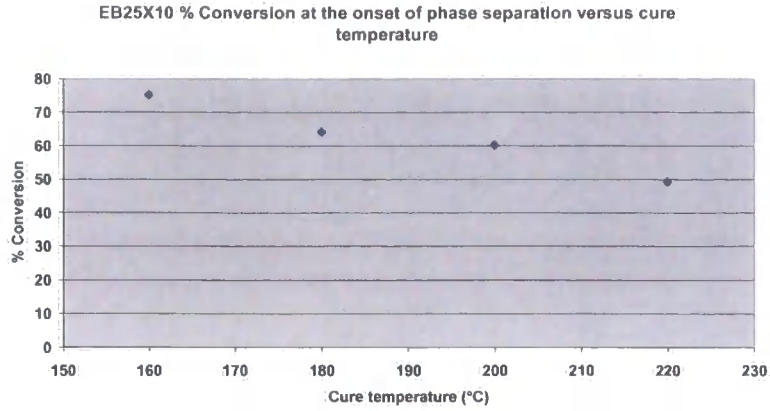

Graph 6.4.8.9 *This graph shows the relationship between % conversion at the onset of phase separation versus the isothermal cure temperature for system EB25X10*

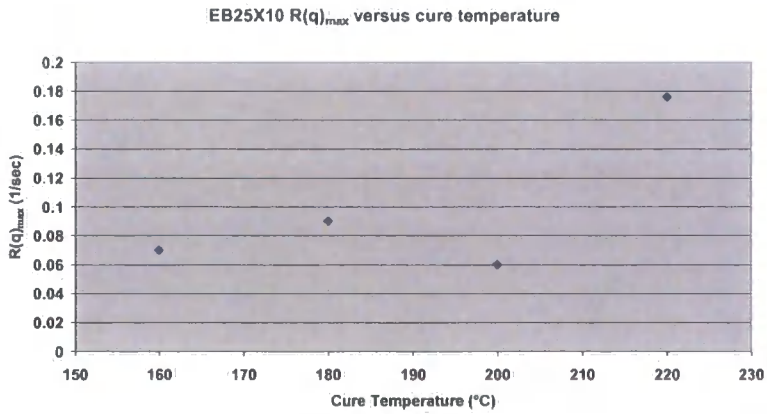

Graph 6.4.8.10 *This graph shows the relationship between $R(q)_{max}$ and the isothermal cure temperature for the spinodal phase separations observed in EB25X10*

The graph 6.4.8.10 shows the $R(q)_{max}$ values for the initial stages of the spinodal decomposition phase separations observed in EB25X10 cured at different isothermal cure temperatures. The increasing trend with increasing temperature seen in this graph further suggests that the system shows LCST.

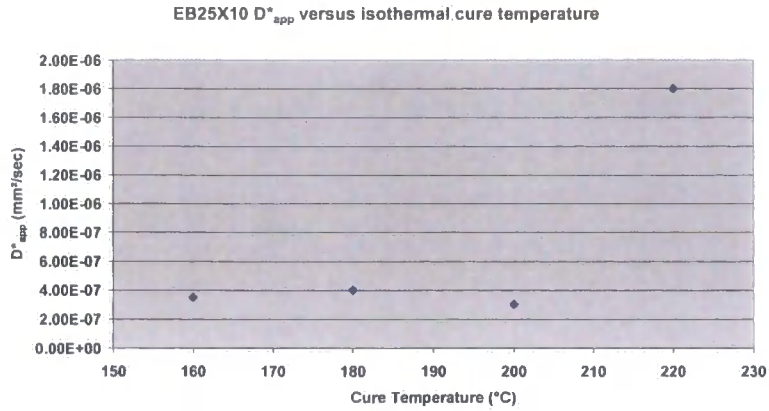

*Graph 6.4.8.11 D*app versus isothermal cure temperature for EB25X10.*

The graph 6.4.8.11 above shows the relationship between the D^*_{app} for the spinodal decomposition process occurring in EB25X10 cured at different isothermal cure temperatures. This shows a general increasing trend with increasing temperature. There is a large increase in the value at 220°C and this may be associated with the Tg of the thermoplastic phase.220°C is above the Tg of the thermoplastic used in these studies so it is likely the D^*_{app} is higher because the thermoplastic rich phase does not readily vitrify at 220°C.

6.5 Discussion

In this section results from chapter 5 which studied a thermoplastic modified di-functional epoxy blend system will be compared with the results from this chapter where a tri-functional epoxy resin, MYO510 has been added to the epoxy blend. This will help give a clear insight into how the inclusion of the tri-functional epoxy resin influences the phase formation behaviour of this blended epoxy system.

It has been shown in both chapter 5 and 6 that the major mechanism for phase separation in this thermoplastic-thermoset blend is by spinodal decomposition. This is contrary to previous work in this area where nucleation and growth has been shown to occur [4] However the final morphology of the systems is very rarely a co-continuous structure. In most cases one of the continuous phases undergoes a percolation to cluster transformation to give a single continuous phase and a dispersed phase [5]. The thermodynamic driving force for the percolation to cluster transformation is the reduction of interfacial energy of the system [6]. In the systems

that have 10 or 15% thermoplastic loading in the blend the morphology is always particulate in nature with a dispersed thermoplastic rich phase and a continuous epoxy rich phase. Previously it has been reported that such dispersed morphologies form in thermoplastic-thermoset blends by nucleation and growth mechanisms [7]. This does not appear to be the case in the blends studied in this thesis. No clear evidence of nucleation and growth was observed.

It has been shown in both this chapter and chapter 5 that this system shows LCST and this has also been reported by previous researchers studying PES toughened reactive epoxy blends[8]

It would appear that secondary phase separation process also occur in these reactive thermoplastic-thermoset blend blends. This has been both predicted from modelling studies and observed practically by several workers [9,10]. This study has confirmed that secondary phase separations do in fact occur readily and seem more common for critical compositions. It is the occurrence of such secondary phase separation and the observation of percolation to cluster transformation behaviour that produces very unique morphologies as seen in the EB20 and EB20X5 formulations. These produce dispersed phases with sub-included phases very similar to salami type morphologies previously reported in rubber toughened thermoplastics such as HIPS and rubber toughened acrylics [3,11]. Such morphologies may have the potential to offer blends with enhanced toughness. This effect will be discussed in the next chapter.

The addition of the tri functional epoxy can have a profound influence on the phase separation behaviour of the blend and ultimately cause changes to the final cured morphology of the system. The first change to note when the tri-functional epoxy resin is added to the blend is that the time to onset of phase separation is increased for any particular isothermal cure temperature. This is shown in the series of graphs 6.5.1 to 6.5.4. These show that the onset of phase separation is delayed in the presence of the MYO510 tri-functional epoxy resin. One exception to this is in the case of EB25X5, there is obviously some inconsistency with this particular sample. This could be due to error in the formulation or preparation of this blended system.

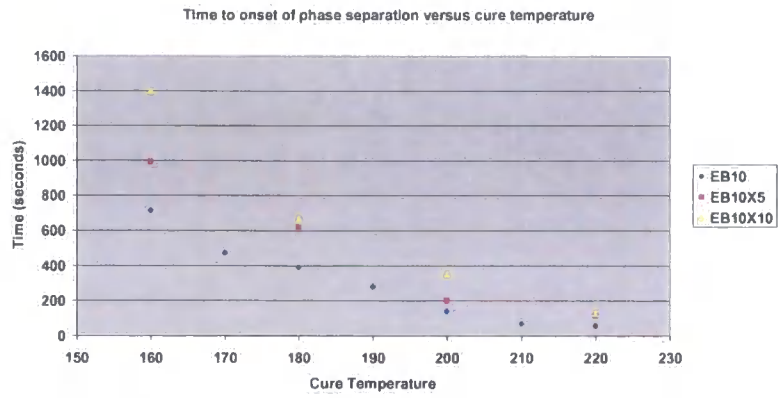

Graph 6.5.1 *Time to onset of phase separation versus cure temperature for EB10 series.*

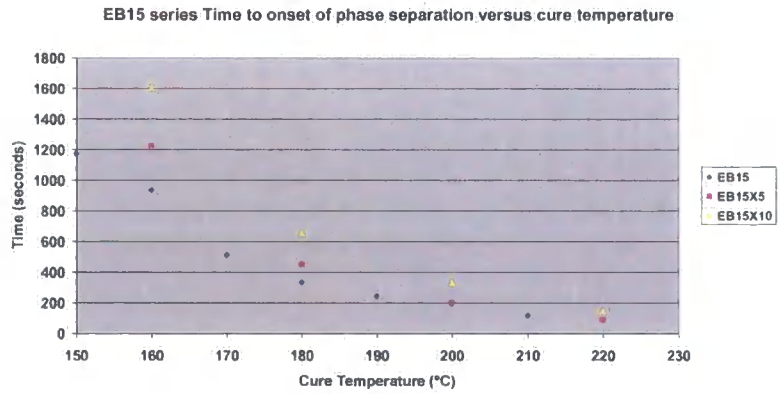

Graph 6.5.2 *Time to onset of phase separation versus cure temperature for EB15 series.*

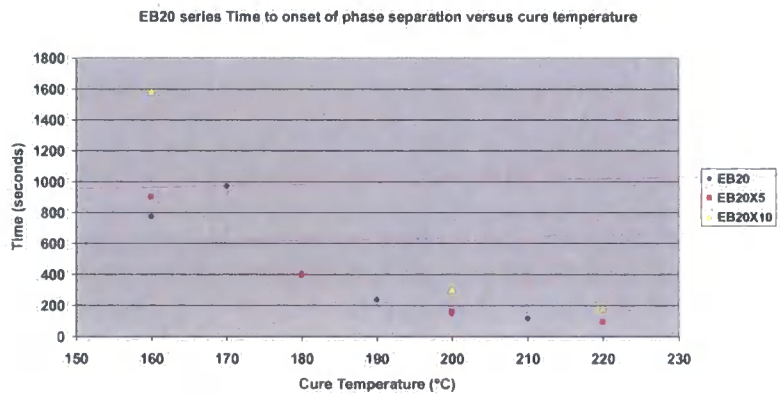

Graph 6.5.3 *Time to onset of phase separation versus cure temperature for EB20 series.*

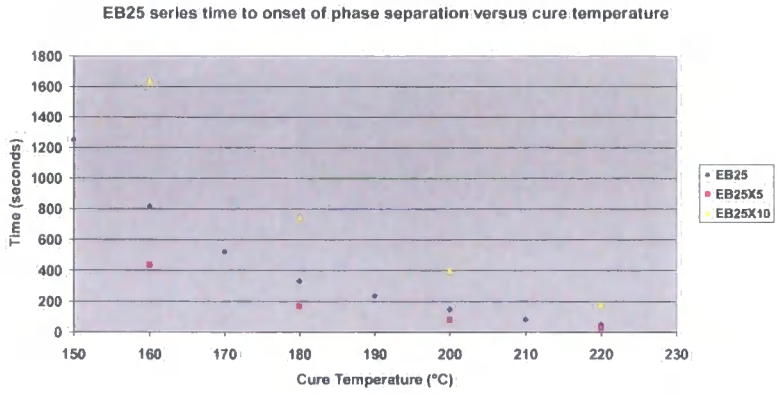

Graph 6.5.4 *Time to onset of phase separation versus cure temperature for EB25 series.*

The results also show that the addition of the tri-functional epoxy resin increases the % conversion at the onset of phase separation. This is shown in the series of graphs 6.5.5 to 6.5.8. The first point to note from these series of graphs is that the % conversion at the onset of phase separation reduces with increasing cure temperature in all cases. This clearly indicates LCST behaviour of this blend system.

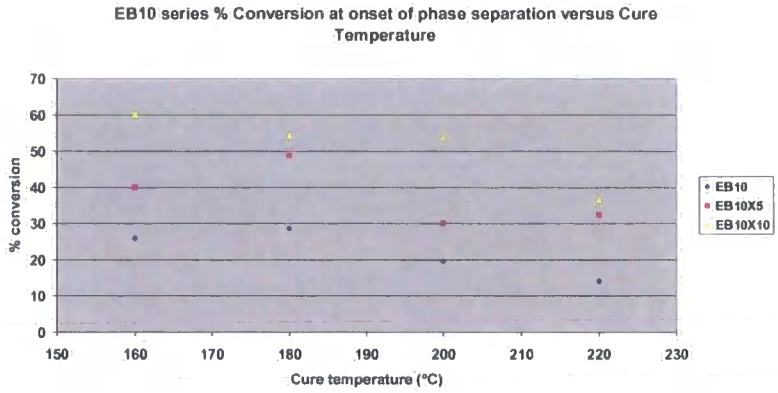

Graph 6.5.5 *This graph shows the % conversion at the onset of phase separation for the EB10 series with different levels of tri-functional epoxy resin.*

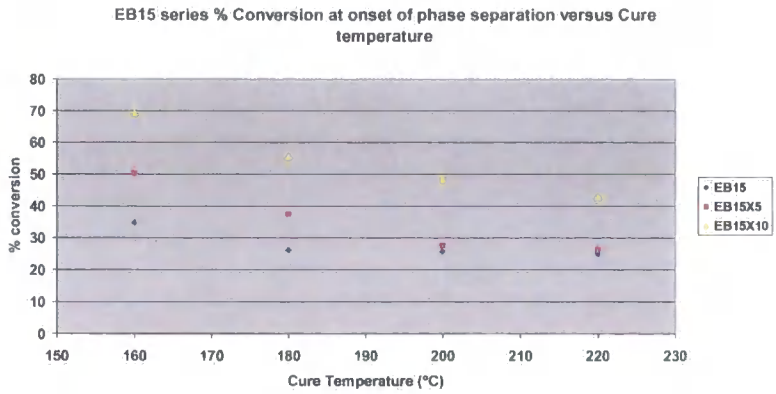

Graph 6.5.6 This graph shows the % conversion at the onset of phase separation for the EB15 series with different levels of tri-functional

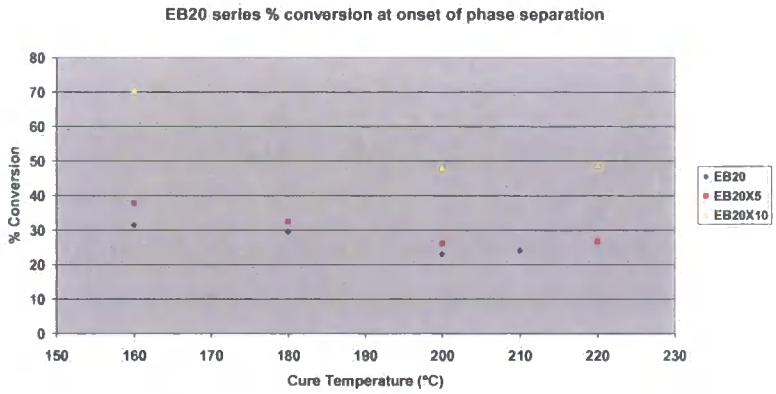

epoxy resin

Graph 6.5.7 This graph shows the % conversion at the onset of phase separation for the EB20 series with different levels of tri-functional epoxy resin

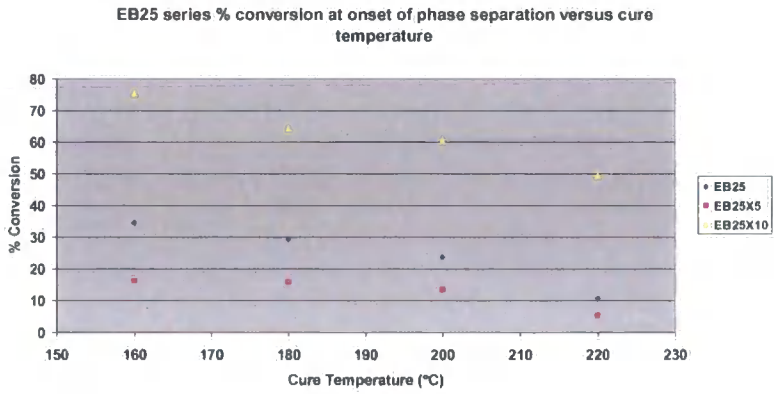

Graph 6.5.8 This graph shows the % conversion at the onset of phase separation for the EB25 series with different levels of tri-functional epoxy resin

From the series of graphs 6.5.5 to 6.5.8 it can be seen that the addition of the tri-functional epoxy resin causes the system to reach a higher level of conversion to

induce phase separation. This suggests that the MYO510 epoxy resin acts to compatibilise the thermoplastic with the epoxy network. This could possibly be due to several reasons. The tri-functional epoxy actually contains a tertiary amine. This has a polar lone pair of electrons that may be more compatible with the polar sulphone groups of the thermoplastic. This may help keep the thermoplastic in solution in the epoxy network. This will have the effect of lowering the exchange energy term of the χ parameter and therefore reduce the thermodynamic driving force for phase separation of the blend.

An alternative explanation may be that the epoxy functionality of the MYO510 resin may preferentially react with the amine end groups of the thermoplastic. This will essentially produce an ABA block copolymer that has a greater solubility with the advancing epoxy network. If this is the case the end group chemistry of the thermoplastic and its ability to react with the epoxy molecules present will have a significant effect on the phase behaviour of the system. It could also be postulated that the molecular weight of the thermoplastic, which will influence the end group concentration, will also be a highly significant factor influencing the phase behaviour of the system. The addition of the tri-functional epoxy resin to an thermoplastic-thermoset blend is usually to increase the glass transition temperature of the system, however it may have the effect of hindering the phase separation of the blend and reduce the toughness of the system.

It is also worth noting that when the tri-functional epoxy is present in the system the % conversion at which phase separation occurs can be relatively high, upto 70% in the case where 10 mole % MYO510 is added to the blend. This is likely to be approaching the gel point of the system. If greater levels of tri-functional epoxy resin are added there may reach a point where phase separation does not occur because the gel point is reached prior to the necessary thermodynamic conditions being achieved to cause phase separation in the system.

If block copolymer formation is occurring in the blends between the thermoplastic and the tri-functional epoxy resin it may also be possible that a very small scale micro-phase formation may also be occurring in these systems. Such small scale morphologies have previously been reported for block-copolymers. However the nano-sized phase size of such morphologies would not usually be detected by SALS

and would need other techniques such as neutron scattering techniques to study in detail.

The $R(q)_{max}$ values for the different systems are shown in the series of graphs 6.5.9 to 6.5.12. These in general show that increasing the level of tri-functional epoxy in the system generally reduces the initial rate of phase separation.

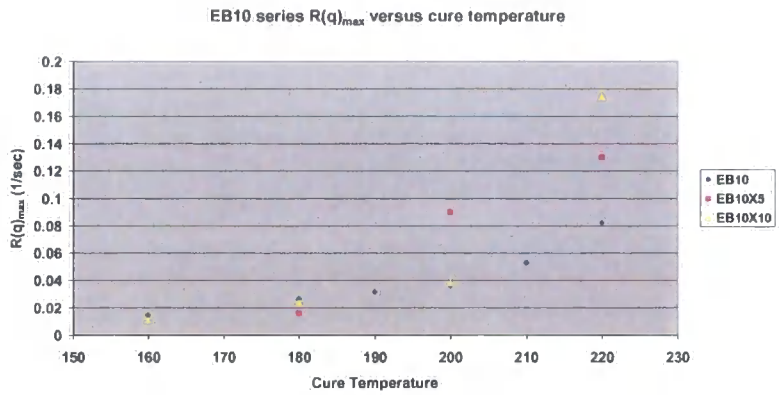

Graph 6.5.9 *R(q)max versus cure temperature for the primary spinodal decompositions in the series EB10*

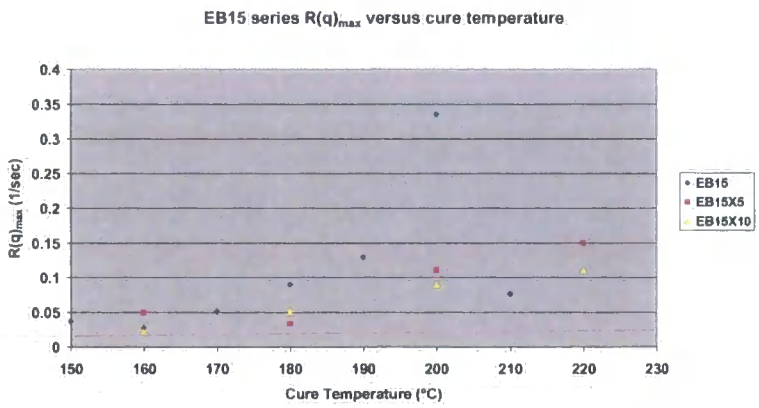

Graph 6.5.10 *$R(q)_{max}$ versus cure temperature for the primary spinodal decompositions in the series EB15*

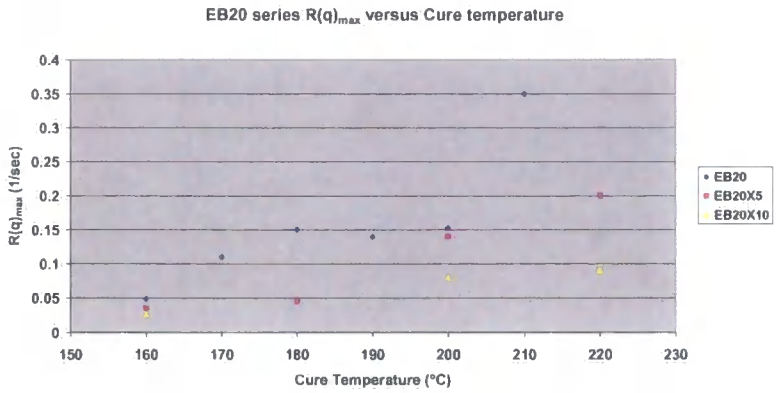

Graph 6.5.11 $R(q)_{max}$ versus cure temperature for the primary spinodal decompositions in the series EB20

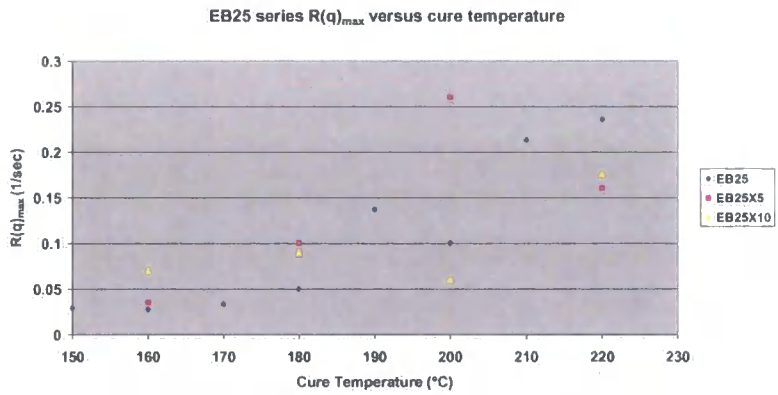

Graph 6.5.12 $R(q)_{max}$ versus cure temperature for the primary spinodal decompositions in the series EB25

The reduction in the $R(q)_{max}$ value with increasing levels of tri-functional epoxy is likely be as a result of the reduction in the thermodynamic driving force for the phase separation process. This is likely due to the reduction in the enthalpy of mixing as opposed to entropic factors. The exchange energy between the two phases is likely to be lower due to either polar interactions or block copolymer formation and this will lower the χ value of the system resulting in a lower thermodynamic driving force fro the phase separation. The reduction in $R(q)_{max}$ with increasing tri-functional epoxy resin may also be due to the observation that the phase separation process occurs at higher levels of conversion closer to the gel point. This may also decrease the rate of phase separation. It is difficult to determine the exact reason why the $R(q)_{max}$ decreases with increasing tri functional epoxy level.

In all cases the $R(q)_{max}$ value increases as the cure temperature increases. This also suggests that that at higher temperatures there is a greater thermodynamic driving force for the phase separation process and this is characteristic of LCST behaviour.

Where secondary phase separations occur it is observed that the $R(q)_{max}$ value for the secondary phase separation are always significantly lower than the $R(q)_{max}$ value for the primary phase separation. This is to be expected for LCST behaviour for secondary phase separations.

The series of graphs 6.5.13 to 6.5.16 show the relationship between D^*_{app} and the isothermal cure temperature for the series containing different levels of thermoplastic. In these graphs the effect of increasing level of tri-functional epoxy resin is also shown. It can be observed from this series of graphs that in general the D^*_{app} value increases with increasing cure temperature, which further confirms the LCST behaviour of this system.

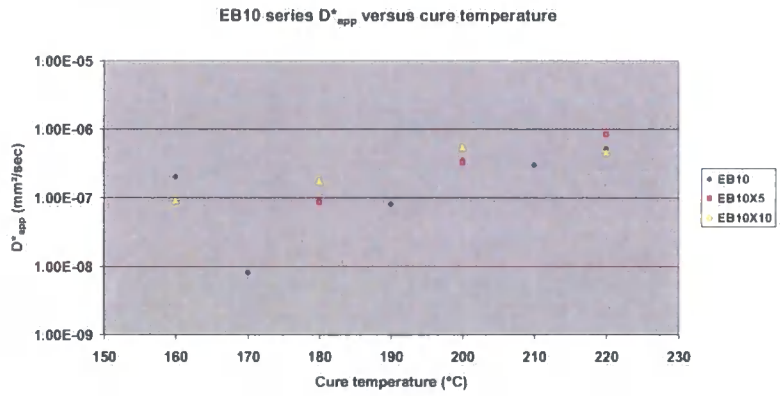

Graph 6.5.13 *D^*_{app} versus isothermal cure temperature for EB10 series.*

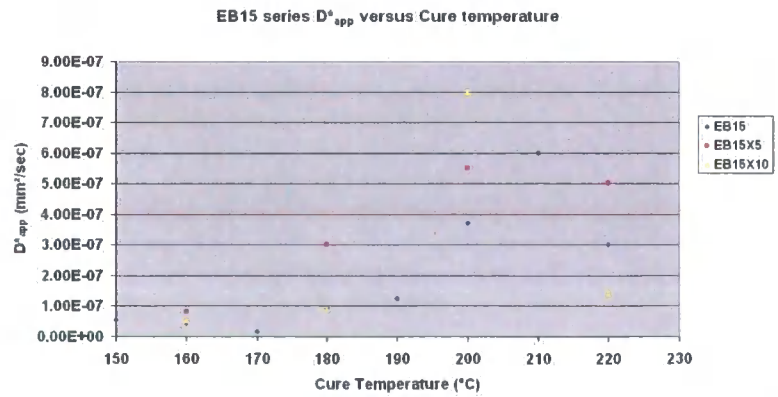

Graph 6.5.14 *D^*_{app} versus isothermal cure temperature for EB15 series*

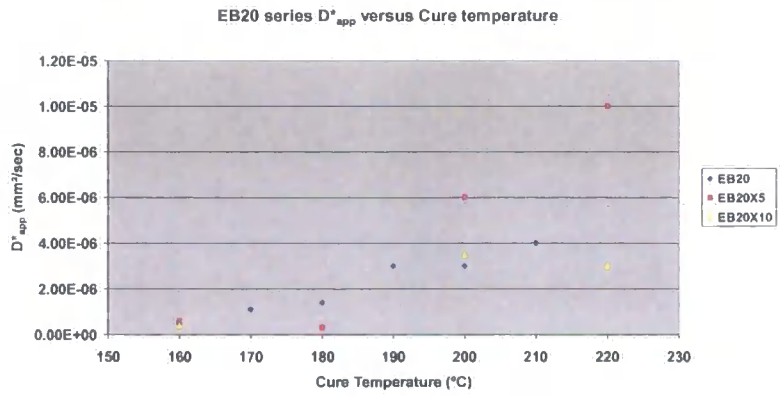

Graph 6.5.15 *D^*_{app} versus isothermal cure temperature for EB20 series*

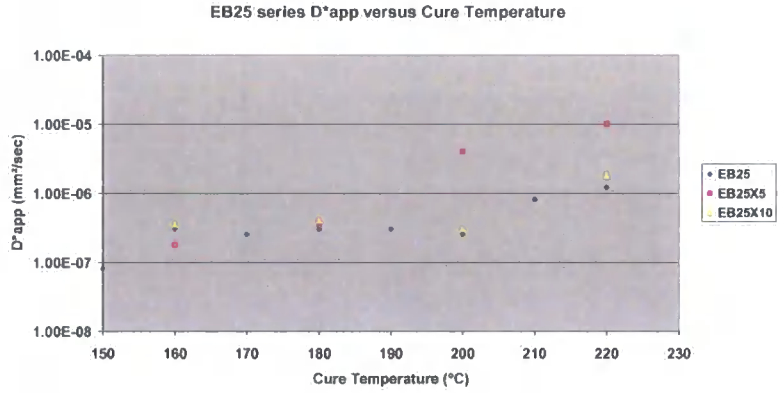

Graph 6.5.16 *D^*_{app} versus isothermal cure temperature for EB25 series*

From this series of graphs is can also be observed that the D^*_{app} value does not change significantly with increasing levels of tri-functional epoxy resin. This would suggest that the apparent uphill diffusion for the spinodal decomposition is largely a temperature dependent parameter. In most cases there is a large increase in the value of D^*_{app} at cure temperatures of 200°C and above. The glass transition temperature of the thermoplastic used in these experiments is 195°C. This may indicate that the phase separation processes at lower temperatures may be kinetically hindered by vitrification. During the early stages of the spinodal decomposition process the emerging thermoplastic rich phase could potentially become vitrified at lower cure temperatures. This is far less likely to be the case at temperatures above 200°C, which are in excess of the Tg of the thermoplastic. It would appear that at low cure temperatures the morphologies produced are non-equilibrium structures that are formed as a result of the vitrification of the thermoplastic rich phases. This indicates

the important role of the Tg of the polymer backbone. Changing the PES:PEES ration of the backbone will alter the Tg of the thermoplastic and hence change the nature of the cured morphology. This work suggests that critical nature of the characteristics of the thermoplastic in determining the morphology of the cured system. End group chemistry, molecular weight and backbone Tg will all play significant roles in the phase separation and morphology formation processes.

From the information reported in this section phase diagrams can be plotted for the system. The phase diagrams are spinodal lines in % conversion versus thermoplastic loading level.

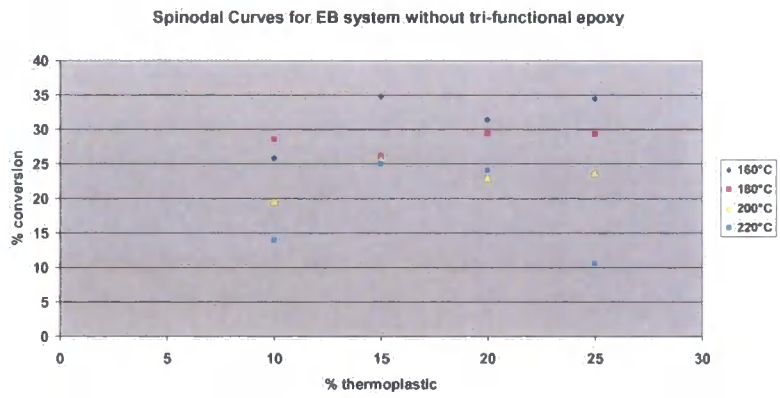

Graph 6.5.17 Phase diagram for EB system with no tri-functional epoxy resin

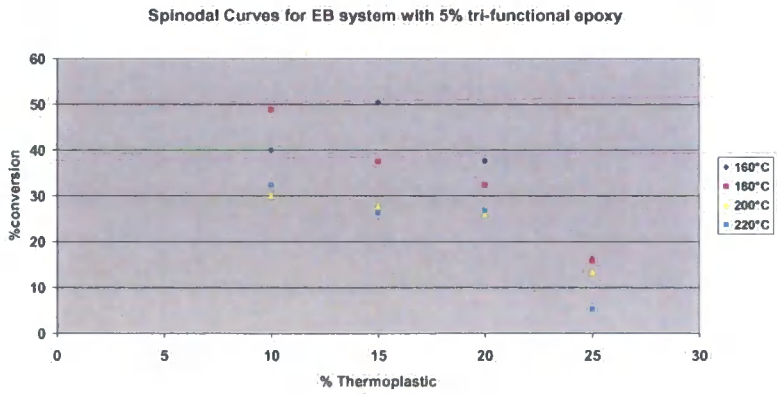

Graph 6.5.18 Phase diagram for EB system with 5% tri-functional epoxy resin MYO510

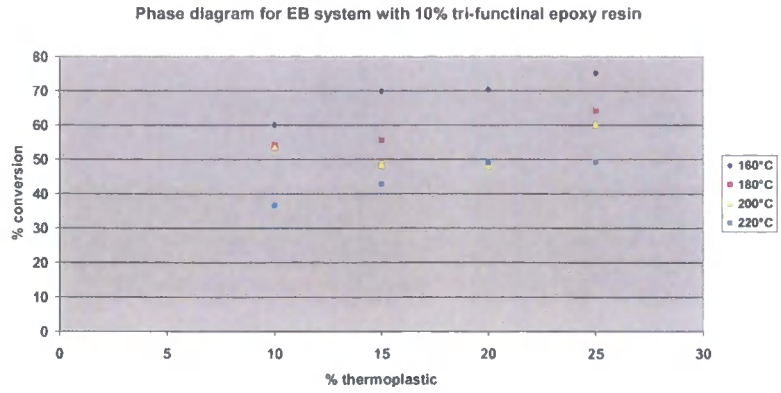

Graph 6.5.19 Phase diagram for EB system with 10% tri-functional epoxy resin MYO510

The series of graphs 6.5.17 to 6.5.19 show the spinodal lines for the EB system at different temperatures with different levels of tri-functional epoxy resin. The first point to notice from these phase diagrams is that the system shows LCST as indicated by the lower % conversion at which phase separation occurs at higher temperatures. Also the spinodal lines are shifted upwards with the addition of tri-functional epoxy resin. As discussed above this is likely due to the MYO510 acting to make the thermoplastic more compatible with the developing epoxy network and reduce the tendency for the system to phase separate. This may be due to the formation of a block copolymer by chain extending the amine ends of the thermoplastic with the MYO510 tri-functional epoxy resin. It may also be due to the more polar nature of the developing epoxy network due to the presence of the nitrogen lone pair on the tertiary amine of the MYO510 molecule.

The phase diagrams also show evidence of an inverted nature which is not usually predicted from binary phase diagrams. This effect is more evident at higher temperatures and may indicate that the phase diagram for these system shows a ternary nature rather than purely a binary nature. This may again be due the reactive nature of end groups of the PES:PEES thermoplastic. As the system begins to react if the initial most favourable reaction is the reaction of the thermoplastic amine end groups with the tri-functional epoxy then the system becomes a ternary mixture of thermoplastic, block copolymer and epoxy/amine. This alters the general nature of the phase diagram to produce an inverted phase diagram which can be predicted from modified Flory-Huggins theory for ternary blends [12]. The inversion of the phase diagram is more evident at elevated temperature. This may indicate that the reaction between the thermoplastic amine end group and the epoxy is more favourable at

higher temperatures than it is at lower temperatures. This again may be due to the influence of the Tg of the thermoplastic polymer.

6.6 Summary

This chapter has studied the influence of adding a tri-functional epoxy resin to a thermoplastic-thermoset blend. It has been demonstrated that the mechanism of phase separation in all cases is spinodal decomposition. Usually one of the emerging phases undergoes a percolation to cluster transformation to produce a dispersed phase. It has been shown that secondary phase separation also can occur in these thermoplastic-thermoset blend systems. This can produce some unusual morphologies in the final cured system such as salami type morphologies previously seen in rubber modified thermoplastics. These may exhibit interesting properties.

It has also been shown that the epoxy blends studied in this chapter show LCST behaviour. The addition of the tri-functional epoxy MYO510 to the formulation acts to make the thermoplastic more soluble in the epoxy network and this delays the onset of the phase separation and also reduces the rate at which the phase separation occurs. In some cases the % conversion at the onset of phase separation can be very close to the gel point of the system. It is predicted that higher levels of MYO510 may prevent the phase separation occurring in the system.

This chapter has also shown that the characteristics of the thermoplastic appear to be key to the phase separation behaviour of the system. It would appear that the end group chemistry, molecular weight and Tg of the toughening thermoplastic will all play a vital role in determining the overall morphology of the system and will therefore dictate the properties of the cured blend.

It may also be the case that this system shows ternary phase diagram behaviour due to the formation of ABA type block copolymers by reaction of the thermoplastic amine end groups with the epoxy resin. These copolymers appear to stabilise the blend and may give a ternary nature to the phase behaviour.

6.7 References

1 Flory, P.J. *Principles of Polymer Chemistry*, Cornell university Press. Ithaca, NY **1953**

2 Confidential ICI Internal Yellow Back Report

3 Bucknall,CB, Partidge IK, Phillips MJ, *Polymer 32*,786 & 636, **1991**

4, Higgins J, Ellianardis S et al, *Polymer*, 1999, 37, 1655

5 Alig I Rullman M, Holst M, Deutes Kunststoff-Institute 2002.

6 http://koken-db.kogaku.kyoto-u.ac.jp/1998/B/PC/98BPC32012.html.

7 Ellianardis S, PhD thesis, C/o Higgins J, Imperial College London 1998

8 R.J.J.Williams, *Reaction Induced Phase Separation In Modified Thermosetting Polymers, Advances In Polymer Science* No128, Springer, **1997**

9 Clarke N, McLiesh TCB, Jenkins S, *Macromolecules 28.* 4650,**1995**

10 Alig,I Jennerger W, Schawe, J. Polymer 2000, 41,1577.

11 ICI internal report on rubber modified acrylic systems

12 Kinetics of Phase separation in Ternary Polymer mixtures: PhD thesis of Bumsuk Jung, Girton College Cambridge March 1999.

Chapter 7

Physical Properties and Toughening Mechanisms of Thermoplastic-Thermoset blends

7.1 Introduction

The overall object of mixing thermoset resins with thermoplastics is to tailor the properties of the blend to meet the needs of a particular application. Chapter 1 discussed the applications of thermosetting polymers and their inherent properties. The major deficiency of thermosetting polymers is their poor toughness. As a result of the low toughness, or resistance to crack growth, thermosetting polymers perform very poorly in a fatigue environment. The low toughness is largely a result of the highly crosslinked networks that produce glassy polymers at ambient temperatures. Chapter 1 also discussed the various approaches that may be used to improve the toughness of thermoset materials, some methods reduce the crosslinked density but in using this approach although fracture toughness is improved it is at the expense of both modulus and Tg. Incorporating high Tg thermoplastics into a thermoset can produce a system that has good toughness without any detrimental impact on the Tg or modulus. This is of commercial advantage in aerospace applications where high temperature properties, impact performance and fatigue performance are of vital importance.

Another significant drawback of thermosetting polymers, in particular epoxy resins, is their inherent ability to absorb moisture. This is primarily due to the open, low-density molecular network, which offers little impedance to small molecules such as water, and also due to the presence of highly polar hydroxyl groups that are present in the network. The hydroxyl groups can hydrogen bond with water molecules and can have a significant plasticisation effect on the network. Also epoxy resin networks are susceptible to hydrolysis especially at elevated temperatures. The plasticising effect of the water molecules on an epoxy network may give some inherent improvement in toughness but Tg and modulus will be reduced. For this reason the moisture uptake properties of thermosetting polymers is of vital importance.

This chapter investigates the fracture toughness and mechanical properties of a phase separated thermoplastic-thermoset blend. It studies how the morphology of the cured blend influences fracture properties. Also the water uptake properties of the blends are investigated to see how the phase separated morphology impacts the moisture diffusivity and saturation levels.

7.2 Experimental

7.2.1 Materials and sample preparation.

For this study a range of systems were chosen that had different phase separated morphologies. The formulations used in this study are detailed in table 7.2.1. The details of the components used are fully described in chapter 3.

	% Composition				
Reference Code	**Di-functional epoxy (PY306)**	**Tri-functional epoxy (MY0510)**	**Cure Agent (MDEA)**	**Thermoplastic (PES:PEES)**	**Morphology**
EBN0	34.47	32.9	32.62	0	Homogeneous
EBN5	32.74	31.25	30.96	5	Particulate
EBN15	23.9	27.97	27.7	15	Particulate
EBN22.5	26.7	25.49	25.3	22.5	Co-continuous
EBN35	22.41	21.38	21.2	35	Phase Inverted

Table 7.2.1 Table of epoxy blend compositions studied in this chapter

For the mechanical characterisation cured resin panels were prepared. The dimensions of these panels were 160 mm x 80 mm x 4 mm. Initially the formulations were prepared using the hot melt method described in chapter 3. The hot blend was transferred into a polished mould that had previously been treated with a release agent. The resin was then degassed in a vacuum oven at 100°C for approximately one hour until all bubbling had ceased. Following the degassing the hot mould was transferred to an air circulating oven and cured. The cure cycle used was 2°C/min to 180°C with a dwell time of 3 hours.

7.2.2 Mechanical Testing

The cured panels were characterised for the following properties, Modulus, yield strength, fracture toughness, K_{IC} and G_{IC} and ductility factor. These properties were measured at 25°C and at a test speed of 1mm/min. The detailed descriptions of these tests are given in chapter 3 section 3.6. The fracture toughness testing procedure used conforms to the European Structural Integrity Society (ESIS) protocol [1]. The modulus and yield strength tests conform to the ASTM standards for polymer testing (ASTM D790 for Modulus, ASTM D695 for yield strength).

To evaluate the effect of moisture on the mechanical properties the samples were tested both dry and after conditioning at 30°C and 85% relative humidity. In order to avoid complicating the results by additional curing the samples were dried at 40°C in a cabinet purged with pre-dried nitrogen. The mass of the samples was monitored approximately daily until a consistent mass was achieved. In general this drying process took around 20-30 days depending on the thickness of the specimen. Once a stable weight was attained the samples were transferred to a dessicator containing silica gel and transported to the testing facility. The necessary tests were carried out within 1 hour of removing from the drying cabinet. The wet conditioning was carried out in a Hereaus environmental chamber (model no HV08/300) set at 30°C and 85% relative humidity. Samples were held in this environment for a period of 30 days. Following this period of conditioning the samples were transported and stored in a dessicator containing moist cotton wool and tested within 1 hour of removing from the environmental chamber.

7.2.3 Toughening Mechanism Evaluation

In order to investigate the toughening mechanisms that occur in phase separated thermoplastic-thermoset blends a combination of fracture mechanics, sectioning and TEM was carried out. Initially a fracture mechanics test was performed on the SENB fracture toughness sample. After testing the samples were sectioned and microtomed at 90° to the fractured surface of the specimen. The microtomed section was taken using a diamond knife microtome under liquid nitrogen. The thickness of the section was approximately 5 microns thick. It was found that for these samples there was enough atomic number contrast between the two phases to produce good well-defined TEM images of the samples without the need for staining.

The samples were carefully sectioned from the fractured SENB specimens so that the region close to the fracture surface could be observed. This was done to look for evidence of toughening mechanisms such as yielding or crazing in the bulk of the sample away from the fracture surface. The crack path could also be observed and the influence of the morphology upon both crack path and toughening mechanism could be investigated. Further details of this evaluation process are given in chapter 3 section 3.6.

7.2.4 Moisture Uptake Properties.

The thermoplastic-thermoset blends in this study were studied for moisture diffusion properties using dynamic vapour sorption apparatus manufactured by Scientific and Medical Systems Ltd [2]. The details of this test are given in chapter 3. From the data moisture diffusion and saturation level can be evaluated at different relative humidity and temperatures.

To study the moisture uptake properties in these thermoplastic-thermoset blends dynamic vapour sorption equipment was employed. This equipment carries out isothermal tests at different relative humidity's (RH). The equipment measures the mass of the samples with time at different RH. For this experimentation the relative himidities selected were 0% (dry), 30%, 60% and 85%. The test initially dries the sample under the set temperature with dry flowing nitrogen (0% RH). This is held until a constant sample mass is achieved. Then the RH is increased to 30% RH and the sample mass is measured until a constant mass is achieved. Then after equilibrium has been established the RH is then changed to 60%. The sample mass is monitored dynamically until equilibrium mass is established. Then following the establishment of equilibrium at 60%RH the environment is changed to 85%RH and the sample mass monitored dynamically until a constant mass is achieved.

Once the sample has established equilibrium at 85%RH the humidity is then set to 60% and the desorption mass change is monitored until equilibrium is established. Then the RH is further reduced to 30% RH and the desorption monitored until equilibrium is established and finally the RH is set to 0% and the final desorption curve is established.

For each of the adsorption and desorption step changes in RH a diffusion coefficient for the process can be calculated using Ficks law. This experimental procedure is detailed in chapter 4.

7.2.5 Dynamic mechanical thermal analysis

Dynamuc mechanical thermal analysis evaluation was carried out using a Polymer Laboratories DMTA. For this test samples of the cured epoxy blend 10mm x 50mm x 2mm were cut from the cured panel. Prior to testing samples were dried in a dry nitrogen cabinet at 40°C until the weight had stabilised. This drying process took approximately 20-30days. The samples were then removed from the drying cabinet and tested immediately. This technique applies a sinusoidal stress to the sample in three point bend mode and measures the phase shift between the stress amplitude and the sample deformation. This calculates the in phase modulus (or storage modulus) of the sample, E' and the out of phase modulus (loss modulus) E" of the sample. The test carried out in this thesis were carried out with a sinusoidal stress frequency of 50Hz. The tests were carried out as a function of temperature between 25°C and 250°C. From the traces phase Tg's can be identified and also rubbery plateau modulus can be estimated.

7.3 Results and Discussion

7.3.1 Mechanical Testing

7.3.1.1 Modulus

The modulus of the EBN series of blends after both drying and moisture conditioning are shown in graph 7.3.1.

The error bars shown on the graph are the standard deviation on a sample size of 6 specimens.

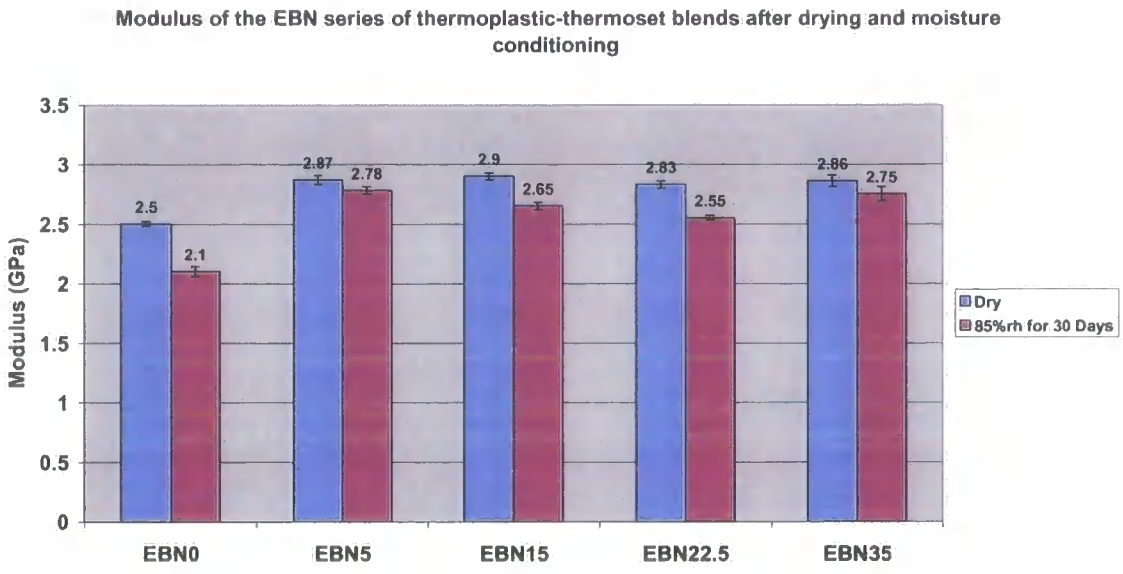

Graph 7.3.1 This graph shows the modulus of EBN series of thermoplastic-thermoset blends after both wet and dry conditioning

Firstly comparing the dry data for the EBN series shows that with the exception of EBN0 that contains no thermoplastic the modulus values are all similar and within experimental scatter. The modulus of the dry EBN0 system is statistically lower that the other blends. This shows that the addition of the aromatic thermoplastic has the effect of increasing the modulus of the blend. This may possibly be due to the effect of the amine end groups on thermoplastic, which could increase the crosslinked density of the system. It may be also likely that the modulus of the base aromatic thermoplastic is higher than that of the cured unmodified epoxy system. However this also shows that increasing the level of thermoplastic does not significantly increase the modulus of the system. There does not appear to be any clear link between the morphology of the system and the modulus of the cured blend.

After moisture conditioning the modulus of the blends drops in all cases. The drop in modulus appears to be more significant in the EB0 blend that does not contain any thermoplastic. It has been reported that when moisture ingresses into an epoxy network the water molecules hydrogen bond to the pendant hydroxyl groups resulting from the ring opening and polymerisation of the epoxy group. This prevents or reduces the level of intra molecular network hydrogen bonding which results in a fall in modulus and plasticisation of the system [3]. The incorporation of the thermoplastic will effectively reduce the concentration of the pendant hydroxyl

groups in the molecular network. This is possibly the reason why the thermoplastic modified epoxy blend shows less of a reduction in modulus after moisture exposure to moisture. It appears that the thermoplastic incorporation is advantageous in preventing plasticisation due to moisture ingress.

7.3.1.2 Yield Strength

The graph 7.3.2.1 shows the yield strength of the EBN series of thermoplastic-thermoset blends before and after moisture conditioning.

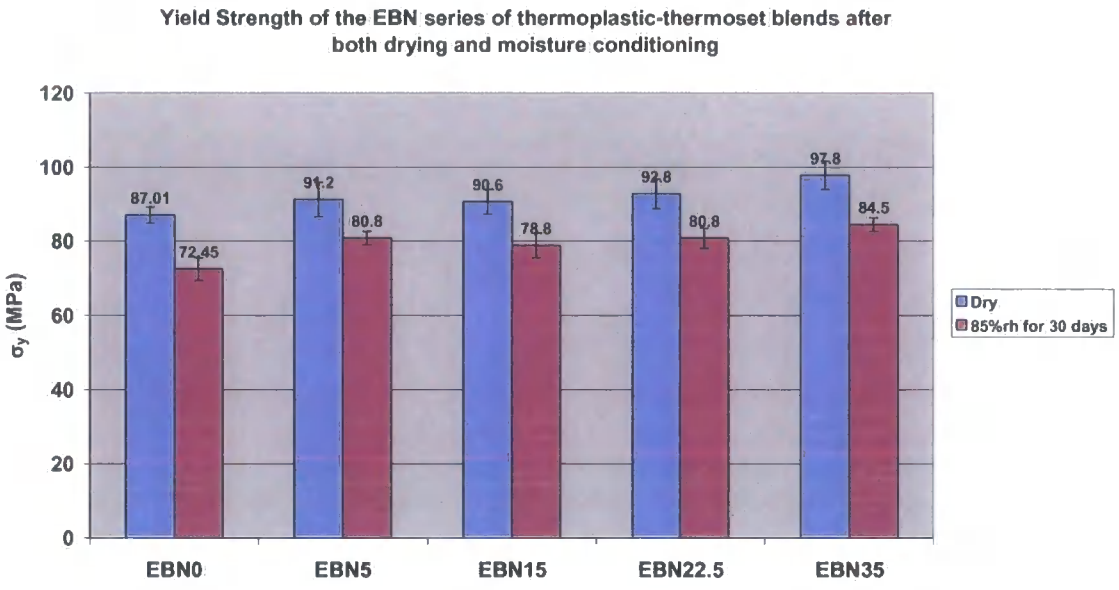

Graph 7.3.2 This graph shows the yield strength of EBN series of thermoplastic-thermoset blends after both wet and dry conditioning. The error bars show the standard deviation on a sample size of 6 specimens.

The dry yield strength values show a general increasing trend with increasing thermoplastic loading. It therefore appears that the PES:PEES thermoplastic has a minor reinforcing effect to the epoxy matrix. On moisture conditioning the yield strength of the thermoplastic-thermoset blends decreases. The most significant decrease in yield strength occurs in the EBN0 sample that contains no thermoplastic. This may be due to either the plasticisation effect as moisture hydrogen bonds to the network or possibly due to some hydrolysis occurring. It appears that the addition of thermoplastic reduces the moisture susceptibility of the system however there is no

obvious link between the yield strength of the system and the phase separated morphology in the thermoplastic-thermoset blends.

7.3.1.3 Strain Energy Release Rate, G_C.

The graph 7.3.3.1 below shows the G_C, strain energy release rates, for the EBN series of epoxy blends for both dry and moisture conditioned samples fracture.

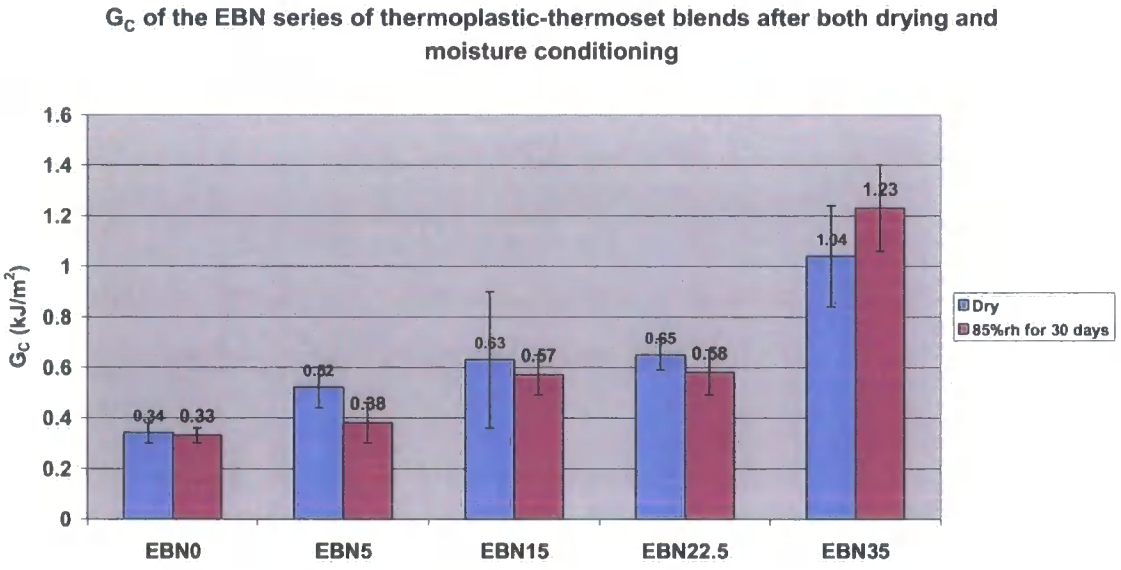

Graph 7.3.3 This graph shows the Gc results for the EBN series of epoxy blends for both dry and moisture-conditioned specimens. The error bars show the standard deviation on a sample size of 6 specimens

The dry G_C results show a clear increasing trend with increasing thermoplastic level. There is a significant increase in G_C in all of the thermoplastic-thermoset blends compared with the EBN0 system that does not contain any thermoplastic. It is clear that the addition of the thermoplastic increases the resistance to fracture of the system and as shown above also increases the modulus. This combination of property improvement is of great commercial significance especially in aerospace applications. Looking at the relationship between the phase separated morphology of the system and the fracture toughness there appears to be a large increase in toughness in the sample EBN35 that has a phase inverted morphology. This has a continuous thermoplastic rich phase containing a dispersed epoxy rich phase. Crack propagation

in this system is likely to be significantly in the thermoplastic rich phase which may explain the high fracture toughness in this sample.

Comparing the samples that have been subjected to moisture it can be seen that the G_C decreases in all cases expect fro the EN35 system that has the phase inverted morphology. It is likely that the crack growth in the EN35 sample is more significantly in the thermoplastic rich phase when compared to the other blended systems. It may be the case that the thermoplastic rich phase increases its fracture toughness on exposure to moisture due to plasticisation and the epoxy rich phase reduces its fracture toughness because of hydrolysis effects.. This may then explain why the G_C of the EN35 sample improves on moisture exposure. Further tests would need to be carried out to test out this hypothesis. If this is a true finding then this also could be of key commercial significance.

7.3.1.4 Critical Stress intensity factor K_C

The graph 7.3.4 shows the K_C results from the EBN series of blends.

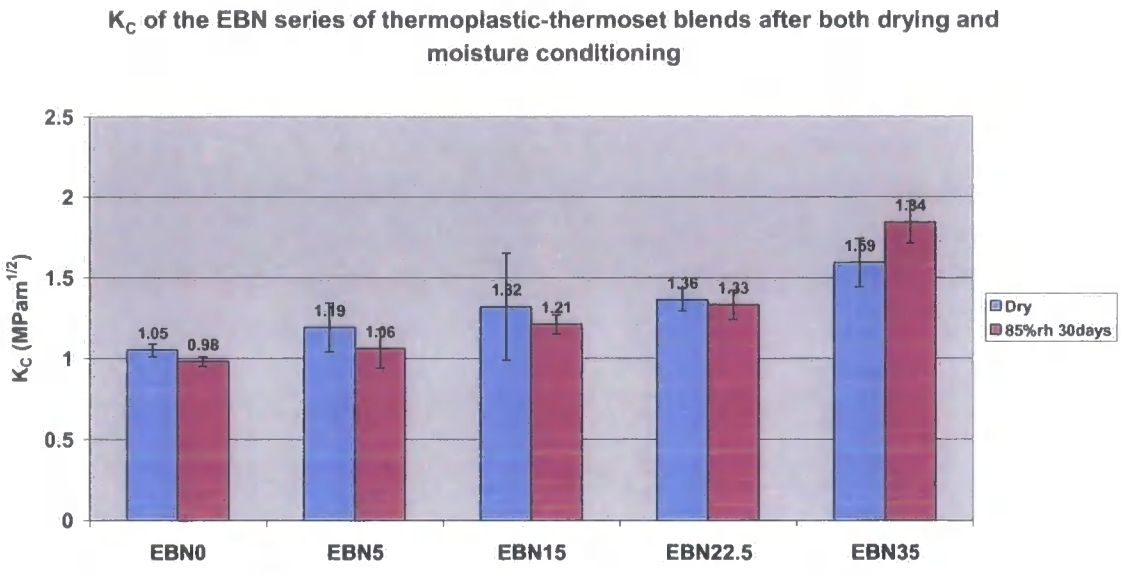

Graph 7.3.4 *This graph shows the Kc results for the EBN series of epoxy blends for both dry and moisture-conditioned specimens. The error bars show the standard deviation on a sample size of 6 specimens*

As expected these K_C results reflect the same trends as shown in the G_C data. In all cases there is a fall in the K_C after moisture conditioning with the exception of EBN35 that shows a significant increase. This may be as a consequence of the morphology of this sample, which has a continuous thermoplastic network. It could be postulated that the continuous thermoplastic rich phase is less affected by moisture ingress and this shields the dispersed epoxy phase from moisture.

7.3.1.5 Ductility factor

The ductility factor of the blends is a ratio of K_C to yield strength and is discussed in chapter 3. Pragmatically this is related to the diameter of plastic zone at the crack tip. This is often of more importance in real applications than KC and GC. Several workers [4, 5] have reported that in polymers the fatigue life of a component correlates more to the ductility factor than either K_C or G_C. The graph 7.3.5 shows the calculated ductility factors for the EBN systems for both wet and dry conditions.

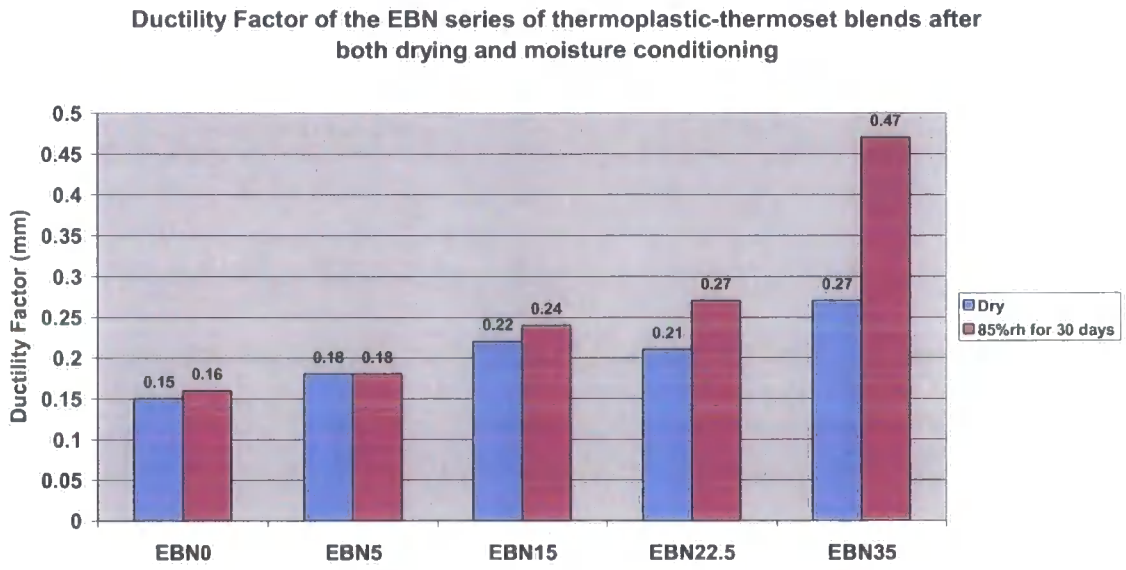

Graph 7.3.5 This graph shows the Kc results for the EBN series of epoxy blends for both dry and moisture-conditioned specimens.

This graph shows that in both wet and dry forms the ductility factor increases with increasing thermoplastic content. What is of greater significance is that in the moisture conditioning appears to have a large effect on the ductility factor especially at higher thermoplastic level. For the case of EBN35 the difference between the dry and wet states is very large. This would therefore suggest that in moist conditions the samples with higher thermoplastic loading are likely to have a superior fatigue life. This indicates that the morphology of the samples does in fact play a significant role in the overall properties of the blend. This also indicates the importance of considering the effect moisture has on the properties of thermosetting epoxy resin systems. Pre-conditioning of the samples prior any mechanical testing is therefore very important in order to reveal the true properties of the polymer blend and make like to like comparisons.

From these results it does appear that there are significant advantages to having a phase-inverted morphology in this particular thermoplastic-thermoset blend. The EBN35 system shows greatly improved toughness and in moist conditions the fracture properties actually increase and this would probably lead to improved fatigue performance in the blend. This is likely due to the continuous thermoplastic rich matrix that exists in this blend. This again could be of commercial relevance in

applications when thermosetting epoxy resin systems are used in hot wet environments where both impact and fatigue properties are of importance.
One drawback of a thermoplastic-thermoset blend with 35% thermoplastic is that the uncured blend may have a higher viscosity and be difficult to process.

7.3.1.6 Dynamic Mechanical Thermal Analysis (DMTA)

DMTA analysis was carried out on the EBN series of specimens using the method outlined in chapter 3. Prior to testing the samples were pre dried at 40°C in cabinet purged with dry nitrogen. The samples weight was monitored immediately regularly and when the samples reached a constant weight they were removed and stored in a dessicator containing silica gel and transported to the testing facility. They were then tested immediately. Samples were DMTA tested within 1 hour of removing from the drying cabinet.
The graph 7.3.6. shows the relationship between the storage modulus and temperature for the EBN series of blends.

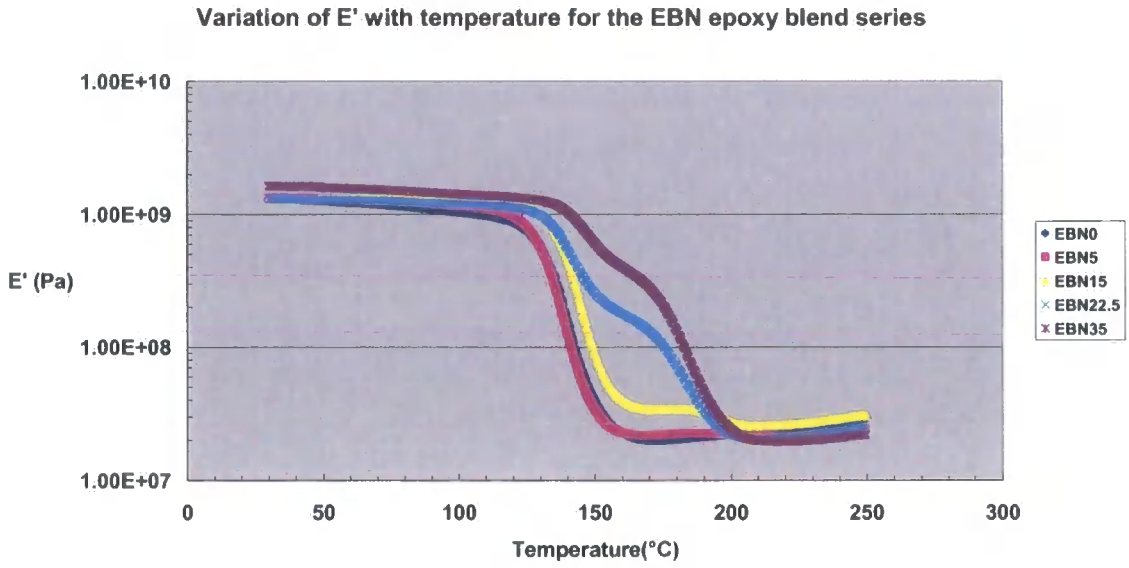

Graph 7.3.6 Variation of E' with temperature for the EBN series of blends.

The graph 7.3.6.1 above shows that as the loading of thermoplastic increases the Tg also increases. The following table shows the primary E' onset Tg's obtained from this data.

Epoxy Blend System	Tg by E' onset
EBN0	122.0°C
EBN5	123.72°C
EBN15	126.4°C
EBN22.5	131.4°C
EBN35	137.8

Table 7.3.1 This table shows the Tg by primary E' onset of the EBN series of blends.

This primary onset Tg is likely to be the Tg of the epoxy rich phase in the blend. As the level of thermoplastic increases it would appear that the level of thermoplastic in the epoxy rich phase also increases and this increases its Tg. This is because for this blend the Tg of the thermoplastic is 195°C and from EBN0 the pure epoxy is 122°C
It can also be seen in graph 7.3.6.1 that a secondary transition occurs at higher temperatures when there is thermoplastic present. This is likely to be the Tg of the thermoplastic rich phase in the phase- separated system. On close examination of this secondary transition it can be seen that as the level of thermoplastic in the system increases the temperature at which the transition occurs falls. Table 7.3.6.2.below shows the temperature of the secondary transition for the different blends

Epoxy Blend System	Secondary Tg by E' onset
EBN0	-
EBN5	189.5°C
EBN15	187.6°C
EBN22.5	170.4°C
EBN35	167.3°C

Table 7.3.2 This table shows the secondary Tg by E' onset of the EBN series of blend

The table 7.3.6.2. above shows the temperature at which the secondary transition occurs . This is likely to be the Tg of the thermoplastic rich phase. The Tg of the thermoplastic used in these blends is 195°C, this suggests that as the level of

thermoplastic increases the greater the level of epoxy in the thermoplastic rich phase. Hence more complete phase separation is occurring in the blends with lower levels ot thermoplastic.

The graph 7.3.7 shows the variation in loss modulus, E'', for the EBN series of blends

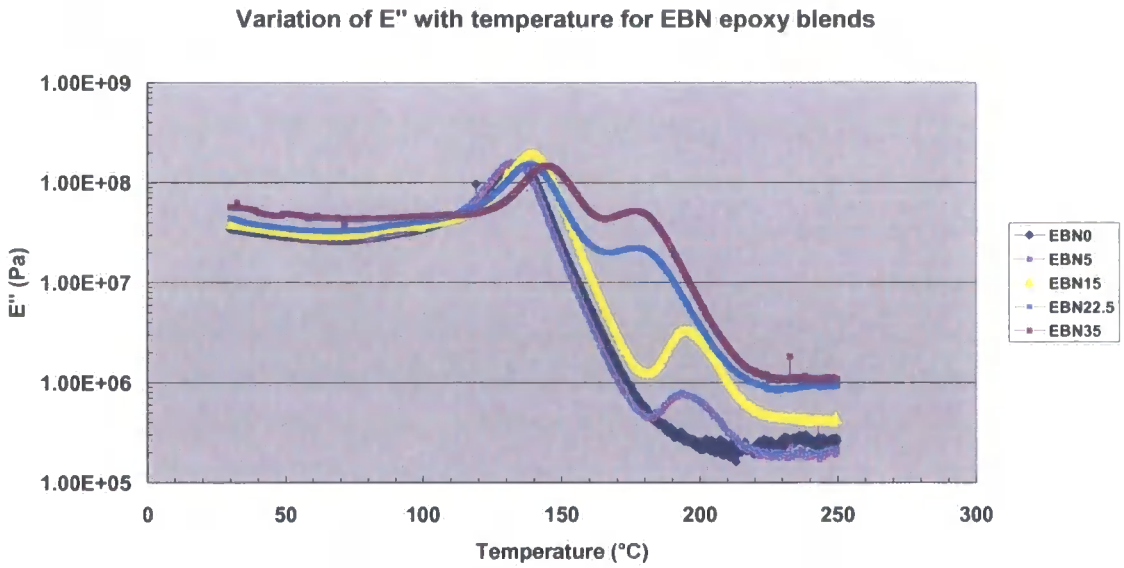

Graph 7.3.7 The variation of E' with temperature for the EBN series of blends.

The E'' data in graph 7.3.7 clearly shows the two phase nature of these epoxy blends. When the thermoplastic is present the two distinct peaks can be observed in the loss modulus curve. Similarly to the E' data the primary peak occurs at progressively higher temperatures as the thermoplastic level increases. The position of the secondary peak shifts to a lower temperature as the level of thermoplastic in the blend increases. This suggests that as the level of thermoplastic in the blend increases the composition of the two separating phases changes. Higher levels of thermoplastic produces less complete phase –separation between the thermoset epoxy and the thermoplastic.

The graph 7.3.8 shows the variation in tan δ with temperature for the EBN series of thermoplastic-thermoset blends

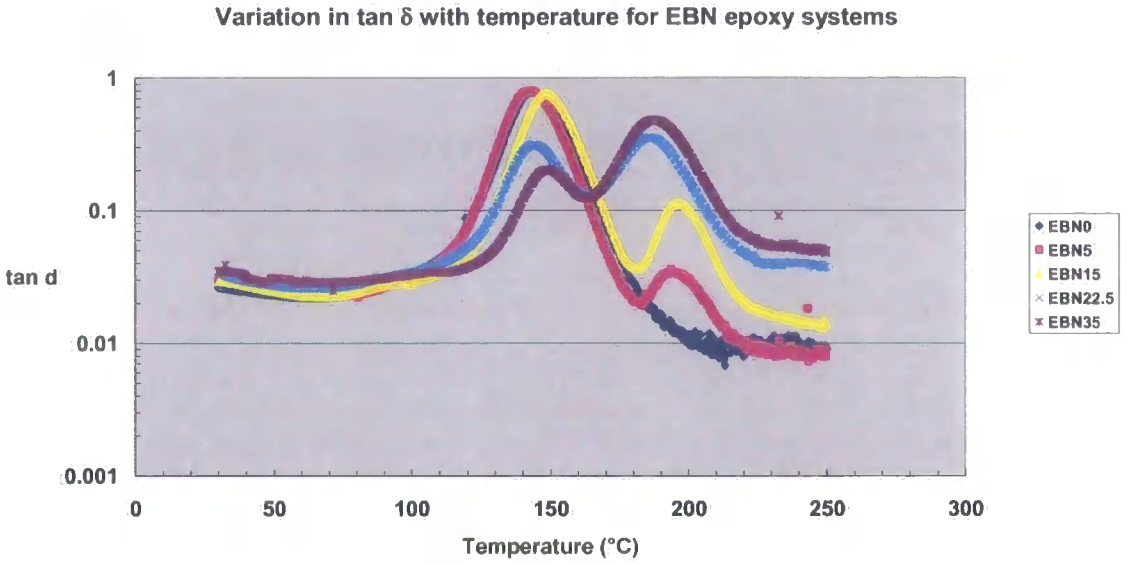

Graph 7.3.8 The variation of tan δ with temperature for the EBN series of blends.

The tan δ data shown in graph 7.3.8 further indicates the two phase nature of these thermoplastic-thermoset blends. Points of interest in the tan data are that the peak heights change as the compositions change. Increasing the thermoplastic concentration decreases the peak height of the primary peak associated with the epoxy rich phase and the height of the secondary peak associated with the thermoplastic rich phase increases. Similarly to both the E" and E' data the Tg's of the thermoset and thermoplastic rich phases change with composition. Increasing the thermoplastic concentration increases the Tg of the thermoset epoxy phase and reduces the Tg of the thermoplastic rich phase. Another point of interest in this data is that at ambient temperatures below the primary Tg the value of tan δ is proportional to the thermoplastic level. At higher thermoplastic levels the value of tan d is correspondingly higher. This is also shown at higher temperatures above the Tg of the thermoplastic rich phase where the higher the thermoplastic loading the higher the higher the tan δ. The value of tan delta is important when the thermoplastic-thermoset blend is subjected to higher frequency cyclic loading. The tan δ is a measure of the energy dissipated per cycle and if this value is high then it is likely that the sample will more rapidly heat up on cyclic loading.

7.3.2 Evaluation of toughening Mechanisms in Thermoplastic-Thermoset blends.

To evaluate the mechanisms by which fracture toughness is improved in these thermoplastic-thermoset blends the fracture mechanics samples were subjected to TEM evaluation. The method used for this is described in detail in chapter 3. Thin film samples for TEM evaluation were taken at 90° from the fracture surface. This enabled both the crack path and any toughening mechanism to be identified. The three blend selected for this study were EBN15, EBN22.5 and EBN35 which have particulate, co-continuous and phase inverted morphologies respectively. The samples used in this study are the exact same samples used for the fracture mechanics tests discussed in section 7.3.1

7.3.2.1 Toughening Mechanisms in system EBN15 with a particulate morphology.

The system EBN15 when cured at 180°C exhibits a particulate morphology. The TEM of this morphology is shown in figure 7.3.1

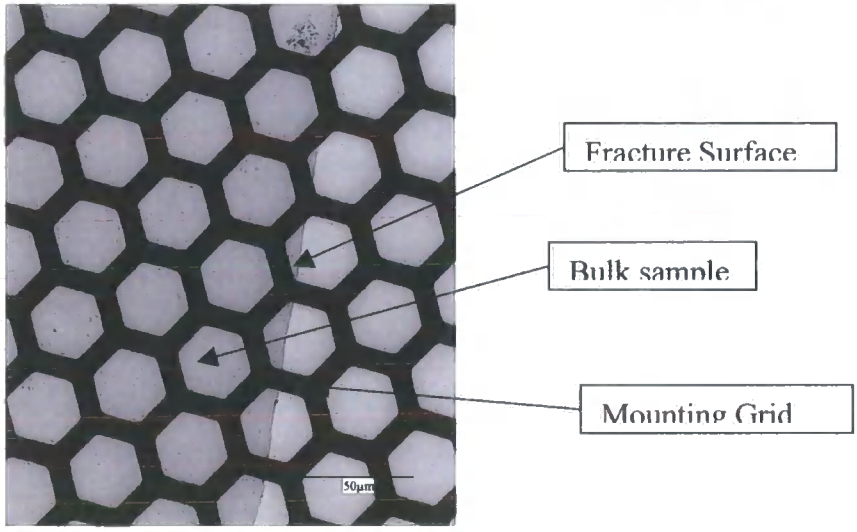

Figure 7.3.1 TEM micrograph of EBN15 showing the particulate morphology. The black honeycomb pattern is the TEM support grid.

The figure 7.4.6.1 shows the fracture surface resulting from the fracture mechanics test. The bulk of the sample shows a particulate morphology with a dispersed

thermoplastic rich phase. The fracture surface appears to be very smooth and generally featureless.

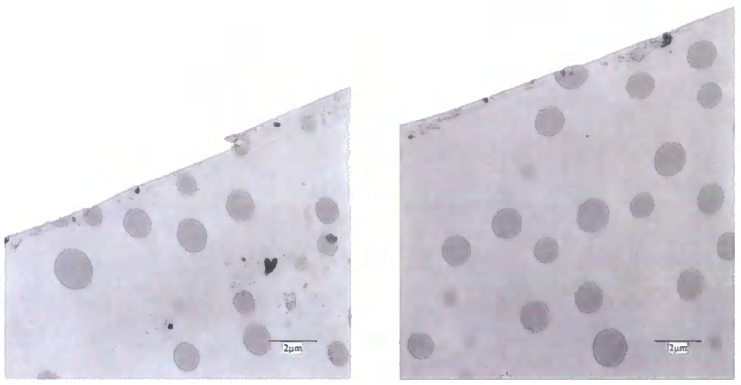

Figure 7.3.2 TEM micrographs of the fracture surface of EBN15.

Figure 7.3.2 above shows the fracture surface of the EBN15 sample. It can be seen that the fracture surface is very smooth and this is especially true when the crack is propagating in the epoxy rich region. However the crack path is deflected of its incident path when it meets a thermoplastic rich particle. It appears that the thermoplastic rich particles are acting to deflect the path of the crack. There is no evidence of any yielding or deformation around the thermoplastic rich particles which is the toughening mechanism observed in rubber modified epoxy resins [6,7suggests that the particles are not necessarily acting as sources of stress concentration to produce a toughening effect. This stress concentration effect has been widely reported for rubber toughened epoxy resins showing particulate morphologies however the thermoplastic rich dispersed phase does not appear to perform a similar toughening process. It does appear that the dispersed particles only act to deflect the propagating crack path.

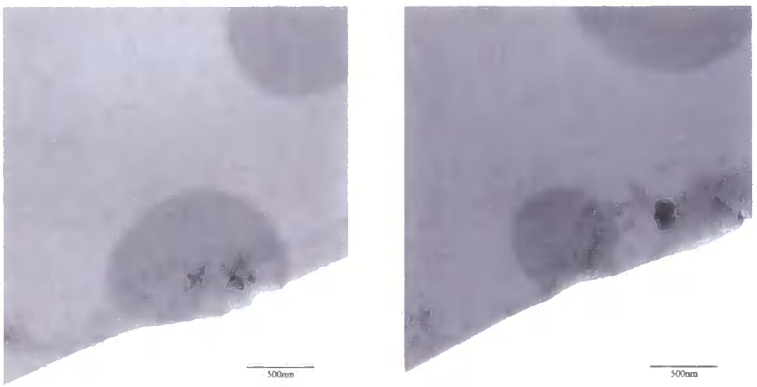

Figure 7.3.3 High Magnification TEM micrographs of the fracture surface of EBN15. This shows that the particulate thermoplastic rich phase acts to deflect the crack path.

The figure 7.3.3 shows a high magnification of a region of the fracture surface where the crack has encountered a thermoplastic rich particle and the crack path has deviated off its original course. The crack actually propagates through the thermoplastic rich particle and not around the particle which suggests good interfacial adhesion between the two separated phases. There is no obvious signs of cavitation or de-bonding of the thermoplastic particle. The fact that the particle is not de-bonded suggests that there is good interfacial adhesion between the two phases in the system. It does appear that the dispersed thermoplastic rich particles do not act in a similar fashion to dispersed rubbery particles in epoxy resins that show shear yielding and cavitation to produce a toughening effect.

7.3.2.2 Toughening Mechanisms in system EBN22.5 with a co-continuous morphology.

The system EBN22.5 when cured at 180°C exhibits a co-continuous morphology. The TEM of this morphology is shown in figure 7.3.4

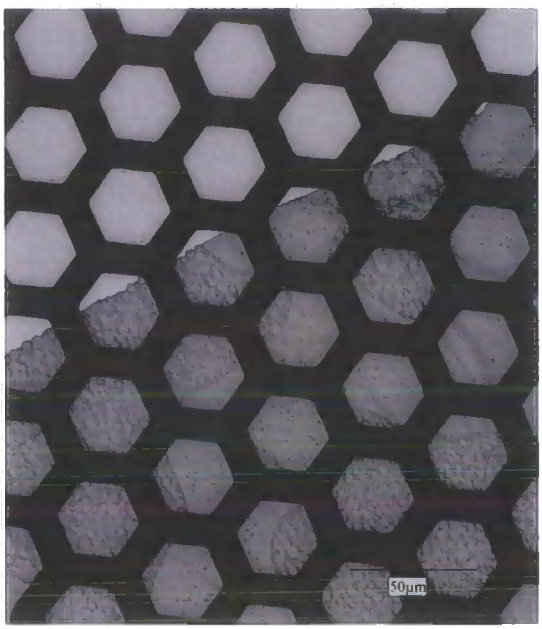

Figure 7.3.4 TEM of EBN22.5 cured at 180°C. This shows a large- scale co-continuous morphology with secondary phase separation occurring in both primary phases.

The figure 7.3.4 shows a TEM micrograph of the fracture region in the EBN22.5 system. This shows a large scale co-continuous morphology with two very distinct primary regions. The epoxy rich phase has a secondary phase of dispersed thermoplastic rich particles. The second primary phase is thermoplastic rich with a dispersed epoxy rich particle phase. A close examination of the fracture region shows that as the crack propagates through the primary epoxy rich phase the crack path is smooth and generally featureless. This is in contrast to the situation when the crack propagates through the thermoplastic rich primary phase where the fracture surface is rough and uneven in comparison to the epoxy rich phase.

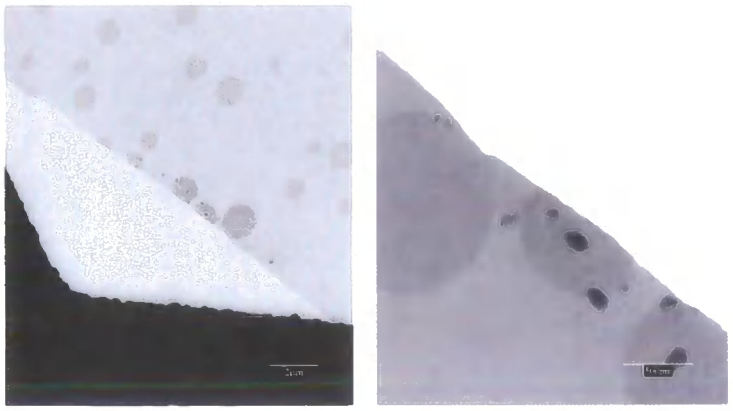

Figure 7.3.5 TEM micrographs of the EBN22.5 system showing the region where the crack is propagating in the primary epoxy rich phase.

Figure 7.3.5 shows the region where the crack propagates in the primary epoxy rich phase. The fracture surface is relatively smooth however the crack path is defected when it encounters secondary phase separated thermoplastic rich particle and the crack path is deflected, this is similar to the behaviour of the EBN15 system shown above. There is no obvious indication of any other toughening mechanisms occurring other than crack path deflection. The crack actually travels through the thermoplastic rich particle however the path of the crack is deflected. This indicates that there is good interfacial adhesion between the two phases.

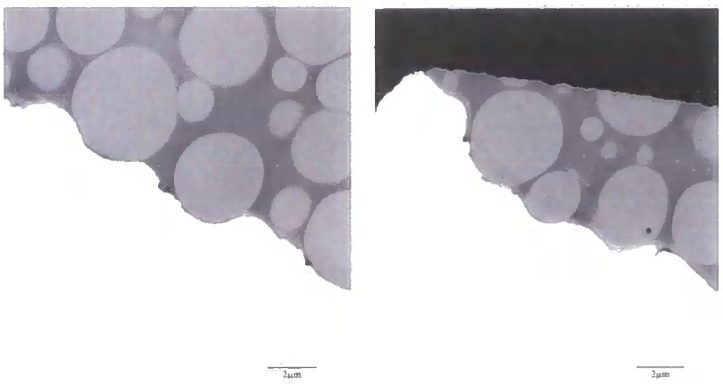

Figure 7.3.6 TEM micrographs of the EBN22.5 system showing the region where the crack is propagating in the primary thermoplastic rich phase

The figure 7.3.6 shows TEM micrographs of EBN22.5 in the region where the crack has propagated though the primary thermoplastic rich region. It can be seen that the crack path is far more undulating as a result of the secondary phase separated epoxy rich particles. The crack propagates around the outer surface of the epoxy rich particles and not through the particles. This suggests that the interfacial adhesion between the phases within the primary thermoplastic rich phase may be weak. However this lower adhesion between the phases may be beneficial in deviating the crack path and producing a toughening effect. There is no obvious evidence in this phase of any toughening effects in the bulk of the material away form the crack propagation region. This is very different to rubber modified epoxy resins where shear yielding and cavitation occur in the bulk of the sample adjacent to the crack propagation region that imparts a significant toughening mechanism. It appears that the toughening effect in thermoplastic-thermoset blends is largely as a result of the crack propagation being deflected and growing though the tougher thermoplastic rich phase. There are no conventional toughening mechanisms observed in this sample.

7.3.2.3 Toughening Mechanisms in system EBN35 with a particulate morphology.

The system EBN35 when cured at 180°C exhibits a phase inverted morphology with a continuous thermoplastic rich phase and a dispersed epoxy rich phase. The TEM of this morphology is shown in figure 7.4.8.1

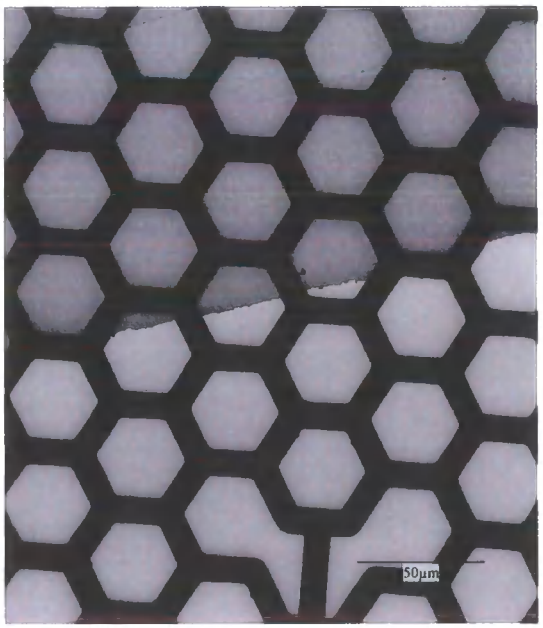

Figure 7.3.7 TEM of EBN35 cured at 180°C. This shows a phase-inverted morphology with a continuous thermoplastic phase with a dispersed epoxy rich phase.

The figure 7.3.7 shows the phase inverted morphology of the EBN35 system in which the fracture surface of this sample is not smooth as in the EBN15 system. Here the fracture surface has a very roughened appearance. This is further emphasised in figure 7.3.8 where it can be seen that the crack has in fact propagated around the dispersed epoxy rich phase in the sample.

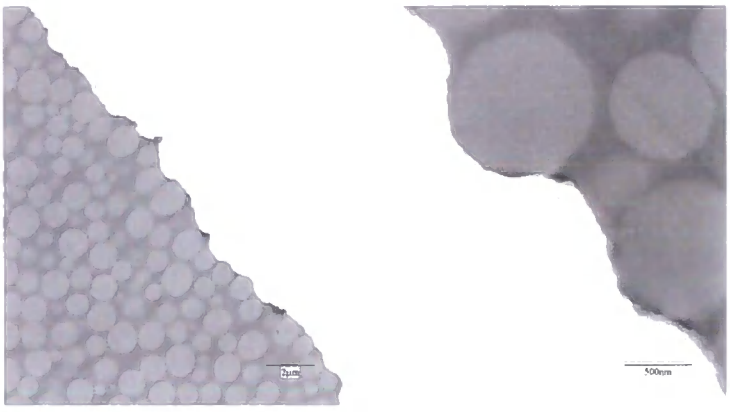

Figure 7.3.8 TEM micrographs of the EBN35 system showing the crack propagation region

Figure 7.3.8 shows that the crack path in this sample has propagated in very close proximity to the interface between the two phases. The crack propagates around the epoxy rich particles. Away from the fracture surface there does not appear to be any distortion of the morphology or any voiding. This suggests that the conventional toughening mechanisms observed in rubber toughened epoxy systems do not appear to operate in these systems. Here it appears that toughening in this sample is achieved by the crack propagation being largely in the thermoplastic rich phase and the crack is deflected around the epoxy rich dispersed phase. The fact that the crack propagates in the thermoplastic rich phase and the crack route becomes more tortuous as a result of the epoxy rich particle gives this particular morphology its much-improved toughness. There does appear to be a significant advantage with this particular morphology in terms of its excellent combination of mechanical properties.

7.3.3 Moisture diffusion properties epoxy blends

For this study EBN15 that has a particulate morphology, EBN22.5 which has a large scale co-continuous morphology and EB35 which has a phase inverted morphology were studied. The adsorption and desorption isotherm relative humidity steps chosen for the experiments were 0%RH (DRY), 30% RH, 60%RH, and finally 85%RH. Initially samples were tested at 25°C but the samples took over 2 weeks to establish

equilibrium at 30%RH, so due to time limitations samples were only testes at 60°C and 85°C.

7.3.3.1 Adsorption and Desorption Isotherms

The adsorption and desorption isotherms for the EBN15 systems at 60°C and 85°C are shown in figures 7.3.6 and 7.3.7 respectively. This sample has a particulate morphology with a dispersed thermoplastic rich phase.

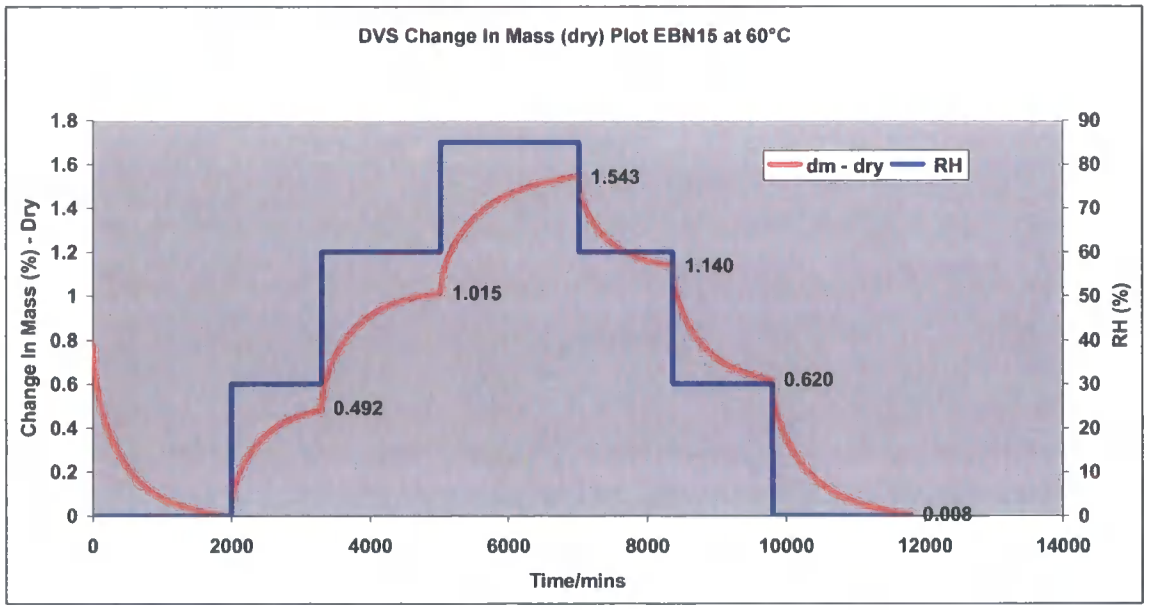

Graph 7.3.6 Moisture adsorption and desorption isotherms at 60℃ for EBN15

A comparison of the adsorption and desorption isotherms for EBN15 at both 60°C and 85°C show that the saturation levels at the different relative humidities are generally similar in value. As expected the time taken to reach equilibrium saturation is shorter at the higher temperature. It should also be noted that the saturation levels on the adsorption and desorption curves are different for any particular relative humidity level. Without exception at both temperatures the equilibrium saturation level is higher on the desorption curve than it is on the adsorption curve. However the final dry weight at the end of the experiment is similar to the starting weight in both cases. This may indicate that some hydrolysis or plasticisation of the network is

occurring on the adsorption run. If some hydrolysis is occurring this would possibly allow for a higher level of moisture to be held in the sample during the desorption. Further studies would need to be carried out in order to prove is this was in fact the case in these samples.

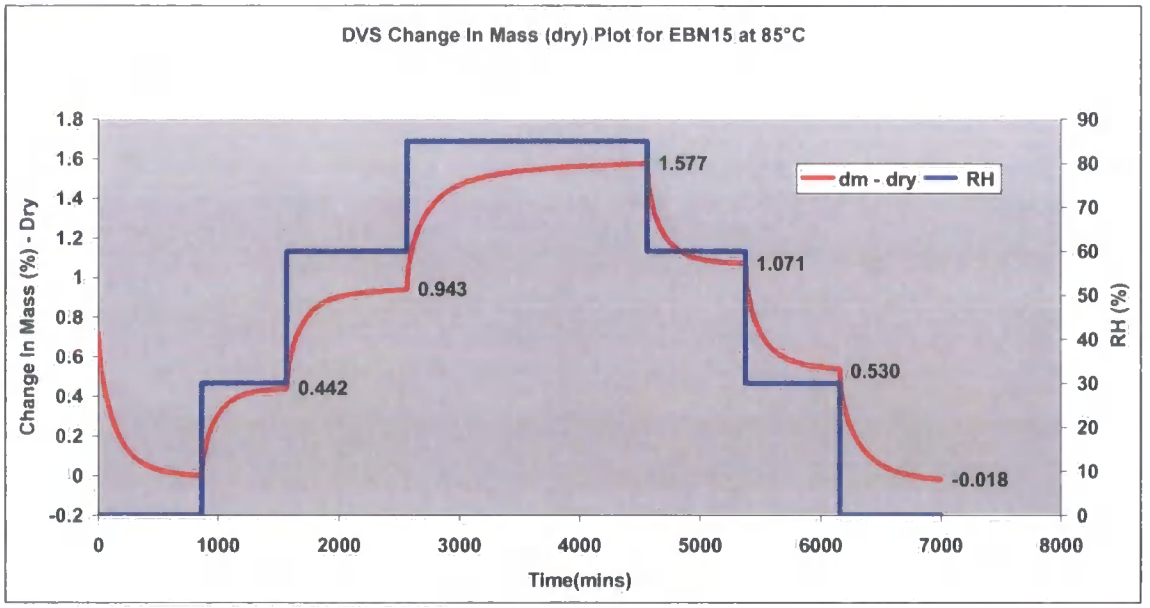

Graph 7.3.7 Moisture adsorption and desorption isotherms at 85°C for EBN15.

The difference in adsorption and desorption curves may also be explained is during the experiment some post curing of the epoxy resin occurred. This may have occurred when holding at 85°C for an extended period of time. More of the epoxy groups may have reacted and produced a higher concentration of polar hydroxyl groups which would hydrogen bond to water molecules and hence increase the saturation level of desorption curve. Multiple runs would have to be carried out on the same sample to prove if this was the explanation for this observed behaviour.

Adsorption and desorption isotherms for EBN22.5 at 60°C and 85°C are shown in figures 7.3.8 & 7.3.9 respectively. This sample shows a large-scale co-continuous morphology. A comparison of these curves shows that the behaviour of this system at both 60°C and 85°C are similar however there appears to be a lower saturation level at all relative humidities for the isotherm at 85°C. It is difficult to postulate why this would be the case as these experiments are all carried out well below any transition

temperature of the system. Further investigations need to be carried out to explain this observation.

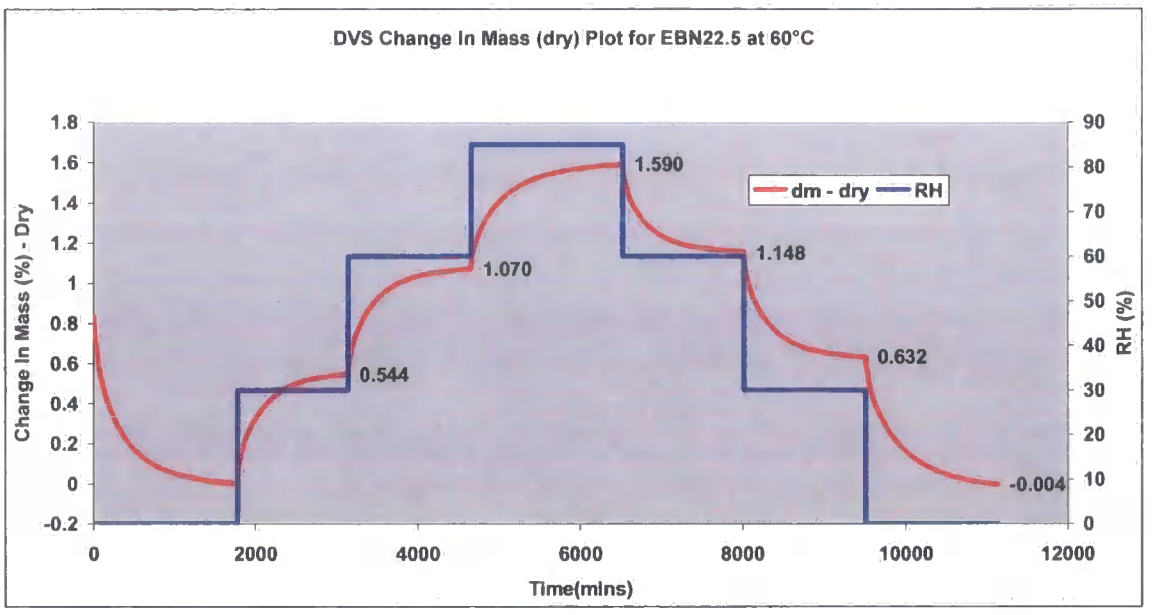

Graph 7.3.8 Moisture adsorption and desorption isotherms at 60℃ for EBN22.5.

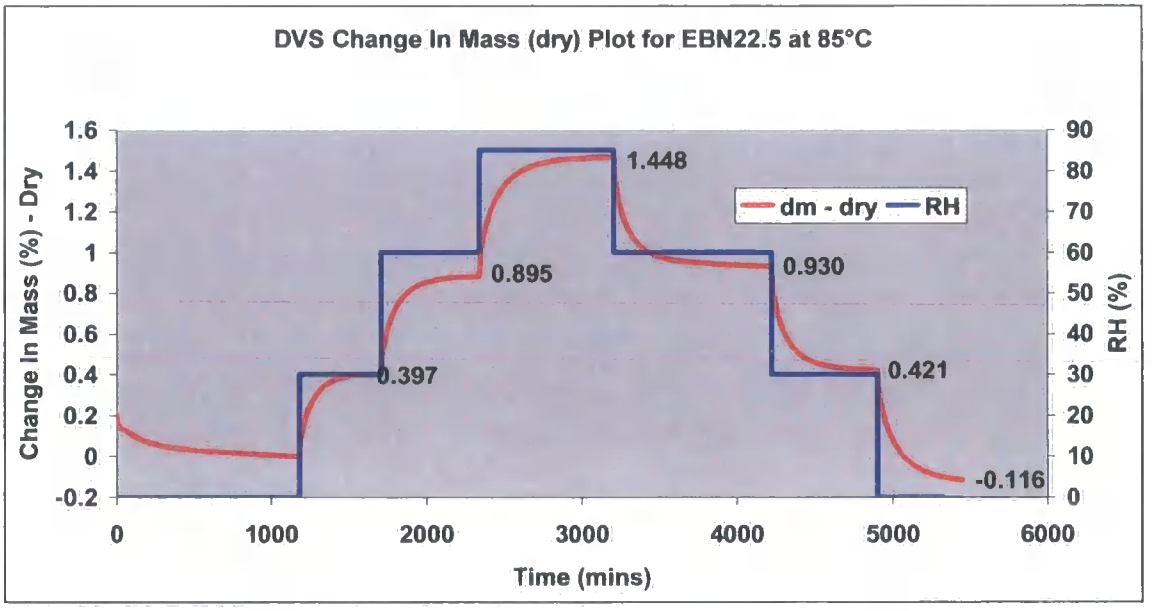

Graph 7.3.9 Moisture adsorption and desorption isotherms at 85℃ for EBN22.5.

The saturation levels for the EBN22.5 system at the different relative humidities are very similar to that seen in the EBN15 system

As was observed in the EBN15 system in all cases the desorption saturation levels are always higher than the adsorption saturation levels. This may indicate either hydrolysis of the network or possibly some post curing occurring during the experiment.

Adsorption and desorption isotherms for EBN35 at 60°C and 85°C are shown in figures 7.3.10 & 7.3.11 respectively. This sample shows a phase inverted morphology which has a continuous thermoplastic rich phase which contains a dispersed epoxy rich phase.

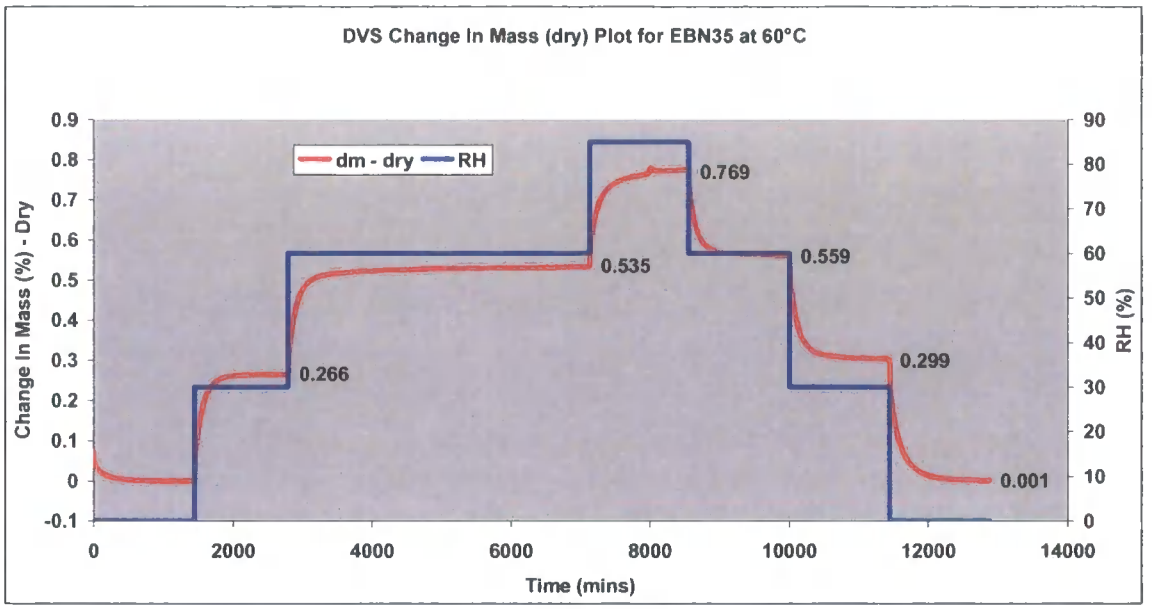

Graph 7.3.10 Moisture adsorption and desorption isotherms at 85°C for EBN35.

It can be observed that the isotherms for EBN35 at both 60°C and 85°C are very similar. However this is to be expected as all experiments here are carried out with the polymer blend in its glassy state. However comparing the EBN35 data with the data from both EB15 and EB22.5 it can be clearly seen that there is a very significant difference in the saturation levels at the different relative humidities. The EBN35 system has saturation levels that are approximately half that of the other systems.

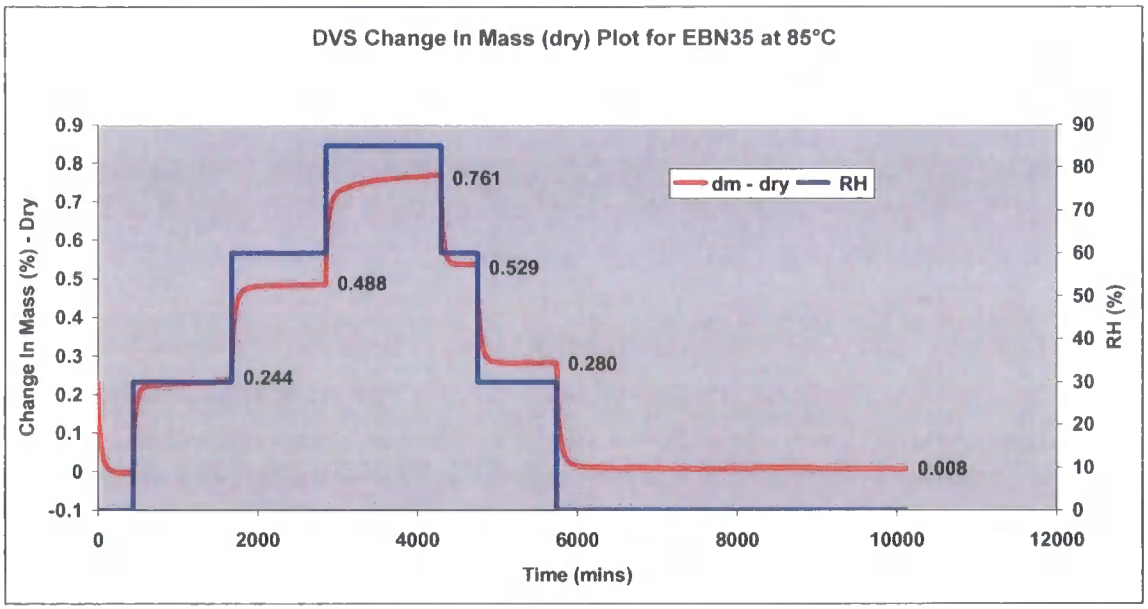

Graph 7.3.11 Moisture adsorption and desorption isotherms at 85°C for EBN35

This observation that the saturation levels are much lower for the EBN35 system may be as a result of the morphology of this system. The continuous thermoplastic rich phase may be acting as a barrier to the moisture. It is likely that the thermoplastic rich phase has a lower level of polar hydroxyl groups so there is less opportunity for the water molecules to diffuse into the system. However it is unlikely that the thermoplastic rich phase will be a total barrier to the moisture from diffusing into the epoxy phase. Another explanation could be due to differences in surface adsorption of the water molecules. Theories of moisture ingress in polymers show that there are several stages to moisture ingress [8,9]. It is thought that the first stage of moisture ingress involves the adsorption of a mono-layer of water molecules on the surface of the sample. In the EBN35 sample it is possible that the surface of the sample is largely a thermoplastic rich phase which is considerable less polar than the epoxy rich phase. This could alter the surface adsorption of water molecules which will change the diffusion characteristics of the system resulting in lower saturation levels.

From the adsorption and desorption curves described above the Fickian diffusion graphs of Mt / Minf versus square root of time / sample thickness can be plotted. The initial slope of this plot is the diffusion coefficient. This can be calculated for both the adsorption and desorption curves. This is detailed in chapter 3.

The diffusion coefficients for the EBN15 system are shown in graph 7.3.12

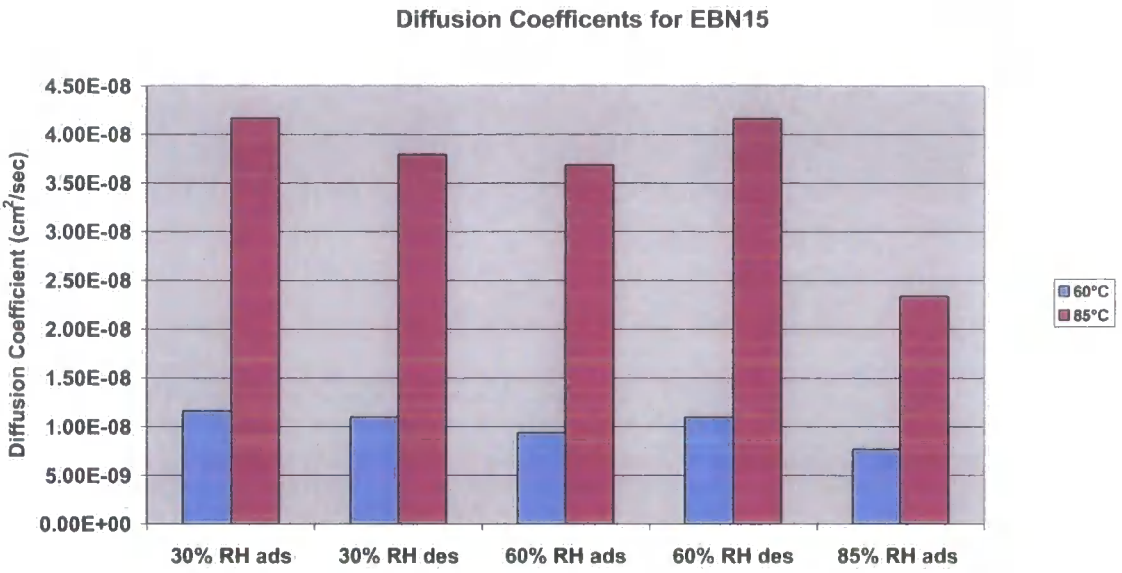

Graph 7.3.12 Diffusion Coefficients for EBN15 for adsorption and desorption isotherms at 60℃ and 85℃. (ads= adsorption, des= desorption)

The diffusion coefficients are shown in graph 7.3.12 for the EBN15 system. The first observation from this data is that the diffusion coefficient is very temperature dependent this is in contrast to the saturation levels which are the roughly the same for both isothermal temperatures evaluated. This indicates that the system saturates more quickly at elevated temperatures, which is largely to be expected due to the increase in Brownian motion of the water molecules at higher temperatures.

The diffusion coefficients appear relatively constant with changing %RH with the exception of the 85% data that shows a fall in diffusion coefficient at both 60°C and 85°C. From this data alone it is difficult to propose an explanation for this observation.

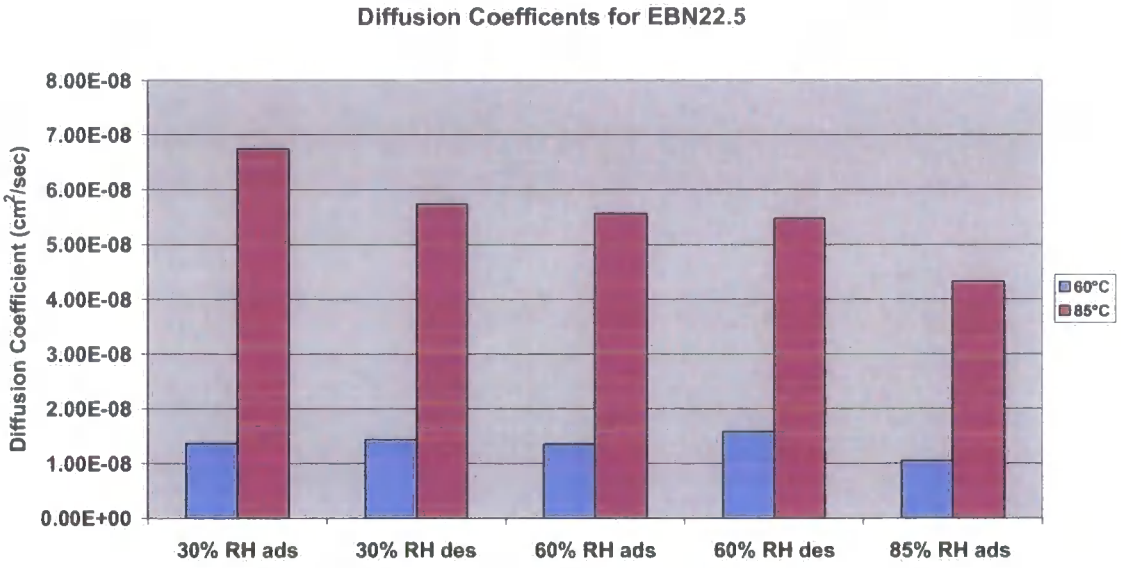

Graph 7.3.13 Diffusion Coefficients for EBN22.5 for adsorption and desorption isotherms at 60℃ and 85℃. (ads= adsorption, des= desorption)

The graph 7.3.13 shows the calculated diffusion coefficients for the EBN22.5 system which has a large scale co-continuous morphology. The obvious feature from this graph is that, as observed in the EBN15 sample, the diffusion coefficient is temperature dependent. There is a significant increase in diffusion coefficient between 60°C and 85°. As was also observed in the EBN15 sample the diffusion coefficients at 85%RH appear to be lower which suggests that this may be a real effect.

Comparing this data with that of EBN15 it can be seen that there is a clear increase in diffusion coefficient under all conditions with EBN22.5. This system has a con-continuous morphology with a continuous thermoplastic rich phase percolating through the sample. It has been reported that the higher the polar group concentration, the greater the tendency for water to hydrogen bond to the network and this results in a lower diffusion coefficient. The fact that the water becomes hydrogen bonded to epoxy network essentially impedes its progress into the sample, which has been reported by several workers [10,11]. It is likely that the continuous thermoplastic rich phase in the EBN22.5 sample has a lower concentration of polar hydroxyl groups and this may have the effect of offering a more rapid route for moisture ingress into the sample and therefore increasing the diffusion coefficient in this sample.

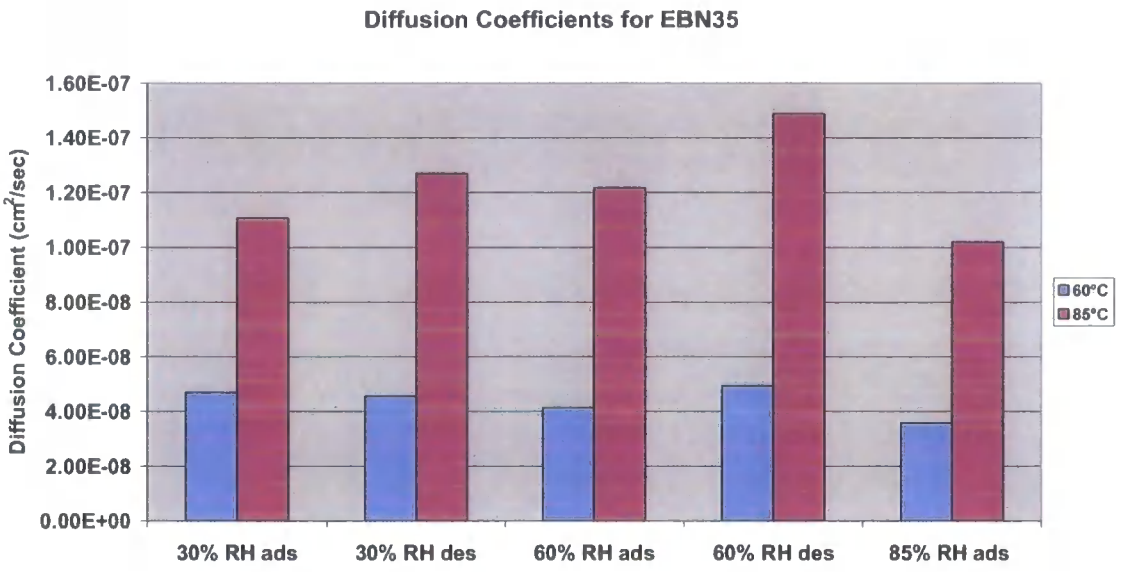

Graph 7.3.14 Diffusion Coefficients for EBN35 for adsorption and desorption isotherms at 60℃ and 85℃. (ads= adsorption, des= desorption)

Graph 7.3.14 shows the diffusion coefficients for the EBN35 system, which has a phase inverted morphology consisting of a continuous thermoplastic rich phase. As observed in the previous samples, EBN15 and EBN22.5, the diffusion coefficient increases with temperature. The significant point from this data is that the value of the diffusion coefficient is significantly higher when compared to EBN15 and EBN22.5. The EBN35 sample had a lower saturation level coupled with a higher diffusion coefficient. This further implies that that the transport of moisture through the thermoplastic rich phase in the system is in fact quicker because it is not hindered by highly polar functional groups that can strongly hydrogen bond to the moisture and impede ingress.

It has also been proposed [11,12] that the ingress of moisture into epoxy systems is initially by ingress into nano-voids in the system and ultimately this gives access to the polar functional groups in the network. It is possible that the thermoplastic rich phase has a higher level of nano-voids in the system which allows for the more rapid ingress of moisture into the sample

It would appear that overall the EBN35 system that has a phase inverted morphology is less susceptible to moisture ingress. This is likely due to the continuous

thermoplastic rich network. This may be of significant advantage when epoxy resins are used in moist environments.

7.4 Summary

In this chapter the physical properties of thermoplastic-thermoset blends with different morphologies have been characterised. It has been shown that there appears to be a significant advantage to having a phase inverted morphology, which consists of a continuous thermoplastic rich phase containing a dispersed epoxy rich phase. This appears to give the blend improved fracture toughness, Tg and reduced moisture uptake. It has also been demonstrated that moisture has a great effect on the mechanical properties of the thermoplastic-thermoset blends and preconditioning of samples is important prior to any accurate physical characterisation of the blend.

It has been shown that the conventional toughening mechanisms seen in rubber toughened epoxy resins are not observed in these thermoplastic-thermoset blends. It appears that toughening occurs in two-phase morphologies largely by crack path deflection. In the phase inverted morphology the crack propagates through the thermoplastic rich phase and is deflected around the dispersed epoxy thermoset phase and this appears to impart the greatest improvement in fracture toughness. One detriment to the phase inverted morphology is that it requires the incorporation of higher levels of thermoplastic, which may impact on rheology and processing.

This chapter has also shown how the incorporation of a high Tg thermoplastic can increase the Tg of the overall system and this is largely thought to be as a result of incomplete phase separation of the blend. The rubbery plateau modulus of the blends is however reduced with increasing thermoplastic content.

Moisture ingress of the thermoplastic-thermoset blends has also been studied in detail and this too has highlighted that the most beneficial morphology is the phase inverted system which exhibits a higher diffusivity as shown by the diffusion coefficient however the overall saturation levels in the phase inverted morphology are significantly lower. It also appears to be the case that the system, which possesses the phase inverted morphology the fracture toughness of the system improves on

exposure to a moist environment that suggests the moisture has a plasticising effect on the thermoplastic rich phase.

This work suggests that the phase separated morphology of thermoplastic-thermoset blends does play a significant role in establishing the overall physical properties of the polymer blend and this could be of significant commercial significance.

7.5 References

1 ESIS publication No 28 ; Fracture Mechanics Testing Methods for Polymers, Adhesives and Composites. Ed. Moore D.R., Williams J.G. Elsevier 2001

2 http://www.oconnor.com.sg/SScien.html

3 Hayward, D.; Hollins, E.; Johncock, P.; McEwans, I.;Pethrick, R. A.; Pollock, E. Polymer 1997, 38, 1151.

4 Moore DR, Emmerson GT, McGrail PT CytecFiberite internal report on Fatigue

5 Kinloch AJ, Young RJ, Fracture Behaviour of Polymers, Applied Science, London 1983.

6 A. Lazzeri and C. B. Bucknall Polymer 36 (1995) 2895

7 Bucknall CB, Maistros G, Gomez CM, Partridge IK. Toughening epoxy resins using functionalized polymers. J Macromol Sci Pure 1994;A31.

8 Kumins, C. A.; Kwei, T. K. In Diffusion in Polymers; Crank, J.; Park, G. S., Eds.; Academic: London,1968; Chapter 4.

9 Theodorou, D. N. Neogi, P., Ed.; Diffusion in Polymers; Marcel Dekker: New York, 1996; Chapter 2.

10 Maxwell, I. D.; Pethrick, R. A. J Appl Polym Sci 1983, 28, 2363.

11 Soles, C. L.; Chang, F. T.; Bolan, B. A.; Hristov, H. A.; Gidley, D. W.; Yee, A. F. J Polym Sci Part B:Polym Phys 1998, 36, 3035.

12 http://msewww.engin.umich.edu/research/groups/yee/publications/Diffusion-model/Diffusion-model

Chapter 8

Conclusions And Suggested Further Work

8.1 Introduction

This chapter briefly summarises the main results and conclusion from this project and suggests areas worthy of further investigation.

8.2 Conclusions

The introduction given in chapter 1 described the commercial uses of thermosetting resins and why they are of significant commercial interest. The drawbacks of thermosetting resins were also outlined with the major disadvantages of epoxy resins being their low toughness, moisture sensitivity and limited high temperature use. Blending high Tg thermally stable thermoplastics into epoxy resins can significantly improve the properties of the overall cured system. During cure an epoxy / thermoplastic blend may undergo phase separation to produce a multi-phase morphology. The nature of this resultant morphology influences the overall physical properties of the blend.

Chapters 5 and 6 studied the nature of the phase separation processes occurring in an epoxy toughened with a PES type thermoplastic. It was shown that the major phase separation process occurring is spinodal decomposition and this is independent of the

blend composition, no evidence of phase separation by nucleation and growth was observed in this study. Particulate morphologies that were previously thought to occur by nucleation and growth actually form from the break up of a percolating co-continuous network. This behaviour is termed a percolation to cluster transformation (PCT). In the PCT process phase separation occurs by spinodal decomposition, however the resultant co-continuous network is not stable and can reduce its energy interfacial energy by one phase breaking up into particles. From this study it appears that both particulate and phase inverted morphologies form from by PCT.
It was also shown in chapters 5 and 6 that multiple phase separations can occur during the cure of an epoxy / thermoplastic blend and this can lead to some very interesting morphologies. Around the critical composition for the blend multiple PCT's can occur which leads to sub-included or salami type morphologies. Such structures have been reported in rubber modified acrylic and polystyrene resins, but have not been previously reported for epoxy / thermoplastic blends.

Cahn-Hilliard analysis was used to determine the kinetics of the phase separation process. This study shows that Cahn-Hilliard theory does not fully describe the spinodal decomposition processes occurring in these reactive systems. This is likely due to the highly dynamic nature of the reacting system where the molecular masses and functionalities of the components is rapidly changing. However Cahn-Hilliard theory can be useful in extracting kinetic information about the early stages of the spinodal decomposition processes occurring in the reactive blends.

The application of Cahn-Hilliard theory showed that the blends studied in this thesis show typical LCST behaviour. And for this particular epoxy / thermoplastic blend the critical composition is around 20% thermoplastic.

It also appears that the rate of phase separation is greatly increased when cured above the Tg of the aromatic thermoplastic. It is likely that the spinodal decomposition process is hindered when the blends are cured at temperatures below the Tg of the thermoplastic. Curing the system at or above the Tg of the thermoplastic is likely to promote phase separation in the systems. Further studies need to be carried out to see how varying the thermoplastic Tg and the cure temperature of the system can control the morphology.

It was shown in chapter 6 that the addition of small levels of tri-functional epoxy delays the phase separation process dramatically. This is thought to be as a result of the tri-functional epoxy resin acting as a highly effective solvent for the thermoplastic which delays the onset of phase separation until a high level of epoxy conversion is reached. It is possible that with high levels of tri-functional epoxy resin present the system will gel prior to any phase separation occurring.

In chapter 7 it was shown that the mechanical properties of the epoxy blend are significantly influenced by the morphology. It does appear that there is a significant advantage to a phase inverted morphology where a continuous thermoplastic rich phase is present in the system. This morphology improves the fracture toughness and its properties are less influenced by moisture. It does appear that with the phase inverted morphology that the moisture solubility is significantly reduced. It is also shown that with a phase inverted morphology the presence of moisture actually has a toughening effect on the blend which is not readily seen with other morphologies.

Chapter 7 showed how moisture can significantly alter the physical properties of the cured epoxy / thermoplastic blends. This needs to be considered when screening mechanical properties of epoxy resin blends.

Chapter 7 also looked at possible toughening mechanism in phase separated epoxy / thermoplastic blends. The conventional toughening mechanisms of shear yielding and cavitation were not observed in these blends. The major toughening mechanism appears to be crack path deflection and this mechanism is maximised with a phase inverted morphology.

8.3 Suggested Further Work.

Several areas are probably worthy of further investigation and these are as follows:

- A further study looking at changing the Tg of the thermoplastic in relation to the cure temperature and how this influences the cured morphology may be a useful study. It may be possible to achieve a phase inverted morphology at lower thermoplastic content. This may be a route to higher toughness without significantly impacting on uncured viscosity.
- Several interesting novel morphologies have been reported in this thesis, in particular the sub-included or salami structures. A study of the mechanical properties of these blends could yield some interesting results.
- A theoretical modelling study of the PCT process may yield some useful information on the mechanisms and factors that influence this process. This may predict ways to control morphology.
- The effect of fillers on both phase separation and mechanical properties requires further investigation and understanding.
- It has been shown that the methodology of SALS/DSC and microscopy is highly effective in studying phase separation in thermoplastic-thermoset blends. This approach should be more widely adopted when developing new formulations in order to fully understand the relationship between phase separation and processing. This would lead to formulations with more reproducible properties.
- The effect of morphology on adhesion to different substrates should be studied.
- It has been shown how moisture significantly influences mechanical properties of these epoxy / thermoplastic blends. The effect of moisture should be taken into consideration when performing any physical evaluation of polymeric system.